Proceedings E-Book

International Symposium for

Agricultural Biomedical Research Network

The Fusion of Natural Product Chemistry and Medical Information Engineering for Advancement of Medicine – 2025

第２回天然物化学・情報医工学融合によるアグリバイオメディカル研究セミナー

9th - 10th January 2025

at UNISERV Chiang Mai University

Chiang Mai, Thailand

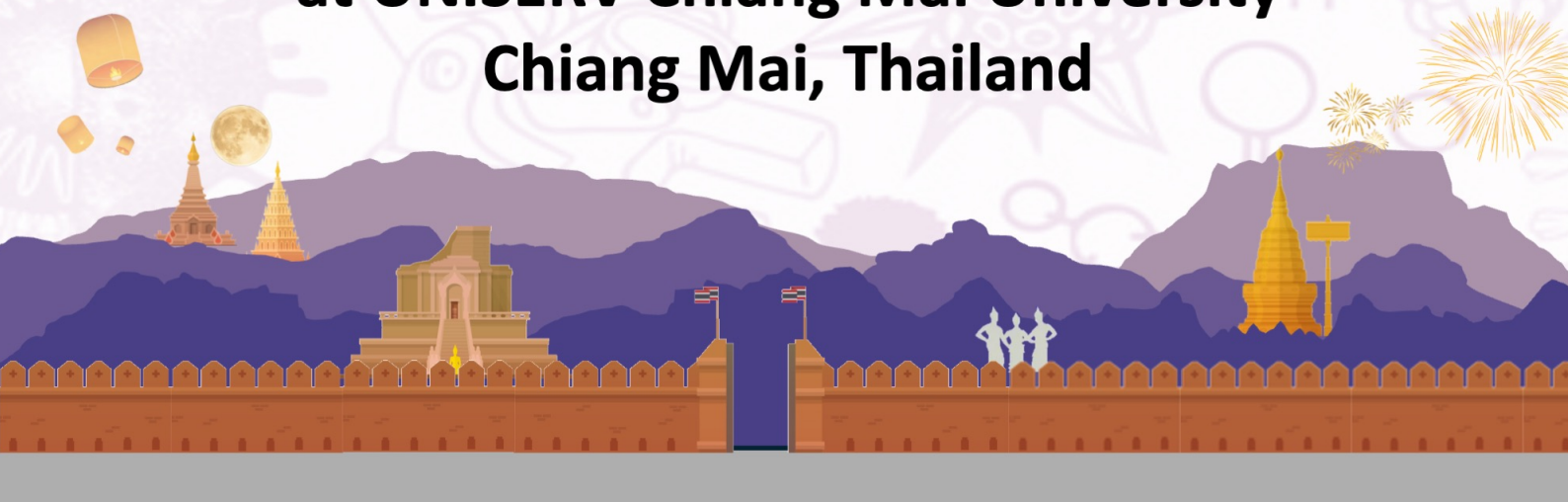

CONTENTS

Welcome Address

Dear all perspective participants,

On behalf of all organizers, we wish welcoming to our esteemed cross-disciplinary research conference, hosted by Chiang Mai University in collaboration with the Kyoto Institute of Technology (KIT) and other network institutions from Japan, Myanmar, Vietnam, and Cambodia.

The International Symposium for Agricultural Biomedical Research Network stands as a testament to our commitment to integrating cross-disciplinary research, which is vital for developing innovations and technologies that respond to the dynamic changes of our contemporary world. Our aim is to transcend the boundaries of individual disciplines and foster a collaborative environment where diverse fields can converge, share insights, and build upon each other's strengths.

Over the course of this event, you will have the opportunity to engage with distinguished speakers from various countries and disciplines, present your own research, and participate in enriching discussions. The program includes oral presentations from invited experts, selected participant presentations, poster sessions, and the publication of peer-reviewed proceedings. We believe that these activities will provide immense value, especially for our master's degree students, who can leverage the published proceedings as part of their graduation requirements.

We are honored to host this platform for you to publicly present your work, exchange ideas, and establish valuable connections. Together, we can advance the frontiers of cross-disciplinary research and forge pathways to meaningful innovation.

We look forward to your participation and to the impactful collaborations that will emerge from this conference.

Warm regards,

Bannakij LOJANAPIWAT, M.D.
Professor (Specialist) and Dean of Faculty of Medicine
Chiang Mai University, Thailand

Welcome Address

Dear all perspective participants,

We are pleased to have an opportunity to organize this international symposium hosted by Chiang Mai University in cooperation with other partnership institutions in Vietnam and Cambodia.

This symposium has been a part of the Japan-ASEAN Seminar series organized by Kyoto Institute of Technology (KIT) since 2018 with partner institutions, and its origins lie in the Japan-Vietnam Seminars, which have been held 15 times from 2003 to 2017.

KIT is a relatively compact university in Japan, but it includes a diverse range of specialists in many fields such as biology, chemistry, and information sciences, and is actively involved in many international research projects with the partner institutions, especially in ASEAN countries.

These symposiums are the core events of such research projects and have led to many new research collaborations and the acceptance of international students.

We hope that young researchers and students in related fields will join this symposium, not only to share their valuable insights but also to use it as an opportunity for future collaborations.

We look forward to seeing you in Chiang Mai.

Acknowledgments: Our international research network, including this symposium, is supported by the Japan Society for the Promotion of Science (JSPS) Core-to-Core Program. On behalf of the organizers, we would like to thank JSPS and all our partners who have contributed to establish this network.

KAMEI Kaeko, Ph.D.
Vice-President, Professor of Faculty of Molecular Chemistry and Engineering
Kyoto Institute of Technology, Japan

FUKUZAWA Masayuki, Ph.D.
Coordinator of KIT's Core-to-Core Program, Associate Professor of Faculty of Information and Human Sciences
Kyoto Institute of Technology, Japan

List of Committees

INTERNATIONAL ADVISORY COMMITTEE

KAMEI Kaeko	Kyoto Institute of Technology, Japan
FUKUZAWA Masayuki	Kyoto Institute of Technology, Japan
YOSHIDA Hideki	Kyoto Institute of Technology, Japan
KUMADA Yoichi	Kyoto Institute of Technology, Japan
SIRIARAYA Panote	Kyoto Institute of Technology, Japan

LOCAL ORGANIZING COMMITTEE

Honorary Chair

Bannakij LOJANAPIWAT	Dean of the Faculty of Medicine, Chiang Mai University, Thailand

Honorary Vice Chair

Arisa BONNESS	Associate Dean for Graduate Studies, Chiang Mai University, Thailand

General Chairs

Teera CHEWONARIN	Head of the Department of Biochemistry, Chiang Mai University, Thailand
Supanimit TEEKACHUNHATEAN	Head of the Department of Pharmacology, Chiang Mai University, Thailand

General Committee

Pornngarm DEJKRIENGKRAIKUL	Chiang Mai University, Thailand
Thanyaluck PHITAK	Chiang Mai University, Thailand
Somdet SRICHAIRATANAKOOL	Chiang Mai University, Thailand
Wirote TUNTIWECHAPIKUL	Chiang Mai University, Thailand
Supachai YODKEEREE	Chiang Mai University, Thailand

Convenor

Pornsiri PITCHAKARN	Chiang Mai University, Thailand

Subcommittees:

Program, Book of Abstracts and Proceedings

Jirayu BOONYAKIDA	Chiang Mai University, Thailand
Pensiri BUACHEEN	Chiang Mai University, Thailand
Orawan KHANTAMAT	Chiang Mai University, Thailand
Weerakit TAYCHAWORADITSAKUL	Chiang Mai University, Thailand
Ariyaphong WONGNOPPAVICH	Chiang Mai University, Thailand

Registration and Reception

Arisa BONNESS	Chiang Mai University, Thailand
Jirayu BOONYAKIDA	Chiang Mai University, Thailand
Pensiri BUACHEEN	Chiang Mai University, Thailand
Salinee JANTRAPIROM	Chiang Mai University, Thailand
Pimpisid KOONYOSYING	Chiang Mai University, Thailand
Woranontee KORSIEPORN	Chiang Mai University, Thailand
Weerakit TAYCHAWORADITSAKUL	Chiang Mai University, Thailand

Publicity and Information Technology

Sivamoke DISSOOK	Chiang Mai University, Thailand
Pimpisid KOONYOSYING	Chiang Mai University, Thailand
Peraphan POTHACHAROEN	Chiang Mai University, Thailand

Sponsorship and Finance

Ratchanu PHOKUM (Treasurer)	Chiang Mai University, Thailand
Peraphan POTHACHAROEN	Chiang Mai University, Thailand

Venue and Audiovisual Coordination

Jittasak KHOWSATHIT	Chiang Mai University, Thailand
Jetsada RUANGSURIYA	Chiang Mai University, Thailand

List of Reviewers for ISABRN 2025 Proceedings

Jirayu BOONYAKIDA	Chiang Mai University, Thailand
Kongsak BOONYAPRANAI	Chiang Mai University, Thailand
Pensiri BUACHEEN	Chiang Mai University, Thailand
Wittaya CHAIWANGYEN	University of Phayao, Thailand
Ratchadawan CHEEWANGKOON	Chiang Mai University, Thailand
Chaowanee CHUPEERACH	Mahidol University, Thailand
Sivamoke DISSOOK	Chiang Mai University, Thailand
Nahathai DUKAEW	Mae Fah Luang University, Thailand
Panichakorn JAIYONG	Mae Fah Luang University, Thailand
Napapan KANGWAN	University of Phayao, Thailand
Fahsai KANTAWONG	Chiang Mai University, Thailand
Varongsiri KEMSAWASD	Mahidol University, Thailand
Orawan KHANTAMAT	Chiang Mai University, Thailand
Jittasak KHOWSATHIT	Chiang Mai University, Thailand
Sarunya KITDUMRONGTHUM	Mahidol University, Thailand
Nut KOONRUNGSESOMBOON	Chiang Mai University, Thailand
Pimpisid KOONYOSYING	Chiang Mai University, Thailand
Warunee KUMSAIYAI	Chiang Mai University, Thailand
Puwapong NIMKINGRATANA	Chiang Mai University, Thailand
Sakaewan OUNJAIJEAN	Chiang Mai University, Thailand
Sirichatnach PAKDEEPROMMA	King Mongkut's Institute of Technology, Thailand
Chatchawin PETCHLERT	Burapha University, Thailand
Thanyaluck PHITAK	Chiang Mai University, Thailand
Kanokkarn PHROMNOI	University of Phayao, Thailand
Komsak PINTHA	University of Phayao, Thailand
Pornsiri PITCHAKARN	Chiang Mai University, Thailand
Saranyapin POTIKANOND	Chiang Mai University, Thailand
Patcharee PRIPDEEVECH	Mae Fah Luang University, Thailand
Khanittha PUNTUREE	Chiang Mai University, Thailand
Jetsada RUANGSURIYA	Chiang Mai University, Thailand
Yuraporn SAHASAKUL	Mahidol University, Thailand
Tuangporn SUTHIPHONGCHAI	Mahidol University, Thailand
Uthaiwan SUTTISANSANEE	Mahidol University, Thailand
Weerakit TAYCHAWORADITSAKUL	Chiang Mai University, Thailand
Piya TEMVIRIYANUKUL	Mahidol University, Thailand
Wirote TUNTIWECHAPIKUL	Chiang Mai University, Thailand
Ariyaphong WONGNOPPAVICH	Chiang Mai University, Thailand

List of Supporting Organizations

Faculty of Medicine, Chiang Mai University, Thailand

Japan Society for the Promotion of Science (Core-to-Core Program), Japan

Kyoto Institute of Technology, Japan

The Biochemistry and Molecular Biology Section (BMB), The Science Society of Thailand
Under the Patronage of His Majesty the King, Thailand

List of Sponsors

Advanced Medical Science Co., Ltd.

Applied Chemical and Instrument Company Limited

Bang Trading 1992 Company Limited

Bara Scientific Co., Ltd.

Becton Dickinson (Thailand) Ltd.

ESCO Lifesciences (Thailand) Company Limited

Life Science Ap Co., Ltd.

Merck Limited

P S Bioscience Company Limited

P. International Equipment Company Limited

RI Technologics Company Limited

S.M. Chemical Supplies

Union Science. Co., Ltd

Proceedings

A (Agriculture and Biology)

B (Biomedical Science)

D (Data Science and IT)

A Comparative Study of Physical Extraction Methods on Spirulina's Bioactive and Volatile Organic Composition

Sithu Lwin[1], Suthat Surawang[2], and Thanyaporn Siriwoharn[1,*]
[1] Division of Food Science and Technology, Faculty of Agro-Industry, Chiang Mai University, Chiang Mai, Thailand
[2] Division of Product Development Technology, Faculty of Agro-Industry, Chiang Mai University. Chiang Mai, Thailand
*Corresponding author's email: thanyaporn.s@cmu.ac.th

Abstracts:
Although spirulina is widely recognized for numerous health benefits, it has been underutilized in the food industry due to its undesirable odor. This research aimed to establish information between extraction and the obtained bioactive and volatile organic compounds (VOC) to enable wider ingredient usage. Aqueous extractions using ultrasonication and conventional homogenization at 10, 20, and 30 min were performed and compared to the control. The bioactive compounds, antioxidant activity, and undesirable VOC in the extract were determined. The ultrasonicated extracts were significantly higher in total phycocyanin (3.9-4.2 times), chlorophyll (1.8-2.3 times), carotenoid (12-38 times), and antioxidant activity (1.8-2.4 times) than the homogenized extracts ($P<0.05$). The higher efficiency in extracting bioactive compounds led to increased VOC content. The ultrasonicated extract at 30 min had the highest 3-methyl-butanal (27.9 ± 0.28%), hexanal (8.44 ± 1.05%), and 1-Octen-3-ol (1.38 ± 0.35%). This research provided an important foundation for customizing spirulina extraction for functional food applications.

Keywords: *Arthrospira platensis*; Homogenization; Ultrasound-assisted extraction; Phycocyanin; Off-odor; Blue-green algae

Introduction

Spirulina *(Arthrospira platensis),* a blue-green micro-algae, is one of water's largest quantities of cyanobacteria. It is recognized for its high protein content (60 - 70 g/100 g) and excellent nutritional values including fatty acids, vitamins, minerals, and bioactive substances like phycocyanin, chlorophyll, and carotenoids (1). Phycocyanin is a water-soluble component representing approximately 15% of proteins in spirulina. It has been reported to have antioxidant, anticancer, and anti-inflammatory properties (2). There have been many attempts to utilize phycocyanin along with bioactive substances of spirulina in food applications including cookies (3), pasta (4), snacks, and confectionary products (5). However, the dosage was not able to exceed 10% due to its sensory properties (4).

The odor and gritty texture of spirulina are major factors impacting consumers' acceptability (3-5). These undesirable sensory attributes arise from odorous compounds in the vacuoles and chloroplasts. Generally, the overall scent of food products typically arises from a combination of various odorants rather than from a single compound (6-8). Previous studies have linked this earthly musty flavor to the combination of terpenoid breakdown, lipid oxidation, and other volatile compounds caused by amnio acid degradation by bacteria (6, 7). The volatile organic compounds (VOC) in commercial spirulina were identified as aldehydes, pyrazines, furans, and furanones. The 3-methyl-butanal was from leucine degradation, while hexanal, furans, and oct-1-en-3-ol were derivatives of fatty acids (6, 7). Although these compounds have been linked to the characteristic green and fishy odor, robust data is lacking to support these associations conclusively.

Since these VOC are located in the intercellular organelles, their release is unavoidable when spirulina is extracted using conventional solvent or physical methods (7). Recently extraction combined with mechanical cell rupture methods such as ultrasonication and homogenization have gained popularity in the micro-algae industry due to its sustainability and high product yield for protein and bioactive compounds (2, 9). However, no research has been done to determine the impact

of these physical extractions on the extracted bioactive compounds alongside the VOC. Therefore, this study aimed to evaluate the effects of aqueous extractions using ultrasonication and conventional homogenization on bioactive compounds and the main undesirable VOC in spirulina extract. The knowledge could lead to the development of optimized extraction to enhance spirulina's benefits while maintaining sensorial acceptability and expanding its utilization in food and nutraceutical industries.

Material and Methods

Raw material and chemical

Spirulina powder was obtained from Green Diamond Farm, Chiang Mai, Thailand. The chemicals and solvents used in the study were analytical grade and purchased from Union Science Co. Ltd., Chiang Mai, Thailand.

Extraction

For ultrasonication extraction, 10 g of spirulina powder was added to 200 ml of distilled water and sonicated using a high-intensity ultrasonic processor (VCX 750W, Sonics, Newtown, CT, USA) at 20 kHz, 40% amplitude for 10, 20, or 30 min. Then it was centrifuged at 6,000 rpm (Hitachi Koki Co., Ltd., Minato, Tokyo, Japan) for 30 min. The supernatant was collected and made up to a known volume using distilled water. The final extract was analyzed for chemical and volatile composition. For homogenization extraction, the same procedure was performed except instead of ultrasonication, a conventional homogenizer (T25 digital, IKA Works Co. Ltd., Bangkok, Thailand) was used at 10,000 rpm for 10, 20, and 30 min. The control was an aqueous extract without ultrasonication and homogenization treatments.

Determination of phycocyanin content

The analysis was performed according to the method of Bennett and Bogorad (10). The extract was diluted 100-fold, placed in a 96-well plate, and measured absorbance (OD) at 620 and 652 nm using Spark® 10M multimode microplate reader (Tecan Trading AG, Männedorf, Switzerland). The phycocyanin content (mg/g) was obtained using the following equation:

$$Phycocyanin\ (mg/g) = \frac{\left(OD_{620\,nm} - 0.474(OD_{652\,nm})\right) \times Volume\ of\ solution}{5.34 \times Sample\ weight}$$

Chlorophyll and carotenoid contents

One ml of extract was mixed with 4 ml of methanol and centrifuged at 5,000 rpm for 10 min. The amounts of carotenoid and chlorophyll contents in the supernatant were measured at 470, 652, and 665 nm using the microplate reader according to the method of Lichtenthaler and Buschmann (11).

Antioxidant activity

Antioxidant activities were performed using 1,1-diphenyl-2-picryl-hydrazyl stable radical (DPPH) according to the method of Brand-Williams, Cuvelier and Berset (12) with some modification Briefly, 0.1 mM solution of DPPH in methanol was prepared, and this solution (200 µl) was added to the sample solution (25 µl) which was diluted to 10 fold in the methanol, and the mixture was shaken thoroughly, then placed on a 96-well plate. The mixture was kept at room temperature for 30 min and measured using the microplate reader at the absorbance, of 517 nm. The sample containing without the sample served as a control.

Determination of volatile organic compounds (VOC)

The major aromatic volatile components of spirulina samples were analyzed by headspace combined with gas chromatography-mass spectrometry (HS-GC–MS/MS). The GC-MS/MS analyses were performed on EVOQ GC-TQ MS (Bruker, Billerica, MA, USA) coupled with a Multi-purpose

Sampler MPS system (GERSTEL GmbH & Co.KG, Mülheim an der Ruhr, Germany). Five ml extract was incubated at 70 °C for 15 min in a screw-cap glass vial. After incubation, the HS syringe (2500 µl, 65 mm) was exposed to the headspace of the vial for 5 min and subsequently injected the volatile into the gas chromatography equipped with the Rxi-5Sil MS quartz capillary column (30 m × 0.25 mm i.d., 0.25 µm film thickness; Restek Corp., Bellefonte, PA, USA) using 10:1 split mode. The injector temperature was 250 °C. The carrier gas was pure helium at a 1 ml/min flowing rate.

The GC analysis was performed as follows: the oven temperature was held at 45 °C for 2.5 min, then increased to 80 °C at 10 °C/min (held for 3 min), 200 °C at 15 °C/min (held for 1 min), and finally 250°C at 20 °C/min (held for 30 s). The MS condition was electron ionization (EI) mode at 70 eV and full scan data were obtained in a mass range of 45-350 *m/z*. The target compounds were identified based on selected ions, and by comparing the MS spectra to the reference spectra with the National Institute Standard and Technology (NIST) 2020 database, with a similarity index of at least 80%. The relative content of each compound was calculated using the peak area of the identified compound.

Statistical analysis

All data were reported as mean ± standard deviation (SD) and analyzed using SPSS 17.00 software (SPSS Inc., Chicago, IL, USA). Significant differences were determined by analysis of variance (ANOVA) and Duncan's Multiple range test (*$P<0.05$).*

Results and Discussion

Bioactive Compounds and Antioxidant Activity

The type of extraction method and time significantly affected the phycocyanin, chlorophyll, and carotenoid contents of spirulina extract (Table 1). The ultrasonication and homogenization treatments significantly enhanced the content of bioactive compounds in the spirulina extract compared to the control. The ultrasonication extracts were superior to those of homogenization in extracting phycocyanin (3.92-4.16 times), chlorophyll (1.77-2.32 times), and carotenoid (12.2-37.8 times) contents. The phycocyanin, carotenoid, and antioxidant activity positively correlated with the extraction time (*$P<0.05$*). The highest phycocyanin content (84.26 ± 0.53 mg/g) was found in the ultrasonication extract at 30 min. This was in agreement with Khandual (2) who reported a higher phycocyanin content (54.65 mg/g) with aqueous extraction using ultrasonication compared to sonication and freeze/thaw extraction methods, which yielded the phycocyanin content of 46.65 mg/g and 48.88 mg/g, respectively. Tavakoli (9) also reported that a water extraction with 20 min sonication gave the optimal phycocyanin (0.4 mg/ml) compared to ethanol-water extracts (0.02-0.1 mg/ml), which resulted in 4 times less than water extracts. In our present work, the highest phycocyanin content was obtained at 30 min and this is possibly because of temperature and amplitude control of the solution during the ultrasonication extraction.

For chlorophyll and carotenoid contents, the ultrasonication extract at 30 min had the highest carotenoid content (265.04 ± 4.30 µg/g), and the ultrasonication extract at 20 min had the highest chlorophyll content (328.14 ± 5.56 µg/g). An increase in chlorophylls and carotenoids with increased extraction time contradicted a study by Tavakoli (9) who reported no change in chlorophyll content in the aqueous spirulina extract in ultrasonication at 5 to 30 min and a decrease in carotenoid content with a longer extraction time compared to water-ethanol extracts. The researcher suggested that carotenoids had low polarity, and ethanol would be a better solvent for chlorophyll and carotenoid than water. Overall our findings were consistent with the previous research that ultrasonication was more effective in disrupting cell walls and enhancing the release of intracellular compounds (2, 9). The cavitation effect of ultrasonication improved solvent penetration and solubilization of target compounds from algal cells while the mechanical shearing mechanism of homogenization was less effective in extraction (9).

Table 1. Contents of bioactive compounds and antioxidant activity of spirulina extracts after homogenization (H) and ultrasonication (U) treatments at 10, 20, and 30 min.

Samples	Phycocyanin (mg/g)	Chlorophyll (µg/g)	Carotenoid (µg/g)	Antioxidant activity (Trolox mg/L)
Control	$10.17^{f} \pm 0.28$	$89.19^{e} \pm 1.15$	$2.39^{f} \pm 1.03$	$87.86^{b} \pm 0.24$
H-10	$17.23^{e} \pm 0.15$	$126.08^{d} \pm 8.35$	$3.84^{ef} \pm 1.58$	$65.31^{c} \pm 0.80$
H-20	$18.94^{de} \pm 1.43$	$141.67^{cd} \pm 8.71$	$17.69^{de} \pm 1.92$	$61.48^{c} \pm 2.02$
H-30	$20.27^{d} \pm 0.34$	$160.00^{c} \pm 1.39$	$21.80^{d} \pm 1.43$	$52.72^{c} \pm 0.79$
U-10	$67.58^{c} \pm 0.26$	$264.42^{b} \pm 8.57$	$145.23^{c} \pm 6.40$	$121.35^{a} \pm 9.54$
U-20	$75.60^{b} \pm 0.43$	$328.14^{a} \pm 5.56$	$231.19^{b} \pm 6.49$	$133.50^{a} \pm 0.77$
U-30	$84.26^{a} \pm 0.53$	$282.53^{b} \pm 4.01$	$265.04^{a} \pm 4.30$	$133.05^{a} \pm 10.75$

Mean ± Standard deviation; Different letters indicate significant differences between samples ($P<0.05$); H-10, 20, 30 = extracts using homogenization at 10, 20, 30 min; U-10, 20, 30 = extracts using ultrasonication at 10, 20, 30 min

For antioxidant activity (Table 1), only the ultrasonication extracts had higher antioxidant activity than the control. The homogenization treatment adversely affected the antioxidant activity of spirulina extracts, ranging from 25.7-40.0% reduction. Nonetheless, the extraction time did not influence the antioxidant activity of the extracts within the same treatment ($P>0.05$). This trend is consistent with findings from other research indicating that prolonged extraction times could enhance the bioavailability of antioxidants by facilitating their release from cellular matrices in ultrasonication (9). However, conventional homogenization showed lesser activity because the mechanical sheering conceivably caused stresses to the integrity of the structures in bioactive compounds over a prolonged time, and thermal effect and oxidation were greater in comparison to ultrasonication where cavitation in air served as an insulating medium and the amplitude and temperature was under control.

Volatile organic compounds (VOC)

Figure 1 shows the VOC profiles of homogenization and ultrasonication extracts. Four important VOCs, consisting of 3-methyl-butanal, hexanal, oct-1-en-3-ol, and 2-pentyl-furans, were monitored because they have been linked to the undesirable characteristics of spirulina (6, 7). The highest VOC content was 3-methyl-butanal (7.30-27.90%), followed by hexanal (1.52-8.44%), oct-1-en-3-ol (0.47-1.38%), and 2-pentyl-furans (0.45-1.08%), respectively.

Table 2. Main volatile organic compounds in spirulina extracts after homogenization (H) and ultrasonication (U) treatments at 10, 20, and 30 min.

Sample	3-methyl-butanal	Hexanal	1-Octen-3-ol	2-pentyl-furan^{ns}
H-10	$7.30^{d} \pm 0.13$	$1.52^{d} \pm 0.79$	$0.47^{b} \pm 0.19$	0.45 ± 0.18
H-20	$10.73^{c} \pm 0.46$	$2.61^{d} \pm 0.16$	$0.52^{b} \pm 0.04$	0.44 ± 0.10
H-30	$15.41^{c} \pm 3.18$	$3.09^{cd} \pm 0.23$	$0.54^{b} \pm 0.10$	0.50 ± 0.42
U-10	$21.23^{b} \pm 3.48$	$5.51^{b} \pm 0.39$	$0.63^{b} \pm 0.02$	0.60 ± 0.30
U-20	$26.86^{a} \pm 0.52$	$4.98^{bc} \pm 0.02$	$0.66^{b} \pm 0.02$	0.68 ± 0.10
U-30	$27.90^{a} \pm 0.28$	$8.44^{a} \pm 1.05$	$1.38^{a} \pm 0.35$	1.08 ± 0.45

Mean ± Standard deviation; Different letters indicate significant differences between samples ($P<0.05$); ns = no significant difference; H-10, 20, 30 = extracts using homogenization at 10, 20, 30 min; U-10, 20, 30 = extracts using ultrasonication at 10, 20, 30 min

Changes in these VOCs, shown in Table 2, highlighted the significant influence of extraction treatments and extraction time. The long extraction time led to a higher content of these compounds with ultrasonication treatment causing a higher release than homogenization. Ultrasonication extracts had significantly higher 3-methyl-butanal (1.81-2.91 times) and hexanal (1.91-3.63 times) than the homogenization extracts of the same extraction time ($P<0.05$). There was no significant change among the treatments in 1-octen-3-ol except that of the ultrasonication extract at 30 min. The content of 2-pentyl-furan was also not affected by the treatment and extraction time ($P>0.05$). The

homogenization extract at 10 min had the least amount of 3-methyl-butanal. In contrast, hexanal was lowest in homogenization extracts with no significance between extraction time (*P>0.05*).

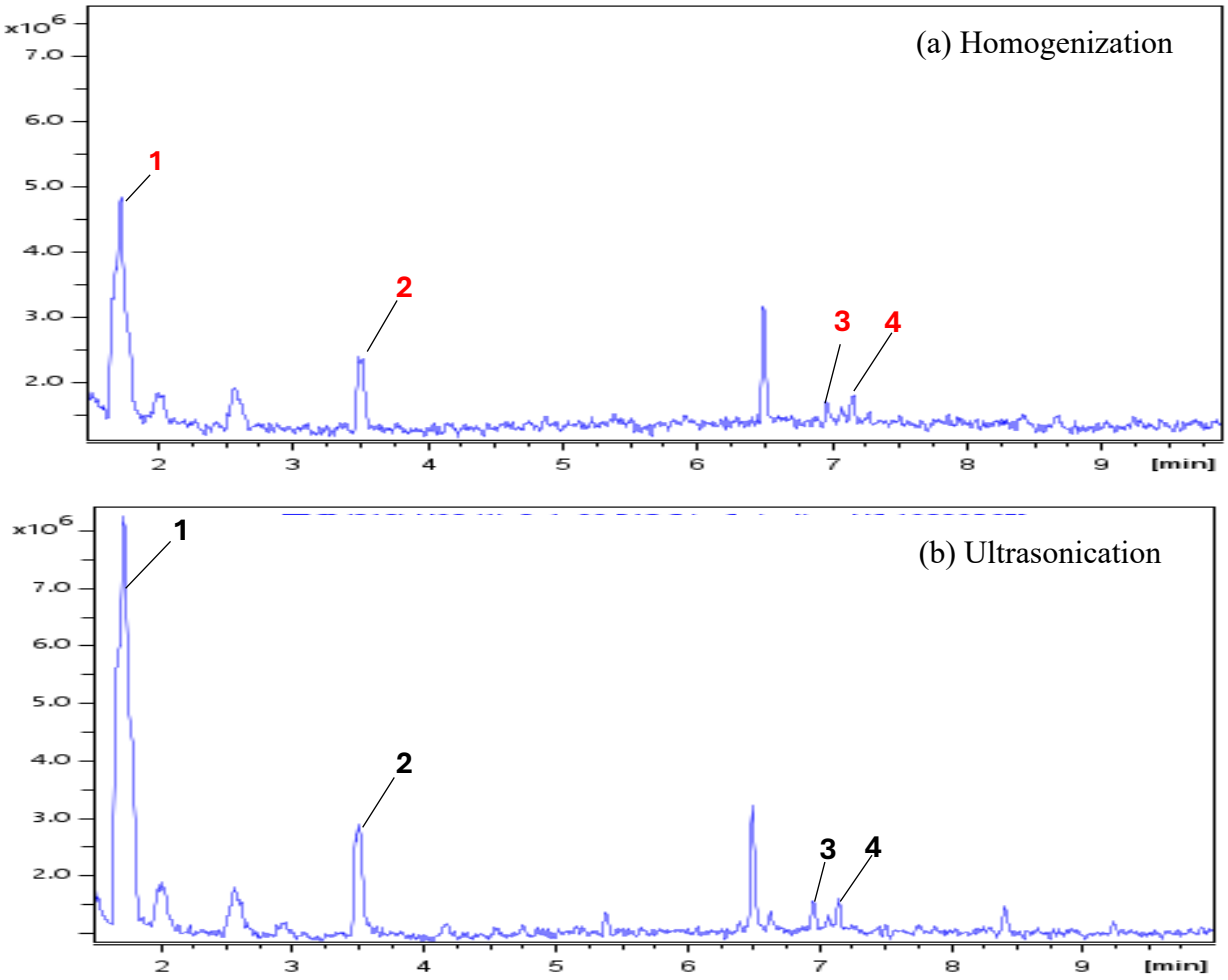

Figure 1. Volatile organic compound profile of spirulina extracts (a) homogenization treatment and (b) ultrasonication treatment; Peak (1) 3-methyl-butanal, (2) hexanal, (3) 1-octen-3-ol, and (4) 2-pentyl-furan.

The 3-methyl-butanal is associated with a malty, fermented aroma. It possibly originated from the biological process of spirulina involving amino acid metabolism (8) and was enhanced by protein degradation in the course of Maillard reaction due to thermal effect by cavitation and mechanical force (9, 13). As for hexanal which is characterized as green, fatty off-odor, and 1-octen-3-ol which is associated with a mushroom-like musty odor, they come from lipid oxidation and chlorophyll degradation due to stress upon cell breakage by ultrasonication and homogenization. 2-pentyl-furan is generated also from the degradation of fatty acids such as linoleic acid (6, 8).

Conclusion

This research illustrated the connection between bioactive compounds and VOC in spirulina extract. Overall ultrasonication was more efficient in extracting bioactive compounds from spirulina than homogenization. However, both treatments and the prolonged extraction time unavoidably generate undesirable VOCs. Our results suggested that ultrasonication at 30 min gave the best condition for obtaining the highest bioactive compounds and antioxidant activity. However, homogenization extraction offered a more acceptable spirulina extract than ultrasonication in terms

of minimizing undesirable VOCs. This insight provides valuable knowledge in developing additional processes to manage the drawbacks of spirulina for food applications.

Conflict of interest statement

The authors declare no conflicts of interest.

Acknowledgment

This research was supported by the Master's Degree Program in Food Science and Technology, Faculty of Agro-industry, Chiang Mai University under the CMU Presidential Scholarship, for the year 2022.

Reference

1. AlFadhly NK, Alhelfi N, Altemimi AB, Verma DK, Cacciola F, Narayanankutty A. Trends and technological advancements in the possible food applications of Spirulina and their health benefits: A Review. Molecules. 2022;27(17):5584.
2. Khandual S, Sanchez EOL, Andrews HE, de la Rosa JDP. Phycocyanin content and nutritional profile of *Arthrospira platensis* from Mexico: Efficient extraction process and stability evaluation of phycocyanin. BMC chemistry. 2021;15(1):1-13.
3. El Nakib D, Ibrahim M, Mahmoud N, Abd El Rahman E, Ghaly A. Incorporation of Spirulina (*Athrospira platensis*) in traditional Egyptian cookies as a source of natural bioactive molecules and functional ingredients: Preparation and sensory evaluation of nutrition snack for school children. European Journal of Nutrition & Food Safety. 2019;9(4):372-97.
4. Grahl S, Strack M, Mensching A, Mörlein D. Alternative protein sources in Western diets: Food product development and consumer acceptance of spirulina-filled pasta. Food Quality and Preference. 2020;84:103933.
5. Agustini TW, Maâ WF, Widayat W, Suzery M, Hadiyanto H, Benjakul S. Application of *Spirulina platensis* on ice cream and soft cheese with respect to their nutritional and sensory perspectives. Jurnal Teknologi. 2016;78(4-2).
6. Paraskevopoulou A, Kaloudis T, Hiskia A, Steinhaus M, Dimotikali D, Triantis TM. Volatile Profiling of Spirulina Food Supplements. Foods. 2024;13(8):1257.
7. Cuellar-Bermúdez SP, Barba-Davila B, Serna-Saldivar SO, Parra-Saldivar R, Rodriguez-Rodriguez J, Morales-Davila S, et al. Deodorization of *Arthrospira platensis* biomass for further scale-up food applications. Journal of the Science of Food and Agriculture. 2017;97(15):5123-30.
8. Coleman B, Muylaert K, De Witte B, Van Poucke C, Robbens J. The potential of microalgae as flavoring agent for plant-based seafood alternatives. 2023.
9. Tavakoli S, Hong H, Wang K, Yang Q, Gahruie HH, Zhuang S, et al. Ultrasonic-assisted food-grade solvent extraction of high-value added compounds from microalgae Spirulina platensis and evaluation of their antioxidant and antibacterial properties. Algal Research. 2021;60:102493.
10. Bennett A, Bogorad L. Complementary chromatic adaptation in a filamentous blue-green alga. The Journal of cell biology. 1973;58(2):419-35.
11. Lichtenthaler HK, Buschmann C. Chlorophylls and carotenoids: Measurement and characterization by UV-VIS spectroscopy. Current protocols in food analytical chemistry. 2001;1(1):F4. 3.1-F4. 3.8.
12. Brand-Williams W, Cuvelier M-E, Berset C. Use of a free radical method to evaluate antioxidant activity. LWT-Food science and Technology. 1995;28(1):25-30.
13. Morita K, Kubota K, Aishima T. Comparison of aroma characteristics of 16 fish species by sensory evaluation and gas chromatographic analysis. Journal of the Science of Food and Agriculture. 2003;83(4):289-97.

Diversity and Antimicrobial Activity of Culturable Fungi Associated with *Rhodomyrtus tomentosa* (Aiton) Hassk. in Songkhla, Thailand.

Nureeda Che-alee* and Lakkhana Kanhayuwa Wingfield
Division of Biological Science, Faculty of Science, Prince of Songkla University,
Hat Yai, Songkhla, 90110 Thailand
*Corresponding author's email: nureedachealee@gmail.com

Abstract:

Our study represents the first report of the fungal community associated with *Rhodomyrtus tomentosa* (Aiton) Hassk. The species identification based on molecular and morphological characteristics classified fungi into twenty-three genera belonging to eight orders, Chaetothyriales, Eurotiales, Hypocreales, Mucorales, Mycosphaerellales, Onygenales, Pleosporales and Venturiales, from five classes, Eurotiomycetes, Dothideomycetes, Mucoromycetes and Sordariomycetes of the two phyla Ascomycota and Mucoromycota. The most frequent genera were *Diaporthe* and *Daldinia*. Twenty-six of the 329 isolates produced antimicrobial metabolites which inhibited various microbial pathogens. Most of these active isolates were identified as *Aspergillus, Penicillium* and *Trichoderma.* Our findings offer new insights into the fungal diversity associated with *R. tomentosa* (Aiton) Hassk. and suggest opportunities for further biotechnological research.

Keywords: Fungal diversity; *Rhodomyrtus tomentosa*; Antimicrobial activity

Introduction

Endophytic microorganisms, including bacteria, fungi, and algae, are vital sources of natural products with bioactive potential. Endophytic fungi, in particular, are known for their ability to produce various secondary metabolites, including pigments, antioxidants, and anti-inflammatory substances (1). These fungi live within plant tissues without causing harm and present a promising resource for biotechnological development.

Medicinal plants are rich sources of endophytic diversity, often leading to the discovery of novel bioactive natural products with pharmaceutical importance. These plants produce valuable secondary metabolites to adapt to harsh environments, making them key elements in traditional medicine. *Rhodomyrtus tomentosa* (Aiton) Hassk., known as downy rose myrtle and widely used in Thai traditional medicine, is notable for its variety of structurally diverse and biologically active metabolites. Exploring the endophytic fungal diversity within *R. tomentosa* holds great potential for discovering new functional compounds that could benefit industries such as food, cosmetics, textiles, and pharmaceuticals, offering sustainable alternatives to synthetic agents (2,3,4). Numerous strains of endophytic fungi have shown valuable properties for applications across different industrial sectors, highlighting the potential of *R. tomentosa* as a future biotechnological innovation.

Materials and Methods

Plant materials and soil sampling

A representative community of *Rhodomyrtus tomentosa* (Aiton) Hassk. plants and associated soil samples were collected from Thung Lung and Tha Kham, Hat Yai District, Songkhla Province, Thailand. Healthy *R. tomentosa* plant components, including leaves, fruits, flowers, and stems, were randomly collected. Soil sample was separated into three fractions including, bulk soil (BS), rhizosphere soil (RP), and rhizoplane fraction (RP) as followed by the standardized protocol described in Barillot et al. (2013). Details of geographic locations, sampling sites, and plant characteristics were shown in Figure 1.

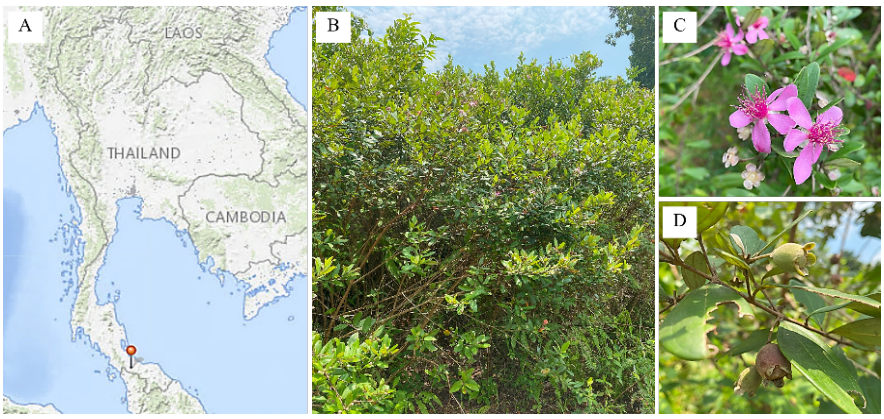

Figure 1. Plant properties and sampling sites. A) Geographic location of the sampling sites. B) Characteristics of the sampling sites. C) Characteristics of *R. tomentosa* flowers. D) Characteristics of *R. tomentosa* fruits.

Isolation of soil fungi and endophytic fungi

Soil fungi were isolated using the protocol described Barillot et al. (5) with minor modification. One mL of each soil suspension was serially diluted in 9 mL of 0.85% sterile normal saline solution (NSS) and spread on Corn Meal Agar medium (CMA) containing chloramphenicol. Plates were incubated at 25°C for 5-7 days. Different tissues (leaf, fruit, flower, and stem) of plant samples were rinsed with sterile distilled water. Surface sterilization procedures were performed on clean tissue pieces by dipping into 70% ethanol for 2 min, followed by 2% sodium hypochlorite treatment for 4 min and 70% ethanol treatment for 2 min. Plates were incubated at 25 °C and inspected for hyphal growth for 7 days. Fungal growth was observed daily. Pure cultures were isolated and stored at the Mycology Laboratory, Department of Microbiology, Prince of Songkla University.

Morphological and molecular identification of fungi

Fungal isolates were identified based on their macroscopic morphological characteristics. The microscopic appearance of individual fungi was observed using the slide culture technique and the observed mycelial and reproductive structures were used. Molecular techniques were performed using the internal transcribed spacer (ITS) region of rDNA was amplified and sequenced with primers ITS5 (5'-GGAAGTAAAAGTCGTAACAAGG-3') and ITS4 (5'-TCCTCCGCTTATTGATATGC-3'). Genomic DNA was extracted according to a protocol described by Wingfield and Atcharawiriyakul (2021). PCR amplificaton was performed using the protocol described by Wingfield and Atcharawiriyakul (2021). The closest matched sequences were searched in the National Centre for Biotechnology Information (NCBI) GenBank database. MEGA software, version 11 was used to construct the sequence alignments and phylogenetic tree. The phylogenetic trees were inferred using the maximum-likelihood algorithm by bootstrap analysis with 1,000 replications.

Antimicrobial assays

The antimicrobial activity was tested against seven pathogenic bacteria (*Micrococcus luteus* (ATCC9341), *Staphylococcus aureus* (ATCC25923), methicillin-resistant *S. aureus* (MRSA), *Escherichia coli* (ATCC25922), *Pseudomonas aeruginosa* (ATCC27853), *Salmonella* Typhi and *Vibrio cholerae*) and two pathogenic fungi (*Candida albicans* (ATCC90028) and *Aspergillus fumigatus* Af293) strains were tested by using agar well diffusion method described by Wingfield et al. (6) with some modification. Fungal isolates were cultivated in a potato dextrose broth (PDB) for 21 days at 28 °C. The bacteria were grown on Mueller-Hinton agar (MHA) at 35 ºC for 18 h; the yeast was grown on Sabouraud dextrose agar (SDA) at 28 ºC for 24-48 h; and the filamentous fungus was grown on SDA at 28 °C for 48 h. After incubation, inhibition zones were reported as the mean of the clearing zone in triplicate measurements. Vancomycin and gentamicin were used as standard antibacterial agents and amphotericin B was used as standard antifungal agents. After preliminary

screening of fungi for their antimicrobial activity, those that revealed potent antimicrobial effects were further tested to determine MIC and MBC against pathogenic bacteria and pathogenic fungi according to a modification of the Clinical and Laboratory Standards Institute guidelines.

Results and Discussion

Isolation, identification, and characterization of fungi

Rhodomyrtus tomentosa has garnered attention for its rich repertoire of structurally diverse and biologically active metabolites (3,7). However, very few attempts have been made to evaluate the diversity of fungi associated with this valuable plant. We investigated the diversity of endophytic and soil fungi associated with *R. tomentosa*. In this study, a total of 329 fungal colonies were found. A total of 234 fungal colonies (isolation rate, 1.56%) were isolated from 150 tissue segments of the *R. tomentosa* plant including, 185(1.85%), 20(1%), 19(0.95%), and 10(1%) colonies from leaf, flower, fruit, and stem tissue samples, respectively. In addition, 95 colonies were isolated from soil samples. The 329 colonies were allocated to 52 morphotypes [leaf(18), flower(3), fruit(5), stem(2), and soil(24)] based on their culture characteristics on PDA plate. Microscopical analysis and colony morphology were used to identify fungi (Figure 2). Furthermore, ITS-based rDNA sequence analysis was used to carry out their molecular identification. The phylogenetic tree based on ITS of the isolates at genus, order, and class levels was generated (Figure 3).

The endophytic fungal isolates were classified into 23 genera, mostly belonging to Ascomycota phylum (96.7%) followed by Mucoromycota phylum (2.7%) based on the BLAST searches analysis, while two isolates (0.6%) could not be identified. Five classes Sordariomycetes (71.1%), Dothideomycetes (14.6%), Eurotiomycetes (10.3%), Pezizomycetes (0.6%), and Mucoromycota (2.7%), and eleven orders Hypocreales (12.2%), Glomerellales (2.4%), Sordariales (0.6%), Xylariales (22.8%), Diaporthales (33.1%), Botryosphaeriales (11.2), Pleosporales (2.7%), Muyocopronales (0.6%), Eurotiales (10.3%), Pezizales (0.6%), and Mucorales (2.7%). *Diaporthe* was the most represented genus (31.6%). Our findings were similar to those reported in studies of foliar endophytic fungal diversity and soil fungi around the world, but different frequencies were observed (8-10).

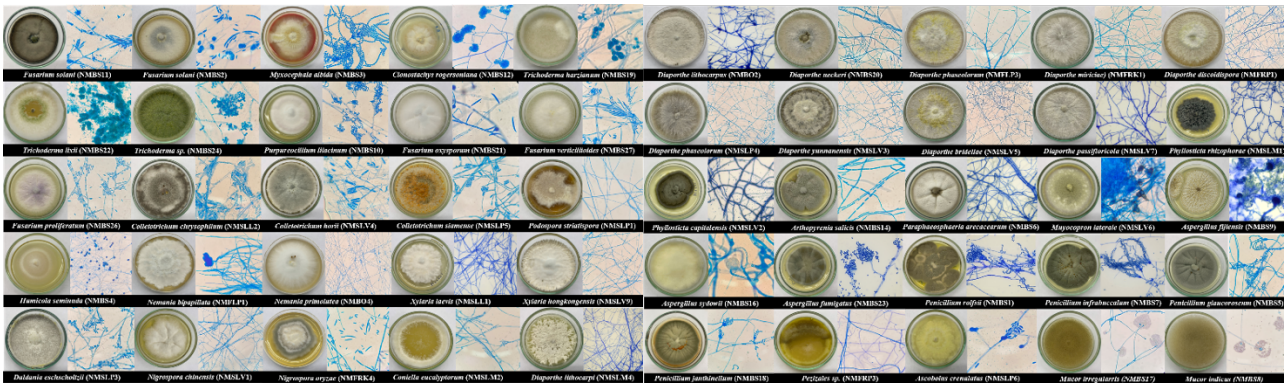

Figure 2. Representative fungal morphotypes of the isolated fungi associated with *R. tomentose* (Aiton) Hassk. Morphotyping was based on macroscopic and microscopic observation (magnification ×100). All isolates were grown on PDA plates for 7-14 days at 28°C.

Figure 3. The phylogenetic analysis of fungi associated with the *R. tomentosa* (Aiton) Hassk.

Antimicrobial activity

The antimicrobial potential of the selected fungal endophytes was assessed against clinical strains of Gram-positive, and Gram-negative bacteria, yeast, and pathogenic fungi by the agar well diffusion method. Twenty-six out of 135 isolates (19.26%) showed antimicrobial activity against at least one pathogen using the culture broth filtrate (Table 1). Eleven out of 135 isolates (8.15%) had broad-spectrum antibacterial activity to inhibit Gram-positive and Gram-negative test bacteria and another ten isolates had a narrow spectrum. In the ability to inhibit pathogenic fungi, nine isolates could inhibit yeast whereas, four isolates had activity against fungi. Only one isolate (HII7B) had broad-spectrum antifungal activity (against yeast and fungi). Meanwhile, three out of 135 isolates (2.22%; HII6P, HII7Pe2, and E3) had broad-spectrum antimicrobial activity against Gram-positive and Gram-negative bacteria; and yeast. Out of 135 fungal isolates screened, the majority showed antimicrobial activity against *Micrococcus luteus*, followed by *Candida albicans*, *Vibrio cholerae*, *Staphylococcus aureus*, methicillin-resistant *S. aureus*, *Pseudomonas aeruginosa*, *Salmonella* Typhi, *Aspergillus fumigatus*, and *Escherichia coli*. The best activity was exhibited by T8 against *M. luteus* and *V. cholerae* with the zone of inhibition diameter of 21.5 and 22.5 mm, respectively, followed by E5, HII7B, and T9.

The antimicrobial activity of the soil fungi and endophytic fungi was also determined by the broth microdilution method (Table 2). The highest antimicrobial activity during the agar well diffusion method (*Arcopilus cupreus* T8, *Aspergillus fumigatus* E5, *Diaporthe citri* HII7B, and *Pestalotiopsis menezesiana* T9) was selected to determine its minimum inhibitory concentration (MIC) at various concentrations (2-1024 µg/ml) of crude fungal isolates of their culture broths and mycelia. The results showed that crude fungi of the culture broths have better inhibition against several test pathogens than mycelia. Crude fungal isolates have shown MIC ranging from 1024 to 128 µg/ml. In this study, Crude supernatant of *Arcopilus cupreus* T8 isolated form *R. tomentosa* showed the strongest activity against *Micrococcus luteus* and *Candida albicans* with a MIC value of 128 µg/ml, respectively. No activity was observed against MRSA, and *A. fumigatus*.

Table 1 Antimicrobial assays of fungi associated with *R. tomentosa* using the agar-well diffusion method.

Isolate	Zone of inhibition (mm)									Total
	Gram-positive bacteria			Gram-negative bacteria				Yeast	Fungi	
	ML	SA	MRSA	EC	PA	ST	VC	CA	AF	
Endophytic fungi										
HII6V1						17.4±0.2				1
HII1P	12.5±0.3	8.5±0.7						9.1±0.4		3
HII6P	10.1±0.4					14.8±0.5		16.0±0.2		3
HII3Pe1	10.4±0.2									1
HII6Pe								10.2±0.5		1
HII7Pe1								10.0±0.2		1
HII7Pe2	12.2±0.4	8.5±1.0			19.5±1.0			13.4±0.5		4
HII10Pe1								15.1±0.4		1
HII7B								**20.9±0.7**	14.0±0.5	2
HII4F	12.4±0.3	10.0±0.5	10.8±0.1			11.8±0.8	14.2±0.5			5
HII5F								12.4±0.2		1
HII10F	15.7±0.3		9.9±0.1						12.3±0.9	3
T2	18.1±0.5						14.2±0.2			2
T3	14.8±0.1	8.3±0.2							9.5±0.6	3
T7							16.4±0.0			1
T8	**21.5±0.2**						**22.5±0.6**			2
T9	15.0±0.0	8.8±0.3	8.3±1.0			**20.0±0.4**	9.5±0.4			5
T10	13.5±0.8		10.9±0.2							2
T12							16.0±1.2			1
T13	17.2±0.4		11.9±0.4						10.7±0.0	3
T14	14.2±0.6						18.1±0.6			2
Soil fungi										
E2	12.6±0.2	14.4±0.8		11.3±0.2						3
E3			10.7±1.2		17.7±0.5			25.0±0.4		3
E5	14.6±0.4	14.0±0.2	13.8±0.2	13.6±0.8	**21.3±0.2**		10.4±0.4			6
E10					13.0±0.0					1
E16	13.8±0.4				14.8±0.2					2
Total no.	16	7	7	2	5	4	8	9	4	
Positive control (20 µg/mL)	**ML**	**SA**	**MRSA**	**EC**	**PA**	**ST**	**VC**	**CA**	**AF**	
Vancomycin	24.4±0.0	15.6±0.2	14.4±0.0							
Gentamicin				16.9±0.3	14.6±0.1	20.0±0.0	17.5±0.2			
Amphotericin B								13.3±0.2	12.7±0.0	

*ML: *Micrococcus luteus* (ATCC9341), SA: *Staphylococcus aureus* (ATCC25923), MRSA: methicillin-resistant *S. aureus* (MRSA), EC: *Escherichia coli* (ATCC25922), PA: *Pseudomonas aeruginosa* (ATCC27853), ST: *Salmonella* Typhi (ATCC19430), VC: *Vibrio cholerae*, CA: *Candida albicans* (ATCC90028), and AF: *Aspergillus fumigatus* (AF293). The hyphen - indicates no activity.

Table 2 Minimum inhibitory concentration of fungi associated with *R. tomentosa* using broth microdilution method.

Isolate	Ext.	Minimum inhibitory concentration (µg/mL)								
		Gram-positive bacteria			Gram-negative bacteria				Yeast	Fungi
		ML	SA	MRSA	EC	PA	ST	VC	CA	AF
Diaporthe citri HII7B	B	-	-	-	512	512	1024	1024	-	-
	C	-	1024	-	-	-	-	-	-	-
Arcopilus cupreus T8	B	128	-	-	1024	256	512	1024	128	-
	C	-	-	-	1024	256	512	-	-	-
Pestalotiopsis menezesiana T9	B	-	-	-	-	512	-	1024	-	-
	C	-	-	-	-	-	-	-	-	-
Aspergillus fumigatus E5	B	-	-	-	-	512	-	1024	256	-
	C	-	-	-	1024	256	512	-	256	-

*ML: *Micrococcus luteus* (ATCC9341), SA: *Staphylococcus aureus* (ATCC25923), MRSA: methicillin-resistant *S. aureus* (MRSA), EC: *Escherichia coli* (ATCC25922), PA: *Pseudomonas aeruginosa* (ATCC27853), ST: *Salmonella* Typhi (ATCC19430), VC: *Vibrio cholerae*, CA: *Candida albicans* (ATCC90028), and AF: *Aspergillus fumigatus* (AF293). Ext: extract, B: broth, C: cell, the hyphen - indicates no activity.

Conclusion

Fungal community associated with *Rhodomyrtus tomentosa* including their bioactive metabolites, and mycoviruses wete investigated. The species identification based on molecular and morphological characteristics revealed fungi of twenty-three genera belonging to eight orders, and five classes with the most frequent genera of *Diaporthe* and *Daldinia*. This diversity highlights the potential of these fungi as sources of bioactive compounds. Their unique metabolites offer promising prospects for future applications in pharmaceuticals, cosmetics, agriculture, and other industries.

Acknowledgement: Research Assistantship (contract no. 1-2565-02-019) from Faculty of Science Research Fund, Prince of Songkla University.

References

(1) Arnold AE, Mejía LC, Kyllo D, Rojas EI, Maynard Z, Robbins N, et al. Fungal endophytes limit pathogen damage in a tropical tree. Proc Natl Acad Sci U S A. 2003;100(26):15649–54. Available from: http://dx.doi.org/10.1073/pnas.2533483100

(2) Wang W, Liao Y, Chen R, Hou Y, Ke W, Zhang B, et al. Chlorinated azaphilone pigments with antimicrobial and cytotoxic activities isolated from the deep sea derived fungus *Chaetomium sp*. NA-S01-R1. Mar Drugs. 2018;16(2):61. Available from: http://dx.doi.org/10.3390/md16020061

(3) Xu Y, Wei B, Zuo Y, Yin L, Fang P, Gong J, et al. Research Progress on the Effects of Low Temperature on the Accumulation of Secondary Metabolites of Medicinal Plants. Molecular Plant Breeding. 20(5):1708–15.

(4) Lim TK. *Rhodomyrtus tomentosa*. In: Edible Medicinal And Non Medicinal Plants. Dordrecht: Springer Netherlands; 2012. p. 732–7.

(5) Barillot CDC, Sarde C-O, Bert V, Tarnaud E, Cochet N. A standardized method for the sampling of rhizosphere and rhizoplan soil bacteria associated to a herbaceous root system. Ann Microbiol. 2013;63(2):471–6. Available from: http://dx.doi.org/10.1007/s13213-012-0491-y

(6) Wingfield LK, Atcharawiriyakul J, Jitprasitporn N. Diversity and characterization of culturable fungi associated with the marine sea cucumber *Holothuria scabra*. PLoS One. 2024;19(1):e0296499. Available from: http://dx.doi.org/10.1371/journal.pone.0296499

(7) Vo TS, Ngo DH. The health beneficial properties of *Rhodomyrtus tomentosa* as potential functional food. Biomolecules. 2019;9(2):76. Available from: http://dx.doi.org/10.3390/biom9020076

(8) Gaddeyya G, Niharika S, Bharathi P, Kumar R. Isolation and identification of soil mycoflora in different crop fields at Salur Mandal. Adv Appl Sci Res. 2012;3:2020–6.

(9) Rosas-Medina M, Maciá-Vicente JG, Piepenbring M. Diversity of fungi in soils with different degrees of degradation in Germany and Panama. Mycobiology. 2020;48(1):20–8. Available from: http://dx.doi.org/10.1080/12298093.2019.1700658

(10) Tedersoo L, Bahram M, Põlme S, Kõljalg U, Yorou NS, Wijesundera R, et al. Fungal biogeography. Global diversity and geography of soil fungi. Science. 2014;346(6213):1256688. Available from: http://dx.doi.org/10.1126/science.1256688

Impact of Covalent and Non-covalent Conjugation on the Properties of Whey Protein Isolate-Resveratrol Complexes

Tanaporn Manochai[1], Suthaphat Kamthai[2], Pairote Wiriyacharee[3], and Thanyaporn Siriwoharn[1,*]

[1] Division of Food Science and Technology, Faculty of Agro-Industry, Chiang Mai University, Chiang Mai 50100, Thailand

[2] Division of Packaging Technology, Faculty of Agro-Industry, Chiang Mai University, Chiang Mai 50100, Thailand

[3] Processing and Product Development Factory, The Royal Project Foundation, Chiang Mai 50100, Thailand

*Corresponding author's email: thanyaporn.s@cmu.ac.th

Abstract:

Covalent conjugation is recognized as a sustainable process for modifying bioactive compounds. However, its efficacy depends on the compatibility between the method and the specific compound. This study aimed to investigate the effect of the non-covalent method (mixing process) and covalent method (alkaline process) on whey protein isolate (WPI)-resveratrol conjugation. The samples were prepared using WPI:resveratrol at ratios of 1:5 and 1:10. The molecular weight and structural changes were determined using SDS-PAGE, UV-Vis spectroscopy, and FTIR. The functional and antioxidant properties of the mixtures and conjugates were also assessed. Although the alkaline and mixing processes did not prominently affect the molecular weight band on SDS-PAGE, their secondary structure changed. The α-helix structure of conjugates was significantly lower, and the β-sheet structure was higher than that of the mixture and WPI ($p < 0.05$). In comparison, the mixtures had the highest β-turn. The conjugates demonstrated almost twice the water solubility than the mixtures and 15-20 times higher than the native resveratrol. However, the alkaline process did not increase the emulsifying properties compared to WPI. The antioxidant activity of compounds positively correlated with the amount of resveratrol used. Conjugating resveratrol with WPI provides an alternative approach to enhancing the applicability of health-promoting resveratrol in food products. The 1:5 ratio conjugates were best for water-based foods while the 1:10 ratio conjugates were best for antioxidant purposes.

Keywords: Protein-phenolic conjugate; Solubility; Emulsion; Stilbene; Modification

Introduction

Phytochemicals, secondary metabolites of plants, are associated with significant health benefits. Resveratrol, a main bioactive compound found in mulberries, is widely known for its antioxidant properties and beneficial biological activities. However, the application of resveratrol in food products is limited due to its poor solubility and sensitivity to light, pH, and high temperatures (1). According to the literature, conjugating polyphenols with proteins may alleviate the problems associated with polyphenols (2, 3, 4).

Conjugation is a sustainable process that involves linking bioactive compounds such as proteins, peptides, and polyphenols by covalent or non-covalent bonds. This modification impacts the molecules' chemical structure and influences the functional properties of the final compounds, such as solubility, gelling, emulsifying, foaming, and antioxidants. Several factors affect the efficiency of conjugation, including the conjugation method, the characteristics of the substrates, and the ratio of reactants (2, 4). The alkaline reaction method is commonly used for covalently cross-linking proteins with polyphenols due to stronger and more permanent molecular interactions with high stability (2).

Since there is scarce research information in this area for resveratrol, this study aimed to compare the impact of non-covalent and covalent conjugation methods (a mixing process vs. alkaline process) as well as the substrate ratio on the structural, functional, and antioxidant properties of whey protein isolate (WPI)–resveratrol compounds. The findings could provide additional insights and

potentially facilitate the development of reservoir-based food additives and nutraceuticals for functional food, pharmaceutical, and biomaterial industries.

Materials and Methods

Materials

Whey protein isolate (WPI, purity > 90%) and resveratrol (purity > 98%) were purchased from Scidict Plus Co., Ltd. (Bangkok, Thailand). Analytical-grade chemicals and standards used in the experiments were obtained from Sigma-Aldrich (St. Louis, MO, USA) and RCI Labscan Limited (Bangkok, Thailand). SDS-PAGE protein marker was purchased from Bio-Rad Laboratories (Hercules, CA, USA).

Sample preparation

The non-covalent sample (WPI-R mixture) was prepared by mixing WPI (1 g) with resveratrol (5 g or 10 g in 10 mL ethanol) in 190 mL deionized water, thoroughly shaking, and incubating at room temperature for 24 h. Then the solution was filtered through a 10 kDa filter (Merck Millipore, Darmstadt, Germany) using centrifugation at 5,000 rpm for 15 min. The final solution was freeze-dried (FreeZone 4.5L, Labconco, Kansas City, MO, USA) and stored at -18°C until used. The covalent sample (WPI-R conjugate) was prepared the same way but replaced deionized water with sodium phosphate buffer (pH 9) according to the alkaline process of Liu et al. (5).

SDS-PAGE analysis

The sample solution (10 mg/mL) was diluted in the loading buffer at a 1:1 ratio. The loading volume of samples and protein marker was 10 mL. The electrophoresis was run at 120 V for 70 min. After that, the gel was stained with Coomassie blue for 24 h. Then the gel was destained and scanned for an image to estimate the molecular weight of the sample.

UV-Vis spectra analysis

The sample solution of 1.0% concentration (w/v) was prepared. The absorbance was measured at 200 to 400 nm using a microplate reader (Spark, Tecan, Männedorf, Switzerland) to determine changes in the spectral graph compared to WPI and resveratrol.

Fourier transform infrared (FTIR) spectroscopy analysis

Two mg of the sample was mixed with 200 mg Potassium Bromide (KBr) powder and placed in an FTIR spectrometer (Tensor 27, Bruker, Ettlingen, Germany). The FTIR spectra in the 400-4,000 cm^{-1} range were measured. The characteristic major peaks of the α-helix, β-sheet, β-turn, and random coil were fitted into a Gaussian curve using OriginPro 8.5.1 (OriginLab Corporation, M.A., USA) for data analysis.

Functional properties

Measurements of water solubility and emulsifying properties were conducted at pH 3, 5, and 7, as this range encompasses pH conditions commonly found in food systems and biological processes.

Water solubility

The water solubility property was determined using a method of Rui et al. (6). The sample was dissolved in distilled water (10 mg/mL), adjusted the pH (3, 5, and 7) using 0.1% hydrochloric acid and sodium hydroxide, and stirred for 30 min. Then the solution was centrifuged at 5,000 rpm for 15 min. The supernatant was collected and freeze-dried. Water solubility was calculated using the following equation:

$$\% \text{ Water solubility} = \frac{\text{Weight of sample after freeze-drying}}{\text{Weight of sample before freeze-drying}} \times 100$$

Emulsifying properties

The method of Sui et al. (7) was used to determine the emulsifying properties. The sample was dissolved in distilled water (1 mg/mL) and adjusted the pH to 3, 5, and 7. Then 5 mL of soybean oil was added to 15 mL of sample solution and homogenized (Ultra TURRAX homogenizer, T25digital, IKA, Staufen, Germany) at 10,000 rpm for 1 min. Fifty µL of the emulsion was added to 5 mL of 0.1% SDS solution and mixed well. Absorbance measurements were recorded at 500 nm immediately after mixing (A_0) and after waiting 10 min (A_{10}). The emulsifying activity index (EAI) and emulsion stability index (ESI) were calculated using the following equations:

$$\text{EAI } (m^2/g) = \frac{460.6 \times A_0}{0.003125}$$

$$\text{ESI (min)} = \frac{A_0 \times 100}{A_0 - A_{10}}$$

Antioxidant activity

2,2-Diphenyl-1-picrylhydrazyl (DPPH) radical scavenging assay

DPPH radical scavenging was determined using the method of Liu et al. (8) with modification. In brief, 200 µL of DPPH solution (0.1 mmol in methanol) was mixed with 25 µL of the sample solution (1 mg/mL in water) and stored in the dark for 30 min. The absorbance was measured at 517 nm using a microplate reader (Spark, Tecan, Männedorf, Switzerland). The DPPH values were calculated as µmol Trolox equivalent per g using the Trolox standard curve.

Ferric Reducing Antioxidant Power (FRAP) assay

The FRAP assay was determined using the method of Rui et al. (6) with modification. The FRAP reagent was prepared by mixing acetate buffer (300 mM, pH 3.6), ferric chloride (hexahydrate) solution (20 mM), and TPTZ solution (10 mM) at a ratio of 10:1:1. Next, 200 µL of FRAP reagent was mixed with 25 µL of the sample solution (1 mg/mL in water) and stored in the dark for 8 min. The absorbance was measured at 593 nm using a microplate reader (Spark, Tecan, Männedorf, Switzerland). The FRAP values were calculated as µmol Trolox equivalent per g using the Trolox standard curve.

Statistics analysis

All experiments were conducted in triplicate, and all data were analyzed using one-way analysis of variance (ANOVA) and Duncan's test on SPSS software version 17.0 (SPSS Inc., Chicago, IL, USA) for analysis with a significant level of $p < 0.05$.

Results and Discussion

SDS-PAGE

Figure 1 shows the SDS-PAGE of WPI-R mixtures and WPI-R conjugates compared to WPI and resveratrol. WPI displayed three main bands at approximately 14, 17, and 66 kDa, corresponding to α-lactalbumin, β-lactoglobulin, and bovine serum albumin, respectively (9). Resveratrol was a small molecule of 228.25 g/mol; therefore, it was not detected on the gel. Overall, the band distribution of WPI-R mixtures and WPI-R conjugate were comparable to the original WPI. When the ratio of resveratrol in the process increased, no prominent change in molecular weight was observed. The absence of distinct changes in the SDS-PAGE gel may be attributed to the small molecular size of resveratrol. This finding is consistent with Liu et al. (5), who reported minimal changes in electrophoresis upon conjugation with small molecules.

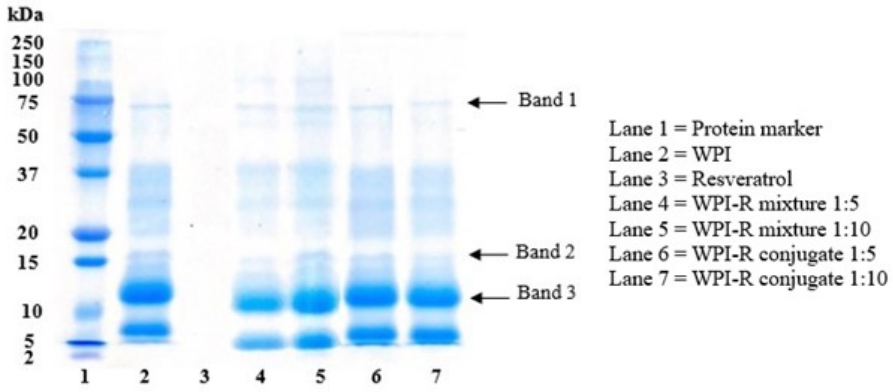

Figure 1. SDS-PAGE of WPI, Resveratrol, WPI-R mixture at 1:5 ratio, WPI-R mixture at 1:10 ratio, WPI-R conjugate at 1:5 ratio, and WPI-R conjugate at 1:10 ratio.

UV-Vis spectra

The UV-Vis spectra of WPI exhibited absorbance maxima at 280 nm (Figure 2a) corresponding to aromatic amino acids (tryptophan and tyrosine) present in whey protein isolate (3). Resveratrol displayed an absorption maximum of 306 nm. After mixing, the WPI-R mixtures showed a significant increase in absorption at 306 nm with a positive correlation to the amount of resveratrol added. In contrast, WPI-R conjugates had characteristic peaks at 280 and 290 nm without the absorbance at 306 nm. These changes in the spectra indicated the formation of a covalent interaction between WPI and resveratrol after the alkaline process (3, 5).

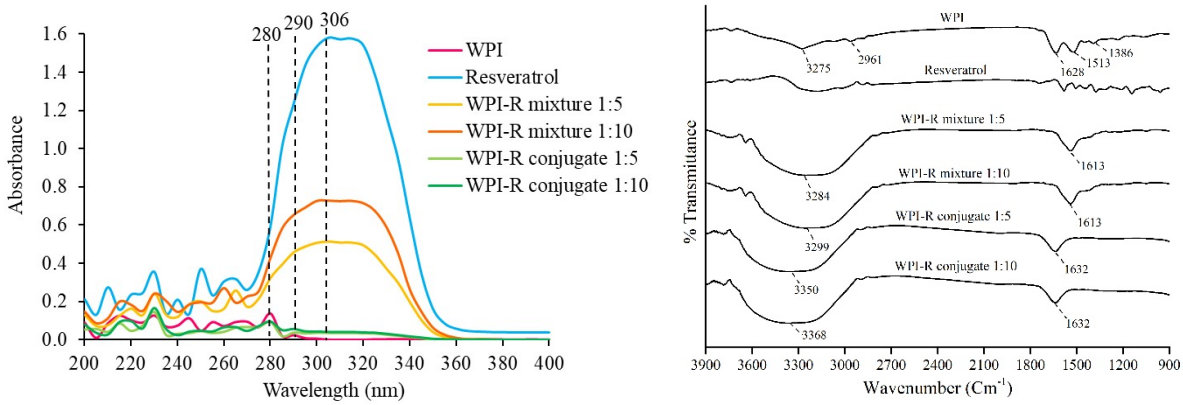

Figure 2. (a) UV–Vis spectra and (b) FTIR spectra of WPI, Resveratrol, WPI-R mixture at 1:5 ratio, WPI-R mixture at 1:10 ratio, WPI-R conjugate at 1:5 ratio, and WPI-R conjugate at 1:10 ratio.

FTIR analysis

Figure 2b shows changes in the FTIR spectra of the substrates and samples. The WPI spectrum showed characteristic absorption peaks at 3275 cm^{-1} (amide A, -OH linked to $-NH_2$), 1628 cm^{-1} (amide I, C=O stretching vibration), 1513 cm^{-1} (amide II, N-H and C-N bonds stretching vibration), and 1386 cm^{-1} (amide III, C-N and N-H bonds stretching vibration) (3). After the process, the amide A peak shifted to a higher frequency from 3172 to 3284-3299 cm^{-1} for WPI-R mixtures and 3350-3368 cm^{-1} for WPI-R conjugates. In addition, there was a minor shift on the amide I peak from 1628 to 1613 cm^{-1} for WPI-R mixtures and 1632 cm^{-1} for WPI-R conjugates. These shifts indicated changes in the structure of the WPI after interacting with resveratrol, in which the covalent reaction exerted stronger shifts than the non-covalent reaction (2, 8). Regardless of the process, the increase in resveratrol content only affected the amide A peak of the compounds.

Based on the secondary structure (Table 1), WPI and WPI-R mixtures had the same amount of α-helix and β-sheet ($p > 0.05$) but the structure of WPI-R mixtures had a higher content of β-turn than WPI. This suggested that the non-covalent interaction between WPI and resveratrol through the mixing process converted the random coil structure of WPI to a more ordered structure of β-turn (7, 10). Compared to the alkaline process, a significant structural change of WPI-R conjugates was a conversion of α-helix to β-sheet ($p < 0.05$). This finding was consistent with the literature that the covalent conjugating process induced the reaction by unfolding the protein structure (3, 10).

Table 1. Secondary structure (%) of WPI, WPI-R mixture at 1:5 ratio, WPI-R mixture at 1:10 ratio, WPI-R conjugate at 1:5 ratio, and WPI-R conjugate at 1:10 ratio.

Sample	α-helix	β-sheet	β-turn	Random coil
WPI	15.30 ± 0.08^{a}	58.60 ± 0.31^{b}	22.65 ± 0.60^{b}	3.42 ± 0.44^{a}
WPI-R mixture 1:5	15.02 ± 0.20^{a}	58.88 ± 0.61^{b}	24.21 ± 0.84^{a}	1.90 ± 0.23^{b}
WPI-R mixture 1:10	14.77 ± 0.35^{a}	59.04 ± 1.00^{b}	24.47 ± 1.23^{a}	1.72 ± 0.93^{b}
WPI-R conjugate 1:5	13.69 ± 0.36^{b}	60.60 ± 1.09^{a}	22.14 ± 1.60^{b}	3.57 ± 0.76^{a}
WPI-R conjugate 1:10	13.80 ± 0.58^{b}	60.62 ± 1.48^{a}	22.36 ± 2.01^{b}	3.22 ± 1.12^{a}

Values are means ± SD ($n = 3$). Different letters in the same column indicate significant differences ($p < 0.05$).

Water solubility

The solubility values of all samples at pH 5 were generally lower than those of pH 3 and 7 due to the influence of WPI's isoelectric point (pH 4.8–5.2) causing a zero net charge and reducing electrostatic repulsion that leads to aggregation and precipitation (9). WPI-R mixtures and WPI-R conjugates displayed significantly higher water solubility than the single resveratrol (Figure 3a) at all studied pH ($p < 0.05$). Only WPI-R conjugates had equal or higher solubility than WPI. This showed the superiority of covalent conjugation over non-covalent conjugation on resveratrol's solubility improvement. Conjugation altered the protein's net charge and secondary structure by decreasing the structure of the α-helix and increasing the β-sheet. This exposed more hydrophilic amino acids, enhancing hydrophilicity and solubility (2, 7, 12). On the other hand, the non-covalent conjugation created more β-turn which may partially hinder hydrophilic amino acids and lead to precipitation (11). The enhanced solubility of WPI-R conjugates positions them as viable carriers for delivering resveratrol in aqueous-based food products such as soft drinks, energy drinks, and milk.

Emulsifying properties

Although neither WPI-R mixtures nor WPI-R conjugates exhibited better emulsifying properties than WPI (Figures 3b and 3c), their emulsifying activities were greater at pH 7 than at pH 3 and 5. For the WPI-R mixture, a decrease in random coil structure may reduce the flexibility of the protein and its ability to interact with the oil-water interface (13). While an increase in β-sheet in the WPI-R conjugates could enhance interfacial adsorption and stabilization, excessive unfolding due to conjugation may weaken emulsion. This may also be partially attributed to polyphenol aggregation, which could lead to protein aggregation and a weakened interfacial network structure (2, 14). pH has a major impact on emulsifying properties. All samples demonstrated the lowest emulsifying properties at pH 5 due to protein aggregation near the isoelectric point, which led to oil droplet coalescence (9, 14). Consequently, WPI-R mixtures and WPI-R conjugates would not be suitable for applications requiring high emulsion properties, such as mayonnaise, salad dressings, butter, and dairy products.

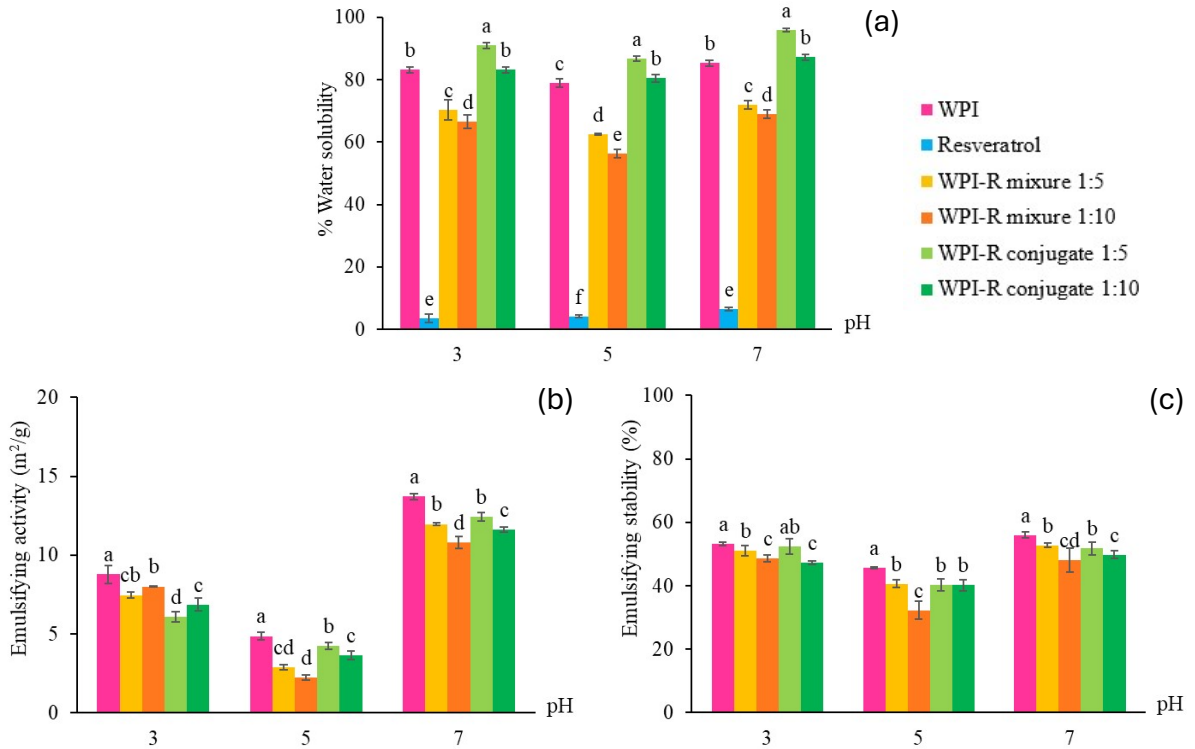

Figure 3. Water solubility (a), emulsifying activity (b), and emulsifying stability (c) of WPI, resveratrol, WPI-R mixtures, and WPI-R conjugates at 1:5 and 1:10 ratios and pH 3, 5, and 7. Different letters within the same pH indicate significant differences ($p < 0.05$)

Antioxidant activity

WPI exhibited the lowest DPPH and FRAP values (Table 2). The antioxidant activity of WPI-R mixtures and WPI-R conjugates positively correlated with the amount of resveratrol used. The enhanced antioxidant activity may be attributed to the introduction of hydroxyl groups from resveratrol, which increased the complexes' hydrogen-donating capacity and free radical scavenging ability (2, 4). However, the lower antioxidant activities of WPI-R conjugates compared to WPI-R mixtures of the same ratio may be due to the degradation of resveratrol during the alkaline conjugation process. Resveratrol generally deprotonates hydroxyl groups at pH 8-10 and consequently loses its antioxidant activity (1).

Table 2. Antioxidant activity of WPI, Resveratrol, WPI-R mixture at 1:5 ratio, WPI-R mixture at 1:10 ratio, WPI-R conjugate at 1:5 ratio, and WPI-R conjugate at 1:10 ratio.

Sample	DPPH (µmol Trolox eq./g)	FRAP (µmol Trolox eq./g)
WPI	48.79 ± 1.68^{f}	26.79 ± 2.30^{f}
Resveratrol	434.01 ± 0.63^{a}	457.21 ± 5.55^{a}
WPI-R mixture 1:5	119.24 ± 3.96^{d}	155.44 ± 0.87^{d}
WPI-R mixture 1:10	138.06 ± 3.66^{c}	181.83 ± 1.15^{b}
WPI-R conjugate 1:5	90.04 ± 1.68^{e}	147.65 ± 1.99^{e}
WPI-R conjugate 1:10	146.10 ± 3.88^{b}	171.27 ± 3.40^{c}

Values are means ± SD (n = 3). Different letters in the same column indicate significant differences ($p < 0.05$).

Conclusion

This study illustrated the impact of non-covalent conjugation (mixing process) and covalent conjugation (alkaline process) on the structure, functional properties, and antioxidant activity of WPI-resveratrol complexes. The UV-Vis and FTIR spectra revealed significant structural differences between the processes. Although the covalent conjugates were superior to the non-covalent mixtures,

the solubility of resveratrol was significantly improved after conjugating with WPI in both cases ($p < 0.05$). Overall WPI-R mixtures showed a higher antioxidant activity than WPI-R conjugates. However, the conjugation processes did not enhance emulsifying properties. The ratio of WPI:resveratrol affected functional properties and antioxidant activity at different levels. Therefore, the type of conjugation and substrate ratio are important factors when designing WPI-resveratrol complexes for specific applications and purposes.

Conflict of interest statement: The authors declare no conflicts of interest.

Acknowledgements: This research was supported by the Agricultural Research Development Agency (Public Organization) under a Graduate Research Scholarship in Agriculture and Agro Industry, for the fiscal year 2022.

References

(1) Zupančič Š, Lavrič Z, Kristl J. Stability and solubility of trans-resveratrol are strongly influenced by pH and temperature. European Journal of Pharmaceutics and Biopharmaceutics. 2015;93:196-204.
(2) Quan TH, Benjakul S, Sae-leaw T, Balange AK, Maqsood S. Protein–polyphenol conjugates: Antioxidant property, functionalities and their applications. Trends in Food Science & Technology. 2019;91:507-17.
(3) Liu J, Yong H, Yao X, Hu H, Yun D, Xiao L. Recent advances in phenolic–protein conjugates: synthesis, characterization, biological activities and potential applications. RSC Advances. 2019;9(61):35825-40.
(4) Czubinski J, Dwiecki K. A review of methods used for investigation of protein–phenolic compound interactions. International Journal of Food Science & Technology. 2017;52(3):573-85.
(5) Liu F, Ma C, McClements DJ, Gao Y. A comparative study of covalent and non-covalent interactions between zein and polyphenols in ethanol-water solution. Food Hydrocolloids. 2017;63:625-34.
(6) Rui L, Xie M, Hu B, Zhou L, Saeeduddin M, Zeng X. Enhanced solubility and antioxidant activity of chlorogenic acid-chitosan conjugates due to the conjugation of chitosan with chlorogenic acid. Carbohydrate Polymers. 2017;170:206-16.
(7) Sui X, Sun H, Qi B, Zhang M, Li Y, Jiang L. Functional and conformational changes to soy proteins accompanying anthocyanins: Focus on covalent and non-covalent interactions. Food Chemistry. 2018;245:871-8.
(8) Liu X, Song Q, Li X, Chen Y, Liu C, Zhu X, et al. Effects of different dietary polyphenols on conformational changes and functional properties of protein–polyphenol covalent complexes. Food Chemistry. 2021;361:130071.
(9) Kinsella JE, Whitehead DM. Proteins in Whey: Chemical, Physical, and Functional Properties. In: Kinsella JE, editor. Advances in Food and Nutrition Research. 33: Academic Press; 1989. p. 343-438.
(10) Zhang Q, Cheng Z, Wang Y, Fu L. Dietary protein-phenolic interactions: characterization, biochemical-physiological consequences, and potential food applications. Critical Reviews in Food Science and Nutrition. 2021;61(21):3589-615.
(11) Prigent SVE, Voragen AGJ, van Koningsveld GA, Baron A, Renard CMGC, Gruppen H. Interactions between globular proteins and procyanidins of different degrees of polymerization. Journal of Dairy Science. 2009;92(12):5843-53.
(12) Ozdal T, Capanoglu E, Altay F. A review on protein–phenolic interactions and associated changes. Food Research International. 2013;51(2):954-70.
(13) Kim W, Wang Y, Selomulya C. Emerging technologies to improve plant protein functionality with protein-polyphenol interactions. Trends in Food Science & Technology. 2024;147:104469.
(14) Bock A, Kieserling H, Rohn S, Steinhäuser U, Drusch S. Impact of Phenolic Acid Derivatives on β-Lactoglobulin Stabilized Oil-Water-Interfaces. Food Biophysics. 2022;17(4):508-22.

Developing a Rice-Based Beverage with Potential Health Benefits: A Foodomics Approach

Misbah Saleem[1,2], Wachira Jirarattanarangsri[1], Nut Koonrungsesomboon[3], and Sukhuntha Osiriphun[1,*]

[1] Department of Food Science and Technology, Faculty of Agro-Industry, Chiang Mai University, Thailand
[2] Graduate Student of Department of Food Science and Technology, Faculty of Agro-Industry, Chiang Mai University, Thailand
[3] Department of Pharmacology, Faculty of Medicine, Chiang Mai University
*Corresponding author's email: Sukhuntha.o@cmu.ac.th

Abstract:

Rice serves as a staple food for billions, and its glycemic Index (GI) has variations, directly impacting postprandial blood glucose levels very significantly in the management of diabetes, so understanding of its varieties with respect to how they would affect the blood sugar levels is important for developing dietary strategies in diabetic patients. This study investigates the development of a rice-based beverage using a pasteurization process. The research examines the impact of varying concentrations of rice flour (3%, 7%, and 11%) on the color, pH, total sugar content, and microbial content of the beverage. During the methodology, rice samples were ground into flour and then sieved for uniformity to be processed into rice-based beverages. Enzymatic digestion using α-amylase of the prepared samples was followed by pasteurization. Preliminary results indicate that the rice-based beverages have a pH of 4.2, which is acidic, and a total sugar content of 100,945 µg/ml. The color values measured using Hunter Lab colorimeter (Color Quest XE) were L= 87.632.06a, a= 4.310.60ns, and b*= 26.891.22. The drinks were safe for consumption from the results of microbial content. Expected preliminary results of such a study might point to the Thai rice variety that have lower GI and hence can improve insulin sensitivity, thus offering functional benefits to diabetic patients. Results may show the existence of bioactive oligosaccharides in rice, which modulate glucose metabolism, thus demonstrating potential as a functional food. This research could form a basis for further studies in metabolomics research on rice in establishing optimal diet therapy for improving health outcomes in diabetic patients. Ultimately, identifying rice varieties with health-promoting properties could contribute to personalized nutrition strategies for better management of diabetes.

Keywords: Rice oligosaccharides; Foodomics; Antioxidant properties; Diabetes management.

Introduction

Diabetes mellitus is a chronic metabolic disorder characterized by persistent hyperglycemia and has emerged as a major health problem globally, affecting over 422 million people worldwide. Management of diabetes generally involves lifestyle intervention through diet, exercise, or medication that keeps blood glucose within a normal range and avoids the complications associated with the disease [1].

Rice is the staple food for billions worldwide and is also criticized due to its high GI, raising concerns over its suitability for diabetic people. However, recent studies reveal that rice contains bioactive compounds such as oligosaccharides, which may have potential health benefits in diabetes management. Oligosaccharides are short-chain carbohydrates resistant to rapid enzymatic digestion, promoting a gradual release of glucose and supporting gut microbiota through fermentation [2].

This research focuses on the development of a rice-based beverage, studies of its sugar content, pH, and microbial properties, which will add to the knowledge of potential benefits for diabetes management. By investigating these aspects, the study lays the foundation for further research into the oligosaccharide composition of rice and its implications for glycemic control. Moreover, the safety of this drink will be evaluated, which can prove it to be a functional food that could help control diabetes over a long period of time [3].

Materials and Methods

The materials used in the experiment included 20 kilograms of rice grains, a hammer mill, a 100-mesh sieve, polyethylene plastic bags, a double-layered boiling vat, an enzyme digestion machine, a Brix refractometer, HDPE plastic bottles, a Color Quest XE machine, a pH meter, and PCA agar.

To prepare the rice flour, rice grains were ground using a hammer mill, and the resulting powder was sieved twice through a 100-mesh sieve to obtain 100-mesh rice flour. This sieved flour was then stored in bags and divided into three portions based on weight to create electrolyte drink formulations at 3%, 7%, and 11% concentrations.

For the preparation of the rice-based beverage, the rice flour was mixed with water at a 1:6 ratio (using water that met GMP consumption standards). The mixture was heated in a double-layered boiling vat to 90°C for 5 minutes to gelatinize the starch. After gelatinization, the mixture was transferred to an enzyme digestion machine, where α-amylase enzyme was added at a concentration of 62.92 mol and incubated for 138.31 minutes at 35°C. The digestion process was halted by boiling the mixture for 5 minutes. The mixture was then filtered to retain only the clear part, with the sediment stored for other uses. The sweetness of the rice starch water was measured using a Brix refractometer, yielding a value of 17 Brix. The clear liquid was stored in polyethylene plastic bags or cold bags at -18°C in a freezer until pasteurization [8].

To produce the rice-based drink, the frozen clear liquid was thawed and transferred to a double-layered boiling pot. The required amount of liquid for each formulation (3%, 7%, and 11%) was calculated. For the 3% formula, 7.04 liters of clear liquid was mixed with 32.96 liters of water. For the 7% formula, 16.48 liters of clear liquid was combined with 23.52 liters of water. For the 11% formula, 14.12 liters of clear liquid was mixed with 25.88 liters of water [9].

In the pasteurization step, the solidified rice starch water was reheated to obtain a liquid, which was then pasteurized at 75°C for 30 seconds. The pasteurized drink was filled into 250-milliliter HDPE plastic bottles while hot and cooled by passing them through cold water. The bottles were stored at 4°C for analysis.

For the analysis of the characteristics and properties of the beverage, several tests were conducted. The color value was measured using the Color Quest XE machine, following a specific procedure to ensure accurate readings. The total sugar content was tested using the Phenol-Sulfuric reaction method, with the absorbance measured at 490 nm and a glucose standard curve used to determine the sugar content. The acidity-alkalinity of the beverage was analyzed using a pH meter, with the pH recorded after dipping the electrode into the beverage sample. Finally, microbial content was analyzed using the pour plate technique on PCA agar to determine the total bacterial count [10].

Statistical analysis was conducted using appropriate software, and differences between groups were considered statistically significant at $p < 0.05$.

Results and Discussion

This research investigates the development of a rice-based drink using a pasteurization process.

The findings show that the rice-based beverage had desirable attributes, including light color (L* values 87.34–89.42) with a slight yellow tint (b* values 26.72–26.92) and consistent acidic pH (4.2), critical for microbial stability. Sugar content increased with rice concentration, ranging from 23,108 µg/ml (3%) to 100,945 µg/ml (11%). Microbial analysis confirmed that all formulations were safe for consumption.

These results demonstrate the potential of rice-based beverages as a nutritional and functional drink. However, while rice oligosaccharides are recognized for their prebiotic benefits and their role in glycemic control, this study did not include direct analysis of oligosaccharides or glycemic index (GI).

Table 1: Color, Total sugar, and pH analysis of beverages using Hunter Lab colorimeter (Color Quest XE)

Formulation	Color analysis			pH	sugar content (µg/ml.)	Total Bacteria (MeanLogCFU±S.D./ml
	L*	a*	b*			
3%	89.42±2.72[a]	-4.49±0.71[ns]	26.92±1.32 [ns]	4.2	23,108	4.30±0.02
7%	87.34±5.42[ab]	-4.34±0.57[ns]	26.72±2.46 [ns]	4.2	57,837	4.40±0.02
11%	87.63±2.06[a]	-4.31±0.60[ns]	26.89±1.22 [ns]	4.2	100,945	4.30±0.02

Notes:
* The letters ns in the column indicate values that are not significantly different at the 95% confidence level.
** The letters a and b in the column indicate significant differences at the 95% confidence level.
*** All experiments were conducted in triplicate.

Discussion

The findings of this study indicated that the rice-based beverage was desirable in color, pH, and sugar content. The color of the drink was acceptable and within the range of other drinks available within the market. The pH of the beverage was below the neutrality level, acidical (4.2), a condition necessary to prevent the growth of bacteria and thus make the product safe. The sugar content of the drink was 100,945 µg/ml. Microbial analysis showed that the drink was safe to drink, hence suitable for the target audience.

These findings provide further insight into the varied oligosaccharide composition of rice and some benefits such rice may offer to diabetic patients. Oligosaccharides present in rice might help reduce the GI of the beverage, therefore providing an added advantage to diabetic patients in their blood sugar management. Further, prebiotic effects of rice oligosaccharides may promote gut health by encouraging the proliferation of beneficial microbiota that may lead to good overall health.

Future Directions

The present investigation thus forms the foundation for exploring rice-based beverages as functional foods. Therefore, further studies on rice-based beverages are necessary to study the following:

- Oligosaccharide Profiling: The in-depth oligosaccharide profiling in rice beverages may reveal prebiotic characteristics of the molecules.
- Glycemic Index Evaluation: Measuring the glycemic index (GI) of rice-based beverages will help assess their suitability for individuals managing blood sugar levels, such as diabetic patients.
- Optimized Processing: Investigating different processing techniques to enhance the oligosaccharide content and nutritional value of rice beverages could improve their functional properties.
- In Vitro and In Vivo Studies: Preclinical and clinical studies will be performed with rice oligosaccharides to test their efficacy on gut microbiota and metabolic markers in order to validate functional benefits for diabetes management.

By addressing these aspects, rice-based beverages could be further developed toward gut health, metabolic wellness, and blood sugar management to offer a promising dietary option for people with certain health needs.

Conclusion

The aim of the research was the development of a beverage based on rice from rice flour and determination of nutritional-functional parameters. By the results, it has been revealed that the developed beverage corresponds to specifications: pH was 4.2; the content of sugar was 100,945 µg/ml; color value-L* was 87.63 ± 2.06; a*-4.31 ± 0.60; and b* 26.89 ± 1.22.

The results from this study provide some preliminary insights into the characteristics of rice-based beverages. Further studies should be conducted to determine whether rice-based drinks can contribute to health benefits for diabetic consumers in terms of the glycemic index, oligosaccharide content, and prebiotic action of rice oligosaccharides. Further optimization of rice processing could improve the nutritional and functional quality of such beverages, thereby aiding in the improvement of general health.

Conflict of interest statement: The authors declare no conflict of interest.

Acknowledgements: The authors gratefully acknowledge Ms. Warangkana Temiya, chemist, and Ms. Wannipa Khamwangsawadi, microbiologist, at the Faculty of Agro-Industry, Chiang Mai University, for assisting in the laboratory work. This research work was supported by the Faculty of Agro-Industry, Chiang Mai University. This research was partially supported by Chiang Mai University, "Graduate and Master's Degree Program in Food Science and Technology, Faculty of Agro-Industry, Chiang Mai University, under the CMU Presidential Scholarship".

References

(1) Kaur P, Mittal A, Nayak SK, Vyas M, Mishra V, Khatik GL. Current strategies and drug targets in the management of type 2 diabetes mellitus. Curr Drug Targets. 2018;19(15):1738-66. doi: 10.2174/1389450119666180727142902.
(2) Ahmad MS. Glycemic index, antioxidant activity and starch composition of various varieties of *Oryza sativa* L. (rice) available in Pakistan. Diabetes & Obesity International Journal. 2023;16:268. doi:10.23880/doij-16000268.
(3) Mondal D, Awana M, Mandal S, Pandit K, Singh A, Syeunda CO, Thandapilly SJ, Krishnan V. Functional foods with a tailored glycemic response based on food matrix and its interactions: Can it be a reality? Food Chemistry: X. 2024;16:101358. doi:10.1016/j.fochx.2024.101358.
(4) Khan M, Singh K, Pandey S. Quality aspects of rice based fermented beverage. Biol. J. Sci. & Tech. Res. 2021;34:005609. doi: 10.26717/BJSTR.2021.34.005609.
(5) Mishra S, Aravind SM, Ajlouni S, Ranadheera CS, Singh BP, Chakkaravarthi S. Optimization of fermentation process and characterization of non-alcoholic functional beverage from pigmented rice varieties. Biocatal. Agric. Biotechnol. 2024; 40:103213. doi: 10.1016/j.bcab.2024.103213.
(6) Pereira C, et al. Rice compounds with impact on diabetes control. Foods. 2021;10(9):1992. doi: 10.3390/foods10091992.
(7) Saji N, Francis N, Schwarz LJ, Blanchard CL, Santhakumar AB. Rice bran derived bioactive compounds modulate risk factors of cardiovascular disease and type 2 diabetes mellitus: an updated review. Nutrients. 2019;11(11):2736. doi: 10.3390/nu11112736.
(8) Tian Y, Ding L, Liu Y, Shi L, Wang T, Wang X, Dang B, Li L, Gou G, Wu G, Wang F, Wang L. The effect of different milling methods on the physicochemical and in vitro digestibility of rice flour. Foods. 2023;12(16):3099. doi: 10.3390/foods12163099.
(9) Sun Z, Lyu Q, Ding W, et al. Impact of different preparation methods on the properties of brown rice flour and the cooking stability of brown rice noodles and the underlying mechanism: Microstructure, starch-protein distribution, moisture migration. LWT. 2023;176:114697. doi: 10.1016/j.lwt.2023.114697.
(10) Mishra S, Aravind SM, Ajlouni S, Ranadheera CS, Singh BP, Chakkaravarthi S. Optimization of fermentation process and characterization of non-alcoholic functional beverage from pigmented rice varieties. Biocatal. Agric. Biotechnol. 2024;40:103213. doi: 10.1016/j.bcab.2024.103213.

Health Benefits of Pulsed Electric Field-enhanced Extracted Anthocyanin from Purple Rice Leaves in Obese Rats

Phacharapong Inyasri*, Thanyaporn Siriwoharn, and Wachira Jirarattanarangsri
Division of Food Science and Technology, Faculty of Agro-Industry, Chiang Mai University, Chiang Mai 50100, Thailand
*Corresponding author's email: phacharapong.inyasri@gmail.com

Abstract:

This study provides the first comprehensive analysis of PEF-enhanced anthocyanin extraction from purple rice leaves and demonstrates its potential as a novel functional ingredient for improving metabolic health in an obesity model. The levels of C3G, TPC and antioxidant activity (measured by DPPH and ABTS) were tested under different electric field intensity (5, 7.5, and 10 kV/cm) and pulse numbers (2000, 3000, and 4000). Results showed that higher field strength and more pulses increased TPC and antioxidant activity but lowered C3G because of heat damage. Optimal extraction conditions (5 kV/cm, 2000 pulses) balanced high C3G content with enhanced antioxidant activity. The health benefits of the C3G extract were tested in male Wistar rats on normal and high-fat diet. The extract lowered LDL, triglycerides and cholesterol while raising HDL. It also improved blood sugar control, shown by lower glucose levels and AUC during the OGTT. These findings highlight the potential of PEF-extracted anthocyanins as a sustainable approach to enhance metabolic health, with promising applications in functional foods, nutraceuticals, and agricultural byproduct valorization.

Keywords: Anthocyanin; Cyanidin-3-Glucoside (C3G); Purple rice leaves; Pulsed electric field (PEF); Lipid profile

Introduction

The export volume of Thai rice has shown an upward trend, rising from 5.7 million tons in 2020 to 8.7 million tons in 2023, an average increase of 15.33% per year (7). As a result, agricultural
by-products such as rice straw and husks have also increased, particularly in the northern region, where purple rice is commonly grown. Studies found that purple rice leaves contain high levels of anthocyanins, which contribute to strong antioxidant properties (9).

Anthocyanins are found in many forms and Cyanidin-3-O-glucoside (C3G) is one of the most common. It helps regulate blood sugar, burn fat, reduce inflammation, improve insulin sensitivity, and lower blood sugar levels (15). Anthocyanins can also inhibit enzymes involved in starch and sugar digestion, reducing post-meal blood sugar spikes (6). They help regulate lipids by lowering LDL cholesterol and increasing HDL (3).

Efficient anthocyanin extraction depended on factors such as temperature, pH, solvent type, and extraction time. Environmentally friendly solvents were essential because traditional solvents were often toxic and harmful to the environment. PEF technology provided several advantages over traditional methods, including non-thermal processing that preserved heat-sensitive nutrients, higher extraction efficiency with increased yields of bioactive compounds, and reduced processing time and energy consumption. PEF produced better results than UAE (Ultrasound-Assisted Extraction) and HVED (High Voltage Electrical Discharge) because it used high-voltage pulses to break cell membranes through electroporation, allowing anthocyanins like C3G to be released more easily. It operated as a non-thermal process, keeping the temperature below 10 °C, which preserved heat-sensitive compounds. PEF also extracted more efficiently and faster while consuming less energy. Additionally, it maintained the stability and bioactivity of compounds better than other methods since it avoided toxic solvents and high heat. PEF was environmentally friendly and suitable for industrial applications due to its scalability and reduced environmental impact (12).

Although anthocyanins from purple rice have been widely studied, the health effects of extracts from rice leaves in rats have not been studied before. This study aimed to extract

anthocyanins from these leaves and evaluate their health benefits by measuring lipid profiles and the body's ability to use sugar in *Rattus norvegicus* rats. If the results are positive, purple rice leaves could be used as a value-added agricultural byproduct, providing additional income for farmers.

Materials and Methods

Chemicals

Potassium chloride buffer (pH 1.0), sodium acetate buffer (pH 4.5), C3G were purchased from SM Chemical Supplies Co., Ltd. (Thailand). Folin - Ciocalteu reagent was purchased from Merck (Germany). DPPH (2,2-diphenyl-1-picrylhydrazyl), Gallic acid, ABTS (2,2′-azinobis-3-ethylbenzothiazoline-6-sulfonic acid) were purchased from Sigma-Aldrich (USA). Hydrochloric acid was purchased from RCI Labscan Ltd. (Thailand). Potassium persulfate was purchased from Panrea (Spain). 95% Ethanol was purchased from Union Science Co Ltd. (Thailand). Dri-chem slide for high-density lipoprotein (HDL), triglyceride, cholesterol and glucose were purchased from Meditop Co., Ltd. (Thailand). All other chemicals were analytical grade or above.

Sample preparation

Doi Saket purple rice leaves (*Oryza sativa* L.) were collected from the Lanna Rice Research Center, Chiang Mai University (Chiang Mai, Thailand) during the winter season, between November 24 - 27, 2022. The leaves were then washed and dried in a hot air oven at 60°C until they reached a constant weight, resulting in a moisture content of about 2%. After drying, the leaves were finely ground using a powder grinder (Sgethai, Bangkok, Thailand) and passed through the sieve (120 Mesh). Then, stored in a high-density polyethylene (HDPE) bag at -20°C.

Extraction of anthocyanin

The method and parameters were adapted from Salee et al. (10) that extracted C3G from seeds. These studies showed that the optimal conditions for extracting C3G were an E of 4 kV/cm with 3681 pulses and 5.7 kV/cm with 2000 pulses. These conditions provided the highest yield of C3G. The extraction ratio of purple rice leaves to 95% ethanol was set at 1:10 (w/v). A 100 ml mixture of purple rice leaves in 95% ethanol (0.1 g/ml) was placed in the PEF equipment. The extraction conditions varied, with electric field strength ranging from 5-10 kV/cm, a pulse width of 1 μs, and a frequency of 10 Hz. A 500 W power supply and a 0.1 μF capacitor at 20 kV were used. Electric field intensity (E) of 5, 7.5 and 10 kV/cm were applied, with number of pulses (N) set at 2000, 3000 and 4000. After the initial extraction, the solution was filtered with Whatman No.1 filter paper, and the remaining leaves powder was re-extracted. The two extracts were then combined and concentrated using a rotary evaporator (BUCHI Thailand Ltd., Bangkok, Thailand) at 40 °C, 30 mbar at 50 rpm. The concentrated residue was washed with deionized water and adjusted to a final volume of 25 ml. The extract was centrifuged at 3000 rpm for 10 minutes at 25°C to remove insoluble debris before storage at -20°C.

Purification of Anthocyanins

The method was adapted from Gao et al. (2). First, glass wool was placed at the bottom of the column to hold the silica gel (Merck, Germany) in place. Then, silica gel saturated with ethanol was poured into the column. Solvent was added to smooth out the silica gel and remove any air bubbles, ensuring that the solvent level was just above the gel to prevent bubble formation. Next, 50 mL of the extract was added. The column was sequentially eluted with 0.01% hydrochloric acid to remove sugars and fats, followed by ethyl acetate to clear out non-anthocyanin polyphenols, and finally 0.01% hydrochloric acid in ethanol to elute the anthocyanins until the purple color faded. Afterward, the solvent was evaporated at 40°C. DI water was then used to rinse the residue and the volume was adjusted to 25 mL. The sample was stored at -20°C until further analysis.

Animals Testing Model

Animal Preparation

Twenty-four (4 - 5 weeks of age) male Wistar rats were purchased from the National Laboratory Animal Center, Mahidol University, Salaya (Nakorn-Pathom, Thailand). They were housed in the Animal House, Laboratory Animal Center (LAC), Chiang Mai University, Chiang Mai, Thailand, under controlled conditions (12-hour light/dark cycle, 50 ± 10% humidity, at 21 ± 1°C) and were provided with food and tap water ad libitum. All procedures were conducted according to the experimental protocols approved by the Animal Ethics Committee of LAC, Chiang Mai University (approved protocol No. RT0020/2566).

Animal Use Protocol

The method was adapted from Pratchayasakul et al. (8). A C3G dose of 2.37 mg kg^{-1} body (BW) was used which showed a significant reduction in blood sugar levels in obese rats (14). The rats were randomly divided into two diet groups (n = 12 in the high-fat diet group and n = 12 in the normal diet group). The normal diet (ND) was provided by Smart Heart Hamster (Bangkok, Thailand) whereas the other group received a diet with fat mainly from lard (59.3% of energy). At week 12, each diet group was split into two subgroups. The first subgroup received 0.9% normal saline solution at 2 ml kg^{-1} BW/day and the second subgroup received the extract at the same dosage for 4 weeks. Before blood collection, the rats were fasted for 12 hours. Blood samples of 1 ml kg^{-1} BW were collected from the saphenous vein at weeks 0, 12, and 16 to analyze HDL, triglycerides, cholesterol and LDL. Then, blood was centrifuged to separate the serum for analysis at a speed of 3000 rpm, at 25°C, for 10 min. After 4 weeks of extract administration, an Oral Glucose Tolerance Test (OGTT) was conducted by administering glucose at 2 g kg^{-1} BW/day by gavage. Blood samples were collected at 0, 30, 60 and 120 min. The plasma samples were stored at -80 °C until analysis, which was performed using a FUJI DRI-CHEM 3500i (Burladingen, Germany).

Analysis

Determination of Total Phenolic Content (TPC)

For each sample, 50 µL was used, and 100 µL of Folin-Ciocalteu reagent was added to each well. The mixture was shaken for 1 minute and then left for 4 min. After that, 50 µL of sodium carbonate solution was added to each well. This was done three times for each sample. The 96-well plate with the samples was kept in the dark for 2 hours. After that, the absorbance at 765 nm was measured with a microplate reader. TPC was calculated using a gallic acid standard curve and expressed as grams of gallic acid equivalents per ml extract (g GAE/ml extract). (1)

Determination of C3G content

High-performance liquid chromatography (HPLC) was used to separate and measure the amount of C3G in the extract, following the method by Siriwoharn et al. (11). The HPLC system used for this analysis was from Hitachi High-Tech Corporation, Tokyo, Japan, and it included a C18 column (HC-C18 Column, 4.6 x 150 mm, 5 µm, 400 bar, Agilent, United States). The mobile phase had two parts: mobile phase A was 100% HPLC-grade acetonitrile, and mobile phase B was a mix of 1% glacial phosphoric acid in deionized water. To ensure the solvents and samples were clean, they were filtered using a 13mm Nylon syringe filter with a pore size of 0.22µm. The chromatographic program followed a precise sequence: (a) 0 min, 2% A; (b) 0-25 min, employing a linear gradient that transitioned from 2% to 20% A; (c) 25-30 min, with a linear gradient ranging from 20% to 40% A; (d) 30-35 min, with a linear gradient returning from 40% to 2% A. Simultaneous monitoring of the chromatographic separation was conducted at 520 nm, with a constant flow rate of 1 mL/min and an injection volume of 10 µL.

Determination of antioxidant activity

Determination of DPPH radical scavenging activity

100 µL of the extract solution was mixed with an equal volume of DPPH solution and allowed to stand for 30 min in darkness during the incubation period. Subsequently, the absorbance of the

resulting mixture was measured at 17 nm. The capacity to scavenge DPPH radicals within the samples was calculated employing Equation

$$\% \text{ DPPH scavenging activity} = ((C - S) / C) \times 100\ \%$$

where C was UV absorbance of control solution and S was UV absorbance of the sample solution. (10)

ABTS radical scavenging activity assay

The ABTS solution was prepared by combining 2.45 mM of $K_2S_2O_8$ with 7 mM of ABTS solution at a ratio of 1:2 (v/v), followed by a 24-hour incubation period in darkness. During the analysis, 50 µL of each sample was mixed with 100 µL of the ABTS solution in a 96-well plate and left at room temperature for 30 min. Next, the absorbance of the samples was measured at 734 nm using a microplate reader. The standard regression equation was plotted between the absorbance and the Trolox concentration at various levels. Antioxidant capacity was calculated and expressed as grams of Trolox equivalent antioxidant capacity per milliliter of extract (g TEAC/g extract). (10)

Lipid Profile and Oral Glucose Tolerance Test (OGTT) Analysis

The rats received a glucose solution (2 g/kg weight) through gavage feeding. Blood samples were collected from the saphenous vein at 0, 30, 60 and 120 min after glucose administration. The area under the curve (AUC). AUC were calculated using the formula:

$$AUC = (0.25 \times \text{fasting value}) + (0.5 \times 30\ \text{min}) + (0.75 \times 60\ \text{min}) + (0.5 \times 120\ \text{min})$$

For glucose levels was calculated using the trapezoidal formula to assess glucose tolerance. The Lipid Profile analysis and glucose measurement were conducted using the FUJI DRI-CHEM analyzer. First, the appropriate DRI-CHEM slides were selected for cholesterol, triglycerides, HDL, and glucose. Approximately 10 µL of serum or plasma was applied to the sample area on each slide using a pipette, and the analyzer lid was closed. The start button was pressed to initiate the measurement. After a few min, the results were displayed on the screen and recorded. LDL was calculated using the Friedewald equation:

$$LDL = \text{total cholesterol} - ((HDL + (\text{triglycerides}/5)) \quad (13)$$

Statistics analysis

All experiments were conducted in triplicate, and all data were analyzed using one-way analysis of variance (ANOVA) and Duncan's test on SPSS software version 17.0 (SPSS Inc., Chicago, IL, USA) for analysis with a significant level of $p < 0.05$.

Results and Discussion

Effect of PEF process variables on C3G, TPC, DPPH, ABTS and Temperature values.

Table 1 presents the TPC, antioxidant activities, and C3G content of extracts under various PEF extraction conditions. The C3G content ranged from 3.43 ± 0.04 to 178.4 ± 24.1 mg/g extract, while TPC varied between 96.7 ± 0.1 and 242.46 ± 1.8 mg GAE/g extract. Antioxidant activities were measured using the DPPH and ABTS tests. DPPH (% inhibition) ranged from 36.7 ± 1.8 to 89.6 ± 0.3, and ABTS (g TEAC/g extract) ranged from 1.0 ± 0.2 to 4.9 ± 0.2. Increasing the E reduced the C3G content but increased the TPC and enhanced radical scavenging activities in both DPPH and ABTS. Similarly, increasing the N decreased the C3G content while boosting the TPC and enhancing radical scavenging activities in both DPPH and ABTS. Both independent variables increased the temperature. A previous study (4) used water at 100°C to extract C3G by soaking for 3 minutes and obtained 0.0468 mg/g. In this study, the highest C3G yield was 16.4 mg/g, which is about 350 times higher than the traditional method.

This was consistent with the study by Salee et al. (10) on PEF-assisted extraction of purple rice grain, which found that increasing the E and the N resulted in a higher amount of bioactive compounds. This occurred because the density of pores in the cell membrane and cell wall of the rice changed, allowing for increased mass transfer through the cell walls that contained the bioactive

compounds. However, anthocyanin content decreased significantly as the temperature increased, especially at temperatures above 40°C, leading to notable degradation of anthocyanins.

Table 1. The C3G, TPC, DPPH, ABTS, and temperature of the purple rice leaf extracts by using the PEF technique.

E	Pulsed	C3G (mg/g extact)	TPC (mg GAE/g extact)	DPPH (% inhibition)	ABTS (g TEAC/g extact)	Temperature (°C)
5	2000	164.0±9.7^{a}	96.75±0.1^{j}	36.7±1.8^{i}	4.9 ± 0.1^{a}	37.3±0.5^{i}
5	3000	54.56±2.0^{c}	105.4±0.3^{i}	58.79±0.4^{h}	3.0 ± 0.5^{c}	41.0±0.0^{h}
5	4000	35.75±0.3^{de}	114.3±2.7^{h}	58.32±0.5^{h}	1.0 ± 0.2^{f}	44.3±0.5^{g}
7.5	2000	41.11±1.1^{cd}	124.69±0.8^{g}	65.06±0.7^{g}	2.8 ± 0.4^{cd}	45.0±0.0^{f}
7.5	3000	35.74±1.8^{de}	130.34±1.4^{f}	80.50±0.18^{e}	2.0 ± 0.1^{e}	41.0±0.0^{e}
7.5	4000	34.72±0.4^{de}	139.32±0.5^{d}	78.55±0.3^{f}	4.3 ± 0.3^{b}	54.3±0.5^{d}
10	2000	22.87±0.9^{ef}	195.02±4.1^{c}	84.55±0.3^{bc}	2.5 ± 0.4^{d}	59.0±0.0^{fc}
10	3000	9.45±0.3^{fg}	213.15±0.2^{b}	85.39±0.4^{b}	2.1 ± 0.5^{e}	60.0±0.0^{b}
10	4000	3.43±0.0^{h}	242.46±1.8^{a}	89.63±0.3^{a}	1.9 ± 0.2^{e}	65.0±0.0^{a}

Values are means ± SD (n = 3). $^{a, b, c, d}$ indicate significant differences ($p < 0.05$) between groups.

Figure 1 showed a correlation heatmap with significant relationships ($p < 0.05$) between E, N, C3G content, TPC, DPPH, ABTS and temperature. The E was positively correlated with TPC, DPPH, ABTS and temperature. This meant that increasing the E improved phenolic content and antioxidant activity but also increased the extraction temperature. However, there was a negative correlation between E and C3G showing that higher intensities caused a loss of C3G, potentially resulting from thermal degradation. The N also showed a negative correlation with C3G , indicating that more pulses further reduced C3G content. C3G was negatively correlated with TPC. This suggested that higher phenolic content and antioxidant activity led to lower C3G levels, likely due to heat-related degradation during extraction.

Therefore, E and N significantly affected TPC and extraction temperature, where higher TPC was associated with increased antioxidant activity in DPPH. In contrast, C3G decreased significantly as both TPC and DPPH antioxidant activity increased. Thus, an electric field intensity of 5 kV/cm with 2000 pulses was chosen, as it yielded the highest amount of C3G and required the shortest extraction time.

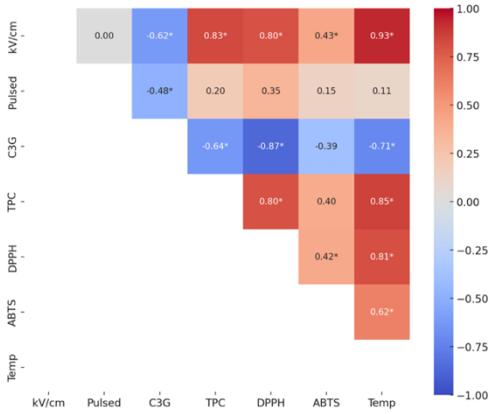

Figure 1. correlation heatmap ($p < 0.05$) between The C3G, TPC, DPPH, ABTS, and temperature with positive correlations in red and negative in blue.

Effect of C3G extract for Lipid profile

Table 2 illustrates the positive effects of C3G supplementation on body weight and lipid profiles in both HFD and ND groups. In the HFD group, body weight increased significantly from 571.7 ± 25.4 g to 602.9 ± 33.1 g, whereas the HFD+C3G group maintained a stable weight of 573.2 ± 32 g. The ND+C3G group showed a slight weight increase to 447.4 ± 18.3 g at 16 weeks, while the ND group reached 561.6 ± 16.5 g. These findings suggested that C3G helped control weight gain in the normal diet group, leading to less weight gain compared to the ND group without C3G.

Triglyceride levels increased in the HFD group from 148 ± 8.4 mg/dL to 174.5 ± 6.3 mg/dL. However, significant reductions were observed in the HFD+C3G group (128.7 ± 3.4 mg/dL), with the lowest triglyceride levels recorded in the ND+C3G group (89 ± 5.2 mg/dL). Cholesterol levels also increased in the HFD group, while the HFD+C3G group experienced a reduction to 77.3 ± 3.6 mg/dL, similar to ND+C3G (79.7 ± 2.4 mg/dL). HDL levels were highest in the ND+C3G group at 61 ± 2.2 mg/dL, whereas LDL levels were reduced with C3G, reaching 16.2 ± 1.7 mg/dL in HFD+C3G and 5.3 ± 1.1 mg/dL in ND+C3G.

Table 2. Effect of 4-week anthocyanin extract administration on body weight, triglyceride, cholesterol, HDL, and LDL between groups fed with a normal diet (ND) and a high-fat diet (HF diet).

Parameter	Week	HFD	HFD+C3G	ND	ND+C3G
Body weight (g)	12	571.7 ± 25.4^{a}	575.6 ± 30.7^{a}	504.6 ± 16.5^{ab}	442.3 ± 15.7^{b}
	16	602.9 ± 33.1^{a}	573.2 ± 32^{a}	$561.6 \pm 16.5^{*,a}$	$447.4 \pm 18.3^{*,b}$
Triglyceride (mg/dL)	12	148 ± 8.4^{bc}	159.7 ± 4^{c}	100.2 ± 1.9^{ab}	106.3 ± 5.2^{a}
	16	$174.5 \pm 6.3^{*,a}$	$128.7 \pm 3.4^{*,b}$	102.8 ± 1.9^{c}	$89 \pm 5.2^{*,d}$
Cholesterol (mg/dL)	12	107.2 ± 5.7^{a}	107.3 ± 2.1^{a}	80.8 ± 2^{b}	83.2 ± 2.6^{b}
	16	$112.8 \pm 6^{*,a}$	$77.3 \pm 3.6^{*,b}$	$85.2 \pm 2.7^{*,b}$	$79.7 \pm 2.4^{*,b}$
HDL (mg/dL)	12	44.2 ± 1.2^{bc}	42 ± 1.4^{c}	48.7 ± 2.2^{ab}	53.3 ± 2.5^{a}
	16	42.3 ± 1.1^{c}	41.5 ± 3.3^{c}	50.7 ± 2.2^{b}	$61 \pm 2.2^{*,a}$
LDL (mg/dL)	12	40.7 ± 6.1^{a}	41.2 ± 2.1^{a}	16.8 ± 0.9^{b}	13.8 ± 1.4^{b}
	16	$44 \pm 6.5^{*,a}$	$16.2 \pm 1.7^{*,b}$	18.8 ± 1.2^{b}	$5.3 \pm 1.1^{*,c}$

$^{a, b, c, d}$ indicate significant differences ($p < 0.05$) between groups. * indicates significant differences ($p < 0.05$) within the same group compared to its baseline.

Figure 2 showed the effects of C3G extract on various health markers. For body weight (A), ND without C3G experienced significant weight gain whereas the HFD group with C3G gained less weight, indicating its potential in weight control. Triglyceride levels (C) significantly decreased in groups treated with C3G but remained high in non-supplemented groups. HDL levels (B) showed no significant changes. however, C3G seemed to maintain or slightly improve HDL levels compared to decreases in non-C3G groups. LDL levels (D) dropped significantly in both ND and HFD groups with C3G. Cholesterol levels (E) exhibited the most substantial reduction in the HFD group with C3G, highlighting its cholesterol-lowering properties.

C3G improved lipid metabolism by inhibiting HMG-CoA reductase, thereby reducing LDL production and enhancing LDL receptor expression for efficient clearance. It also supported HDL functionality by promoting reverse cholesterol transport, returning excess cholesterol to the liver for elimination (1). Additionally, C3G activated the Nrf2 pathway, reducing oxidative stress and inflammation. These findings were consistent with prior research demonstrating that anthocyanins enhanced lipid profiles, reduced LDL and increased HDL, thereby mitigating cardiovascular risks in high-fat diet conditions. (5, 7)

.

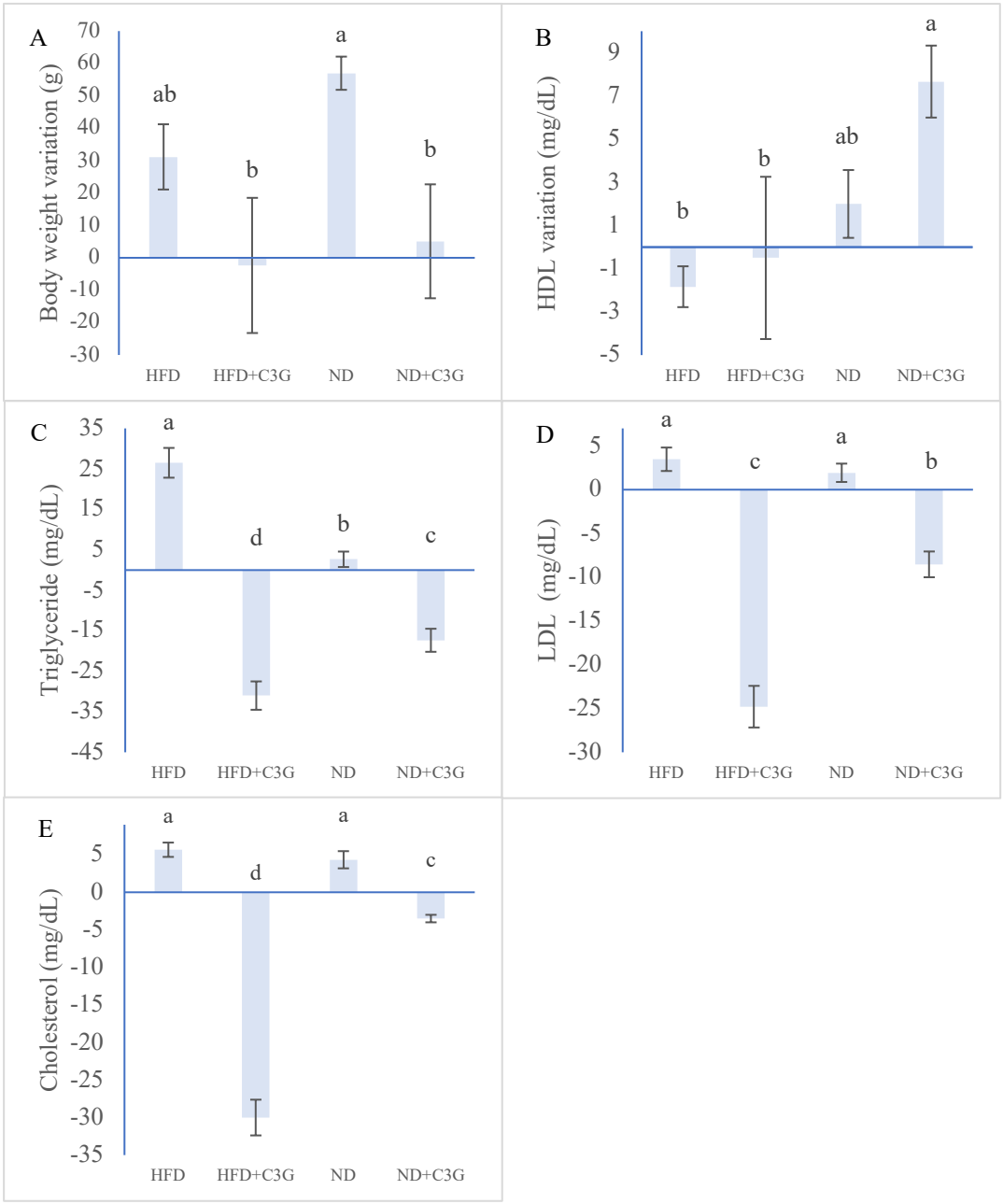

Figure 2. variations in body weight, triglyceride, cholesterol, HDL, and LDL after C3G administration. [a, b, c, d] indicate significant differences ($p < 0.05$) between groups.

Effect of C3G extract for OGTT

Figure 3 illustrates the effects of C3G extract on plasma glucose levels during the OGTT and the corresponding AUC. The HFD group displayed the highest glucose levels, peaking at 60 minutes, indicative of poor glucose tolerance. The HFD+C3G group demonstrated significantly lower glucose levels compared to the HFD group, suggesting that C3G improved glucose metabolism. Similarly, the ND+C3G group exhibited a smaller glucose peak and a faster return to baseline compared to the ND group.

In B, the AUC values confirmed these findings. The HFD+C3G and ND+C3G groups displayed significantly lower AUCs compared to their respective controls, with the ND+C3G group showing the lowest AUC. This suggested that C3G reduced glucose levels and improved glucose regulation. These findings indicated that C3G supplementation supported better glucose control in both normal and high-fat diet groups.

The improvement was likely attributed to the antioxidant properties of anthocyanins, which increased insulin sensitivity and supported improved β-cell function. Anthocyanins influenced key pathways, such as the Nrf2 pathway, to enhance antioxidant defenses and protect cells from damage. The AUC, representing the overall glucose response during the OGTT, further supported these results. Lower AUC values in treated groups suggested better glucose regulation, possibly due to enhanced insulin signaling. These findings aligned with studies that demonstrated anthocyanin-rich diets reduced post-meal glucose and lipid levels (12).

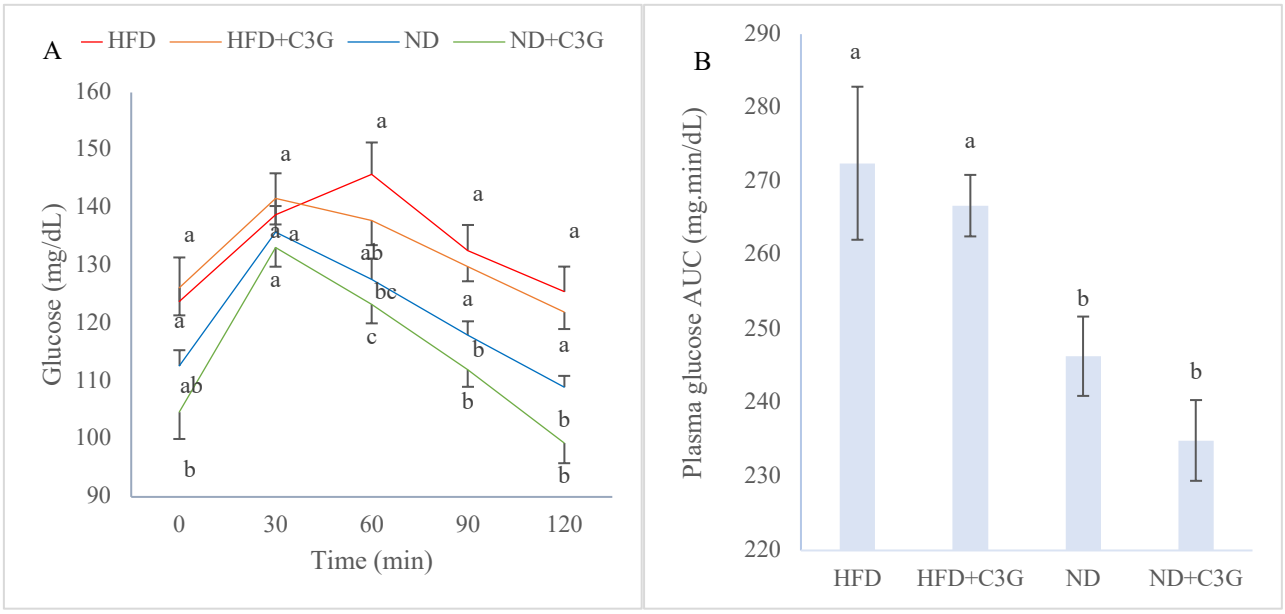

Figure 3. plasma Glucose Levels During OGTT (A) and AUC for Plasma Glucose During OGTT (B). ^{a,b,c,d}, $p < 0.05$ indicate comparisons between groups at the same time point.

Conclusion

The study showed that PEF extraction significantly affected the antioxidant properties and chemical composition of purple rice leaf extracts, including C3G, TPC, DPPH, and ABTS levels. Lower electric field intensities and pulse numbers preserved higher C3G content but resulted in lower TPC and antioxidant activities. In contrast, higher field intensities and pulse numbers increased TPC and antioxidant activities but reduced C3G content due to thermal degradation. The optimal extraction conditions, which balanced high C3G content and antioxidant activity, were achieved at 5 kV/cm with 2000 pulses.

C3G supplementation improved lipid profiles and glucose metabolism in both HFD and ND rat groups. It reduced LDL, triglycerides, and cholesterol, increased HDL levels and improved glucose tolerance as shown by OGTT results. These effects were likely due to the antioxidant properties of C3G, which enhanced insulin sensitivity, supported β-cell function, and activated key pathways like Nrf2. C3G improved lipid regulation and glucose control. These findings suggest that C3G could be a potential dietary supplement for improving metabolic health.

Conflict of interest statement: The author declares no conflict of interest.

Acknowledgements: The author wishes to thank the Agricultural Research Development Agency (Public Organization) for supporting this work through the Agricultural and Agro-Industrial Graduate Scholarship. Special appreciation is extended to the Lanna Rice Research Center, Chiang Mai University, for providing the purple rice leaves used in this research. The author would also like to thank Assistant Professor Dr. Arthit

Yawutthi for granting access to the Pulsed Electric Field equipment. Additionally, sincere gratitude is expressed to Assistant Professor Wachira Jiraratanarangsri and Assistant Professor Dr. Thanyaporn Siriwohan, the research advisors, for their invaluable guidance throughout this study. Finally, the author thanks the Experimental Animal Center at Chiang Mai University for their support, consultation, and assistance in facilitating the animal studies in this research.

References

(1) Fatchiyah F, Meidinna HN, Suyanto E, editors. The cyanidin-3-O-glucoside of Black Rice inhibits the interaction of HMG-CoA and HMG-CoA Reductase: three-and two-dimension structure. Journal of Physics: Conference Series; 2020: IOP Publishing.

(2) Gao Z. Extraction, separation, and purification of blueberry anthocyanin using ethyl alcohol. Kemija u industriji: Časopis kemičara i kemijskih inženjera Hrvatske. 2017;66(11-12):655-9.

(3) Jang H-H, Hwang I-G, Lee Y-M. Effects of anthocyanin supplementation on blood lipid levels: a systematic review and meta-analysis. Frontiers in Nutrition. 2023;10:1207751.

(4) Jirarattanarangsri W., Budprom P. Effect of Different Processing on Phenolic Content, Anthocyanin Content, and Antioxidant Capacity. Srinakharinwirot University Journal of Sciences and Technology. 2017;9(17, January-June):91-103.

(5) Laorodphun P, Arjinajarn P, Thongnak L, Promsan S, Swe MT, Thitisut P, et al. Anthocyanin-rich fraction from black rice, Oryza sativa L. var. indica "Luem Pua," bran extract attenuates kidney injury induced by high-fat diet involving oxidative stress and apoptosis in obese rats. Phytotherapy Research. 2021;35(9):5189-202.

(6) Moein S, Moein M, Javid H. Inhibition of α-Amylase and α-Glucosidase of Anthocyanin Isolated from Berberis integerrima Bunge Fruits: A Model of Antidiabetic Compounds. Evidence-Based Complementary and Alternative Medicine. 2022;2022(1):6529590.

(7) OAE. rice export. Available at: URL: https://impexpth.oae.go.th/export . Accessed Nov 1, 2024.

(8)Pratchayasakul W, Kerdphoo S, Petsophonsakul P, Pongchaidecha A, Chattipakorn N, Chattipakorn SC. Effects of high-fat diet on insulin receptor function in rat hippocampus and the level of neuronal corticosterone. Life sciences. 2011;88(13-14):619-27.

(9) Rice Science Center, Kasetsart University Kamphaeng Saen Campus. color rice. Available at: URL: https://dna.kps.ku.ac.th/index.php/about-rsc-rgdu/rice-research-and-knowledge/402-rainbow-rice-thailand. Accessed Nov 1, 2024.

(10) Salee N, Chaiyana W, Yawootti A, Naruenartwongsakul S, Klangpetch W, Walter P, et al. Optimization of the pulse electric field assisted extraction of black rice grain for antioxidant and sirtuin1 enzyme stimulation activities. Scientific Reports. 2022;12(1):6459.

(11) Siriwoharn T, Wrolstad RE, Finn CE, Pereira CB. Influence of cultivar, maturity, and sampling on blackberry (Rubus L. Hybrids) anthocyanins, polyphenolics, and antioxidant properties. Journal of agricultural and food chemistry. 2004;52(26):8021-30.

(12) Tena N, Asuero AG. Up-to-date analysis of the extraction methods for anthocyanins: Principles of the techniques, optimization, technical progress, and industrial application. Antioxidants. 2022;11(2):286.

(13) Tung Y-T, Chen Y-L, Fan T-Y, Fong T-H, Chiu W-C. Effects of dietary adjustment of n-3: n-6 fatty-acid ratio to 1: 2 on anti-inflammatory and insulin-signaling pathways in ovariectomized mice with high fat diet-induced obesity. Heliyon. 2023;9(10).

(14) Wongmekiat O, Lailerd N, Kobroob A, Peerapanyasut W. Protective effects of purple rice husk against diabetic nephropathy by modulating PGC-1α/SIRT3/SOD2 signaling and maintaining mitochondrial redox equilibrium in rats. Biomolecules. 2021;11(8):1224.

(15) Ye X, Chen W, Huang X-F, Yan F-J, Deng S-G, Zheng X-D, et al. Anti-diabetic effect of anthocyanin cyanidin-3-O-glucoside: data from insulin resistant hepatocyte and diabetic mouse. Nutrition & Diabetes. 2024;14(1):7.

Blockchain Technology for Risk Hazard Assessment in Seafood: Enhancing Food Safety and Traceability

Noman Aslam[1,2], Wachira Jirarattanarangsri[1], Ekkarat Boonchiang[3], and Sukhuntha Osiriphun[1,*]

[1] Department of Food Science and Technology, Faculty of Agro-Industry, Chiang Mai University, Thailand
[2] Graduate Student of Department of Food Science and Technology, Faculty of Agro-Industry, Chiang Mai University, Thailand
[3]Department of Computer Science, Faculty of Science, Chiang Mai University, Thailand
*Corresponding author's email: sukhuntha.o@cmu.ac.th

Abstract:

Fish in the scombroid family, including mackerel, have proteins that are rich in the amino acid histidine. The amino acid histidine can be transformed into histamine through a decarboxylation process facilitated by the enzyme histidine decarboxylase, which is generated by bacteria from the Enterobacteriaceae family commonly found in the intestines, gills, and skin of fish. Histamine is a toxic substance in food that poses a chemical hazard, causing food poisoning. Therefore, high levels of histamine are undesirable in food as they affect allergic in consumer health. This research investigated the application of Blockchain technology for risk hazard assessment in seafood, specifically focusing on histamine levels in mackerel. By implementing a blockchain-based system, we aimed to enhance food safety and traceability throughout the supply chain. Our study involved analyzing histamine levels in mackerel samples stored at different temperatures (4°C and 30°C) for up to 120 hours using a fluorometer with the fluorescence method. We found that the control sample stored at 30°C showed the highest increase in histamine levels from the initial value of 2.316 μg/g to 186.432 μg/g. This method used a fluorometer that analyzed results with graphs and standard concentration values, resulting in very little variation in histamine levels across three repeated measurements. Our findings demonstrated that blockchain technology can effectively record and track histamine levels in mackerel, providing real-time data for risk assessment. The system allowed for the identification of potential hazards early on, enabling timely interventions to prevent foodborne illnesses. By leveraging the decentralized and immutable nature of blockchain, we can enhance transparency, accountability, and consumer trust in the seafood industry.

Keywords: Blockchain technology; Risk hazard assessment; Seafood; Food safety; Traceability; Histamine concentration.

Introduction

Seafood consumption is a vital part of a healthy diet, providing essential nutrients. However, seafood safety is a critical concern due to the potential for contamination with pathogens and hazardous substances. Traditional food safety systems often rely on paper-based documentation, which can be prone to errors, manipulation, and delays, making it challenging to track the origin and history of seafood products. Blockchain technology emerges as a revolutionary solution to address these challenges, offering a secure, transparent, and immutable platform for managing and sharing information throughout the seafood supply chain. ((Rani et al., 2024))

Histamine is a naturally occurring biogenic amine found in various foods, particularly in fish belonging to the scombroid family, including mackerel. This compound is produced by the enzymatic decarboxylation of histidine, catalyzed by histidine decarboxylase, an enzyme secreted by bacteria, primarily from the Enterobacteriaceae family, commonly found in the intestinal tracts, gills, and skin of fish. Elevated levels of histamine in food are a serious public health concern due to its potential to cause allergic reactions, known as scombroid poisoning, characterized by symptoms like flushing, headache, nausea, and vomiting. (Comas-Basté et al., 2019)

Traditional food safety methods for histamine detection often rely on time-consuming laboratory analysis, which can delay timely interventions and potentially compromise food safety. This study aims to address this issue by exploring the application of blockchain technology to enhance food safety and traceability in the seafood industry, focusing specifically on the control of histamine levels in mackerel.

This paper explores the potential of Blockchain technology for enhancing food safety and traceability in the seafood industry. The focus is on its application for risk hazard assessment, a crucial step in preventing foodborne illnesses and maintaining consumer confidence. By leveraging the decentralized and tamper-proof nature of Blockchain, this study aims to demonstrate its effectiveness in creating a robust system for tracking seafood from source to consumer, enabling efficient identification of potential hazards, early intervention, and improved risk management practices.

Blockchain technology provides a decentralized and immutable platform for recording and sharing data, enabling greater transparency and accountability throughout the supply chain. Its decentralized nature offers resistance to tampering, ensuring the integrity and reliability of recorded information. This study investigates the potential of blockchain technology to revolutionize food safety practices by integrating real-time monitoring of histamine levels, enabling prompt identification of potential hazards and timely interventions to mitigate risks of scombroid poisoning. The findings of this study have the potential to contribute to the development of robust and efficient food safety protocols, ultimately promoting consumer confidence and trust in the seafood industry. ((Yu et al., 2024))

Materials and Methods

Materials:

- Fresh mackerel (Scomber scombrus) obtained from local fish markets.
- Phosphate-buffered saline (PBS) solution
- Histamine standard (Sigma Aldrich)
- Fluorometer (Thermo Scientific)
- Blockchain platform (Ethereum)
- Temperature-controlled storage equipment

Methods:

1. Sample Collection and Preparation: Fresh mackerel samples were purchased from local fish markets. Samples were immediately transported to the laboratory and stored at 4C.

2. Histamine Extraction: The mackerel samples were homogenized in PBS solution, and the homogenate was centrifuged at 10,000 rpm for 10 minutes to remove any debris. The supernatant was collected and stored at -20C until analysis.

3. Histamine Analysis: Histamine levels were measured using a fluorometer (Thermo Scientific) based on the method described by [reference]. Briefly, histamine reacts with o-phthalaldehyde (OPA) to produce a fluorescent product that can be quantified by measuring its fluorescence intensity.

4. Bacterial enumeration: Total plate count was determined using the spread plate method with Tryptic soy broth (TSA) as the growth medium. Incubation conditions: Plates were incubated at 35C for 24 hours. Colony counting: Colonies were counted on plates with 25-250 colonies. Results expression: Total plate count was reported as colony-forming units per gram (CFU/g).

5. Temperature Storage and Monitoring: The mackerel samples were stored at two different temperatures: 4C (refrigerated) and 30C (room temperature). The samples were stored for up to 120 hours, and histamine levels were measured at regular intervals. ((Koo & Lim, 2023))

6. Statistical Analysis: Data was analyzed using statistical software (SPSS). One-way ANOVA was performed to compare histamine levels between different storage temperatures and time points. (Mohamed et al., 2023)

Results and Discussion

Results

The results of this study revealed a significant increase in histamine levels in mackerel samples stored at 30C over time. The initial histamine level in the control sample was 2.316 µg/g. After 120 hours of storage at 30C, the histamine level increased significantly to 186.432 µg/g. This substantial increase in histamine levels at elevated temperatures highlights the importance of proper storage conditions to prevent the accumulation of histamine in seafood.

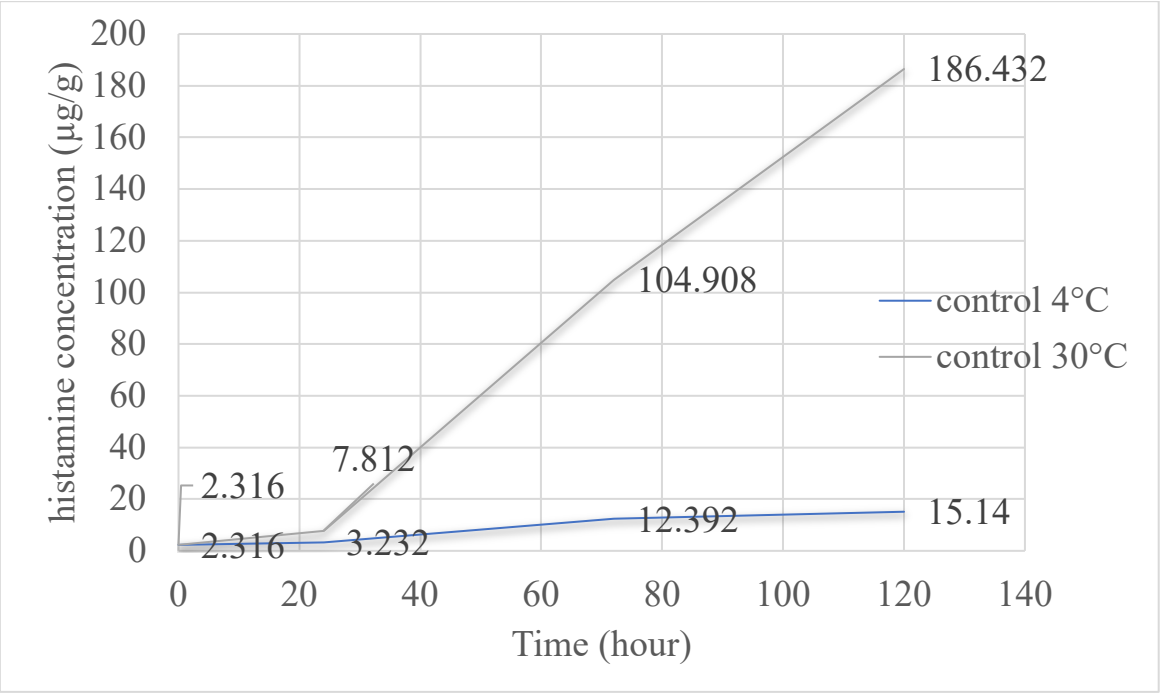

Figure 1. The histamine concentration of samples at various time of storage and storage temperatures

Table 1: Microbiological analysis

Temperature (°C)	Time (hour)	Total plate count (LogCFU/g)
4	24	4.44
	72	TNTC
	120	TNTC
30	24	TNTC
	72	TNTC
	120	TNTC

From Table 1, the total plate count of fresh mackerel stored at 4C was 4.44 LogCFU/g at the start of the experiment and 1.7×10^4 CFU/g after 24 hours. The total plate count of fresh mackerel stored at 30C was too numerous to count (TNTC) after 72 hours.

The blockchain system effectively recorded and tracked the histamine levels in mackerel samples, providing real-time data for risk assessment. This system enabled timely identification of potential hazards and facilitated prompt interventions to mitigate the risk of scombroid poisoning.

The key elements of blockchain used in this study:

• Decentralization: Blockchain technology allows for a decentralized record-keeping system, meaning that data is not stored in a single location. This makes it difficult for unauthorized individuals to alter the data, which improves trust and accountability.

• Immutability: Once a transaction is recorded on the blockchain, it cannot be altered or deleted. This ensures the integrity of the data and provides a reliable source of information.

• Transparency: Blockchain allows for transparent data sharing, meaning that all participants in the supply chain can access and track the history of the seafood product.

• Traceability: By using blockchain, the origin and journey of the seafood can be tracked throughout the supply chain, allowing for immediate identification of any potential issues or contamination.

The research focused on tracking histamine levels in mackerel. They used blockchain to record and track these levels, providing real-time data for risk assessment and enabling timely interventions to prevent foodborne illnesses.

This approach enhances transparency, accountability, and consumer trust in the seafood industry, ultimately improving food safety and quality. ((Iles, 2007))

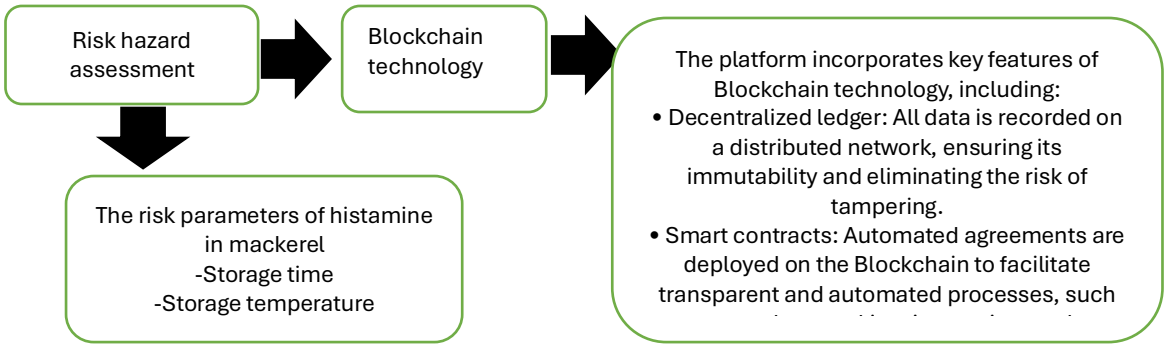

Figure 2 The schematic diagram of elements of block chain technology use in this study

From Figure 2, The success concept model for this research is to utilize blockchain technology to enhance food safety and traceability in the seafood industry, specifically focusing on histamine levels in mackerel. By implementing a blockchain-based system, the research aims to achieve the following:

• Enhance food safety: The blockchain system will allow for real-time monitoring of histamine levels in mackerel throughout the supply chain. This will enable timely interventions to prevent foodborne illnesses and ensure the safety of consumers.

• Improve traceability: The blockchain system will create a transparent and immutable record of the origin, handling, and storage conditions of mackerel. This will allow consumers to track the source of their seafood and ensure its quality.

• Increase consumer trust: The blockchain system will increase consumer trust in the seafood industry by providing a transparent and reliable system for tracking food safety and traceability.

• Foster collaboration: The blockchain system can be used to facilitate collaboration between stakeholders in the seafood supply chain, such as producers, processors, distributors, and retailers. This will help to improve communication and coordination, leading to a more efficient and effective food safety system.

The success of this model will depend on the following factors:

• Adoption by industry: The blockchain system must be adopted by key players in the seafood industry, such as producers, processors, and retailers.

• Technical feasibility: The blockchain system must be technically feasible and scalable to meet the needs of the seafood industry.

• Consumer acceptance: Consumers must be willing to adopt the blockchain system and trust the information provided.

If these factors are addressed, the blockchain technology for risk hazard assessment in seafood has the potential to significantly improve food safety, traceability, and consumer trust in the seafood industry. (Thompson & Rust, 2023)

Discussion

The findings of this study demonstrate the effectiveness of blockchain technology in enhancing food safety and traceability in the seafood industry. The decentralized and immutable nature of blockchain ensures data integrity and transparency throughout the supply chain. The real-time data generated by the blockchain system allows for timely identification of potential hazards, enabling prompt interventions to prevent foodborne illnesses. This study highlights the potential of blockchain technology to revolutionize food safety practices in the seafood industry.

The results of this study also demonstrate the importance of proper storage conditions in controlling histamine levels in seafood. Storing mackerel samples at 30C resulted in a significant increase in histamine levels over time, highlighting the importance of maintaining appropriate temperatures to prevent spoilage and ensure food safety.

Future research should investigate the effectiveness of blockchain technology in a larger-scale setting and explore its integration with other food safety interventions, such as improved sanitation practices and more effective quality control measures. This research lays the foundation for the development of innovative and robust food safety protocols that leverage the benefits of blockchain technology and contribute to the safety and security of the global seafood industry.

Conclusion

Refrigeration (4°C) significantly reduced the total plate count of fresh mackerel, demonstrating its effectiveness in preserving the quality of the fish. This emphasizes the importance of maintaining a cold chain for fresh mackerel to minimize microbial spoilage.The findings of this study highlight the potential of blockchain technology to enhance food safety and traceability in the seafood industry. By implementing a blockchain-based system, we were able to effectively record and track histamine levels in mackerel, providing real-time data for risk assessment. This allows for the identification of potential hazards early on, enabling timely interventions to prevent foodborne illnesses. Leveraging the decentralized and immutable nature of blockchain also enhances transparency, accountability, and consumer trust in the seafood industry. Overall, our research suggests that blockchain technology has the potential to significantly improve the safety and quality of seafood products for consumers.

Conflict of interest statement: The authors declare no conflict of interest.

Acknowledgements: The authors gratefully acknowledge Ms. Warangkana Temiya, chemist, and Ms. Wannipa Khamwangsawadi, microbiologist, at the Faculty of Agro-Industry, Chiang Mai University, for assisting in the laboratory work. This research work was supported by the Faculty of Agro-Industry, Chiang Mai University. This research was partially supported by Chiang Mai University, “Graduate and Master’s Degree Program in Food Science and Technology, Faculty of Agro-Industry, Chiang Mai University, under the CMU Presidential Scholarship”.

References

1. Rani, P., Sharma, P., & Gupta, I. (2024, January). From Sea to Table: A Blockchain-Enabled Framework for Transparent and Sustainable Seafood Supply Chains. In International Conference on Advances in Distributed Computing and Machine Learning (pp. 111-123). Singapore: Springer Nature Singapore.
2. Comas-Basté, O., Latorre-Moratalla, M. L., Sánchez-Pérez, S., Veciana-Nogués, M. T., & Vidal-Carou, M. D. C. (2019). Histamine and other biogenic amines in food. From scombroid poisoning to histamine intolerance (Vol. 1). London, UK: IntechOpen.
3. Yu, J., Yue, Y., Zhang, J., Jia, Z., & Yang, J. (2024). Advances in technologies to detect histamine in food: Principles, applications, and prospects. Trends in Food Science & Technology, 104385.
4. Koo, P. L., & Lim, G. K. (2023). A review on analytical techniques for quantitative detection of histamine in fish products. Microchemical Journal, 189, 108499.
5. Mohamed, W. A., Hassanen, E. I., Mansour, H. A., & Mahmoud, M. A. (2023). Immunohistochemical evaluation of histamine levels and hygienic aspect of little tunny (Euthynnus alletteratus) musculature at different environment time and temperature. Journal of Aquatic Food Product Technology, 32(8-9), 637-653.
6. Iles, A. (2007). Making the seafood industry more sustainable: creating production chain transparency and accountability. Journal of Cleaner Production, 15(6), 577-589.
7. Thompson, B. S., & Rust, S. (2023). Blocking blockchain: Examining the social, cultural, and institutional factors causing innovation resistance to digital technology in seafood supply chains. Technology in Society, 73, 102235.
8. Surya, T., Sivaraman, B., Alamelu, V., Priyatharshini, A., Arisekar, U., & Sundhar, S. (2019). Rapid methods for histamine detection in fishery products. Int. J. Curr. Microbiol. Appl. Sci, 8, 2035-2046.
9. Debeer, John & Bell, Jon & Nolte, Fred & Arcieri, Julian & Correa, Gerson. (2021). Histamine Limits by Country: A Survey and Review. Journal of Food Protection. 84. 10.4315/JFP-21-129.

Perilla Seed Residue Ameliorates the Development of Insulin Resistance in Rats

Pattharaphong Deethai and Teera Chewonarin*
Department of Biochemistry, Faculty of Medicine, Chiang Mai University, Chiang Mai 50200, Thailand
*Corresponding author's email: teera.c@cmu.ac.th

Abstract:

Seed residue of *Perilla frutescens* from oil production contains high in bioactive phytochemicals, including luteolin, rosmarinic acid, and apigenin. The residue also still contains a variety of biological activities. This study explored the preventive effects and proposed mechanisms of perilla seed residue crude extract (PCE) against insulin resistance in rats fed high-fat diet (HFD). Male Wistar rats were divided into 4 groups, with 8 rats in each group: normal group, HFD control group, and HFD groups with PCE administered at low (100 mg/kg.bw) and high (1,000 mg/kg.bw) doses daily for 4 weeks. During 10 weeks of experiment, fasting blood sugar was measured weekly, and the oral glucose tolerance test (OGTT) was determined in the last week before sacrifice. Fat pads and liver were collected and weighed to calculate relative organ index, and the serum was measured for fasting insulin and determined systemic oxidative stress-related molecules, including malondialdehyde (MDA) and antioxidant capacity. The results showed that PCE treatment significantly mitigated the weight gain typically induced by HFD, reduced fat pads size, and lowered fasting blood sugar levels. Additionally, PCE reduced insulin secretion, leading to the improvement of HOMA-IR values significantly compared to normal controls. PCE also reduced oxidative stress by increasing antioxidant capacity and reducing the level of MDA. These findings suggested that PCE could prevent insulin resistance in rats fed with HFD by its phytochemical properties. Therefore, the mechanisms of perilla seed residue as a therapeutic intervention to obesity and insulin resistance will be further investigated.

Keywords: Insulin resistance; Oxidative stress; Obesity; *Perilla frutescens*; Antioxidant

Introduction

Insulin resistance is a condition in which the body's cells do not respond effectively to insulin. Although insulin resistance may initially be a transient condition; however, it may progress to type 2 diabetes if left untreated (1). High-fat diet (HFD) consumption is a key factor that contributes to obesity and insulin resistance. Obesed adipocytes secrete adipokines, which stimulate macrophages that trigger inflammation within the adipose tissue and contribute to the development of insulin resistance (2). Therefore, contoling of bodyweight and consumption of healthy foods are one of the ways to protect obesity and insulin resistance (3). Importantly, antioxidant and anti-inflammatory effects within adipose tissue may reduce the risk of developing insulin resistance. *Perilla frutescens* is a local herb that is rich in nutrients in every parts. The leaves exhibit high concentrations of antioxidants and phytochemicals, along with potential anti-inflammatory properties, such as apigenin, caffeic acid, catechin, ferulic acid, luteolin, rosmarinic acid, and ursolic acid (4). The seeds are also abundant in fatty acids, proteins, carbohydrates, and other phytochemicals similar to those found in the leaves. After oil isolation from the seeds, the residual material, still remains high in bioactive phytochemicals like luteolin, rosmarinic acid, and apigenin (5). Thomas and colleagues demonstrated that this residue possesses beneficial properties that may aid in managing obesity and insulin resistance (6). Moreover, this phystochemials in seed residue exhibit anti-inflammation and antioxidant properties (5). However, the potential effects of perilla seed residue on obesity-related insulin resistance have not been clearly reported. Therefore, this study aims to explore whether seed residue can prevent insulin resistance. Specifically, the effects of the extract from perilla seed residue crude extract (PCE) on the growth, fat accumulation the alteration of glucose metabolism in rats recieved HFD have been determined.

Materials and Methods

Perilla seed residue crude extract preparation

Hundred grams of dried perila seed residue was 1:10 extracted by 80% ethanol PCE. Dry powder of PCE was suspended in 10% DMSO to form an emulsion, which then was administered to experimental rats.

Animal model and treatment

Animal experiment protocol received ethical approval from the Faculty of Medicine, Chiang Mai University (No. 02/2567). Eight-weeks old male Wistar rats were housed and divided for 4 group with 8 rats each. Twenty-four of these rats were fed a high-fat diet for 6 weeks to increase bodyweight and insulin resistance, while Group 1 (8 rats) was maintained on a normal diet throughout the experiment. After the induction phase, the 24 rats were divided into 3 groups (Group 2-4), which were continuously fed a HFD. Group 2 served as the HFD control and was fed with 10% of DMSO. Groups 3 and 4 received HFD along with low (100 mg/kg.bw) and high (1,000 mg/kg.bw) concentrations of PCE, respectively, every day for 4 weeks.

The rats were weighed weekly, and fasting blood glucose levels at week 0, 1, 3, and 5 before PCE administration, and at week 6 to 10 during PCE treatment were measured using a glucose meter. A glucose tolerance test was conducted on the last day of the experiment, according to the method of Tang et al.(7). At the day before sacrifice, all rats were fasted for 12 hours, blood was collected from portal vein. Liver and epididymal fat pads were also collected.

Determination of obesity, glucose homeostasis and oxidative stress

Fasting blood sugar levels was measured weekly by glucometer (Pharmahof, Taiwan), and on the last day, glucose utilization will be assessed by conducting an Oral Glucose Tolerance Test (OGTT). Additionally, insulin levels in serum were determined using ELISA kit (Merck Millipore, USA) to calculate the Homeostatic Model Assessment for Insulin Resistance (HOMA-IR), according to the method of Sama et al. (8) and calculate using formula as show in Formula 1. Serum antioxidant capacity will be determined using the ABTS (2,2'-azino-bis(3-ethylbenzothiazoline-6-sulfonic acid)) assay (9), while oxidative stress was assessed through the serum level of MDA (malondialdehyde) measurement (10).

Formula 1: HOMA-IR calculation

$$\text{HOMA-IR} = \frac{\text{HOMA-IR score Fasting insulin serum (ng/ml) x Fasting blood glucose (mg/dl)}}{405.1} \quad (1)$$

Statistical Analysis

All calculations were done using Microsoft excel and presented as mean ± SD. The statistical analysis for significant differences between all data was analyzed using Prism version 9.5 (GraphPad Software, Canada) with one-way ANOVA and Bonferroni which applied at $p \leq 0.05$ level

Results and Discussion

Effect of PCE on body weight, fasting blood sugar and insulin

The results showed that HFD-fed rat (531 ± 30 g) had significantly increased body weight compared to the normal control group (486 ± 37 g) at week 10, when fed both 100 and 1,000 mg/kg.bw of PCE extract, rats resisted weight gain (470 ± 20 and 468 ± 42 g, respectively) compared to rat fed HFD alone as show in **Figure 1**. Specifically, the HFD group demonstrated markedly elevated fasting blood sugar levels (116±5 mg/dl) as well as insulin levels (4.9±2 ng/ml) when compared to the normal group (normal fasting blood 103±5 mg/dl and insulin 3.6±1 ng/ml). The results are in accordance with the research of Liu *et al.* (11). This suggested that rats fed HFD for 4 weeks or more developed impairments in glucose tolerance and increase weight gain more than normal diet rats. Feeding rats with PCE at 100 and 1,000 mg/kg.bw significantly reduced fasting blood sugar (100±7 and 100±2 mg/dl, respectively) and insulin (3.1±0.8 and 3.4±0.9 ng/ml,

respectively) when compared to rat fed HFD alone as show in **Figure 2 (A and B)**. Moreover, HFD control rats had significantly higher HOMA-IR values (1.4±0.6) compared to the normal control group (0.8±0.3). However, the PCE extract at doses of 100 and 1,000 mg/kg.bw significantly reduced HOMA-IR values (0.7±0.2 and 0.8±0.2, respectively) compared to the HFD control group as show in **Figure 2 (C)**. These results indicated that PCE prevent the increasing in body weight from HFD induce that might led to reduce insulin resistance.

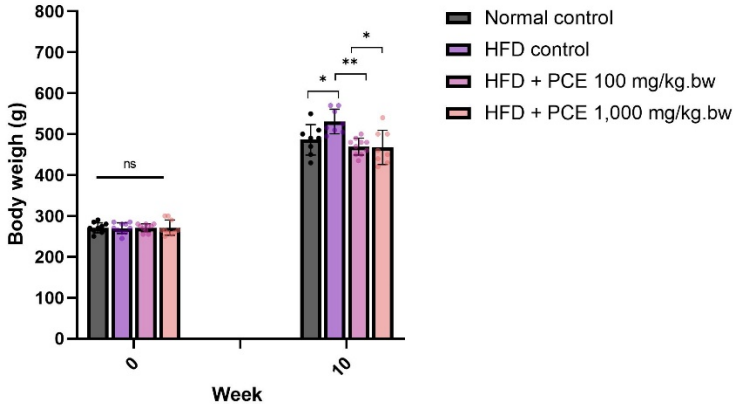

Figure 1. Effect of PCE on body weight. Results were presented as mean ± standard deviation (n = 8 each group). *p<0.05, **p<0.01, ***p <0.001

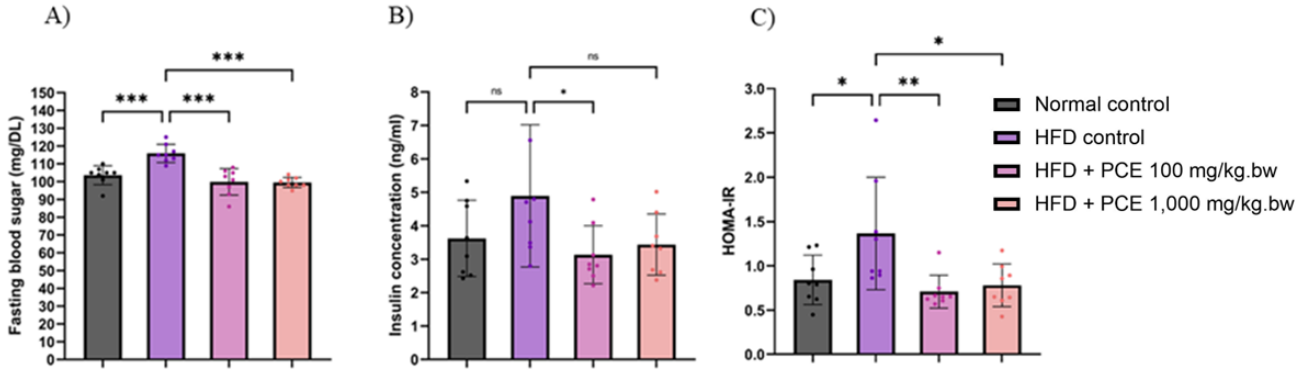

Figure 2. Effect of PCE on (A) serum fasting blood sugar, (B) fasting insulin and (C) calculated HOMA-IR value. Results were presented as mean ± standard deviation (n = 8 each group). *p<0.05, **p<0.01, ***p <0.001

Effect of PCE on improve glucose utilization by OGTT

The results from OGTT curves were calculated for area under curve (AUC) and presented in **Figure 3**. Rats received HFD showed similar in rising phase at 60 min, but the AUC was higher when compared to normal rats. The AUC in the group received HFD with PCE 100 and 1,000 mg/kg.bw groups showed a downward trend of AUC compared to the HFD control group (**Figure 3B**). These results indicate that PCE reduced fasting blood glucose (FBG) levels and improved glucose tolerance in HFD treated rats. Therefore, rats received HFD exhibited mild insulin resistance. It might be related to the increasing of visceral fats and the inflammation.

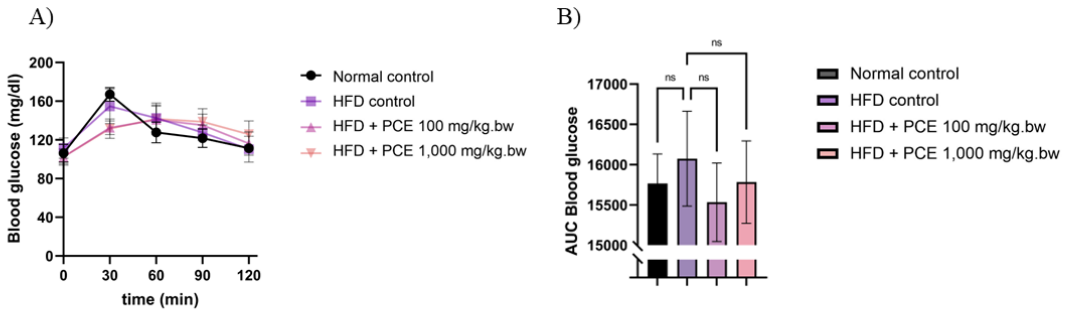

Figure 3. Effect of PCE on glucose utilization presented by (A) oral glucose tolerance curved (OGTT) and (B) calculated area under OGTT curve (AUC). Results were presented as mean ± standard deviation (n = 8 each group). *p<0.05, **p<0.01, ***p <0.001

Effect of PCE on relative liver and fat pads weight

The relative weight of fat pads demonstrated that rats recieved HFD control group had a significantly increased fat pads mass (75±10 g) compared to the normal group (56±9 g). HFD is a key factor for increasing body weight and all fat composition in rat body according to an increasing of calories from fat. Although PCE treatment at both concentrations tended to reduce this fat mass ratio (67±9 and 64±14 g in 100 and 1,000 mg/kg.bw of PCE, respectively), the reduction was not statistically significant when compared to the HFD control group. According to one study reported that after 6 weeks on an HFD, the epididymal fat pads weight increased by approximately 100%, mesenteric fat pads by 90%, and perirenal fat pads by 134% as well as liver (29±1 g) compared to control groups fed a normal diet (26±2 g) (12). However, treatment with PCE at both 100 and 1,000 mg/kg.bw of PCE significantly reduced the liver-to-body mass ratio (26±2 and 26±2 g, respectively) compared to the HFD control group as show in **Figure 4**. These results demonstrated that PCE treatment could reduce fat accumulation in adipose tissue and might prevent HFD-induced fat deposit in liver. The fat content in liver should be measured, according to a report from Di Majo D *et.al.* that showed HFD substantially increase fat accumulation in the liver of rats, leading to conditions such as hepatic steatosis and potentially progressing to more severe liver diseases due to associated oxidative stress and inflammation in rats (13).

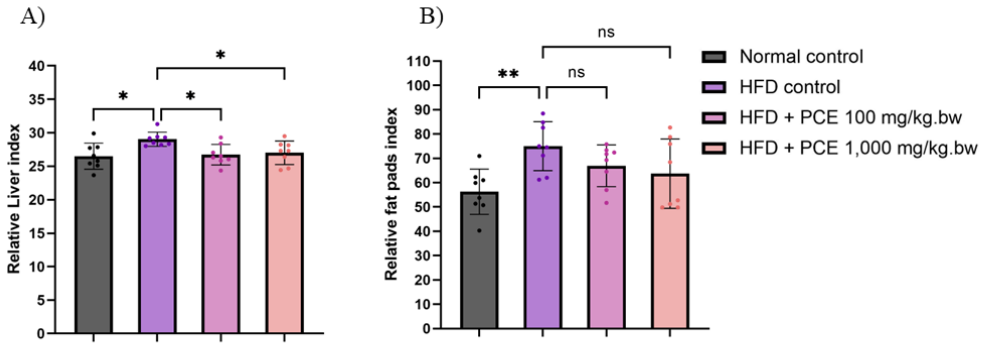

Figure 4. Effect of PCE on relative organ weights of (A) liver and (B) fat pads. Results were presented as mean ± standard deviation (n = 8 each group). *p<0.05, **p<0.01, ***p <0.001

Effect of PCE on systemic oxidative stress

Total antioxidant capacity in rat serum revealed that the HFD control group (93±3 %) had lower antioxidant capacity compared to normal rats (100±3 %). This might cause from the increasing of oxidative stress which showed in the higher level of MDA (1.4±0.4 µM) compared to normal rats (1.1±0.3 µM), according to Pieri, et al. (14). This suggests that HFD can induce oxidative stress that showed decreasing antioxidant capacity and increasing lipid peroxidation in rats. However, when

PCE was administered at both 100 and 1,000 mg/kg.bw, only the 1,000 mg/kg.bw of PCE (99±4 %) significantly increased antioxidant levels compared to the HFD control group. Similarly, the administration of both doses of PCE could reduce the level of serum MDA (1.1±0.2 and 1.0±0.2 µM, respectively) with related to their antioxidant capacity but significant difference were not observed as show in **Figure 5**. This results were similar to pevious report of Furukawa S *et.al.* They demonstrated that the preventing weight gain and reducing relative fat pad size can significantly reduce oxidative stress from production of pro-inflammatory cytokines and improved antioxidant enzyme activity in rats fed a HFD (15).

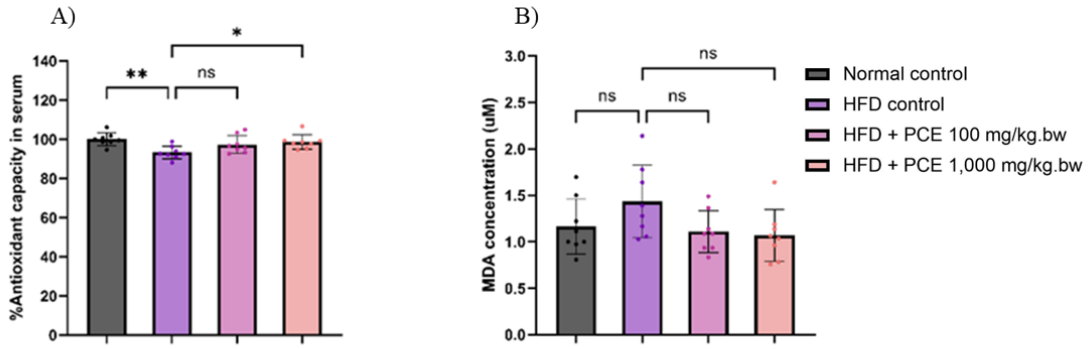

Figure 5. Effect of PCE on (A) serum antioxidant capacity and (B) MDA level. Results were presented as mean ± standard deviation (n = 8 each group). *p<0.05, **p<0.01, ***p <0.001

Conclusion

Perilla seed residue crude extract (PCE) showed the ability to prevent the development of early-insulin resistance induced by a high-fat diet. Administration of PCE can improve glucose utilization that might cause from the reduction of oxidative stress from hypertrophy of adipose tissue in HFD-rats. The underlying mechanism will be further investigated.

Conflict of interest statement

The authors declare that they have no conflicts of interest.

Acknowledgements: This writing of this article was supported by Fundamental Fund (FF67), 2023, Chiang Mai University, Thailand.

References

1. Lee SH, Park SY, Choi CS. Insulin Resistance: From Mechanisms to Therapeutic Strategies. Diabetes Metab J. 2022;46(1):15-37.
2. Ouchi N, Parker JL, Lugus JJ, Walsh K. Adipokines in inflammation and metabolic disease. Nat Rev Immunol. 2011;11(2):85-97.
3. Klein S, Sheard NF, Pi-Sunyer X, Daly A, Wylie-Rosett J, Kulkarni K, et al. Weight management through lifestyle modification for the prevention and management of type 2 diabetes: rationale and strategies: a statement of the American Diabetes Association, the North American Association for the Study of Obesity, and the American Society for Clinical Nutrition. Diabetes care. 2004;27(8):2067-73.
4. Adam G, Robu S, Flutur M-M, Cioanca O, Vasilache I-A, Adam A-M, et al. Applications of *Perilla frutescens* Extracts in Clinical Practice. Antioxidants. 2023;12(3):727.
5. Chantana W, Hu R, Buddhasiri S, Thiennimitr P, Tantipaiboonwong P, Chewonarin T. The Extract of P*erilla frutescens* Seed Residue Attenuated the Progression of Aberrant Crypt Foci in Rat Colon by Reducing Inflammatory Processes and Altered Gut Microbiota. Foods. 2023;12(5):988.

6. Thomas SS, Kim M, Lee SJ, Cha YS. Antiobesity effects of purple perilla (*Perilla frutescens* var. acuta) on adipocyte differentiation and mice fed a high-fat diet. Journal of food science. 2018;83(9):2384-93.
7. Tang D, Liu L, Ajiakber D, Ye J, Xu J, Xin X, et al. Anti-diabetic effect of *Punica granatum* flower polyphenols extract in type 2 diabetic rats: Activation of Akt/GSK-3β and inhibition of IRE1α-XBP1 pathways. Frontiers in endocrinology. 2018;9:586.
8. Sama S, Jain G, Kant R, Bhadoria AS, Naithani M, Kumar A. Quantifying the Homeostatic Model Assessment of Insulin Resistance to Predict Mortality in Multi-organ Dysfunction Syndrome. Indian Journal of Critical Care Medicine: Peer-reviewed, Official Publication of Indian Society of Critical Care Medicine. 2021;25(12):1364.
9. Re R, Pellegrini N, Proteggente A, Pannala A, Yang M, Rice-Evans C. Antioxidant activity applying an improved ABTS radical cation decolorization assay. Free radical biology and medicine. 1999;26(9-10):1231-7.
10. Chaiyasut C, Kusirisin W, Lailerd N, Lerttrakarnnon P, Suttajit M, Srichairatanakool S. Effects of phenolic compounds of fermented Thai indigenous plants on oxidative stress in streptozotocin-induced diabetic rats. Evidence-Based Complementary and Alternative Medicine. 2011;2011(1):749307.
11. Liu S, Duan R, Wu Y, Du F, Zhang J, Li X, et al. Effects of vaspin on insulin resistance in rats and underlying mechanisms. Scientific reports. 2018;8(1):13542.
12. Charradi K, Elkahoui S, Limam F, Aouani E. High-fat diet induced an oxidative stress in white adipose tissue and disturbed plasma transition metals in rat: prevention by grape seed and skin extract. The journal of physiological sciences. 2013;63:445-55.
13. Di Majo D, Sardo P, Giglia G, Di Liberto V, Zummo FP, Zizzo MG, et al. Correlation of metabolic syndrome with redox homeostasis biomarkers: evidence from high-fat diet model in wistar rats. Antioxidants. 2022;12(1):89.
14. Pieri BLdS, Rodrigues MS, Farias HR, Silveira GdB, Ribeiro VdSGdC, Silveira PCL, et al. Role of Oxidative Stress on Insulin Resistance in Diet-Induced Obesity Mice. International Journal of Molecular Sciences. 2023;24(15):12088.
15. Furukawa S, Fujita T, Shimabukuro M, Iwaki M, Yamada Y, Nakajima Y, et al. Increased oxidative stress in obesity and its impact on metabolic syndrome. The Journal of clinical investigation. 2017;114(12):1752-61.

Cytotoxic Activity of Beta-Caryophyllene on MRC5 and A549 Cell Lines and Its *In Vitro* Antioxidant Properties

Chanachinat Booraphet[1], Wanwipha Woonnoi[1], Wiwit Suttithumsatid[2], Supita Tanasawet[1], and Wanida Sukketsiri[1,*]

[1] Division of Health and Applied Sciences, Faculty of Science, Prince of Songkla University, Hat Yai, Songkhla, 90110, Thailand

[2] Department of Pharmacognosy and Pharmaceutical Botany, Faculty of Pharmaceutical Sciences, Prince of Songkla University, Songkhla, 90110, Thailand

*Corresponding author's email: wanida.su@psu.ac.th

Abstract:

There is currently an increasing emphasis on studying the health benefits of important natural substances. β-caryophyllene (BCP), a natural bicyclic sesquiterpene and a major component of essential oil, exhibits a variety of effects, including anti-inflammatory, anticancer, and antioxidant properties. Antioxidants play a crucial role in combating age-related issues, inflammation, and oxidative stress. This study investigates the *in vitro* antioxidant effects of BCP and assesses its cytotoxicity on MRC5 and A549 cells. The antioxidant activity of BCP was assessed at 0-5.0 mM using the ABTS assay, with vitamin C as a positive control. Cell viability at 0-1000 µM was evaluated over 72 hours using the MTT assay for MRC5 and A549 cells. The results indicated that BCP significantly increased free radical scavenging at concentrations of 0.01, 0.05, 0.1, 0.5, 1.0, and 5.0 mM compared to the negative control. BCP was found to be safe for MRC5 cells at concentrations of 1, 5, 10, 25, 50, 100, 250, 500, and 1000 µM, with cell viability reaching up to 95%, indicating non-toxicity to normal cells. In contrast, BCP decreased the viability of A549 cells; however, cell viability remained above 80%. Notably, concentrations of 5 and 250 µM resulted in cell viability of approximately 70%, indicating mild toxicity to the cancer cells. In conclusion, BCP demonstrates antioxidant properties and exhibits cytotoxicity toward cancer cells without affecting normal cells. Future research should investigate the potential pharmacological effects of BCP on cancer cells.

Keyword: β-caryophyllene; Antioxidant; MRC5; A549; Cytotoxicity

Introduction

BCP is a naturally occurring bicyclic sesquiterpene found in various essential oils, particularly in clove oil derived from the stems and flowers of *Syzygium aromaticum*. It is also present in the essential oils of copaiba, hops, cinnamon, black pepper, rosemary, and *Cannabis sativa* (1). The U.S. Food and Drug Administration (FDA) has approved BCP as a food additive, taste enhancer, and natural flavoring agent (2, 3).

BCP demonstrates a variety of pharmacological effects, including anti-inflammatory, cytotoxic, antioxidant, antispasmodic, anticancer, antimicrobial, hypolipidemic, and neuroprotective properties (4-8). These characteristics underscore its potential for further investigation in the treatment of liver cancer. Studies have indicated that related compounds, such as cedrol- a sesquiterpene lactone- can inhibit the proliferation of human leukemia and colorectal carcinoma cells by reducing oxidative stress and inflammation while promoting apoptosis (4). Additionally, BCP has been shown to protect liver cells against fibrosis induced by carbon tetrachloride (5). Moreover, BCP significantly diminishes inflammation and modulates the immune response in chronic inflammatory conditions (6).

However, the effects of BCP on lung cancer therapy remain unclear. Therefore, this study aims to elucidate the antioxidant effects of BCP as well as its cytotoxicity on normal MRC5 cells and the lung adenocarcinoma A549 cell line.

Materials and Methods

Cell Culture and Chemical

The A549 cell line (lung carcinoma epithelial cells) and the MRC5 cell line (human fetal lung fibroblast cells) were obtained from ATCC in the USA. Both cell lines were cultured in Dulbecco's Modified Eagle Medium (DMEM), enriched with 10% fetal bovine serum, 1% L-glutamine, and 1% penicillin (100 units/mL) along with streptomycin (100 mg/mL). The cells were incubated at 37 ºC in a 5% CO_2 environment, with media changes occurring every 3 to 4 days. BCP was sourced from Nacalai Tesque, Inc. in Kyoto, Japan. DMEM, fetal bovine serum, antibiotics (streptomycin and penicillin), L-glutamine, and trypsin-EDTA were acquired from Gibco (Waltham, MA, USA). Vitamin C, dimethyl sulfoxide (DMSO), 2,2'-azino-bis-3-ethylbenzothiazoline-6-sulphonic acid (ABTS), and 3-(4,5-dimethylthiazolyl-2)-2,5-diphenyltetrazolium bromide (MTT) were obtained from Sigma (St. Louis, MO, USA).

ABTS Free Radical Scavenging Assay

The antioxidant activity of BCP and vitamin C was evaluated using the ABTS assay. This method utilizes the oxidized ABTS radical cation ($ABTS^{\bullet+}$) to react with antioxidants, resulting in the reduction of the ABTS radical and a corresponding color change from blue-green to a lighter hue (7). For the assay, a 0.7 mM solution of $ABTS^{\bullet+}$ was prepared, and 90 µL of this solution was added to 96-well plates. BCP was tested at concentrations of 0, 0.01, 0.05, 0.1, 0.5, 1.0 and 5.0 mM (with a control consisting of 10 µL of ethanol), while vitamin C was tested at concentrations of 0, 0.0057, 0.028, 0.057, 0.28, and 0.57 mM (with a control consisting of 10 µL of distilled water). The mixture was subsequently incubated in the dark at room temperature on a shaker for 30 minutes. After incubation, absorbance was measured at a wavelength of 734 nm using a microplate reader. Each experiment was conducted in triplicate. The radical scavenging activity was calculated using the following formula: % Scavenging = $[(Abs_0 - Abs_1) / Abs_1] \times 100$, where Abs_0 represents the absorbance of the control and Abs_1 denotes the absorbance of the test compound at varying concentrations.

Cytotoxicity of BCP by MTT Assay

The cytotoxicity of BCP was assessed using the MTT assay, which measures cell viability and metabolic activity by detecting formazan crystals (purple color) produced from mitochondrial activity. The intensity of the formazan color is directly proportional to cell viability (8). A549 and MRC5 cells were seed in 96 well-plates at a density 1×10^4 cell/well and incubated overnight under conditions of 37˚C, 5%CO_2, and 95% humidity in DMEM medium. Following incubation, the cells were treated with 20 µL of BCP at concentrations of 0, 1, 5, 10, 25, 50, 100, 250, 500, and 1000 µM for a duration of 72 hours. After this period, MTT solution was added to assess cell viability in the BCP-treated cells. A concentration of 0.5 mg/mL of MTT solution was prepared in DMEM without serum and incubated for 2 hours. Subsequently, 100 µL of DMSO was added to each well to dissolve the formazan crystals. Finally, cell viability was measured by recording the absorbance at 570 nm using a microplate reader. Cytotoxicity was calculated using the formula: Cell viability (%) = $(Abs_1\times100)/Abs_0$, where Abs_0 represents the absorbance of the control and Abs_1 denotes the absorbance of the test compound at various concentrations.

Statistical Analysis

All results are presented as mean ± standard error of the mean (SEM). The data reported are based on at least three or four independent experiments. Statistical analysis was performed using one-way ANOVA, followed by the Duncan tests, utilizing SPSS version 16.0. A p-value of less than 0.05 was deemed statistically significant.

Results and Discussion

Determination of antioxidant activity pf BCP by ABTS scavenging assay

The ABTS scavenging activity of BCP was assessed to evaluate its antioxidant capacity. The percentage of ABTS scavenging activity showed a significant increase in relation to the concentration of BCP. At a concentration of 5 mM, BCP demonstrated the highest ABTS scavenging value at 18.70% (Figure 1A) However, vitamin C, recognized as a standard antioxidant, exhibited greater ABTS scavenging activity compared to BCP (Figure 1B). These findings indicate that BCP possesses antioxidant activity by scavenging free radicals, with the IC50 value for BCP being higher than 5 mM. The antioxidant activity of BCP has been previously documented, with IC_{50} values from the 2,2-Diphenyl-1-picrylhydrazyl (DPPH) assay and the ferric reducing antioxidant ability (FRAP) assay reported as 1.25 ± 0.06 and 3.23 ± 0.07 μM, respectively. The IC_{50} value of BCP using DPPH assay was also noted to be 132 μg/mL at low concentration (5). Additionally, BCP effectively enhances scavenging activity against hydroxyl radicals, exhibiting scavenging activities of 53.8% and 56.8% at concentrations of 1 μM and 10 μM, respectively. For superoxide anion radical scavenging activity, concentrations of 0.1, 1, 5 and 10 μM resulted in activities of 20.1%, 91.5%, 131.2% and 205.9%, respectively. Furthermore, BCP has been shown to inhibit superoxide anion-dependent cytochrome c release and reduce lipoxygenase-dependent oxidation of linoleic acid, supporting its role as a potent antioxidant (5). These findings are consistent with the results of this study, further confirming that BCP possesses antioxidant properties. The evaluation of BCP's antioxidant capacity using ABTS assays highlights its potential therapeutic applications in combating oxidative stress-related conditions. Overall, the evidence suggests that BCP could be a valuable compound for developing antioxidant therapies.

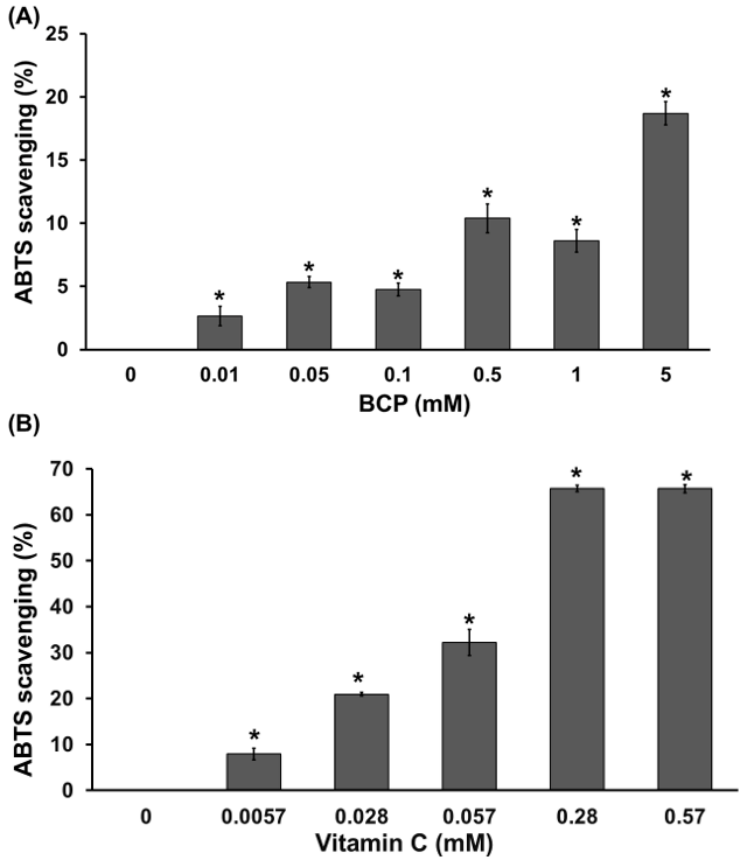

Figure 1. ABTS scavenging activity of BCP, with vitamin C serving as a positive control. (A) ABTS scavenging of BCP. (B) ABTS scavenging of vitamin C The mean values are shown, and the error bars represent the standard error of the mean (n = 3). *$p < 0.05$ when compared to the 0 μg/mL group.

Cytotoxicity of BCP by MTT assay

This study examines the in vitro cytotoxicity of BCP in MRC5 and A549 cells. Evaluating the toxicity of natural product extracts or bioactive compounds is essential, particularly regarding their potential use in human health. Such assessments raise important safety considerations in the development of new drugs or nutraceuticals (9, 10). The cytotoxicity results demonstrated the percentage of cell viability in both MRC5 and A549 cell lines following treatment with various concentrations of BCP (0, 1, 5, 10, 25, 50, 100, 250, 500, and 1000 µM; with 0 µM serving as the negative control containing only media). MRC5 cells, which are normal lung fibroblasts, maintained up to 95% viability across all BCP concentrations, suggesting that BCP is non-toxic to these cells (Figure 2A). In contrast, A549 lung cancer cells exhibited a lower viability of 85% at concentrations of 1, 10, 25, 50, 100, 500, and 1000 µM. Additionally, at concentrations of 5 and 250 µM, cell viability decreased to approximately 70%, indicating mild toxicity (Figure 2B). However, the cytotoxicity of BCP against other lung cancer cell lines should be further confirmed. This study suggests that while BCP can reduce the proliferation of lung cancer cells, it does so without being overtly harmful at lower doses. BCP has garnered attention for its potential cytotoxic effects on various cancer cells, including lung cancer and hepatocellular carcinoma (2,15). Moreover, BCP has been found to enhance the efficacy of traditional chemotherapeutic agents such as cisplatin. When combined with cisplatin, BCP not only improved the anti-tumor activity of the chemotherapy but also reduced the effective dose required for cytotoxicity (15). In normal cells, BCP has been shown to protect CFSC-2G hepatic stellate cells from oxidative stress, where cell survival decreased to 93.3% without treatment. However, when these cells were exposed to BCP at concentrations of 1 and 10 µM, survival rates increased to 98.8% and 99.3%, respectively, indicating a significant protective effect against oxidative damage (10). This suggests that BCP can be safely used without adversely affecting cell viability in normal cells, which aligns with our study's findings. Overall, BCP demonstrates promising cytotoxicity against lung cancer cells while exhibiting minimal toxicity to normal cells at moderate doses.

Conclusion and Suggestion

The study revealed that BCP exhibits antioxidant activity by promoting free radical scavenging. Additionally, the findings suggest that BCP demonstrates promising cytotoxicity against lung cancer cells while exhibiting minimal toxicity to normal cells at moderate doses. Future research should focus on examining the additional effects of BCP, including its molecular mechanisms of action and its effectiveness in various biological models. Furthermore, investigating the potential applications of BCP in the development of therapeutic products, nutraceuticals, or functional foods could provide important insights into its health benefits for humans.

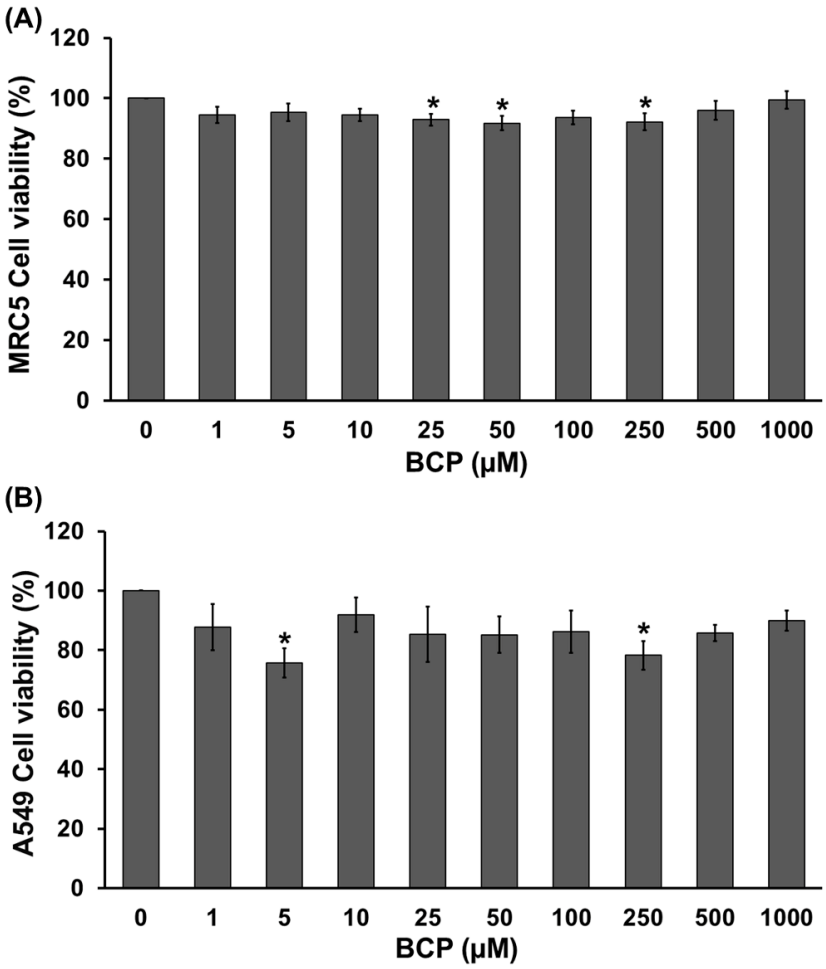

Figure 2. Cytotoxicity of BCP in MRC5 and A549 cells. (A) MRC5 cell line and (B) A549 cell line. The cells were treated with BCP at concentrations of 0, 1, 5, 10, 25, 50, 100, 250, 500, and 1000 μM for 72 hours. Cell viability was evaluated using the MTT assay. The results are expressed as mean ± SEM from four independent experiments. *$p < 0.05$ compared to the untreated control group.

Acknowledgements

Chanachinat Booraphet was supported as a research assistant from Faculty of Science Research Fund (Contract no.1-2566-02-029), Prince of Songkla University, Songkhla, Thailand.

References

1. Maffei, M. E. Plant Natural Sources of the Endocannabinoid (E)-β-Caryophyllene: A Systematic Quantitative Analysis of Published Literature. Int J Mol Sci 2020; 21(18).
2. Ahmad, Z., Jain, S. K., & Mishra, S. K. Beta-caryophyllene attenuates experimental hepatocellular carcinoma through downregulation of oxidative stress and inflammation. J Biochem Mol Toxicol 2024; 38(10): e23850.
3. Fidyt, K., Fiedorowicz, A., Strządała, L., & Szumny, A. β-caryophyllene and β-caryophyllene oxide-natural compounds of anticancer and analgesic properties. Cancer Med2016; 5(10): 3007-3017.
4. Dickson, K., et al., Antibacterial and Analgesic Properties of Beta-Caryophyllene in a Murine Urinary Tract Infection Model. Molecules, 2023. 28(10): p. 4144.
5. Dahham, S.S., et al., β-Caryophyllene Induces Apoptosis and Inhibits Angiogenesis in Colorectal Cancer Models. Int J Mol Sci, 2021. 22(19).

6. Francomano, F., Caruso, A., Barbarossa, A., Fazio, A., La Torre, C., Ceramella, J., Mallamaci, R., Saturnino, C., Iacopetta, D., & Sinicropi, M. S. β-Caryophyllene: A Sesquiterpene with Countless Biological Properties. Applied Sciences 2019; 9(24): 5420.
7. Scandiffio, R., Geddo, F., Cottone, E., Querio, G., Antoniotti, S., Gallo, M. P., Maffei, M. E., & Bovolin, P. Protective Effects of (E)-β-Caryophyllene (BCP) in Chronic Inflammation. Nutrients 2020; 12(11): 3273.
8. Gushiken, L.F.S., et al., Beta-caryophyllene as an antioxidant, anti-inflammatory and re-epithelialization activities in a rat skin wound excision model. Oxid Med Cell Longev 2022; p. 9004014.
9. Mishra, S. K., Bae, Y. S., Lee, Y. M., Kim, J. S., Oh, S. H., & Kim, H. M. Sesquiterpene Alcohol Cedrol Chemosensitizes Human Cancer Cells and Suppresses Cell Proliferation by Destabilizing Plasma Membrane Lipid Rafts. Front Cell Dev Biol 2020 ; 8: 571676.
10. Calleja, M. A., Vieites, J. M., Montero-Meterdez, T., Torres, M. I., Faus, M. J., Gil, A., & Suárez, A. The antioxidant effect of β-caryophyllene protects rat liver from carbon tetrachloride-induced fibrosis by inhibiting hepatic stellate cell activation. British Journal of Nutrition 2013; 109(3): 394-401.
11. Cano, A., Maestre, A. B., Hernández-Ruiz, J., & Arnao, M. B. ABTS/TAC Methodology: Main Milestones and Recent Applications. Processes 2023; 11(1): 185.
12. Ghasemi, M., Turnbull, T., Sebastian, S., & Kempson, I. The MTT Assay: Utility, Limitations, Pitfalls, and Interpretation in Bulk and Single-Cell Analysis. Int J Mol Sci 2021; 22(23).
13. Aenglong, C., Woonnoi, W., Tanasawet, S., Klaypradit, W., & Sukketsiri, W. Impact of Time and Enzyme Concentration on Sangyod Rice Bran Hydrolysate: Phytochemicals, Antioxidants, Amino Acids, and Cytotoxicity. Rice (N Y) 2024; 17(1): 13.
14. Morobe, I., Mthethwa, N., Bisi-Johnson, M., Vasaikar, S., L, O., Oyedeji, A., Kambizi, L., Eloff, J., & Hattori, T. Cytotoxic Effects and Safety Profiles of Extracts of Active Medicinal Plants from South Africa. Journal of Microbiology Research 2012; 2: 176-182.
15. Ahmed EA, Abu Zahra H, Ammar RB, Mohamed ME, Ibrahim HM. Beta-Caryophyllene Enhances the Anti-Tumor Activity of Cisplatin in Lung Cancer Cell Lines through Regulating Cell Cycle and Apoptosis Signaling Molecules. Molecules 2022; 27(23):8354.

Antioxidant Properties and Cytotoxic Effects of Sangyod Rice Extract and Rice Bran Extract on Skin Keratinocytes

Nattawadee Yingbut[1], Wanwipha Woonnoi[1], Wiwit Suttithumsatid[2], Supita Tanasawet[1], and Wanida Sukketsiri[1,*]

[1]Division of Health and Applied Sciences, Faculty of Science, Prince of Songkla University, Hat Yai, Songkhla, 90110, Thailand

[2]Department of Pharmacognosy and Pharmaceutical Botany, Faculty of Pharmaceutical Sciences, Prince of Songkla University, Songkhla, 90110, Thailand

*Corresponding author's email: wanida.su@gmail.com

Abstract:

Sangyod Rice (*Oryza sativa* L.) is a staple crop in Asia and is recognized for its significance as a primary global food source. Previous research has identified various bioactive compounds in Sangyod Rice, including phenolic compounds, flavonoids, gamma-aminobutyric acid, oryzanol, and anthocyanins, which exhibit various pharmacological effects, such as antioxidant, antimicrobial, antifungal, antidiabetic, cancer chemoprotective, and hypolipidemic activities. This study investigates the antioxidant capabilities of Sangyod Rice Extract (SRE) and Sangyod Rice Bran Hydrolysate (SRB-H), as well as their cytotoxic effects on HaCaT human epidermal keratinocytes. We employed the DPPH assay, ABTS assay, and MTT assay for these evaluations. Our findings reveal that SRE significantly enhances both DPPH and ABTS scavenging activities in a dose-dependent manner at concentrations of 0, 0.1, 0.25, 0.5, 0.75, 1, and 1.5 mg/mL. Cytotoxicity assessments indicated that SRE concentrations ranging from 0-1000 µg/mL did not adversely affect the viability of HaCaT cells. In the DPPH assay for SRB-H, concentrations of 0, 0.1, 0.25, 0.5, and 0.75 mg/mL demonstrated antioxidant properties in a dose-dependent manner. However, higher concentrations (1 and 1.5 mg/mL) did not exhibit these effects, possibly due to interference from color changes in the method used. The ABTS assay confirmed that all tested concentrations of SRB-H enhanced antioxidant defense in a dose-dependent fashion. Cell viability results showed that SRB-H at concentrations of 10, and 50 µg/mL was non-toxic to HaCaT cells. However, doses of 100, 250, 500, and 1000 µg/mL significantly reduced cell viability, indicating ongoing cell injury leading to cell death. Therefore, future experiments should utilize safer concentrations to further explore the potential effects and mechanisms of action of SRE and SRB-H on HaCaT cells.

Keywords: Sangyod rice; Rice bran; Skin cells; HaCaT; Antioxidant

Introduction

Rice is an essential staple food worldwide, supporting a significant portion of the global population (1,2). Among the many rice varieties, Sangyod rice (*Oryza sativa* L.) is a distinctive type cultivated in southern Thailand, renowned for its unique red hue. This variety is primarily grown in the Songkhla Lake basin, which encompasses the provinces of Phatthalung, Nakhon Si Thammarat, and Songkhla (3,4). Sangyod rice is rich in essential nutrients, including carbohydrates, proteins, amino acids, and vitamins B1 and B2, which contribute to human health and development (5,6). Previous research has identified that Sangyod rice contains various bioactive compounds, including flavonoids, phenolics, gamma-aminobutyric acid, oryzanol, alkaloids, and glycosides. These compounds are linked to several pharmacological benefits, such as antioxidant properties, antifungal and antibacterial activities, and effects on insulin resistance (5,7,8). Additionally, our previous studies reported that the ethanolic extract from Sangyod rice has anti-obesity effects and reduces hepatic steatosis in diabetic rats (4,5).

Additionally, the rice milling process produces a significant amount of by-products, including husk, rice bran, and rice germ (3). Rice bran, which comprises the outer layers of the grain removed during milling, has historically been overlooked and primarily used as animal feed. However, recent studies have highlighted its untapped potential, demonstrating its value across various industries

(3,9). Our previous research indicated that Sangyod rice bran is rich in high-quality protein and essential amino acids, as well as a variety of flavonoids and phenolic compounds (3).

Despite their potential, the beneficial nutraceutical properties of Sangyod rice extract and hydrolysates derived from Sangyod rice bran are still largely unexplored and not well understood. Consequently, this study aims to investigate the antioxidant activity present in Sangyod rice extract (SRE) and Sangyod rice bran hydrolysate (SRB-H), as well as to evaluate their cytotoxic effects on HaCaT human epidermal keratinocytes.

Materials and Methods

Cell Culture and Extract

The HaCaT human keratinocyte cell lines (ATCC, USA) were cultured in high-glucose Dulbecco's Modified Eagle Medium, supplemented with 10% fetal bovine serum, 1% L-glutamine, and 1% penicillin (100 units/mL) and streptomycin (100 µg/mL), collectively referred to as complete medium. The cells were incubated in a 5% CO_2 atmosphere at 37 ºC, and the media were changed every 3 to 4 days. The preparation of SRE and SRB-H was described in our previous report (3,5).

Cell Viability Assay

The HaCaT cells were seeded at a density of 1.0×10^4 cells per well in 96-well plates and maintained in a complete medium for 24 hours. Subsequently, the cells were incubated with various concentrations of SRE (0, 10, 50, 100, 250, 500, and 1000 µg/mL) and SRB-H (0, 10, 50, 100, 250, 500, and 1000 µg/mL) for 72 hours. Cell cytotoxicity was then assessed using a 3-(4,5-dimethylthiazol-2-yl)-2,5-diphenyltetrazolium bromide (MTT) assay. The MTT solution was added at a concentration of 500 µg/mL, and the cells were then incubated in a 5% CO_2 atmosphere at 37 ºC for 2 hours. After incubation, dimethyl sulfoxide was added to solubilize the formazan. The absorbance of each well was measured at 570 nm using a microplate reader, and the results were expressed as the percentage of cell viability.

Determination of Antioxidant activity

***The 2,2-Diphenyl-1-picrylhydrazyl (DPPH) assay*:** The free radical scavenging capability of SRE (0, 0.1, 0.25, 0.5, 0.75, 1, and 1.5 mg/mL), SRB-H (0, 0.1, 0.25, 0.5, 0.75, 1, and 1.5 mg/mL), and vitamin C (0, 1, 5, 10, 50, and 100 µg/mL) were evaluated using the DPPH assay. The samples were mixed with 0.1 mM DPPH and incubated in the dark at room temperature for 30 minutes. The reduction of DPPH resulted in a color change from purple-pink to yellow. The absorbance of the DPPH radical reduction was measured at 517 nm using a microplate reader to assess scavenging activity. The percentage of inhibition was then calculated using the appropriate equation.

$$\text{Radical Scavenging activity (\%)} = [Abs_{blank} - (Abs_{sample} - Abs_{control})/Abs_{blank}]\times100$$

***The 2,2'-azino-bis-3-ethylbenzothiazoline-6-sulfonic acid (ABTS) assay*:** The free radical scavenging ability of SRE (0, 0.1, 0.25, 0.5, 0.75, 1, and 1.5 mg/mL), SRB-H (0, 0.1, 0.25, 0.5, 0.75, 1, and 1.5 mg/mL), and vitamin C (0, 1, 5, 10, 50, and 100 µg/mL) was assessed using the ABTS assay. The samples were mixed with a solution of 0.7 mM ABTS and incubated in the dark at room temperature for 30 minutes. The reduction of ABTS resulted in a color change from blue-green to clear. The absorbance of the reduced ABTS radical was measured at 734 nm using a microplate reader to evaluate scavenging activity, expressed as the percentage of inhibition calculated using the appropriate equation.

$$\text{Radical Scavenging activity (\%)} = [Abs_{blank} - (Abs_{sample} - Abs_{control})/Abs_{blank}]\times100$$

Statistical Analysis

The data were presented as the mean ± standard error of the mean (SEM). Group differences were analyzed using one-way ANOVA, followed by the post-hoc least significant difference (LSD) test. Statistical significance was determined with a p-value of less than 0.05.

Results and Discussion

Impact of SRB-H and SRE on the viability of human keratinocyte epidermal HaCaT cells

Assessing the toxicity of natural product extracts or bioactive compounds is essential, particularly in relation to their potential applications in human health (3). This study is the first to evaluate the cytotoxicity of the natural bioactive compounds SRE and SRB-H in HaCaT cells. HaCaT cells were treated with various concentrations of SRE (0, 10, 50, 100, 250, 500, and 1000 μg/mL) (Figure 1A) and SRB-H (0, 10, 50, 100, 250, 500, and 1000 μg/mL) (Figure 1B) for 72 hours. The results indicated that SRE did not significantly affect cell viability at any concentration (103.44 ± 3.25, 99.60 ± 4.19, 97.60 ± 3.71, 94.72 ± 3.77, 91.91 ± 3.81, and 91.86 ± 5.48), suggesting that it is non-toxic to HaCaT cells (Figure 1A). In contrast, SRB-H exhibited negligible effects on HaCaT cells at doses of 10, 50, and 100 μg/mL (102.84 ± 4.06, 85.86 ± 1.84, and 75.69 ± 1.80), but demonstrated mild toxicity at concentrations of 250, 500, and 1000 μg/mL (63.31 ± 1.57, 61.63 ± 2.67, and 55.96 ± 2.63) (Figure 1B). Consistent with previous study by Woonnoi et al. (4), which reported that concentrations of SRE ranging from 1 to 1000 μg/mL had no observable effects on the cell viability of preadipocyte 3T3-L1 cells. However, after treatment with SRE for 4 days, it was observed that SRE at a concentration of 100 μg/mL effectively decreased the cell viability of 3T3-L1 cell lines (4). Additionally, it has been reported that SRE affects the cell viability of an insulin-resistant HepG2 cell model, revealing that SRE at concentrations of 50 and 100 μg/mL did not impact cell viability (5). This finding is in linet with the results of our study. Figure 1A indicates that SRE concentrations ranging from 10 to 1000 μg/mL did not significantly reduce the viability of HaCaT cells. For hydrolyzed rice bran, Aenglong et al. (3) demonstrated the cytotoxicity of SRB-H at various concentrations ranging from 0 to 1000 μg/mL in myoblast C2C12 cells. Their findings showed that SRB-H consistently maintained cell viability above 70% across the tested concentration range, which aligns with the results of our study.

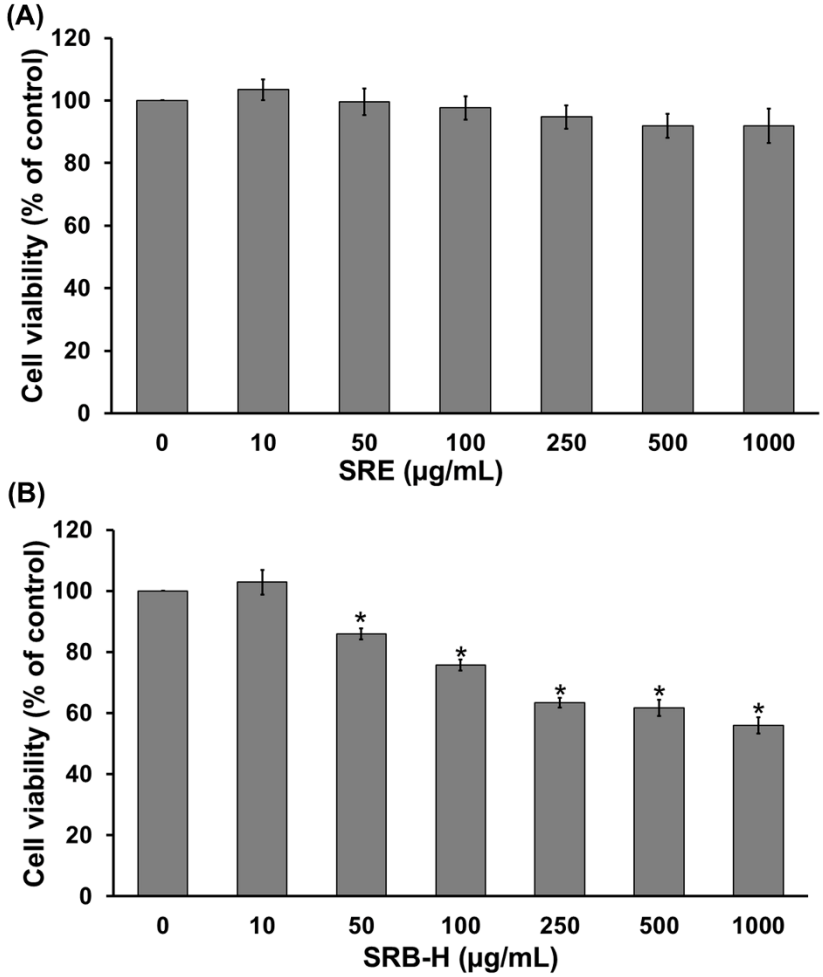

Figure 1. Cytotoxicity of SRE and SRB-H in HaCaT human epidermal keratinocytes. HaCaT cells were treated with (A) SRE (0, 10, 50, 100, 250, 500, and 1000 µg/mL) and (B) SRB-H (0, 10, 50, 100, 250, 500, and 1000 µg/mL) for 72 hours. Cell viability was assessed using the MTT method. The data are presented as mean ± SEM of four independent experiments. $^{*}p<0.05$ compared to the untreated control group.

In vitro antioxidant activity

1. DPPH radical-scavenging activity of SRE, and SRB-H

The DPPH scavenging activity of SRE, SRB-H, and vitamin C was examined to assess their antioxidant potential. The results indicated that concentrations of 0.1, 0.25, 0.5, 0.75, 1.0, and 1.5 mg/mL of SRE significantly enhanced DPPH scavenging activity across all concentrations (Figure 2A). Similarly, concentrations of 0.1, 0.25, 0.5, and 0.75 mg/mL of SRB-H demonstrated a significant increase in radical scavenging activity. However, at concentrations of 1.0 and 1.5 mg/mL, SRB-H significantly decreased these properties due to color interference affecting the results. Vitamin C at doses of 1, 5, 10, 50, and 100 µg/mL also significantly elevated antioxidant activity across all concentrations (Figure 2B). The IC_{50} value for the DPPH assay of SRE was found to be 7.096 mg/mL, while the IC_{50} for SRB-H could not be calculated. The IC_{50} for vitamin C was determined to be 10.88 µg/mL. The findings from our study demonstrate that both SRE and SRB-H exhibit antioxidant activity, as measured by the DPPH assay. Additionally, SRE showed a greater radical scavenging ability compared to SRB-H. In previous studies on antioxidant activities, SRE displayed significant radical scavenging potential, with an IC_{50} value of 0.16 ± 0.01 mg/mL (7). Furthermore, Aenglong et al. (3) demonstrated that SRB-H exhibited high DPPH scavenging activity, effectively decreasing DPPH radicals, with its scavenging efficacy depending on the size of the peptides and the type of enzyme used. Additionally, Kabploy et al. (6) reported that the IC_{50} value of SRB-H was 0.61 mg/mL, indicating its capability to scavenge free radicals by reducing the concentration of DPPH radicals.

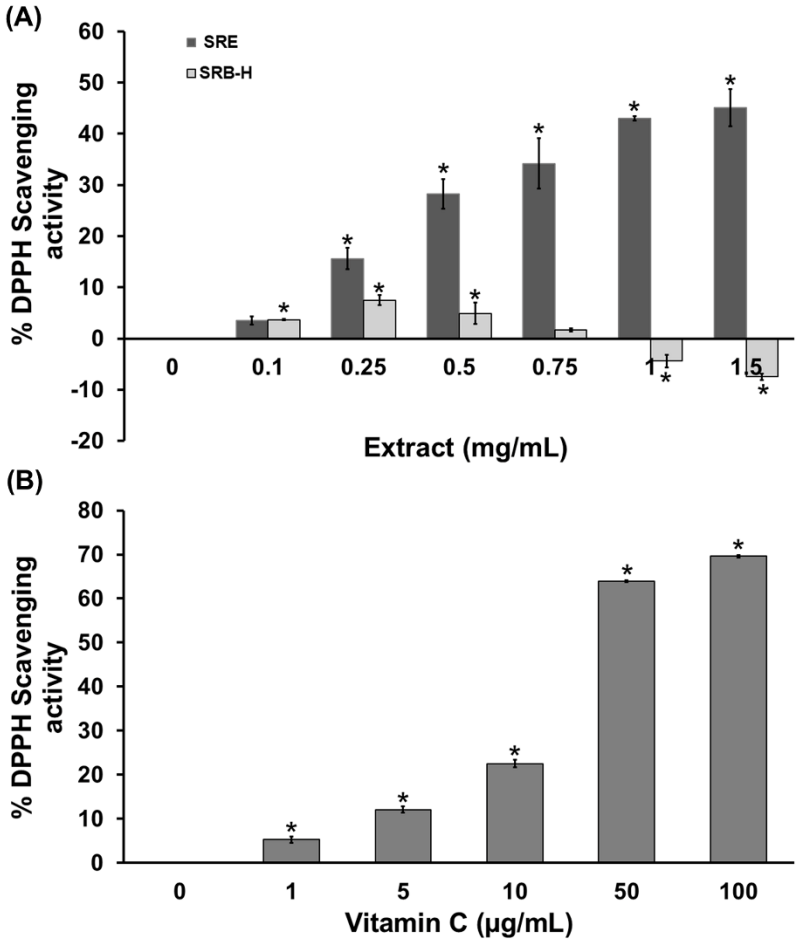

Figure 2. The DPPH radical scavenging activity of SRE, SRB-H, and vitamin C. (A) SRE (0, 0.1, 0.25, 0.5, 0.75, 1.0, and 1.5 mg/mL), and SRB-H (0, 0.1, 0.25, 0.5, 0.75, 1, and 1.5 mg/mL) were tested alongside (B) vitamin C (0, 1, 5, 10, 50, and 100 µg/mL) using DPPH assay. The data are presented as mean ± SEM of three independent experiments. *$p<0.05$ compared to the 0 mg/mL.

2. ABTS radical-scavenging activity of SRE and SRB-H

The analysis of ABTS scavenging activity in SRE, SRB-H (Figure 3A), and vitamin C (Figure 3B) was conducted to evaluate their antioxidant properties. The results indicated that concentrations of 0.1, 0.25, 0.5, 0.75, 1.0, and 1.5 mg/mL of both SRE and SRB-H significantly increased ABTS scavenging activity. Additionally, vitamin C at concentrations of 1, 5, 10, 50, and 100 µg/mL also demonstrated a significant increase in radical scavenging activity. The IC_{50} values for the ABTS assay were found to be 5.61 mg/mL for SRE and 4.44 mg/mL for SRB-H, while the IC_{50} for vitamin C was determined to be 4.56 µg/mL. The findings from our study demonstrate that SRE exhibited greater radical scavenging ability compared to both SRB-H and vitamin C, consistent with the results from the DPPH assay. Previous studies assessing the antioxidant capacity of SRB-H indicated that it displayed ABTS scavenging properties across all treatment conditions (3). Consequently, our study reinforces the antioxidant activity of both SRE and SRB-H.

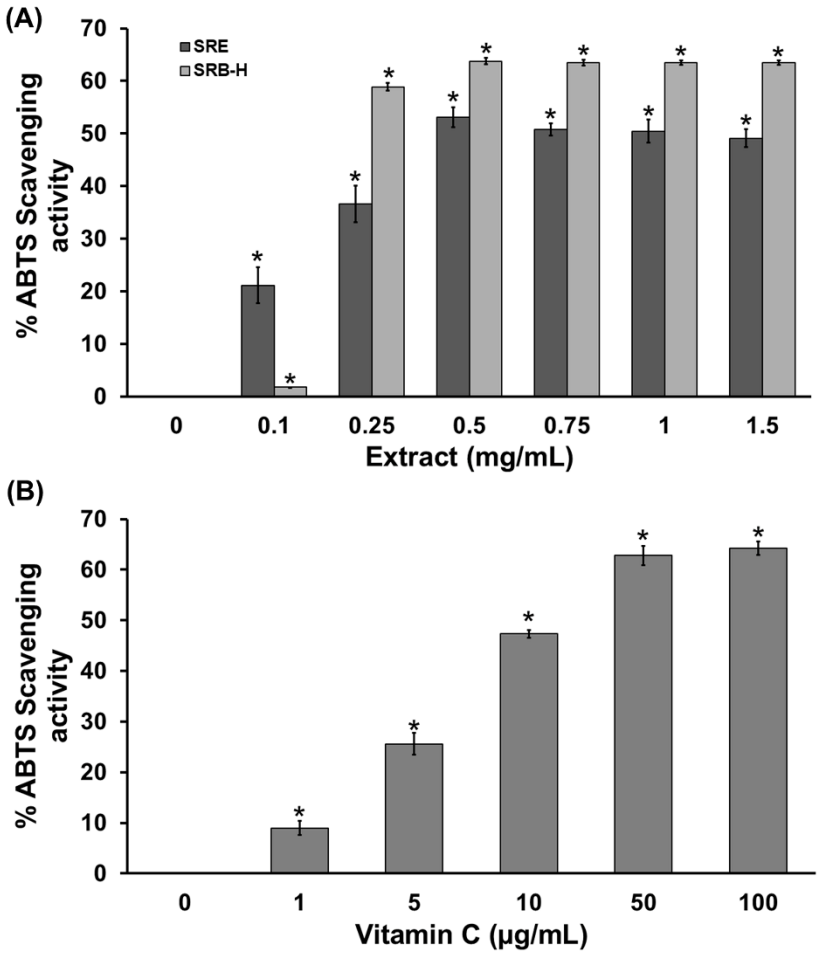

Figure 3. ABTS radical scavenging activity of SRE, SRB-H, and vitamin C. (A) SRE (0, 0.1, 0.25, 0.5, 0.75, 1, and 1.5 mg/mL), and SRB-H (0, 0.1, 0.25, 0.5, 0.75, 1, and 1.5 mg/mL) were tested alongside (B) vitamin C (0, 1, 5, 10, 50, and 100 µg/mL) were analyzed using ABTS assay. The data are presented as mean ± SEM of three independent experiments. *$p<0.05$ compared to the 0 mg/mL group.

Conclusion

In conclusion, these findings indicate that SRE and SRB-H effectively enhance antioxidant activity and are safe for skin cells. However, the antioxidant properties of both SRE and SRB-H should be confirmed in a cell culture model. Future experiments should focus on investigating the specific mechanisms through which SRE and SRB-H exert their antioxidant effects. Additionally, conducting in vitro studies will be essential to evaluate their potential therapeutic applications in treating various skin conditions.

References

(1) Fukagawa, N. K., & Ziska, L. H. Rice: Importance for Global Nutrition. Journal of Nutritional Science and Vitaminology, 2019;65(Supplement): S2–S3.

(2) Mohidem, N. A., Hashim, N., Shamsudin, R., & Man, H. C. Rice for Food Security: Revisiting Its Production, Diversity, Rice Milling Process and Nutrient Content. Agriculture (Switzerland), 2022;12(6):741.

(3) Aenglong, C., Woonnoi, W., Tanasawet, S., Klaypradit, W., & Sukketsiri, W. Impact of Time and Enzyme Concentration on Sangyod Rice Bran Hydrolysate: Phytochemicals, Antioxidants, Amino Acids, and Cytotoxicity, Rice, 2024;17(1):13.

(4) Woonnoi, W., Suttithumsatid, W., Muneerungsee, N., Saetan, J., Tanasawet, S., & Sukketsiri, W. Sangyod rice extract inhibits adipocyte growth and differentiation via mTOR, Akt, and AMPK pathways. Journal of Functional Foods, 2023;111:105913.

(5) Hanchang, W., Woonnoi, W., Saetan, J., Suttithumsatid, W., Tanasawet, S., Sanprick, A., Moolsup, F., & Sukketsiri, W. Sangyod rice extract mitigates insulin resistance in HepG2 cells and hepatic steatosis in diabetic rats via AMPK/mTOR/MAPK signaling pathways. Food Bioscience, 2024;61:104662.

(6) Kabploy, K., Saengsawang, P., Romyasamit, C., Sangkanu, S., Kitpipit, W., Thomrongsuwannakij, T., Wongtawan, T., Daus, M., de Lourdes Pereira, M., & Mitsuwan, W. Sangyod rice bran extract enhances *Lacticaseibacillus paracasei* growth during the exponential phase and antibacterial activity of L. paracasei supernatant against zoonotic and foodborne pathogens. Veterinary World, 2022;15(10):2466–2474.

(7) Chairerk, N., Pongyeela, P., Chungsiriporn, J., & Rakmak, N. Ethanol extraction of active ingredients and antioxidants from germinated sangyod rice. Applied Science and Engineering Progress, 2021;14(1):52–59.

(8) Jeenkeawpieam, J., Rodjan, P., Roytrakul, S., Pruksaphon, K., Mitsuwan, W., Tanthanathipchai, N., Boonkaewwan, C., Tedja, I., & Pongpom, M. Antifungal activity of protein hydrolysates from Thai Phatthalung Sangyod rice (Oryza sativa L.) seeds. Veterinary World, 2023;16(5):1018–1028.

(9) Khongla, C., Chuaingan, J., Siadkhunthod, T., Somnam, P., Musika, S., & Sangsawad, P. Physicochemical Properties of Rice Bran Hydrolysate Prepared in a Pilot Scale Process and Its Application in Milk Tablets. Trends in Sciences, 2022;19(23):2316.

Artocarpus lakoocha Extract Inhibits the Survival and Migration of Human Lung Cancer Cells and Suppressing AKT Activation

Jatuporn Polhiran[1,2], Wutigri Nimlamool[1], Saranyapin Potikanond[1], and Nitwara Wikan[1,*]

[1] Department of Pharmacology, Faculty of Medicine, Chiang Mai University, Chiang Mai 50200, Thailand
[2] Graduate School, Chiang Mai University, Chiang Mai 50200, Thailand.
*Corresponding author's email: nitwara.wik@cmu.ac.th

Abstract:

Artocarpus lakoocha Roxb. (AL), a plant of Thai, is commonly known as Ma-Haad. AL is rich in stilbenoids, particularly oxyresveratrol. Previous studies have explored its potential anti-cancer properties. However, the role of AL in exhibiting anti-cancer properties has not been elucidated in non-small cell lung cancer cells, especially in the aspect of molecular signaling pathways and mechanisms of action. Here, we investigated the molecular mechanisms underlying the anti-cancer activities of AL extract in non-small cell lung cancer cells. We demonstrated that AL extract inhibited \ and migration of lung cancer cells in a dose-dependent manner. Specifically, western blot analysis showed that AL extract inhibited the survival and migration of A549, human lung cancer, cells and suppressed AKT activation through reducing phosphorylation of AKT. These events resulted in reduction in lung cancer cell viability, proliferation, and migration. These findings suggest that AL extract exhibits its anti-cancer activities, in part through suppressing the activation of the AKT kinase. Therefore, AL may be a promising candidate for the development of therapeutic strategies against lung cancer.

Keywords: *Artocarpus lakoocha*; Lung cancer; AKT activation; Anti-cancer; Oxyresveratrol

Introduction

Worldwide, despite recent advance in lung cancer treatment, including chemotherapy, surgery, targeted therapies, and radiation therapy, non-small cell lung cancer (NSCLC) is the most common type of lung cancer that is the primary reason of cancer-related death. According to previous study, NSCLC accounts up to 80% of incidence of all lung cancers, including large cell carcinoma (LCC), squamous cell carcinoma (SCC), and adenocarcinoma (ADC) (1). Most patients with NSCLC are diagnosed at an advanced stage, where treatment is often less effective, and survival rates are poor. NSCLC can be caused by several factors, such as smoking, second-hand smoke, genetic changes and family history as well as carcinogenic chemicals and heavy metals, such as asbestos, radon gas, arsenic (2). The most commonly studied factors are related to genetic mutations such as mutations in the KRAS, EGFR, and ALK genes. These mutations are strongly linked to the AKT pathway, which is important for controlling survival and migration (3, 4). Abnormal activation of the AKT pathway is linked to poor patient outcomes. Therefore, targeting the AKT pathway has become a promising approach for developing new cancer treatments.

The primary active compound in *Artocarpus lakoocha* Roxb. (AL), commonly referred to as Ma-haad, is rich in stilbenoids, particularly oxyresveratrol (trans-2,3′,4,5′-tetrahydroxystilbene). This polyphenolic stilbene is predominantly present in the heartwood of the plant. Additionally, it possesses various pharmacological activities, including anti-inflammatory properties, anti-bacterial, anti-viral, anti-oxidant, and anti-cancer activity (5-8). Previous study have shown that AL extract has anti-inflammatory effects primarily by inhibiting the NF-κB and PI3K/AKT signaling pathways (8). Specifically, AL extract nearly completely suppresses LPS-induced AKT phosphorylation in RAW 264.7 cells (8), inhibits the phosphorylation of AKT and GSK-3β, reduces the expression of the anti-apoptotic protein MCL-1, decreases the migration, and reduces proliferation of cervical cancer cells (7). However, the effects of AL extract on the AKT signaling pathway, as well as its roles on cell migration and survival in human lung cancer cells through the suppressing of AKT activation, have not yet been fully explored. Therefore, the present study aimed to investigate the potential inhibitory

action of AL extract on the activation status of the AKT signal transduction pathways in lung cancer cells.

Materials and Methods

Plant Material with AL Heartwood Extraction

AL heartwood was purchased from Thai Lanna Herbal Industry Company Ltd., located in Chiang Mai, Thailand, and authenticated by comparison with a reference specimen (voucher number 006973) preserved in the herbarium of the Faculty of Pharmacy, Chiang Mai University. Crude extraction of AL followed a previously established protocol (9), where the heartwood was dried at 50 °C for 24 hours, ground into powder, and macerated three times in 95% ethanol for six hours each. The collected ethanolic extracts were concentrated under reduced pressure at temperatures below 45 °C using a rotary evaporator and then stored in a container protected from air and light. A 1 g/mL stock solution was prepared by dissolving 1 g of AL in 1 mL of DMSO, and pre-dilutions were done in the medium for each experiment.

Cell Culture

The human A549 cell line [ATCC® CCL-185 ™] was used in this study. The cells were maintained in complete medium, which was Dulbecco's modified Eagle's medium (DMEM) (Gibco, USA), with the addition of 10% fetal bovine serum (Merck KGaA, Germany), and antibiotics (100 U/mL penicillin and 100 µg/mL streptomycin) (Gibco, USA) and cultured in an incubator at 37°C, with a humid and 5% CO_2 atmosphere. Media were changed every 2–3 days, and cells were sub-cultured when the cells reached approximately 90% confluence.

Cell Viability Assay and Cell Counting

The cell viability of A549 cells treated with AL extract (with extraction process and identification previously reported (9)) was assessed in this instance using 3-(4,5-dimethylthiazol-2-yl)-2,5-diphenyltetrazolium bromide (MTT). In 96-well plates (Thermo Fisher Scientific, USA), we seeded A549 cells at 1×10^4 cells per well in complete media overnight. Next day, AL extract was diluted in the media to a working concentration of 500 µg/mL, then the concentration was further diluted by 2-fold dilution to create a concentration range of 1.95–500 µg/mL. The cells were treated with these varied concentrations of AL extract for 24 and 48 h in the media. Since the stock AL extract was prepared in DMSO, thus DMSO was used as a negative control. The method for DMSO dilution was similar to that of AL extract. After 24 and 48 h of AL extract exposure, MTT reagent (stock 5 mg/mL) was added to each well (25 µL per well), and cells were incubated in a CO_2 incubator for 1 h for formazan formation. After media were aspirated, formazan was dissolved with 100% DMSO (50 µL per well). The difference in color intensity was determined by a microplate reader set at 570 nm. Measurement of cell number was performed at 24 and 48 h post-treatment. For counting cells, the treatment media were discarded, and cells were fixed with 4% paraformaldehyde for 15 min. Then, the nuclei of individual cells were stained with 1 µg/mL of DAPI (4′,6-diamidino-2-phenylindole) for 30 min. Cells were counted and quantified (number of cells per well) by using BioTek Lionheart FX automated microscope with Gen5 imaging software version 3.12.08. (Agilent Technologies, Inc., CA, USA).

Scratch Wound Migration Assay

A549 cells (2.35×10^4 cells) were seeded in 96-well plates and cultured in complete DMEM until they reached 100% confluency. The cell monolayer was scratched to create equal and even scratch wound by using BioTek AutoScratch (Agilent Technologies, Inc.). Then, treatment was done by adding complete media containing AL extract at varied concentrations. Visualization of lung cancer cell migration of wound closure at 0, 6, 12, 18, 24, 36, and 42 h was performed by BioTek Lionheart FX automated microscope with Gen5 imaging software version 3.12.08 and Scratch Assay App version 1.03 (Agilent Technologies, Inc.).

Western Blot Analysis

A549 cells lysates were prepared by adding 1x reducing Laemmli's buffer into the sample dishes. Samples were collected and heated at 100°C for 5 min and then separated in a 10% gel by SDS–PAGE and electroblotted onto PVDF membrane. The membranes were blocked with 5% bovine serum albumin (BSA) dissolved in TBST for 1 h. Membranes were then incubated with primary antibodies at 4°C overnight. After 3 washes with TBST, membranes were incubated with secondary antibodies for 2 h at room temperature. The western blot protein bands were visualized and quantified using the Odyssey® CLx Imaging System (LI−COR Biosciences, USA).

Data Analysis and Statistical Methods

Data were expressed as mean ± SD and analyzed by one-way ANOVA with Tukey's post hoc multiple comparisons test. A p-value < 0.05 was considered significant.

Results and Discussion

Effect of AL extract on lung cancer cells viability

Artocarpus lakoocha Roxb (AL), known as Ma-haad, is rich in oxyresveratrol and exhibits various pharmacological activities, including anti-inflammatory, anti-bacterial, anti-viral, anti-oxidant, and anti-cancer (5-8). This study focused on the anti-cancer of AL extract in NSCLC, particularly through its effect on the AKT signaling pathway.

To determine the effects of AL extract on cell viability, A549 cell line was treated with AL extract, and the cell viability was determined using MTT assay. AL at concentrations ranging from 1.95–500 µg/mL for 24 and 48 h. The toxicity of AL was observed when its concentration was greater than 31.25 µg/mL, with the cytotoxic concentration 50% (CC50) calculated to be 31.30 µg/mL at 24 h (**Figure 1.A**), and greater than 3.91 µg/mL, with the CC50 calculated to be 31.20 µg/mL at 48 h (**Figure 1.B**), comparison to the untreated control group. However, the AL extract at concentrations below 31.25 µg/mL did not affect lung cancer cell viability at 24 h. Therefore, non-toxic concentrations of AL extract at 3.75, 7.5, and 15 µg/mL were chosen for protein analysis using western blotting.

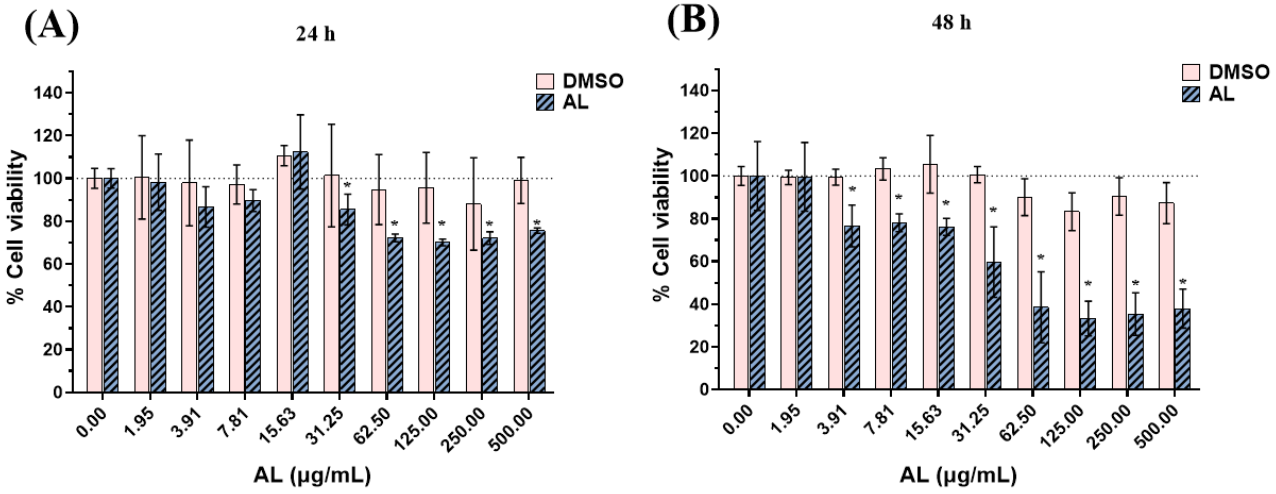

Figure 1. Effect of AL extract on A549 cells viability. Cell viability test (MTT assay) in cells treated with AL extract at 0–500 µg/mL for 48 h. Data are presented as mean ± SD. *p < 0.05 in comparison to the DMSO (vehicle) control.

Effect of AL extract on the proliferation of lung cancer cells

In addition to its role in cell survival, AKT signaling also influences cell survival. We hypothesized that AL extract may inhibit cell proliferation, thus we stained the nucleus of cells with DAPI, a DNA-staining dye, and performed a direct cell counting at day 1 (24 h) and day 2 (48 h) after treated with AL extract. Results showed that direct cell counting confirmed that AL extract at 15.63-500 µg/mL significantly decreased number of cells at day 1 (**Figure 2.A**) while treatment with AL extract at 7.81-500 µg/mL significantly decreased number of cells at day 2. (**Figure 2.B**). Therefore, a concentration of 3.75-60 µg/mL was chosen to confirm the cell migration by scratch wound healing assay.

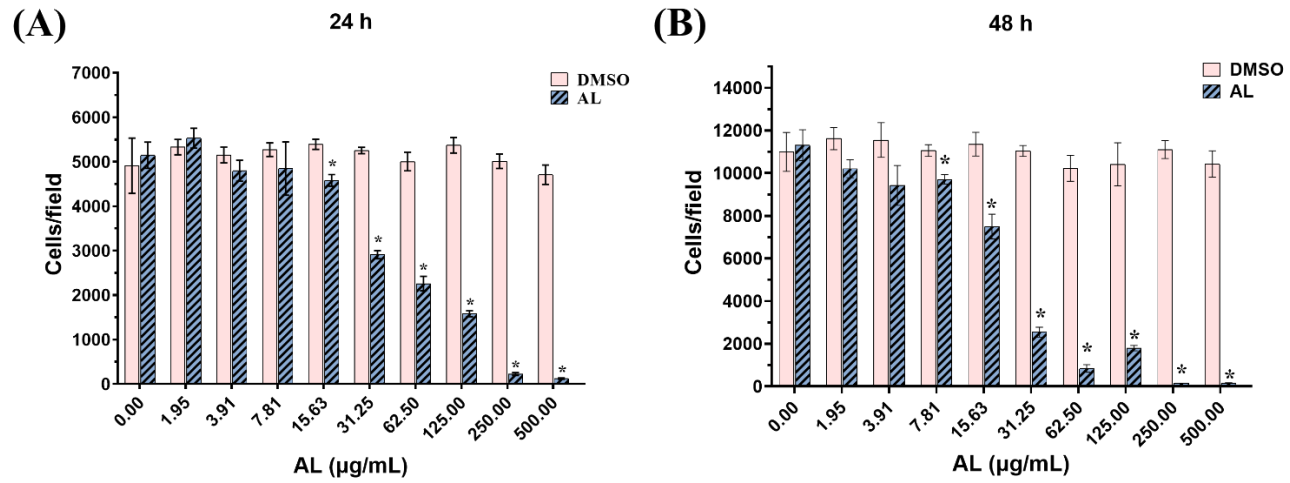

Figure 2. Effect of AL extract on the proliferation of A549 cells. Direct counting for number of cells treated with 0–500 µg/mL of AL extract for day 1 (24 h) and day 2 (48 h). Data are presented as mean ± SD. *$p < 0.05$ in comparison to the DMSO control.

Effect of AL extract on suppressing AKT activation in EGF-induced lung cancer cells

We further investigated the ability of AL extract at 15 µg/mL in inhibiting phosphorylation of AKT (Ser473) at various time points over the course of 2 h after EGF stimulation. The results demonstrated that AL extract almost reduced EGF-induced phosphorylation of AKT in A549 cells at all time points, while the phosphorylation of ERK1/2 remained unaffected (**Figure 3.A–C**). Furthermore, pre-treatment cells with AL extract at concentrations of 3.75, 7.5, and 15 µg/mL for 3 h before EGF stimulation for 0, 15, and 30 min was able to inhibit phosphorylation of AKT (**Figure 3.D–E**). This inhibitory effect was also observed in cells pretreated with AL extract at the same concentrations for 3 h before EGF stimulation for 0, 60, and 120 min (**Figure 3.F–G**), and the inhibition of AKT phosphorylation was observed to be in a concentration-dependent manner.

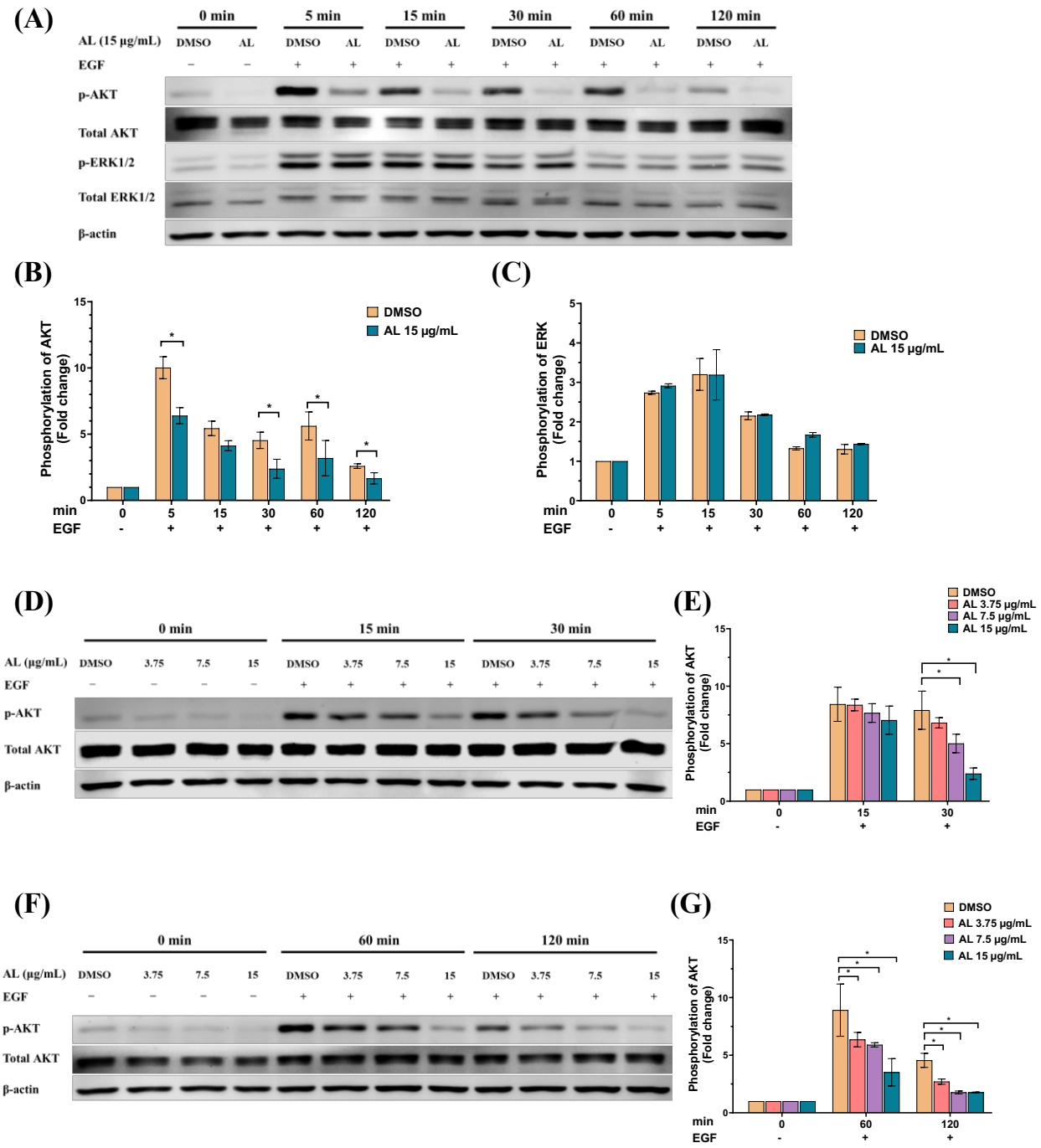

Figure 3. (A) Western blot analysis for the inhibitory effects of AL extract on the phosphorylation of AKT and ERK1/2 upon different treatments (DMSO, AL extract 15 μg/mL) for 3 h before stimulation with EGF (100 ng/mL) for various time points (0, 5, 15, 30, 60, 120 min), total AKT and total ERK1/2 was detected and used as an internal control; (B) quantitative analysis for AKT phosphorylation at Ser473; (C) quantitative analysis for ERK1/2 phosphorylation; (D) the inhibitory effects of AL extract on the phosphorylation of AKT after cells were incubated with various concentrations of AL extract (3.75, 7.5, and 15 μg/mL) for 3 h before stimulation with EGF (100 ng/mL) for various time points (0, 15, 30 min), total AKT was detected and used as an internal control; (E) quantitative analysis for AKT phosphorylation at Ser473; (F) the inhibitory effects of AL extract on the phosphorylation of AKT after cells were incubated with various concentrations of AL extract (3.75, 7.5, and 15 μg/mL) for 3 h before stimulation with EGF (100 ng/mL) for various time points (0, 60, 120 min), total AKT was detected and used as an internal control; (G) quantitative analysis for AKT phosphorylation at Ser473. Data are representatives of three replicates and shown as mean ± SD; * $p < 0.05$ compared to DMSO-treated cells.

Our results indicate that AL extract reduces AKT phosphorylation. which is the main regulator of cell survival, growth proliferation and migration in NSCLC. This inhibition was observed to be concentration dependent. This suggests the potential of AL extract in interfering the physiology of NSCLC. Consistently, previous study have shown that AL extract specifically inhibits AKT signaling without affecting pERK1/2 in RAW 264.7 macrophage cells (8) and cervical cancer cells (7). However, the effects of AL extract on the inhibition of the GSK-3β/MCL-1 axis in A549 cells have not yet been investigated. GSK-3β is a constitutively active kinase associated with several diseases, including Alzheimer's, depression, and neuroinflammation (10). Notably, GSK-3β destabilizes and reduces MCL-1 expression, an important anti-apoptotic protein, which can lead to cell death. Additionally, activated AKT can phosphorylate GSK-3β, inhibiting its function and restoring MCL-1 levels (11). Therefore, this is a key target protein that we aim to investigate in future research.

Effect of AL extract on lung cancer cell migration

To elucidate the effect of AL extract on lung cancer cell migration, we used a scratch wound healing assay to observe and quantify the rate of wound closure over 42 h. As shown in **Figure 4.A** and **Figure 4.B**, the scratch wound of the cells exposed to AL extract at 15 µg/mL exhibited an increased trend of wound closure acceleration. As expected, treatment with AL extract at 30 and 60 µg/mL significantly suppressed cancer cell migration over the course of 42 h. These observations verified that AL extract can be able to delay the migratory activity of NSCLC.

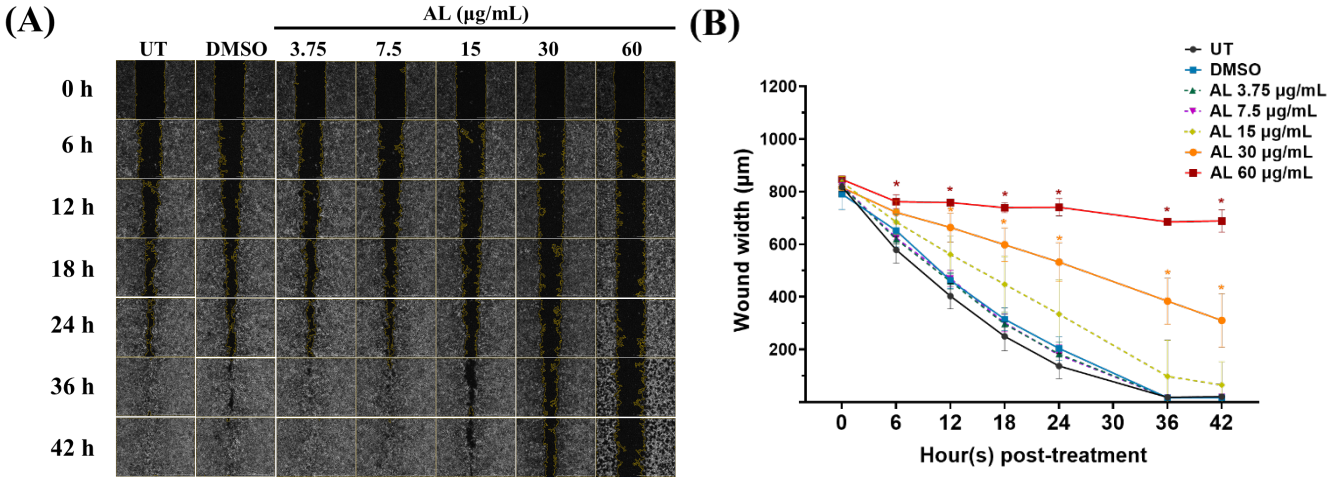

Figure 4. Effect of AL extract on lung cancer cell migration. (A) Scratch wound healing assay of cells treated with DMSO, AL extract at varied concentrations at 0, 6, 12, 18, 24, 36, and 42 h. (B) Quantification of wound width indicating the closure of the scratch wound of A549 cells treated with DMSO, AL extract at varied concentrations at 0, 6, 12, 18, 24, 36, and 42 h. Data are presented as mean ± SD. *$p < 0.05$ in comparison to the DMSO control. UT; untreated cells

Conclusions

AL extract effectively blocks EGF induced AKT activation of A549, human lung cancer, cell, thus suppressing the cell growth and migration. Our findings highlight its potential as a promising candidate for further development as a therapeutic agent for lung cancer.

Conflict of interest statement: All authors declare no conflict of interest.

Acknowledgements: Jatuporn Polhiran was supported by the Faculty of Medicine Graduate Student Scholarship, Chiang Mai University. This work was partially supported by Chiang Mai University.

References

(1) Herbst RS, Morgensztern D, Boshoff C. The biology and management of non-small cell lung cancer. Nature. 2018;553(7689):446-54.
(2) Alduais Y, Zhang H, Fan F, Chen J, Chen B. Non-small cell lung cancer (NSCLC): a review of risk factors, diagnosis, and treatment. Medicine. 2023;102(8):e32899.
(3) Pao W, Girard N. New driver mutations in non-small-cell lung cancer. The lancet oncology. 2011;12(2):175-80.
(4) Alzahrani AS. PI3K/Akt/mTOR inhibitors in cancer: At the bench and bedside. Semin Cancer Biol. 2019;59:125-32.
(5) Majinda R, Mazimba O, Motlhanka D. Antioxidant and antibacterial constituents from Morus nigra. African Journal of Pharmacy and Pharmacology. 2011;5(6):751-4.
(6) Sasivimolphan P, Lipipun V, Ritthidej G, Chitphet K, Yoshida Y, Daikoku T, et al. Microemulsion-based oxyresveratrol for topical treatment of herpes simplex virus (HSV) infection: physicochemical properties and efficacy in cutaneous HSV-1 infection in mice. Aaps Pharmscitech. 2012;13:1266-75.
(7) Tan B, Wikan N, Lin S, Thaklaewphan P, Potikanond S, Nimlamool W. Inhibitory actions of oxyresveratrol on the PI3K/AKT signaling cascade in cervical cancer cells. Biomedicine & Pharmacotherapy. 2024;170:115982.
(8) Hankittichai P, Buacheen P, Pitchakarn P, Na Takuathung M, Wikan N, Smith DR, et al. Artocarpus lakoocha extract inhibits LPS-induced inflammatory response in RAW 264.7 macrophage cells. International Journal of Molecular Sciences. 2020;21(4):1355.
(9) Povichit N, Phrutivorapongkul A, Suttajit M, Leelapornpisid P. Antiglycation and antioxidant activities of oxyresveratrol extracted from the heartwood of *Artocarpus lakoocha* Roxb. Maejo International Journal of Science and Technology. 2010;4(3):454-61.
(10) Beurel E, Grieco SF, Jope RS. Glycogen synthase kinase-3 (GSK3): regulation, actions, and diseases. Pharmacology & therapeutics. 2015;148:114-31.
(11) Maurer U, Charvet C, Wagman AS, Dejardin E, Green DR. Glycogen synthase kinase-3 regulates mitochondrial outer membrane permeabilization and apoptosis by destabilization of MCL-1. Molecular cell. 2006;21(6):749-60.

Prediction Model to Prioritize Colorectal Cancer Screening with Visual Colonoscopy

Suppachai Lawanaskol[1,2,*], Jayanton Patumanond[3], Phichayut Phinyo[4], Narongsak Ratchapakdee[5], and Apichat Tantraworasin[6]

[1] Chaiprakarn hospital, Chiang Mai, 50320, THAILAND

[2] Department of Bioinformatics and Clinical Epidemiology, Faculty of Medicine, Chiang Mai University, Chiang Mai, 50200, THAILAND

[3] Center of Clinical Epidemiology and Clinical Statistics, Faculty of Medicine, Naresuan University, Phitsanulok, 65000, THAILAND

[4] Department of Bioinformatics and Clinical Epidemiology, Faculty of Medicine, Chiang Mai University, Chiang Mai, 50200, THAILAND

[5] Department of Surgery, Kumpawapi hospital, Kumpawapi, Udon Thani, 41110, THAILAND

[6] Department of Surgery, Faculty of Medicine, Chiang Mai University, Chiang Mai, 50200, THAILAND

*Corresponding author's email: suppachai.lawanaskol@gmail.com

Abstract

Visual colonoscopy is a standard procedure for colorectal cancer screening. However, it carries unnecessary operative risks for some patients. Establishing a clinical prediction model to identify high-risk patients who genuinely require urgent colonoscopy is crucial. To develop a clinical prediction model for identifying patients at high risk of colorectal polyps and benign conditions detectable using visual colonoscopy.

This study employed a screening prediction approach using a retrospective cohort observational design. Data were collected in October 2023 at Kumpawapi Hospital and March 2024 at Wangsammo Hospital, located in the northeastern part of Thailand. The study included all patients with a positive fecal immunochemical test. Predictors analyzed included male gender, age, family history of colorectal cancer, prior colonoscopy screening, smoking, alcohol use, diabetes mellitus, clinical symptoms (e.g., bowel habit change, weight loss, decreased stool caliber), and hematocrit level. All patients underwent colonoscopy, during which polyps were endoscopically biopsied and sent for histopathological examination. Multivariable multinomial logistic regression was performed to analyze the predictors. The predictors were selected based on clinical relevance and face validity. Participants were classified into three risk groups based on the highest probability. The accuracy of the classification was assessed.

Among the 953 patients who underwent visual colonoscopy, 66 (23.1%) were found to have benign polyps, 128 (44.8%) had non-advanced adenomas, 84 (29.4%) had advanced adenomas, and 8 (2.8%) had colorectal cancer. Predictor selection was based on clinical significance and face validity. The selected predictors included male gender, age >50 years, family history of colorectal cancer, alcohol use, and abdominal pain. The accuracy of the model was 43.4%. This study demonstrated fair discrimination in identifying higher-risk patients. The clinical prediction rule has potential as an advisory tool for individuals considering voluntary colonoscopy and as a prioritization tool for patients requiring urgent screening.

Keywords: Clinical prediction rule; Polyp; Screening; Colonoscopy; Colorectal cancer; Advanced adenoma

Introduction

The current standard for colorectal cancer (CRC) screening is visual colonoscopy, recommended for individuals aged 45–85 years, with screening intervals of every 10 years (1–4). While effective, colonoscopy requires bowel preparation, is time-intensive, involves significant costs, and often causes discomfort for the participants (5–7). Moreover, only a small fraction of screened individuals are found to have colorectal cancer (8). Screening the entire average-risk population may also be delayed due to resource limitations (9). Various professional societies have proposed different screening methods. In Thailand, occasional screening initiatives targeted individuals aged 50–70

years using the fecal immunochemical test (FIT) or fecal occult blood test (FOBT), reaching only 0.08% (114 out of 137,047 individuals) in a Thai CRC program in Health Region 1. Biopsies are required to confirm diagnosis, potentially delaying treatment under constrained resources.

Non-invasive tests like FIT have a positive predictive value (PPV) of 30.6% (10, 11), which may not be sufficient to identify colorectal cancer effectively. A significant number of patients remain unscreened or undiagnosed. Even among detected cases, only about 3 in 10 benefits from subsequent colonoscopy, as FOBT also has a false negative rate of 27.6%, meaning an additional 3 in 10 cases that could benefit from colonoscopy might not receive it. Although colonoscopy remains the reference standard for screening, FOBT's logistical advantage—such as cost and stool collection requirements—may make it less ideal as a preliminary screening tool before colonoscopy. Screening questionnaires or predictive models can identify at-risk individuals before initiating invasive procedures (12).

This study aims to identify predictors and develop a scoring system tailored to the Thai population. This system will assess the likelihood of detecting colorectal cancer through colonoscopy, potentially optimizing resource use and improving screening efficiency in a resource-limited setting.

Materials and methods

This is a retrospective observational cohort study. The study includes all participants who tested positive for the fecal occult blood test (FOBT) as part of the Occasional Surveillance of Colorectal Cancer Program, conducted in October 2023 at Kumpawapi Hospital and March 2024 at Wangsammo Hospital.

Inclusion Criteria:

• Patients with a positive fecal occult blood test (FOBT) who agreed to undergo visual colonoscopy and successfully completed the preoperative process and bowel preparation.

Exclusion Criteria:

• Patients diagnosed with colorectal cancer.
• Patients who did not undergo colonoscopy for screening purposes.

Study size estimation

Based on the study by Al I Sharara et al. (2020), the risk prediction model demonstrated a C-statistic of 0.73. With 15 predictive factors, a colonic lesion prevalence of 37.3%, and a shrinkage factor of 0.9, this study requires a sample size of 823 patients, including 307 patients with colonic polyps.

Statistical analysis

Categorical data were described with frequency and percentage, tested by Fisher's exact probability test. Normally distributed continuous data were described with mean and standard deviation, tested by independent t-test. Non-normally distributed continuous data were described with median and interquartile range, tested by Mann-Whitney U test. In all analyses, statistical uncertainties are expressed in 95% two-sided confidence intervals. A p value of < 0.05 will indicate statistical significance.

Endpoints

For the endpoints, we identified various disease entities, categorized into three groups. The first group represents a normal colon or negative screening result. The second group includes benign conditions such as diverticulitis, internal hemorrhoids, colitis, and colonic or rectal polyps (e.g., hyperplastic polyps). The third group encompasses malignant conditions, including non-advanced adenoma, advanced adenoma, colonic cancer, and rectal cancer

Predictors

The diagnostic factors for polyps are similar to those for colonic and rectal cancer. These include male sex, age (years), family history of colorectal cancer, history of colonoscopy, alcohol use, smoking, type 2 diabetes mellitus, fatigue, weight loss, hematochezia, decreased stool caliber, bowel habit changes, abdominal pain, abdominal mass, body mass index (BMI, kg/m^2), and hematocrit (%).

Patient history, age, body weight, and body height were recorded prior to colonoscopy. Preoperative hematocrit levels were also assessed. Age, body weight, body height, and hematocrit levels were measured as continuous variables, while all other factors were measured as binary variables.

Model derivation

The type of regression model was selected based on the distribution of the endpoints. A predictive modeling strategy was employed. Statistically driven potential predictors were parsimoniously and directly included, with considerations for face validity. The final model was a multivariable multinomial logistic regression, which predicted the probabilities of three categories: normal, benign condition, and malignant condition. Multivariable relative risk ratios were estimated and reported. The ratio of individual probability (observed) to overall probability (expected) was calculated, and the category with the highest ratio indicated the patient's classification.

Model performance

For the model performance, the model performance is measured using accuracy. Underestimate proportion and overestimate proportion were measured.

Ethical consideration

This protocol was approved by the Ethical Committee of Khumpawapi Hospital (KPEC 3/2567). Other hospitals participating in this study used the same approval document without requiring additional review by their authorized ethics committees.

Results and Discussion

Of 953 patients who underwent visual colonoscopy, 66 (23.1%) had benign polyps, 128 (44.8%) had non-advanced adenomas, 84 (29.4%) had advanced adenomas, and 8 (2.8%) had colorectal cancer. The prevalence of colorectal cancer in patients positive for FOBT was 2.8%. Predictor selection was based on clinical significance and face validity. Significant differences were observed in the proportions of males, alcohol use, smoking, and abdominal pain. The mean age and body mass index also showed significant differences. Hematocrit showed the highest proportion of missing values (4.7%). Following categorization, the proportion of anemia was lower in the malignant group. Most of the missing body mass index values were due to missing body height data. A family history of colorectal cancer and hematochezia were borderline significant.

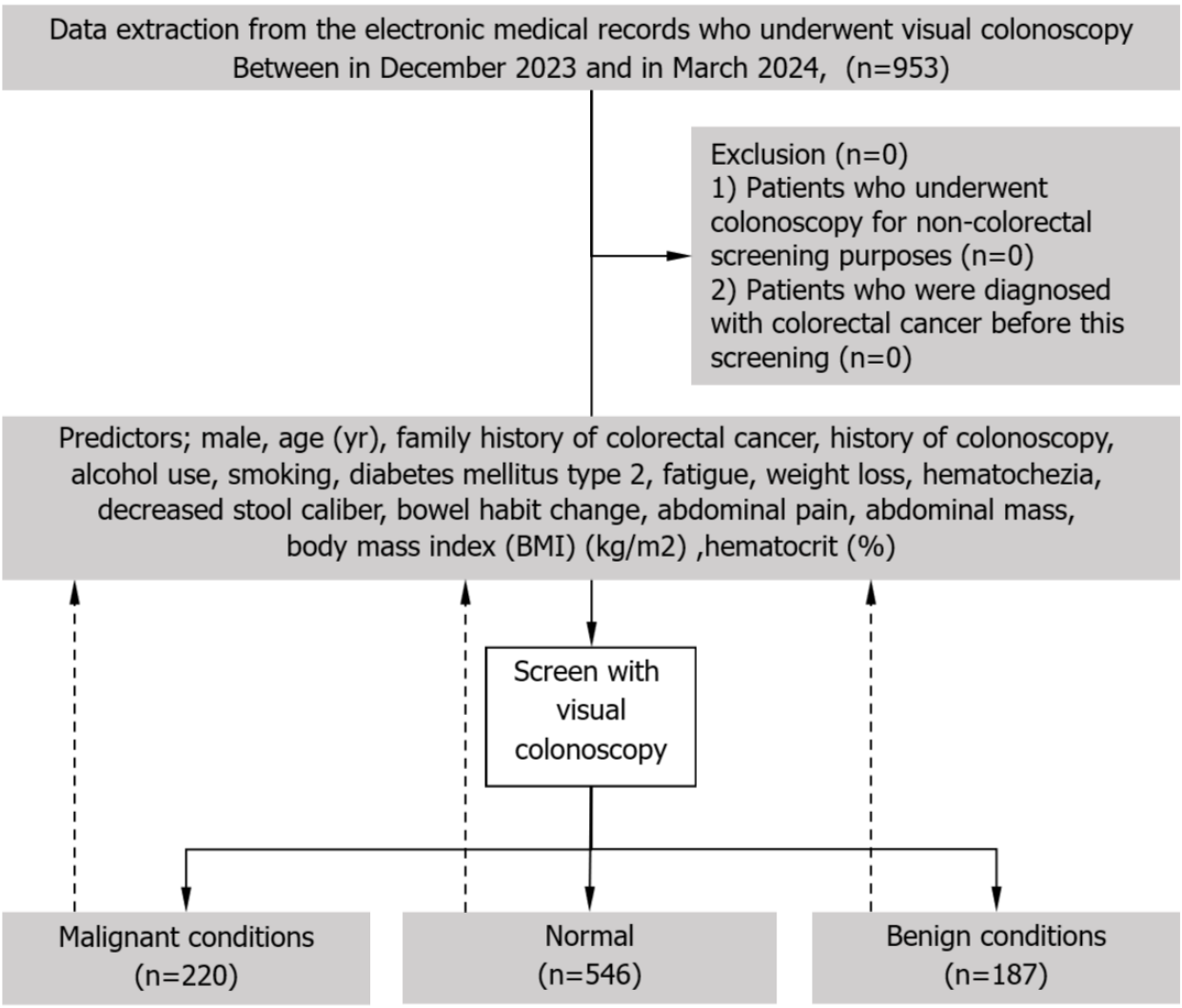

Figure 1 Study flow diagram

Table 1. Multivariable multinomial logistic regression

Predictor	Malignant		Benign	
	mRRR[a] (95% CI[b])	p-value	mRRR (95% CI)	p-value
Male	1.68 (1.18, 2.38)	0.004	1.02 (0.70, 1.50)	0.907
Age >50 years	1.57 (0.83, 2.98)	0.169	1.29 (0.69, 2.40)	0.427
Family history of colorectal cancer	1.42 (0.81, 2.49)	0.218	1.66 (0.96, 2.87)	0.071
Alcohol use	1.68 (1.18, 2.38)	0.004	1.39 (0.96, 2.03)	0.083
Abdominal pain	1.69 (1.09, 2.63)	0.019	1.37 (0.85, 2.22)	0.200

[a]mRRR; multivariable relative risk ratio, [b]CI; confidence interval,

The overestimation proportion was 38.4% (higher than the expected 33%), while the underestimation proportion was 18.1% (lower than the expected 33%). Accuracy increased to 43.5%. (Table 2)

Table 2. Discrimination between true status and predicted status

Predicted status	True status			Total
	Normal	Benign	Malignant	
Normal	252 (26.4)	68 (7.1)	62 (6.5)	382 (40.1)
Benign	111 (11.7)	48 (5.0)	43 (4.5)	202 (21.2)
Malignant	183 (19.2)	71 (7.5)	115 (12.1)	369 (38.7)
Total	546 (57.3)	187 (19.6)	220 (23.1)	953 (100)

Limitations:

This study was conducted only in Udon Thani, limiting its generalizability to other populations. Additionally, the proportion of patients with inadequate bowel preparation was zero, which does not accurately reflect a more symptomatic clinical diagnostic process. Furthermore, Based on the assumption that predictors for colonic polyps would be similar to those for colorectal cancer, the model's performance was not superior to other models that predict cancer alone.

Advantages:

The prevalence of colorectal cancer in patients with a positive FOBT result in this study (2.8%) is significantly lower than that reported in symptomatic populations (30.7%) (10, 11). Additionally, this study provides a more accurate estimate of the positive predictive value, which may vary across a wide spectrum of diseases. For prognostic factors, basic clinical information that can be collected in a primary care setting enhances the practicality of the model.

Implication:

Under routine screening conditions, the authors recommend that high-risk patients undergo endoscopy within one week after adequate preoperative preparation, including bowel preparation. This strategy facilitates a comprehensive, accurate, and precise evaluation of both malignant and non-malignant conditions. For moderate-risk patients, endoscopy is advised within two weeks, while low-risk patients should undergo the procedure within four weeks unless they exhibit prominent cancer-related symptoms or gastrointestinal bleeding necessitating earlier endoscopy. Examples of such indications include concurrent anemia with hematochezia or anemia accompanied by altered stool caliber, both of which are characteristic of malignancy. These cases, categorized as selective criteria, should also undergo endoscopy within one week. However, while the timing of endoscopy may be prioritized as early or delayed, it is not typically categorized as "performed" or "not performed." Delaying endoscopy beyond four weeks may increase cancer-related mortality by 1.06 times (HR 1.06) [13]. Universal scheduling of endoscopy within 1–2 weeks for all patients may be impractical in resource-limited settings. Prioritizing high-risk patients for earlier endoscopy is likely to gain better patient cooperation due to preoperative risk counseling or advice provided as part of the process. For low-risk patients scheduled at four weeks, the additional time allows for further evaluation of anemia or hematochezia at local hospitals, potentially resolving symptoms before the endoscopy. These cases may no longer require urgent endoscopy within four weeks as interim interventions could address the underlying issues during the waiting period.

Conclusion

This study demonstrated fair discrimination in identifying higher-risk patients, with the clinical prediction rule being useful for advising on voluntary colonoscopy and prioritizing urgent screenings. The balance between overestimation and underestimation of the screening process is critical for individual centers.

Conflict of Interest Statement: The authors declare that they have no conflict of interest.

Acknowledgements: The authors would like to express their gratitude to Miss Ruengsiri Panuwet, RN, APN (Anesthetist), for her assistance in facilitating the data collection process.

References

1. Shaukat A, Levin TR. Current and future colorectal cancer screening strategies. Nature Reviews Gastroenterology & Hepatology. 2022;19(8):521-31.
2. Lohsiriwat V, Chaisomboon N, Pattana-Arun J. Current colorectal cancer in Thailand. Annals of Coloproctology. 2020;36(2):78.
3. Ness RM. Updates in Screening Recommendations for Colorectal Cancer. Journal of the National Comprehensive Cancer Network. 2022;20(5.5):603-6.
4. Patel SG, May FP, Anderson JC, Burke CA, Dominitz JA, Gross SA, et al. Updates on age to start and stop colorectal cancer screening: recommendations from the US Multi-Society Task Force on Colorectal Cancer. Gastroenterology. 2022;162(1):285-99.
5. Phimha S, Promthet S, Suwanrungruang K, Chindaprasirt J, Bouphan P, Santong C, et al. Health insurance and colorectal cancer survival in Khon Kaen, Thailand. Asian Pacific Journal of Cancer Prevention: APJCP. 2019;20(6):1797.
6. Phisalprapa P, Ngorsuraches S, Wanishayakorn T, Kositamongkol C, Supakankunti S, Chaiyakunapruk N. Estimating the preferences and willingness-to-pay for colorectal cancer screening: An opportunity to incorporate the perspective of population at risk into policy development in Thailand. Journal of Medical Economics. 2021;24(1):226-33.
7. Matthias MS, Imperiale TF. A risk prediction tool for colorectal cancer screening: a qualitative study of patient and provider facilitators and barriers. BMC family practice. 2020;21(1):1-8.
8. Siripongpreeda B, Mahidol C, Dusitanond N, Sriprayoon T, Muyphuag B, Sricharunrat T, et al. High prevalence of advanced colorectal neoplasia in the Thai population: a prospective screening colonoscopy of 1,404 cases. BMC gastroenterology. 2016;16(1):1-7.
9. Khuhaprema T, Sangrajrang S, Lalitwongsa S, Chokvanitphong V, Raunroadroong T, Ratanachu-Ek T, et al. Organised colorectal cancer screening in Lampang Province, Thailand: preliminary results from a pilot implementation programme. BMJ open. 2014;4(1):e003671.
10. Brenner H, Stock C, Hoffmeister M. Effect of screening sigmoidoscopy and screening colonoscopy on colorectal cancer incidence and mortality: systematic review and meta-analysis of randomised controlled trials and observational studies. Bmj. 2014;348.
11. Sutherland RL, Boyne DJ, Jarada TN, Lix LM, Tinmouth J, Rabeneck L, et al. Development and validation of a risk prediction model for high-risk adenomas at the time of first screening colonoscopy among screening aged Canadians. Preventive Medicine. 2021;148:106563.
12. Min JK, Yang H-J, Kwak MS, Cho CW, Kim S, Ahn K-S, et al. Deep neural network-based prediction of the risk of advanced colorectal neoplasia. Gut and Liver. 2021;15(1):85.
13. Hanna TP, King WD, Thibodeau S, Jalink M, Paulin GA, Harvey-Jones E, et al. Mortality due to cancer treatment delay: systematic review and meta-analysis. bmj. 2020;371.

In Vitro Optimization of Drug-Releasing Fibrin Glue for Bile Duct Cancer Treatment

Hathaichanok Pradabkam[1,3,*], Watcharin Loilome[2,3], Nisana Namwat[2,3], Arporn Wangwiwatsin[2,3], Attapol Titapun[3,4], Poramaporn Klanrit[5], and Poramate Klanrit[2,3]

[1] Department of Biochemistry, Faculty of Medicine, Khon Kaen University, Khon Kaen 40002, Thailand
[2] Department of Systems Biosciences and Computational Medicine, Khon Kaen University, Khon Kaen, 40002, Thailand
[3] Cholangiocarcinoma Research Institute, Khon Kaen University, Khon Kaen 40002, Thailand
[4] Department of Surgery, Faculty of Medicine, Khon Kaen University, Khon Kaen 40002, Thailand
[5] Department of Oral Biomedical Sciences, Faculty of Dentistry, Khon Kaen University, Khon Kaen, 40002, Thailand
*Corresponding author's email: p.hathaichanok@kkumail.com

Abstract:

Fibrin glue (FG) is a natural gel-based biomaterial developed as a tissue adhesive to stop bleeding during surgical procedures, including cholangiocarcinoma. Cholangiocarcinoma (CCA) is a malignant tumor that develops in the bile duct's epithelium and is common in Thailand, especially in the northeastern part of the country. Since fibrin glue is frequently used in surgery as a sealant, a chemotherapeutic agent could be incorporated into fibrin glue for CCA treatment. Gemcitabine (Gem), Cisplatin (Cis), or Gem+Cis, either drug alone or incorporated into FG, were investigated for release into the cell culture medium, leading to cell deaths in vitro of 2D cholangiocarcinoma cell lines (KKU-213A and KKU-213C). The results showed that most conditions of FG vs. drug alone were non-significant ($P > 0.05$), proving that the drug entrapped into FG can be released and normally affected CCA cells. Moreover, 3D assays (migration and live/dead cell assay) reduced migration area but increased significant cell death (red). Finally, the in—house fabrication of fibrin gel can be done with no significant change in compression modulus ($P > 0.05$). Therefore, chemotherapeutic drugs incorporated with fibrin glue have the potential to develop as a drug-releasing tissue sealant for CCA surgery and help eliminate leftover microscopic tumors after surgery. The in-house production and fabrication of drug-incorporated fibrin glue will reduce the cost of production and will be tested with other drugs in the near future.

Keywords: Fibrin glue; Drug delivery; Cholangiocarcinoma; Three-dimensional (3D) Organoid; Cell migration

Introduction

Drug delivery methods are designed to ensure treatments efficiently reach their target sites, minimizing adverse effects and improving patient adherence. As the spectrum of therapeutics expanded from small molecules to more complex entities such as proteins, peptides, nucleic acids, and antibodies, delivery techniques evolved to address new challenges (1). In this broad field of research, researchers attempt to develop a new material or carrier system for more effective delivery of drugs (2). Localized drug delivery is a technique used to provide the drug to the specific body site for its release or transport the active compounds to the site of action to improve the bioavailability of the drug at the site of the disease, decrease the dose frequency, and lower systemic exposure (3). In addition, this approach can directly implant chemotherapeutic agents into the resection cavity after tumor resection (4). In order to make this type of delivery the most effective, the drug should be released in a sustainable fashion (2). Advanced drug delivery systems are being developed using a diverse range of materials, including lipids, polymers, metals, non-metallic inorganics such as silica and graphene, and even viruses. These materials are selected for their exceptional biocompatibility, biostability, biodegradability, high drug-loading capacity, and unique bioactivities, making them ideal candidates for innovative therapeutic applications (5). Fibrin glue is a biologically derived material whose clotting occurs naturally during the wound healing stage. Fibrin glue consists of a

solution of concentrated fibrinogen activated by the addition of thrombin, which mimics the final stages of blood coagulation (6). Because of its non-toxic nature and adaptability, it conforms to irregularly shaped resection cavities. Consequently, considerable research has focused on utilizing fibrin glue as a localized and controlled drug release vehicle by loading neither the drug nor the sensitizer undergoes degradation during uptake into or release from the fibrin glue (7,8).

Cholangiocarcinomas (CCAs) are rare and aggressive tumors with diverse epidemiology worldwide. It is a biliary system neoplasm, starting in the extrahepatic, peri-hepatic, and intrahepatic bile duct. Molecular characterization and immunological evaluation have been essential for the research of novel treatments that have increased the overall survival of these patients, even though CCA still has a high death rate, mostly because of its aggressiveness and late diagnosis (9,10). Patients need to check whether they are resectable or unresectable for effective treatment of CCA. In unresectable or recurrent cases, systemic chemotherapy will be given to the CCA patients by using either gemcitabine combined with cisplatin (first-line chemotherapy) or FOLFOX (second-line chemotherapy). On the contrary, If the patients can be resectable, surgery will be processed and followed by adjuvant chemotherapy (11). This research investigated the potential of drug-incorporated fibrin glue used as a tissue sealant. Also, this material can serve as localized and drug-releasing fibrin glue and help eliminate microscopic tumors after surgery. Moreover, delivering the chemotherapeutic drug concentrated at the local position can help decrease the overall toxicity to the whole body. Hence, it will improve the surgical outcomes of CCA patients and reduce the chance of tumor relapse.

Materials and Methods

Experimental 2D and 3D Cultures

On a routine basis, 2D cell cultures were established in flat-bottom 96-well plates (Corning Life Sciences, Massachusetts, USA) and seeded 5,000-cells/well for KKU-213C and KKU-213A, respectively. 3D multicellular spheroids (MCSs) cultures were established according to the previously published protocol (12) by seeding cells at optimized densities between 5,000 cells/well in an ultra-low-attachment U-bottom plate. 2D cells and 3D MCSs were captured using a phase-contrast microscope (Axiovert 40 inverted microscope, ZEISS) at 4X and 10X objective lens via program iSolution Lite, IMT (i-Solution Inc., New York, USA). For spheroids, the images have measured the diameter and area of shadow projection using ImageJ (The Research Services Branch, National Institute of Mental Health, Bethesda, Maryland, USA.). The spheroids whose sizes deviated more than 10% of the average were excluded from the experiment.

Fibrin Glue Formation

TISSEEL™ fibrin sealant was purchased from Baxter International Inc. (Deerfield, IL, USA). Generally, TISSEEL™ was delivered in a double-chamber syringe. The first chamber contained a sealer protein solution, including fibrinogen, aprotinin, and factor XIII, while the second chamber was composed of a thrombin solution. In the compression modulus measurement, self-made fibrin glue was established from fibrinogen and thrombin purchased separately (Sigma-Aldrich, Gillingham, UK) using the concentrations indicated in TISSEEL™ as a reference. Chemotherapeutic drugs were incorporated into the fibrin clot via the entrapment process for the drug-releasing experiment.

Incorporation of Fibrin Glue with Drugs

A single drug or drug combination was mixed in the thrombin component from TISSEEL™ fibrin glue (Baxter, USA). Then, fibrinogen and thrombin components will be mixed together to form fibrin glue in the ratio 1:1. Gemcitabine (Fresenius Kabi, Germany) was dissolved in Normal Saline Solution (NSS), filtered through 0.22 μm membrane filters, and dissolved in cell culture media to achieve the concentrations 1,000 μM/mL cisplatin (Fresenius Kabi, Germany) was dissolved in sterile DMSO (Sigma-Aldrich) at concentrations 100 μM/ml. Stock aliquots were stored at −80 °C and thawed prior to each experiment for one-time use. A maximal concentration of 0.1% DMSO in cell

culture media was used as a DMSO control. Then, fibrin glue incorporated with the drug was treated to the 2D cells or 3D MCSs cells for 24 and 48 hours.

The 2D Screening of Gemcitabine and Cisplatin on CCA Cell Lines

KKU-213C and KKU-213A cells were seeded at 5,000 cells/well in flat-bottom 96-well plates (Corning Life Sciences, Massachusetts, USA), then cultured at 37°C, 95% humidity, and 5% CO_2 condition for 16 hours to allow cell attachment. On the next day, the quality checking was performed using a phase-contrast microscope (Axiovert 40 inverted microscope, ZEISS) at 4X and 10X objective lens via the program iSolution Lite, IMT (i-Solution Inc., New York, USA). Gemcitabine powder (Fresenius Kabi, Bad Homburg, Germany) was dissolved in Normal Saline Solution (NSS), filtered through 0.22 µm membrane filters, and dissolved in cell culture media to achieve the concentrations of 0.001, 0.01, 0.1, 1, 10, 100, and 1000 µM, respectively. Cisplatin (Fresenius Kabi, Bad Homburg, Germany) was dissolved in cell culture media to achieve concentrations of 0.001, 0.01, 0.1, 1, 10, 100, and 1000 µM, respectively. Stock aliquots were stored at −80 °C and thawed prior to each experiment for one-time use. A maximal concentration of 0.1% DMSO in cell culture media was used as a DMSO control. Cell viability after treatment was assessed by CellTiter-Glo® viability assay.

Migration Assay and Live/Dead Cell Viability Assay

3D Migration Assay

3D MCSs cultures were also established by seeding cells at optimized densities between 5,000 cells/well in an ultra-low-attachment U-bottom plate to study the spheroid-based migration (one spheroid per well). After that, 1,000 µM of gemcitabine, 100 µM of cisplatin, and 1000 µM of gemcitabine plus 100 µM of cisplatin (with or without fibrin glue) were treated to 3D MCSs for 48 hours and followed the migration area of MCSs over time. Imaging and analysis of cell migration were performed by taking images of spheroids at a starting time point at 0 h up to 48 h, using an inverted microscope (at both 10× and 4× objectives). Migration assay was analyzed using software (Image J). The covered area of the spheroids was chosen using a freehand selection tool to select the migration area. Then, the area and fluorescence intensity were measured from GFP (490/525 nm) and Texas Red (585/628 nm) channels.

Live/Dead Cell Viability Assay

Live and dead cell identification was performed using Live/Dead Cell Viability Assay Kit for 3D MCSs culture (Merck-Millipore, Massachusetts, USA) according to the manufacturer's instructions. The kit provided calcein-AM: Ex/Em: 490/515 nm (stains live cells), propidium iodide: Ex/Em: 535/617 nm (stains dead cells), and Hoechst 33342: Ex/Em: 361/486 nm (stains all cells). For 3D MCSs culture, cells were seeded on an ultra-low-attachment U-bottom plate and 200 µl medium per well. The cell culture medium in all wells was discarded and replaced with a new medium containing 5 µl of calcein-AM, 20 µl of propidium iodide, and 8 µl of Hoechst 33342. The plate was incubated for 60 min at 37°C for 3D MCSs. All samples were analyzed for cell count and viability using a fluorescence microscope EVOS M5000 (Thermo Fischer Scientific, Massachusetts, USA) equipped with standard filters, including DAPI (357/447 nm), GFP (490/525 nm), and Texas Red (585/628 nm).

Mechanical Testing via Universal Testing Machine

Young modulus properties were performed by using 40 mg of fibrinogen was mixed with 1U and 2U of thrombin, respectively. Then, the mixture of fibrin glue was cast into the cubic shape with the dimension of 7 mm x 7 mm x 3 mm and placed at 37° C for 30 minutes to allow complete polymerization. The compression stress, strain, and Young's modulus were measured with a universal testing machine (UTM), LR 30K (Lloyd Instruments Ltd., Bog-nor Regis, UK). The samples were placed on a stage and pressed with measuring probes at 100 N load cell and 0.1 mm/min. The plot of compression stress against compression strain and Young's modulus calculation were generated using NEXYGENPlus Materials Testing Software.

Data Analysis

The students' One-way ANOVA was used to analyze intergroup differences between two groups. P-values less than 0.05 were considered statistically significant. The analysis was performed using GraphPad Prism 8.0.1 (GraphPad Software) (San Diego, CA, USA). Densitometry results of migration area and fluorescence intensity were quantified using ImageJ software.

Results and Discussion

The 2D Screening of Gemcitabine and Cisplatin on CCA Cell Lines

The drug screening was carried out in 2 cell lines, including KKU-213A and KKU-213C. The chemotherapeutic drugs, including gemcitabine and cisplatin, were screened for 48 h incubation by varying the concentration in 10-fold dilution (0.001 – 1000 µM) as shown in Figure 1. We used GraphPad Prism 8 software for the data analysis to determine the concentrations. The effect of gemcitabine and cisplatin was determined by using CellTiter Glo assay. For cisplatin, it effectively inhibited CCA cell proliferation in all cell lines. The gemcitabine resistance was observed and was relevant to the results of Wathikthinnakon and team, showing KKU-213A was highly resistant with a IC_{50} value of > 1 mM (13). Other studies showed KKU-213C and KKU-213A were the cell lines with the low sensitivity of gemcitabine, with IC_{50} values of 598.6 and 4629µM, respectively (14). Comparing with cisplatin, all cell lines seem to have higher resistance to gemcitabine. Even in the highest concentration, it still shows a small effect on cell toxicity.

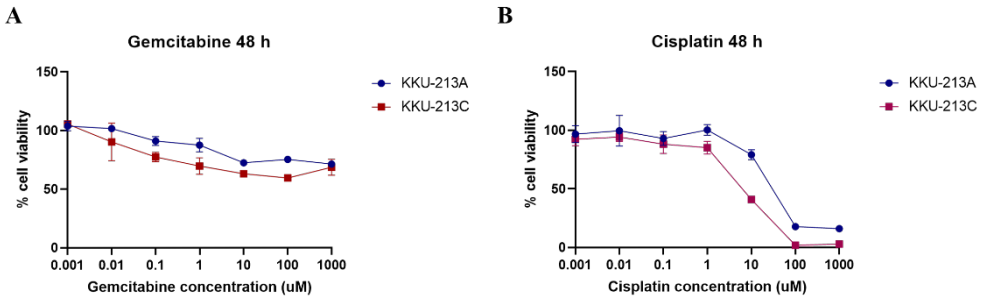

Figure 1. Percentage of CCA cell viability after cells were treated with various concentrations of (A) Gemcitabine and (B) Cisplatin in CCA cell lines (KKU-213C and KKU-213A). This result was determined by a Cell Titer-Glo luminescence cell viability kit.

The 2D Cell Viability when Treated with Fibrin Glue Incorporated with Drugs

Fibrin glue was incorporated with 1,000 µM of gemcitabine, 100 µM of cisplatin, and 1,000 µM of gemcitabine plus 100 µM of cisplatin and forming into glue texture. 2D CCA (KKU-213C, and KKU-213A) were cultured in 24-well plates. Then, they were treated with fibrin glue incorporated with drugs (gemcitabine and/or cisplatin) after 48-hour. After that, a cell viability assay was performed. The result showed that drugs were released from fibrin glue and had an effect on cell viability in all cell types. In some conditions, such as fibrin glue combined with cisplatin and fibrin glue combined with gemcitabine plus cisplatin in KKU-213C and KKU-213A, drug-releasing fibrin glue showed a significantly stronger inhibitory effect than gemcitabine alone, and the result is similar to non-fibrin glue treatment. This indicates that the drug was released into the system (cell culture medium) and had an effect on killing cancer cells.

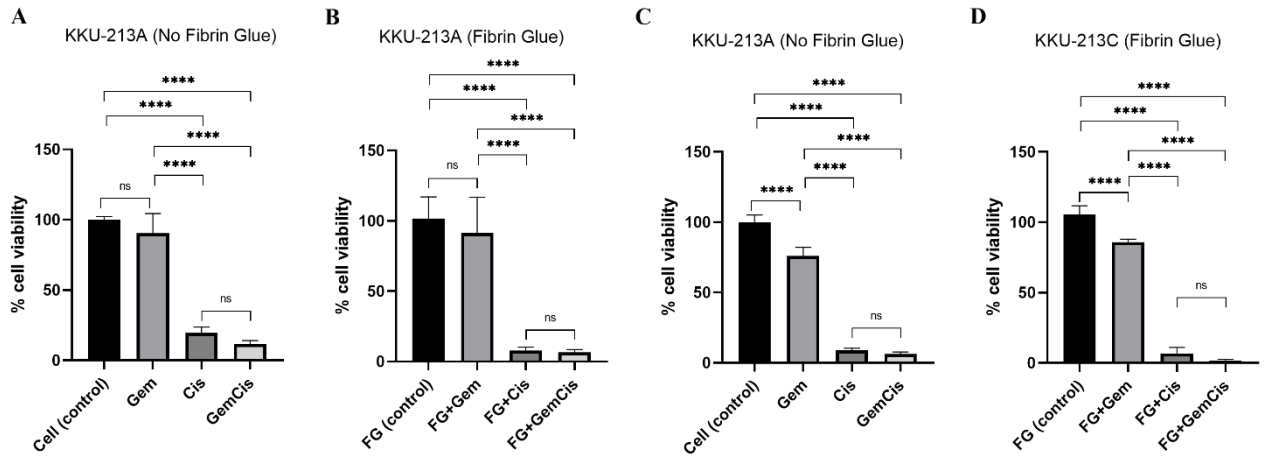

Figure 2. The effect of fibrin glue with the drug on 2D CCA cell viability. Cell viability was measured after treatment with fibrin glue combination with gemcitabine, cisplatin, and gemcitabine plus cisplatin after 48 hours by CellTiter-Glo®. (A) Cell viability of KKU-213A treat with gemcitabine and cisplatin ($P<0.0001$). (B) Cell viability of KKU-213A treat with drug incorporated with fibrin glue ($P<0.0001$). (C) Cell viability of KKU-213C treat with gemcitabine and cisplatin ($P<0.0001$). (D) Cell viability of KKU-213C treat with drug incorporated with fibrin glue ($P<0.0001$).

Spheroid-Based Migration Assay Followed by Live and Dead Cell Viability Assay

Cholangiocarcinoma (KKU-213A) cell lines were chosen for 3D MCSs formation. These results demonstrated 3D MCSs were transferred from an ultra-low attachment plate to a flat-bottomed plate to study the spheroid-based migration (one spheroid per well). After that, 1,000 μM of gemcitabine, 100 μM of cisplatin, and 1000 μM of gemcitabine plus 100 μM of cisplatin (with or without fibrin glue) were treated to 3D MCSs for 48 hours and followed the migration area (cells spread from spheroid) of MCSs over time. Then, live/dead cell assay was also performed to confirm the dead cells. To measure the migration area, Image J program was employed. The results of the cell migration area are shown in Figure 3A, and the migration area was calculated and shown in Figure 3B. Under a microscope, we examined how the formation of spheroids changed after 48 hours of drug treatment, consistently with cell viability. Migration results show that gemcitabine has a less inhibitory effect on 3D MSCSs migration than other conditions (Figure 3B). Live/dead cell assay was performed by calcein-AM and PI staining. The result indicated that gemcitabine only shows high intensity on the green channel (calcein-AM) but low intensity on the red channel (PI). Conversely, cisplatin only and gemcitabine plus cisplatin show high intensity on the red channel, which means cisplatin only and gemcitabine plus cisplatin had more potent inhibitory effects on cell migration and also caused cell death (Figure 4A). The morphology of KKU-213A spheroids was not significantly affected by Gemcitabine treatment, and the spheroids stayed intact with some death cells. Cisplatin, however, dramatically altered spheroid morphology at 100 μM. The measured fluorescence intensity per selected area is shown in the graph (Figure 4B).

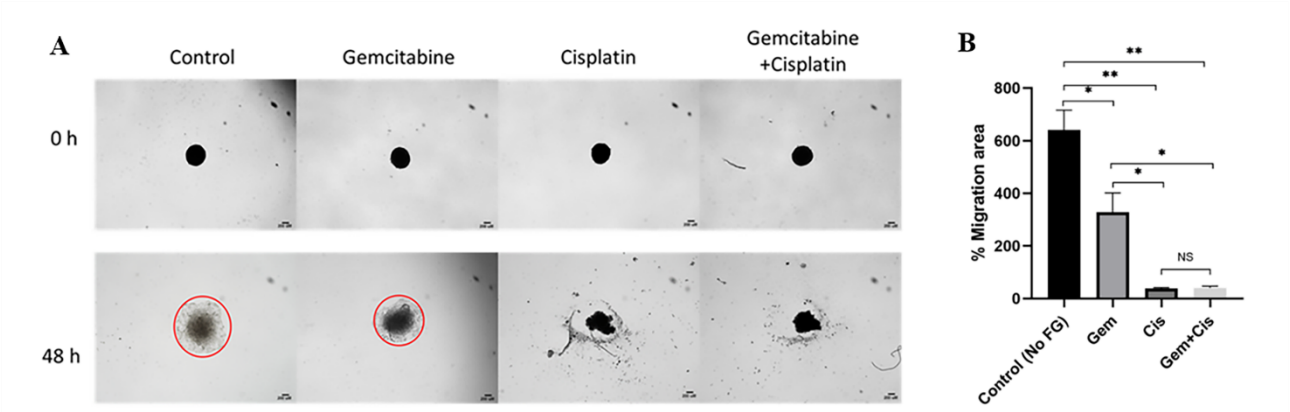

Figure 3. Light micrograph image of 3D MCSs migration of KKU-213A after treating with drugs (Gemcitabine and Cisplatin) for 48 hours and (A) followed the migration area of MCSs over time. (B) Area of the spheroids and migration area was quantified at 48 h using ImageJ.

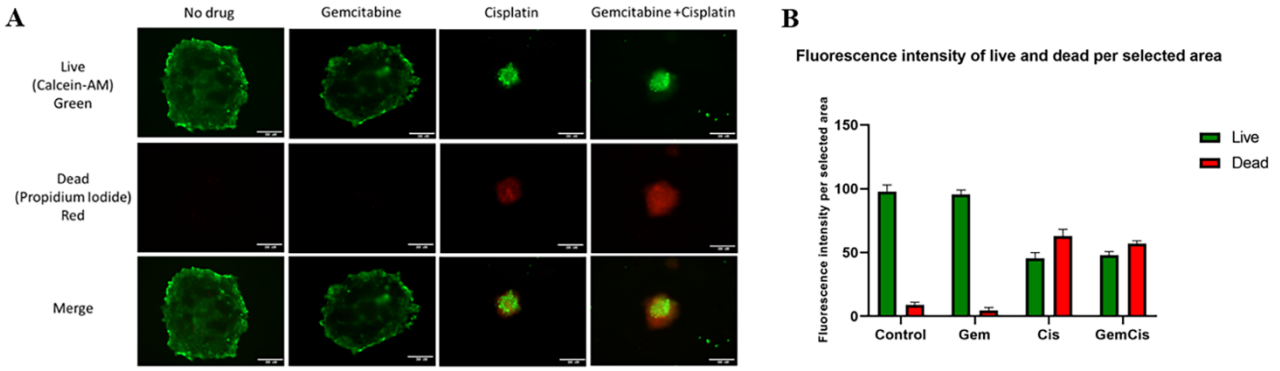

Figure 4. (A) Pictures of 3D MCS cells on cross-sectional morphology treated by gemcitabine and cisplatin. Calcein-PI staining indicated live and dead cells. Propidium iodide (red) represents dead cells and calcein-AM (green) represents live cells of 3D MCSs. (B) Showing fluorescence intensity of live and dead per selected area.

Overall, fibrin glue incorporated with drug results are similar to the conditions treated with drug only, which indicated that drug could be released from fibrin glue and showed an inhibitory effect on cells. In terms of migration, the drug can be released from fibrin glue; however, gemcitabine shows less inhibitory effect on migration. In contrast, cisplatin alone and cisplatin plus gemcitabine show more efficiency inhibitory on cell migration especially cisplatin not only has a high inhibitory effect on cell migration but also has potential in MCS's size reduction (Figure 5A), indicated by the minus value in percent of migration area (Figure 5B). Effects of drug incorporated with fibrin glue on spheroid growth found in Lina and co-worker works, the results show that FG released bleomycin and doxorubicin and effect on spheroids volume which is slightly smaller than controls (15). Live and dead cell assay was performed by calcein-AM and PI staining. The results indicated that fibrin glue with gemcitabine showed high intensity on the green channel but low intensity on the red channel. In contrast, fibrin glue with cisplatin and fibrin glue with gemcitabine plus cisplatin showed high intensity on the red channel, which means cisplatin alone and gemcitabine plus cisplatin had higher efficiency in inhibitory effect on cell migration and also caused some cell death (Figure 6A). The fluorescence intensity of live and dead per selected area is shown in Figure 6B. Studies of Knudsen et al investigated the effect of SB747651A, a multi-target small molecule inhibitor on cell migration. Result shown spheroid cultures that exposed to SB747651A showed significantly impaired cell migration when compared to controls (16). Previous studies show siramesine reduced migration in

T78 spheroids at all concentrations. Exposure to siramesine quickly affected the migration of T78 spheroid. The migratory distance of spheroids that treated with 20 µM siramesine was significantly reduced as early as one day after exposure. In T86 spheroids, a notable reduction in cell Two days following exposure, migration was seen in all exposed groups (17).

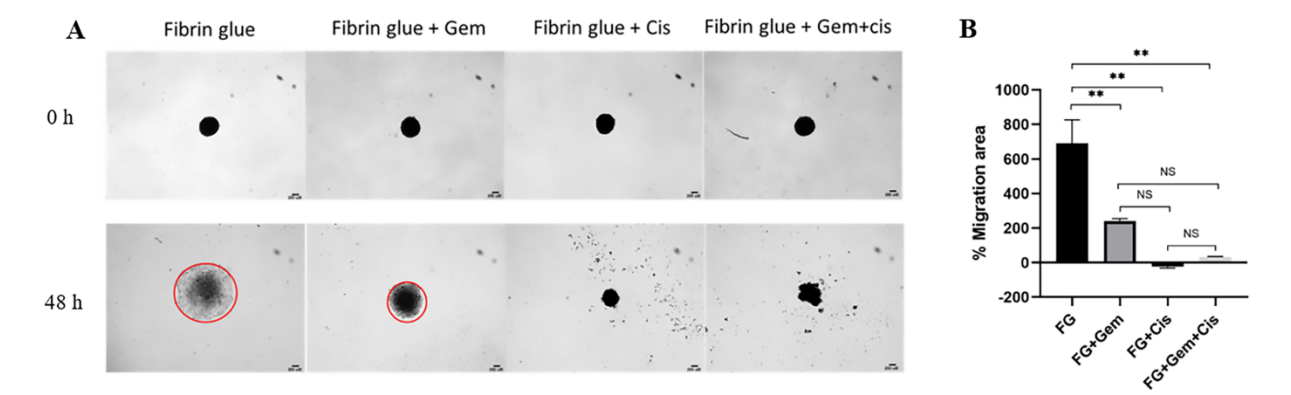

Figure 5. Light micrograph image of 3D MCSs migration of KKU-213A after treating with gemcitabine and cisplatin incorporated with fibrin glue for 48 hours and (A) followed the migration area of MCSs over time. (B) Area of the spheroids and migration area was quantified at 48 h using ImageJ.

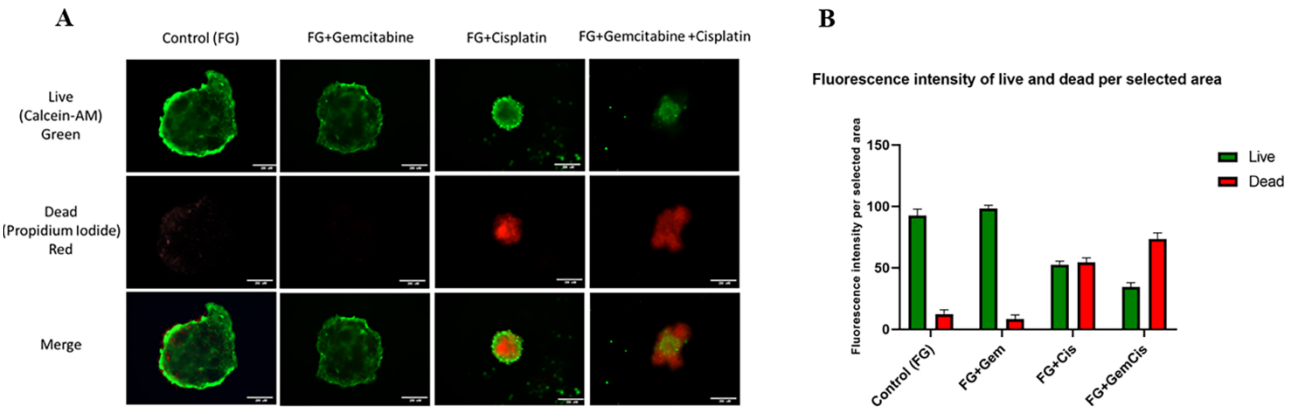

Figure 6. (A) Pictures of 3D MCSs live/dead on cross-sectional morphology after treatment with incorporated fibrin glue. Calcein-PI staining indicated live/dead cells. Propidium iodide (red) represents the dead cell, and calcein-AM (green) represents the live cell of 3D MCSs. (B) Showing fluorescence intensity of live and dead per selected area.

Fibrin Glue Formation and Mechanical Property

TISSEEL™ fibrin glue can be formed by ejecting the solution to mix in the desired container and cast into the designed shape. However, the self-made fibrin glue can be constructed by mixing fibrinogen and thrombin, as demonstrated in this experiment. The compression stress, strain, and compression modulus were assessed via a universal testing machine. The average stress and compression modulus were 0.0008141 N/mm^2 ± 0.0001710 N/mm^2, 0.0007529 N/mm^2 ± 0.0001592 N/mm^2, and 0.0005740 N/mm^2 ± 3.995e-005 N/mm^2, respectively. Although the fibrinogen concentrations in the self-made fibrin glue were lower than TISSEEL™, the self-made fibrin glue still exhibited compression moduli similar to the TISSEEL™ fibrin glue ($P>0.05$). Previous investigations of sealants created with autologous PPP (platelet-poor plasma) fibrinogen and thrombin exhibit adhesion properties comparable to those of commercial allogeneic sealants (e.g.,

TISSEEL™). Results indicate the potential of autologous sources as a viable alternative to commercial products. The study's findings underline the viability of autologous fibrin sealants in cartilage repair, demonstrating that they offer significant benefits without compromising mechanical performance (18).

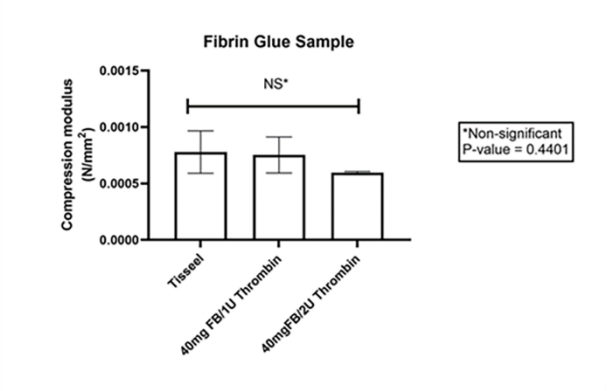

Figure 7. Compression modulus

Conclusion

We have demonstrated that gemcitabine, cisplatin, or Gem+Cis-loaded fibrin glue can develop a ready-to-use drug-loaded fibrin glue. The developed system complies with the original delivery format, which is separated into two components: fibrinogen syringe and thrombin syringe.

The results demonstrated that the mechanical properties did not change, and the drug-loaded fibrin glue showed no difference in cytotoxicity level compared to the drug alone. Applying this modified fibrin glue as an anti-tumor drug delivery material could be used in localized drug delivery after surgery for CCA patients to eliminate microscopic tumors, reduce overall toxicity, and decrease the chance of cancer relapse.

Conflict of Interest Statement: The authors declare that there is no conflict of interest regarding the publication of this paper.

Acknowledgements: This research was supported by the Fundamental Fund research grant from Thailand Science Research and Innovation. We also thank the Faculty of Medicine, Khon Kaen University, for the Invitation Research Grant (IN66033) allocated to Miss Hathaichanok Pradabkam.

References

1. Vargason AM, Anselmo AC, Mitragotri S. The evolution of commercial drug delivery technologies. Vol. 5, Nature Biomedical Engineering. Nature Research; 2021. p. 951–67.
2. Nayak AK, Ahmad SA, Beg S, Ara TJ, Hasnain MS. Drug delivery: Present, past, and future of medicine. In: Applications of Nanocomposite Materials in Drug Delivery. Elsevier; 2018. p. 255–82.
3. Woodring RN, Gurysh EG, Bachelder EM, Ainslie KM. Drug Delivery Systems for Localized Cancer Combination Therapy. Vol. 6, ACS Applied Bio Materials. American Chemical Society; 2023. p. 934–50.
4. Bastiancich C, Malfanti A, Préat V, Rahman R. Rationally designed drug delivery systems for the local treatment of resected glioblastoma. Vol. 177, Advanced Drug Delivery Reviews. Elsevier B.V.; 2021.
5. Han X, Alu A, Liu H, Shi Y, Wei X, Cai L, et al. Biomaterial-assisted biotherapy: A brief review of biomaterials used in drug delivery, vaccine development, gene therapy, and stem cell therapy. Vol. 17, Bioactive Materials. KeAi Communications Co.; 2022. p. 29–48.

6. Pavan A, Gorla GR. Two component preparation of fibrin glue and its clinical evaluation in split skin grafting. Journal of Clinical Sciences. 2019;16(4):133.
7. Madsen SJ, Devarajan AG, Chandekar A, Nguyen L, Hirschberg H. Fibrin glue as a local drug and photosensitizer delivery system for photochemical internalization: Potential for bypassing the blood-brain barrier. Photodiagnosis Photodyn Ther. 2023 Mar 1;41.
8. Lina N, Diane S, Mai T L, Eric O P, Nehal I, Jimmy Nguyen L, et al. Local Drug Delivery by Fibrin Glue for Glioma Treatment: Enhancing Drug Efficacy by Photochemical Internalization (PCI). Insights of Neuro Oncology. 2020 Jul 23;3(1).
9. Halder R, Amaraneni A, Shroff RT. Cholangiocarcinoma: a review of the literature and future directions in therapy. Hepatobiliary Surg Nutr. 2022 Aug;11(4):555–66.
10. Khosla D, Misra S, Chu PL, Guan P, Nada R, Gupta R, et al. Cholangiocarcinoma: Recent Advances in Molecular Pathobiology and Therapeutic Approaches. Vol. 16, Cancers. Multidisciplinary Digital Publishing Institute (MDPI); 2024.
11. Banales JM, Marin JJG, Lamarca A, Rodrigues PM, Khan SA, Roberts LR, et al. Cholangiocarcinoma 2020: the next horizon in mechanisms and management. Nat Rev Gastroenterol Hepatol. 2020;17(9):557–88.
12. Phukhum P, Phetcharaburanin J, Chaleekarn K, Kittirat Y, Kulthawatsiri T, Namwat N, et al. The impact of hypoxia and oxidative stress on proteo-metabolomic alterations of 3D cholangiocarcinoma models. Sci Rep. 2023 Dec 1;13(1).
13. Wathikthinnakon M, Luangwattananun P, Sawasdee N, Chiawpanit C, Lee VS, Nimmanpipug P, et al. Combination gemcitabine and PD-L1xCD3 bispecific T cell engager (BiTE) enhances T lymphocyte cytotoxicity against cholangiocarcinoma cells. Sci Rep. 2022 Dec 1;12(1).
14. Dokduang H, Namwat N, Jusakul A, Bhudhisawasdi V. Determination of Growth Inhibitory Effect of Gemcitabine on Human Intrahepatic Cholangiocarcinoma Cell lines and Comparison of its Inhibition Between the Generic and Reference Form... Determination of Growth Inhibitory Effect of Gemcitabine [Internet]. Vol. 25, Srinagarind Med J. 2553. Available from: https://www.researchgate.net/publication/279650354
15. Lina N, Diane S, Mai T L, Eric O P, Nehal I, Jimmy Nguyen L, et al. Local Drug Delivery by Fibrin Glue for Glioma Treatment: Enhancing Drug Efficacy by Photochemical Internalization (PCI). Insights of Neuro Oncology. 2020 Jul 23;3(1).
16. Knudsen AM, Boldt HB, Jakobsen EV, Kristensen BW. The multi-target small-molecule inhibitor SB747651A shows in vitro and in vivo anticancer efficacy in glioblastomas. Sci Rep. 2021 Dec 1;11(1).
17. Jensen SS, Petterson SA, Halle B, Aaberg-Jessen C, Kristensen BW. Effects of the lysosomal destabilizing drug siramesine on glioblastoma in vitro and in vivo. BMC Cancer. 2017 Mar 7;17(1).
18. Irwin RM, Bonassar LJ, Cohen I, Matuska AM, Commins J, Cole B, et al. The clot thickens: Autologous and allogeneic fibrin sealants are mechanically equivalent in an ex vivo model of cartilage repair. PLoS One. 2019 Nov 1;14(11).

Antibacterial Effect of Lupinifolin on Carbohydrate Metabolism in the Proteomic Profiling of Vancomycin-resistant *Enterococcus faecium*

Chutimon Promthong[1], Sittiruk Roytrakul[2], Kanitta Muangngam[1], and Nantiya Joycharat[3], and Wipawadee Sianglum[1,*]

[1] Division of Biological Science, Faculty of Science, Prince of Songkla University, Hat Yai, Songkhla 90110, Thailand

[2] Functional Proteomics Research Laboratory, National Center for Genetic Engineering and Biotechnology, The National Science and Technology Development Agency, Pathum Thani, Thailand

[3] Faculty of Traditional Thai Medicine, Prince of Songkla University, Hat Yai, Songkhla, Thailand

*Corresponding author's email: wipawadee.s@psu.ac.th

Abstract:

Vancomycin-resistant *Enterococcus faecium* (VREfm) is a growing public health threat, particularly in healthcare settings. The development of resistance to conventional antibiotics requires novel therapeutic compounds. Lupinifolin, a flavonoid isolated from *Albizia myriophylla* Benth., has demonstrated promising antimicrobial activity, but its precise mechanism of action remains unexplored. This study aimed to investigate the proteomic alterations induced by lupinifolin in VREfm using liquid chromatography-tandem mass spectrometry (LC-MS/MS) to understand its mechanism of action at the molecular level. VREfm cultures were treated with 1/2MIC lupinifolin (2 μg/mL) for 6 h incubation. The proteomic profiles of bacterial cells were compared between treated and untreated controls. A bioinformatic tool using a volcano plot was generated to visually represent the significance ($p < 0.05$) and 1.5-fold change of the differentially expressed proteins. The proteomic analysis revealed significant changes in proteins involved in carbohydrate metabolism, including SIS domain-containing proteins and ROK family proteins associating with sugar isomerization and regulation of kinase activity. These proteins play critical roles in bacterial energy production and metabolic regulation, suggesting that their differential expression disrupts essential metabolic pathways after treatment with sub-MIC of lupinifolin. This disruption likely contributes to the antibacterial effects of the compound, highlighting the potential of targeting carbohydrate metabolism in VREfm. The study expands our understanding of action against VREfm and highlights its promise as a potential therapeutic agent against antibiotic-resistant pathogens.

Keywords: Antibacterial activity; LC-MS/MS; Lupinifolin; Proteome; Vancomycin-resistant *Enterococcus faecium*

Introduction

The rise of antibiotic-resistant pathogens presents a significant challenge to global healthcare, with *E. faecium* being a notable concern. Since emerging as a significant cause of resistant infections, enterococci have developed resistance to various antibiotics, leading to severe bloodstream, urinary tract, and surgical wound infections (1). The World Health Organization has recognized vancomycin-resistant *E. faecium* (VREfm) as a top priority among 12 antibiotic-resistant pathogens that pose severe global health risks. Across Asia, the prevalence of VREfm is substantial, with an average prevalence rate of 22.4%, surpassing European levels but remaining lower than in the United States (2). The increasing prevalence of VREfm in Thailand is particularly concerning. Data from Thailand's National Antimicrobial Resistance Surveillance Center indicate that *E. faecium* resistance increased significantly from 0.7% in 2012 to 6.9% in 2020 (National Antimicrobial Resistance Surveillance Thailand 2022). The increasing prevalence of VRE has driven the search to highlight the urgent need for alternative treatment options. In this context, the discovery of antimicrobial compounds from medicinal plants presents a promising avenue for addressing antibiotic resistance. Natural products have long been a source of therapeutic agents, providing a rich reservoir of bioactive compounds with diverse mechanisms of action. Lupinifolin, a natural flavonoid derived from *A. myriophylla,* has shown promising antimicrobial properties, particularly against Gram-positive

bacteria. Previous studies suggest that lupinifolin disrupts cell membranes and interferes with cellular processes (3, 4). To improve our insight into the effects of lupinifolin, this study employs proteomic analysis to investigate how lupinifolin affects the protein expression profile of VREfm after treatment with 1/2MIC lupinifolin. The findings of this study may offer insights into alternative strategies for managing VRE infections, potentially contributing to the development of novel therapeutic options.

Materials and Methods

Bacterial strain, culture condition, and lupinifolin preparation

VREfm HTY0256, a clinical isolate utilized throughout this study. The bacteria were subcultured in Brain Heart Infusion (BHI) broth (BHIB, HiMedia, India) and incubated for 24 h at 35-37°C prior to each experiment. Mueller-Hinton broth (MHB, HiMedia, India) was employed for antimicrobial activity testing. The bacteria were subcultured and counted using BHI agar (BHIA, HiMedia, India). The isolate was stored in BHI broth with 20% glycerol at -80°C for subsequent use. Lupinifolin was extracted from the wood of *A. myriophylla*, collected in southern Thailand, and obtained from the Faculty of Traditional Thai Medicine at Prince of Songkla University in Thailand. The quantification of lupinifolin was quantified and formed using the previously described (5). The compound was dissolved in 100% dimethyl sulfoxide (DMSO, Merck, Germany) and stored at -20ºC in the dark until use. Lupinifolin was freshly prepared for each experiment.

Determination of antibacterial activity

The minimal inhibitory concentration (MIC) of lupinifolin against VREfm was determined using the broth microdilution method following the Clinical and Laboratory Standards Institute guidelines (CLSI, 2020). Briefly, the bacteria was cultured in MHB at 35-37°C until reaching the logarithmic phase, then diluted to approximately 10^6 CFU/mL. A 100 µL of two-fold dilutions of lupinifolin was dispensed into a 96-well microtiter plate. Subsequently, 100 µL of the bacterial suspension was added to each well, achieving a final volume of 200 µL per well and a bacterial density of approximately 5×10^5 CFU/mL and incubated at 35-37°C for 18-24 h.

Protein extraction and trypsin digestion

Protein extraction was conducted on VREfm treated with lupinifolin at 1/2 MIC for 6 h, following a modified previously reported time-kill study method (3), as well as on untreated control samples, using a 0.5% SDS solution. The protein concentration was then quantified by the Lowry assay, with bovine serum albumin as the reference standard (6). For the in-solution digestion, five micrograms of protein were dissolved in 10 mM ammonium bicarbonate (AMBIC). To reduce disulfide bonds, 5 mM dithiothreitol (DTT) in 10 mM AMBIC was added, and the mixture was incubated at 60°C for 1 h. Following this, 15 mM iodoacetamide (IAA) in 10 mM AMBIC was used to alkylate the sulfhydryl groups, with incubation at room temperature for 45 min in the dark. Sequencing-grade trypsin (50 ng/µL) was then added at a 1:20 enzyme-to-protein ratio (Promega, USA), and the digestion continued overnight at 37°C. Following digestion, the samples were dried and acidified with 0.1% formic acid in preparation for injection into the LC-MS/MS system.

Liquid Chromatography-Tandem Mass Spectrometry (LC-MS/MS)

Tryptic peptide samples were analyzed in triplicate by injecting 5 µL of each into an HCTUltra LC-MS system (Bruker Daltonics Ltd, Hamburg, Germany), coupled with a nanoLC setup, the UltiMate 3000 LC-System (Thermo Fisher Scientific, Madison, WI, USA), and using electrospray ionization. A constant flow rate of 300 nL/min was maintained through a nanocolumn (PepSwift monolithic column, 100 µm internal diameter, 50 mm length). Each sample injection included 200 fmol of trypsin-digested bovine serum albumin as an internal standard. Peptide separation was achieved using a mobile phase consisting of solvent A (0.1% formic acid) and solvent B (80% acetonitrile with 0.1% formic acid). A linear gradient was applied from 10% to 70% solvent B between 0 and 13 minutes (retention time), followed by 90% solvent B from 13 to 15 min to elute peptides. Final step involved 10% solvent B from 15 to 20 min to remove any remaining salts.

Bioinformatics analysis

DeCyder MS differential analysis software (DeCyderMS, GE Healthcare) was utilized for protein quantification. The LC-MS raw data were processed, with automated detection of peptides, assignment of charge states, and quantification based on peptide ion intensities, all carried out using the PepDetect module in MS mode. Subsequently, the processed MS/MS data were submitted to Mascot software (Matrix Science, London, UK) for protein identification through a database search. The NCBI database was searched using specific parameters, including the taxonomy set to *E. faecium*, trypsin digestion, and variable modifications such as carbamidomethylation and methionine oxidation. The search also included monoisotopic mass values, unrestricted protein mass, a peptide mass tolerance of 1.2 Da, and a fragment mass tolerance of ±0.6 Da. Peptide charge states of 1+, 2+, and 3+ were considered, with allowance for missed cleavages. Data normalization and protein abundance quantification between control and treated samples were conducted and visualized with Metaboanalyst 6.0 (7). Protein identification was further confirmed by filtering based on the interquartile range (IQR) to minimize false positives. Differentially expressed proteins were identified through a volcano plot (fold change ≥ 1.5, p-value ≤ 0.05, as determined by t-test). Venn diagrams were used to analyze the intersections of protein expression across the different sample groups. To explore protein-protein interactions, STRING version 12.0 (http://string.embl.de) was applied.

Results

Quantitative proteomics of VREfm between with and without lupinifolin treatment

A total of 1,392 proteins were identified by LC-MS/MS-based quantification and compared to the *E. faecium* protein database in NCBI. Three independent biological replicates were conducted for each sample to ensure reproducibility and reliability, and data quality was confirmed by filtering based on interquartile range (IQR) and mean intensity values. A heat map of the 1,392 identified proteins (Figure 1A) illustrates distinct protein expression profiles after treatment for 6 h, revealing noticeable differences between treated and untreated groups. Partial least squares discriminant analysis (PLS-DA) further supported these findings, showing significant clustering separation between the treated and control groups. The Venn diagram analysis allowed for the categorization of proteins into two groups for comparative proteomics analysis. Among the total proteins identified were 1,362 proteins consistently expressed across untreated and 1/2MIC lupinifolin-treated *E. faecium* samples. Venn diagram revealed 8 proteins that were uniquely expressed in the untreated control group and 17 proteins that were unique 1/2MIC lupinifolin treated group (Figure 2A). The analysis of protein-protein interactions (PPIs) for the 17 unique proteins identified in *E. faecium* treated with 1/2MIC lupinifolin, revealed significant insights into potential functional networks influenced by lupinifolin treatment. In this network, 12 key proteins were displayed, indicating their crucial roles within the interaction landscape as shown in Figure 2B. Proteins associated with the carbohydrate metabolic process are highlighted in red, those linked to the phosphoenolpyruvate-dependent sugar phosphotransferase system are shown in blue, and the proteins related to the type II toxin-antitoxin system are marked in green.

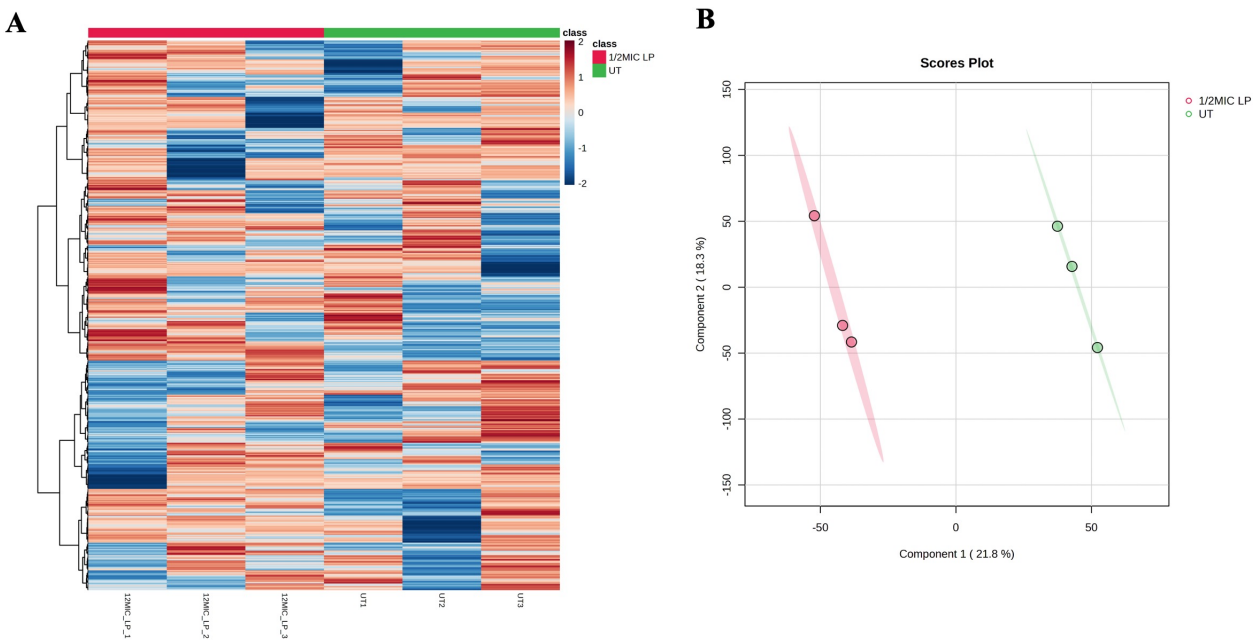

Figure 1. Quantitative proteomics analysis of protein expression in *E. faecium* treated with 1/2MIC lupinifolin (LP) and untreated control (UT). A. Heat map showing the correlation analysis of protein abundance across samples. B. Partial Least Squares Discriminant Analysis (PLS-DA) plot illustrating the separation of samples based on protein expression profiles.

Differential protein expression in VREfm following treatment with lupinifolin

The volcano plot analysis highlighted the differential expression of proteins between samples treated with 1/2MIC lupinifolin and untreated controls, using a 1.5-fold change threshold and $p < 0.05$ to define biological significance. In this plot, each point represents a protein, with the x-axis indicating the $\log_2$ fold-change in expression and the y-axis showing statistical significance ($-\log_{10}$ *p*-value). The plot revealed a subset of proteins with significant expression changes. The volcano plot analysis identified 4 significantly differentially expressed proteins (DEPs), including 4 upregulated proteins in the bacterial cultures treated with 1/2MIC lupinifolin compared to untreated controls. The volcano plot revealed clusters of proteins involved in critical biological processes. This includes those associated with carbohydrate metabolism, hypothetical protein, and phage assembly, indicating pathways that may be impacted by the treatment as shown in the Table 1.

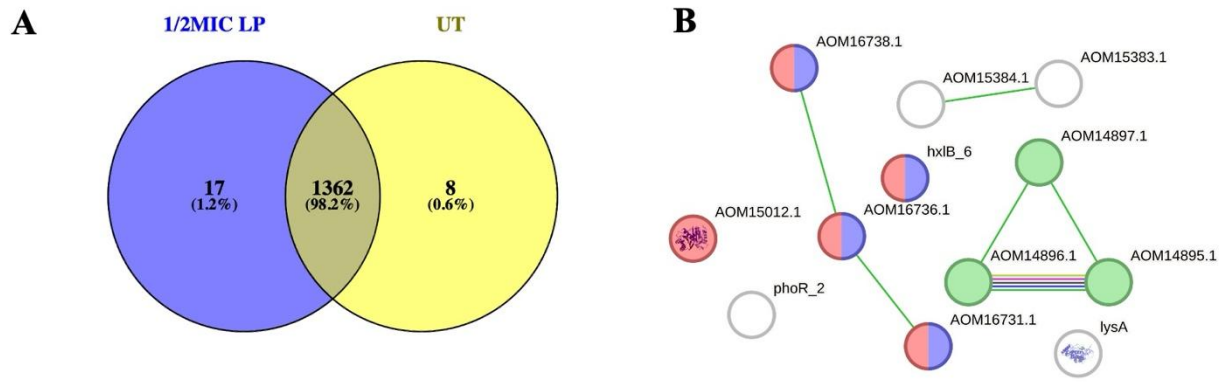

Figure 2. Differentially expressed proteins (DEPs) analysis in *E. faecium* treated with lupinifolin. (A) Venn diagram comparison of the number of proteins in 1/2MIC lupinifolin (LP) treatment and untreated control (UT). (B) STRING protein interaction network for the 17 unique proteins identified at 1/2MIC lupinifolin from venn diagram. (C) Volcano plot depicting significantly regulated DEPs in *E. faecium* treated with 2 µg/mL lupinifolin compared to the untreated control.

Table 1. Significantly differentially expressed proteins of 1/2MIC lupinifolin treated *E. faecium*

Protein ID	Gene Name	FC	Log2 FC	Functional Annotation
gi|491376847	ROK family protein	5.09	2.35	Sugar kinases phosphorylate
gi|1681080463	phage head-tail adapter protein	5.16	2.37	Phage assembly pathway
gi|1567725986	SIS domain-containing protein	5.43	2.44	Carbohydrate sensing and regulation
gi|1425472614	hypothetical protein EA9301329	1.54	0.62	Hypothetical protein

Discussion

Lupinifolin is a natural compound that exhibits excellent antibacterial activity. The efficacy in combating various antimicrobial-resistant bacteria highlights its potential to address the growing challenge of antimicrobial resistance (3, 4, 10, 11). Our findings from the 2MIC lupinifolin study support the idea that lupinifolin exerts its antibacterial effect through a multitarget mechanism (8). In this study, the impact of lupinifolin was examined by comparing protein expression between the bacterial samples treated with 1/2 MIC lupinifolin or 2 µg/mL, and untreated controls using quantitative proteomics. In the analysis of protein-protein interactions, several proteins associated with carbohydrate metabolism were identified, highlighting potential pathways influenced by lupinifolin treatment. The STRING database indicates that AOM1678.1, AOM16736.1, and AOM16731.1 proteins have roles in carbohydrate metabolism, specifically linked to the phosphoenolpyruvate-(PEP)-dependent sugar phosphotransferase system (PTS). Lupinifolin disrupts the phosphoenolpyruvate (PEP)-dependent sugar phosphotransferase system (PTS), a critical bacterial mechanism for sugar uptake and metabolism. Specifically, it inhibits AOM16736.1, a key enzyme in the Entner-Doudoroff (ED) pathway that generates ATP and biosynthetic precursors by catalyzing the cleavage of 2-dehydro-3-deoxy-6-phosphogluconate. This disruption reduces energy production and metabolic flexibility, impairing bacterial growth and stress response. Additionally, AOM1678.1 and AOM16731.1, also involved in carbohydrate metabolism, are likely affected, further enabling it to survive in nutrient-limited environments. Additionally, activation of the type II toxin-

antitoxin system amplifies bacterial stress, further contributing to growth arrest and cell death. These carbohydrate-specific targets, along with other pathways, highlight the potential of lupinifolin as a promising antibacterial agent against resistant strains. The analysis of differentially expressed proteins in carbohydrate metabolism has identified key proteins, including SIS domain-containing proteins and ROK family proteins. The upregulation of SIS domain-containing proteins highlights their pivotal role as regulators within carbohydrate metabolism. These proteins, which bind phosphorylated sugars, are essential for cellular sensing and regulation mechanisms, enabling cells to monitor and respond to internal sugar levels (14). Similarly, ROK family proteins exhibit, which are known to function primarily as transcriptional regulators and are often associated with carbohydrate metabolism (15). The upregulation of ROK family proteins could lead to enhanced regulation of pathways that facilitate the utilization of carbohydrates, thus contributing to the overall metabolic efficiency of the cell. The up-regulation of phage head-tail adapter proteins could interfere with the bacterial virulence factors of the isolate, such as biofilm formation, which is a critical aspect of the ability of VREfm to persist in clinical environments and to resist treatments. Similarly, the up-regulation of a hypothetical protein EA9301329 in response to lupinifolin treatment may suggest that this protein plays a role in the bacterial stress response. Targeting these pathways has several clinical implications that may address the urgent challenge of antimicrobial resistance. This aligns with the findings of previous studies, such as the work on Litsea cubeba essential oil (EO) against Cutibacterium acne. In that study, EO demonstrated significant antibacterial activity by affecting metabolic pathways, including carbohydrate metabolism, energy metabolism, amino acid metabolism, and cell wall and cell membrane synthesis (16). This highlights the broader applicability of natural products in targeting bacterial metabolic pathways and their potential to combat antimicrobial resistance.

Conclusion

This study demonstrates that lupinifolin, significantly impacts the proteomic profile of VREfm. Through quantitative proteomics, we identified critical shifts in metabolic and regulatory pathways, notably in carbohydrate metabolism. The compound upregulated the protein involved in SIS domain-containing proteins and ROK family proteins, which are carbohydrate metabolism and targets of lupinifolin. Overall, this study emphasizes the potential of lupinifolin as a natural antimicrobial agent against VREfm, offering a foundation for developing new antimicrobial therapies to combat antibiotic-resistant infections.

Acknowledgements

This research was supported by a Graduate Fellowship (Research assistant) from the Faculty of Science Research Fund, Prince of Songkla University, under Contract no. 1-2563-02-007 and Prince of Songkla University grant, Contract No. SCI6302099S.

References

(1) Arias CA, Murray BE. The rise of the *Enterococcus*: beyond vancomycin resistance. Nature Reviews Microbiology. 2012;10(4):266-78.
(2) Shrestha S, Kharel S, Homagain S, Aryal R, Mishra SK. Prevalence of vancomycin-resistant enterococci in Asia—A systematic review and meta-analysis. Journal of Clinical Pharmacy and Therapeutics. 2021;46(5):1226-37.
(3) Sianglum W, Muangngam K, Joycharat N, Voravuthikunchai SP. Mechanism of action and biofilm inhibitory activity of lupinifolin against multidrug-resistant enterococcal clinical isolates. Microbial Drug Resistance. 2019;25(10):1391-400.
(4) Yusook K, Weeranantanapan O, Hua Y, Kumkrai P, Chudapongse N. Lupinifolin from *Derris reticulata* possesses bactericidal activity on *Staphylococcus aureus* by disrupting bacterial cell membrane. Journal of natural medicines. 2017;71:357-66.

(5) Joycharat N, Thammavong S, Limsuwan S, Homlaead S, Voravuthikunchai SP, Yingyongnarongkul B-e, et al. Antibacterial substances from *Albizia myriophylla* wood against cariogenic *Streptococcus mutans*. Archives of pharmacal research. 2013;36:723-30.
(6) Lowry OH, Rosebrough NJ, Farr AL, Randall RJ. Protein measurement with the Folin phenol reagent. J biol Chem. 1951;193(1):265-75.
(7) Pang Z, Lu Y, Zhou G, Hui F, Xu L, Viau C, et al. MetaboAnalyst 6.0: towards a unified platform for metabolomics data processing, analysis and interpretation. Nucleic Acids Research. 2024:gkae253.
(8) Promthong C, Sianglum W, Roytrakul S. Effect of lupinifolin on the proteome of multidrug-resistant *Enterococcus faecium* [abstract]. Presented at: International BioScience Conference (IBSC); 2021 Nov 25–26; Novi Sad, Serbia.
(9) Abdallah EM, Alhatlani BY, de Paula Menezes R, Martins CHG. Back to Nature: Medicinal plants as promising sources for antibacterial drugs in the post-antibiotic era. Plants. 2023;12(17):3077.
(10) Kwaengmuang P, Chaiyawong K, Warong T, Rattanakiat S, Pulbutr P. Antibiofilm and antibacterial activities of lupinifolin in combination with protein synthesis inhibitors against methicillin-resistant *Staphylococcus aureus*. Journal of Herbmed Pharmacology. 2023;12(4):549-59.
(11) Limsuwan S, Moosigapong K, Jarukitsakul S, Joycharat N, Chusri S, Jaisamut P, et al. Lupinifolin from *Albizia myriophylla* wood: a study on its antibacterial mechanisms against cariogenic Streptococcus mutans. Archives of Oral Biology. 2018;93:195-202.
(12) Siguier P, Gourbeyre E, Chandler M. Bacterial insertion sequences: their genomic impact and diversity. FEMS microbiology reviews. 2014;38(5):865-91.
(13) Conway T. The Entner-Doudoroff pathway: history, physiology and molecular biology. FEMS microbiology reviews. 1992;9(1):1-27.
(14) Bräsen C, Esser D, Rauch B, Siebers B. Carbohydrate metabolism in Archaea: current insights into unusual enzymes and pathways and their regulation. Microbiology and Molecular Biology Reviews. 2014;78(1):89-175.
(15) Conejo MS, Thompson SM, Miller BG. Evolutionary bases of carbohydrate recognition and substrate discrimination in the ROK protein family. Journal of molecular evolution. 2010;70:545-56.

Elevation of Blood Insulin Resistance after Sub-Chronic Exposure to PM2.5 Based on ^{1}H-NMR

Nitip Liampongsabuddhi[1,2,*], Yutti Amornlertwatana[2], Giatgong Konguthaithip[2], and Churdsak Jaikang[2,*]

[1] Master's Degree in Toxicology, Department of Forensic Medicine, Faculty of Medicine, Chiang Mai University, Chiang Mai 50200 Thailand

[2] Metabolomic Research Group for Forensic Medicine and Toxicology, Department of Forensic Medicine, Faculty of Medicine, Chiang Mai University, Chiang Mai 50200 Thailand

*Corresponding author's email: nitip_liam@cmu.ac.th and churdsak.j@cmu.ac.th; Tel.: +6653-934532

Abstract:

Insulin resistance (IR) is a significant contributor to and coexists with β-cell defects in glucose-stimulated insulin secretion, impaired glucose tolerance, hyperglycemia and type 2 diabetes. Fine particulate matter (PM2.5) is a major air pollutant in Northern Thailand and has become a significant public health concern. The objective of this study was to examine blood levels of IR biomarkers following sub-chronic exposure to PM2.5 in Northern Thailand. Healthy volunteers from areas with high (n = 99) and low (n = 98) PM2.5 levels were enrolled. Healthy volunteers who lived in Mae Jam district (high exposure area) and Watanakorn district (low-exposure area) more than 15 years were enrolled. Blood samples were collected before and during haze periods. IR biomarkers, including 3-methyl-2-oxovaleric acid, N6-carboxymethyllysine, lysine, valine, isoleucine, leucine, pentosidine, 3-hydroxybutyric acid and 2-hydroxybutyric acid were analyzed using proton nuclear magnetic resonance (^{1}H-NMR) spectroscopy. The average PM2.5 concentration was 31 μg/m^{3}/month, exceeding the World Health Organization's guidelines. Nine metabolites significantly increased and are related to branched-chain amino acid synthesis, advanced glycation end-products, ketone body degradation, and oxidative stress. 3-Hydroxybutyric acid and L-isoleucine had significant negative correlations with PM2.5 doses (r = -0.137 and -0.165). These results showed that PM2.5 is associated with IR and may contribute to the development of type 2 diabetes mellitus. In conclusion, exposure to PM2.5 elevates the IR biomarkers and increases the risk of type 2 diabetes. Stronger policy required to substantially reduces PM2.5 sources in Northern Thailand.

Keywords: Insulin resistance; Metabolic biomarkers; Particulate matter; Nuclear magnetic resonance spectroscopy; Environment pollutions; Diabetes

Introduction

In northern Thailand, fine particulate matter (PM2.5) is a major air pollutant and presents significant health risks. PM2.5 is generated from biomass burning, wildfires, vehicle emissions, and industrial activities (1). Level of PM2.5 exceeds standard levels from January to March. It may remain in the environment for prolonged durations, and contains heavy metals, carbon compounds such as polycyclic aromatic hydrocarbons (PAHs) and various volatile chemicals (4). PAHs also activate the aryl hydrocarbon receptor (AhR) while inhibiting the activity of Glutathione S-transferases (GSTs), enzymes crucial for cellular protection against ROS (1). This disruption of redox balance within cells results in damage to DNA, RNA, and proteins through oxidation, contributing to the onset of insulin resistance (2, 3). Moreover, specific PAH metabolites, such as 1-hydroxypyrene (1-OHpyR) and benzo[a]pyrene (B[a]P) (4, 5), have been identified as agents of oxidative damage, further linking PAH exposure to metabolic disturbances.

The extrapulmonary metabolic effects of air pollution have been linked to several pathways, with oxidative stress being the predominant mechanism. Exposure to particulate matter, nitrogen dioxide, and sulfur dioxide induces oxidative stress, which has been strongly associated with the development of diabetes. Long-term exposure to PAHs contributes to this process by promoting oxidative stress, inflammation, and the disruption of sugar metabolism, ultimately leading to insulin resistance (2, 3, 5). PAHs are known to induce the production of reactive oxygen species (ROS)

through multiple mechanisms, further exacerbating metabolic dysfunction (3, 4). Subsequently, it penetrates the bloodstream and disperses throughout the other organs. This can induce inflammation and oxidative stress lead to chronic non-communicable diseases, such as cardiovascular disorders, diabetes, hypertension, cancer and insulin resistance (1, 2, 3, 5).

Insulin resistance, a condition often linked to chronic inflammation of pancreatic beta cells, plays a key role in the development of type 2 diabetes (T2D) (6). Evaluating insulin resistance is essential for monitoring and screening the risk of T2D at its early stages (2, 7). Biomarkers such as fasting blood sugar levels, blood insulin levels, the HOMA-IR index, branched-chain amino acids (BCAAs), and metabolomics data are commonly used to assess insulin resistance.

Metabolomics, an advanced "omics" technology, enables the detailed investigation of metabolites within the body. By analyzing metabolic changes associated with disease progression or exposure to toxic substances, metabolomics enhances our understanding of illnesses and their effects on the body's biochemical processes. Techniques such as Liquid Chromatography-Mass Spectrometry (LC-MS/MS) and proton nuclear magnetic resonance (^{1}H-NMR) are widely used in metabolomics research (7). However, data on the effects of PM2.5 exposure on insulin resistance remain scarce. Thus, this study aims to investigate the impact of sub-chronic exposure to PM2.5 on insulin resistance biomarker levels, providing critical insights into the metabolic consequences of air pollution.

Materials and Methods

The Level of $PM_{2.5}$ in Atmosphere

The levels of PM2.5 were collected from June 2014 to December 2023 by the Thai Metrological Department. The average levels each year at the Mae Jam District (high exposure area) and the Watanakorn District (low-exposure area). PM2.5 concentrations were higher in areas with high exposure, ranging from 23–36 μg/m^3/day compared to low-exposure areas with ranges of 17–25 μg/m^3/day.

Blood Sample Collection

This study was approved by the Ethics Committee of Faculty of Medicine, Chiang Mai University (Study Code: FOR-2567-0610). Healthy volunteers (n=197) were recruited from the Mae Jam District, Chiang Mai Province (n = 99) for the high-exposure area and from Watthana Nakhon District, Sa Kaew Province, Thailand (n = 98) for the low-exposure area. The participants were given 5 mL of blood drawn into heparin tubes by nurses. The samples were kept at 4 °C during transportation and were stored at -80 °C until analysis.

Preparation of Blood Samples

Blood samples were extracted with acetonitrile in ratio 1:1 following the method of Jaikang et al., shaken for 20 minutes, and then centrifuged at 4000 rpm at 4 °C for 10 minutes to precipitate the solids. The supernatant was collected and evaporated using a Lyophilizer Freeze-dryer Alpha 3-4 LSCbasic (Martin Christ, Germany). The evaporated samples were then reconstituted with 0.1 M of 3-(trimethylsilyl)-[2,2,3,3-d4]-1-propionate sodium salt (TSP) solution (Sigma Aldrich, USA) in deuterium oxide (D_2O) as the internal standard. The liquid samples were then transferred into NMR tubes and analyzed using ^{1}H-NMR spectroscopy at 500 MHz, applying a technique to suppress water resonance.

Condition of ^{1}H-NMR Spectroscopy

The proton NMR spectra was obtained at 27°C using a Bruker AVANCE 500 MHz spectrometer (Bruker, Bremen, Germany) with the Carr-Purcell-Meiboom-Gill (CPMG, -RD-90◦-(t-180◦-t) n-acquire) water suppression pre-saturation pulse sequence. A 90° pulse with a number of signal averages (NSA) equal to 16 was administered. The baseline and phase correction were meticulously calibrated using Bruker TopSpin software version 4.0.7. Spectra ranging from 0 to 12 ppm were examined, with data normalized to the total integrated area.

Integration of signals and Insulin resistance biomarkers Identification

Nine insulin resistances metabolites are available, including L-leucine, L-isoleucine, L-lysine, L-valine, 3-hydroxybutyric acid, 2-hydroxybutyric acid, Pentosidine, N6-carboxymethyllysine and 3-methyl-2-oxovaleric acid. Identification of each chemical compound was determined by using the Human Metabolome Database (HMDB) (8). Integration of signals or peak assignment depending on the Cluster Midpoint, peak sequence (Coupling type), number of hydrogen atoms (H's), atomic number, and Coupling constant (*J*-coupling). The interpretation of the NMR spectra relied on the utilization of chemical shift values. These values were crucial for identifying the signal's integration site, determining the integrated region underlying the signal, examining spin-spin coupling, analyzing signal patterns, and evaluating the coupling constant. Identification and adjustment of each peak were necessary to align within 0.01 ppm of the HMDB database, and the same number of occurrences should be observed. Subsequently, the concentration of each chemical can be calculated, following the method outlined (9).

Calculation of metabolites by quantitative NMR

The data were imported into MestReNova software (version 14.1, MestreLab Research, Spain) for metabolite peak identification. All spectra in the chromatogram were adjusted to a baseline of 0 and calibrated using the TSP peak of the internal standard at 0.000 ppm. Afterwards to peak collection, the intensity of all metabolite peaks was quantified to concentration using the equation (10) that follows.

$$C_A = \frac{I_A}{I_{TSP}} \times \frac{H_{TSP}}{H_A} \times C_{TSP}$$

C_A relates to the concentration of the substance.
I_A refers to the intensity value of the substance.
I_{TSP} represents the intensity value of TSP.
H_{TSP} refers to the hydrogen atom of TSP.
H_A represents the hydrogen atom of the substance.
C_{TSP} relates to the concentration of TSP.

It is crucial to ensure chemical compatibility with the database. Specifically, the chemical shift values of each Cluster midpoint must not deviate by more than 0.02, and the same number of occurrences should be observed. Subsequently, the concentration of each chemical can be calculated, following the method outlined (9).

Statistical Analysis

Data are presented as means ± standard deviation (SD) in the demographic table. The Kolmogorov–Smirnov test was used to assess normality. Differences between the high- and low-exposure groups were analyzed using the Mann–Whitney U-test. Results with p values were considered statistically significant.

Results and Discussion

Demographic Data

One hundred and ninety-seven participants were classified into two groups: the high-exposure were included at Mae Jam, Chiang Mai (n=99) and the low-exposure were collected at Wata Nanakorn, Sa Kaew (n=98). The blood samples were collected before exposure haze period and during exposure haze period. Individual volunteers were left out due to inactivity in sampling and lack of response, so we included more subjects during the haze period in each area to complete the sample size. Gender, age, weight, height, blood pressure, and heart rate were similar between the groups. The results are presented in **Table 1**.

Table 1. Demographic data of participants.

	High exposure areas (n=99)			**Low exposure areas (n=98)**		
	HBH	**HDH**	***p* values**	**LBH**	**LDH**	***p* values**
Female (n%)	72 (72.7)			71 (68.5)		0.218
Age (years)	48.9 ± 12.4			42.6 ± 12.1		0.07
BMI (kg/m^2)	23.36 ± 4.0	24.3 ± 4.8	0.443	24.5 ± 3.9	24.9 ± 4.1	0.89
SYS(mmHg)	130.14 ± 16.4	122.8 ± 16.3	0.186	129.1 ± 21.9	122.4 ± 15.4	0.20
DIA (mmHg)	81.20 ± 9.9	77.2 ± 10.6	0.397	81.2 ± 14.0	79.1 ± 8.4	0.46
Heart rate (beats/min)	81.87 ± 11.7	85.1 ± 11.3	0.681	83.9 ± 14.1	82.1 ± 12.0	0.601
Living in the area (year)	36.7 ± 19.2			31 ± 14.0		

Abbreviations: HBH, high-exposure group before exposure haze period; HDH, high-exposure group during exposure haze period; LBH, low-exposure group before exposure haze period; LDH, low-exposure group during exposure haze period; SD, standard deviation; BMI, body mass index; SYS, Systolic pressure; DIA, Diastolic pressure; Results are presented as Mean ± SD.

The IR biomarkers were analyzed both quantitative and qualitative .^{1}H-NMR technique to determine their types and quantities. The study identified 9 metabolites associated with the IR and the results are shown in **Figure 1**.

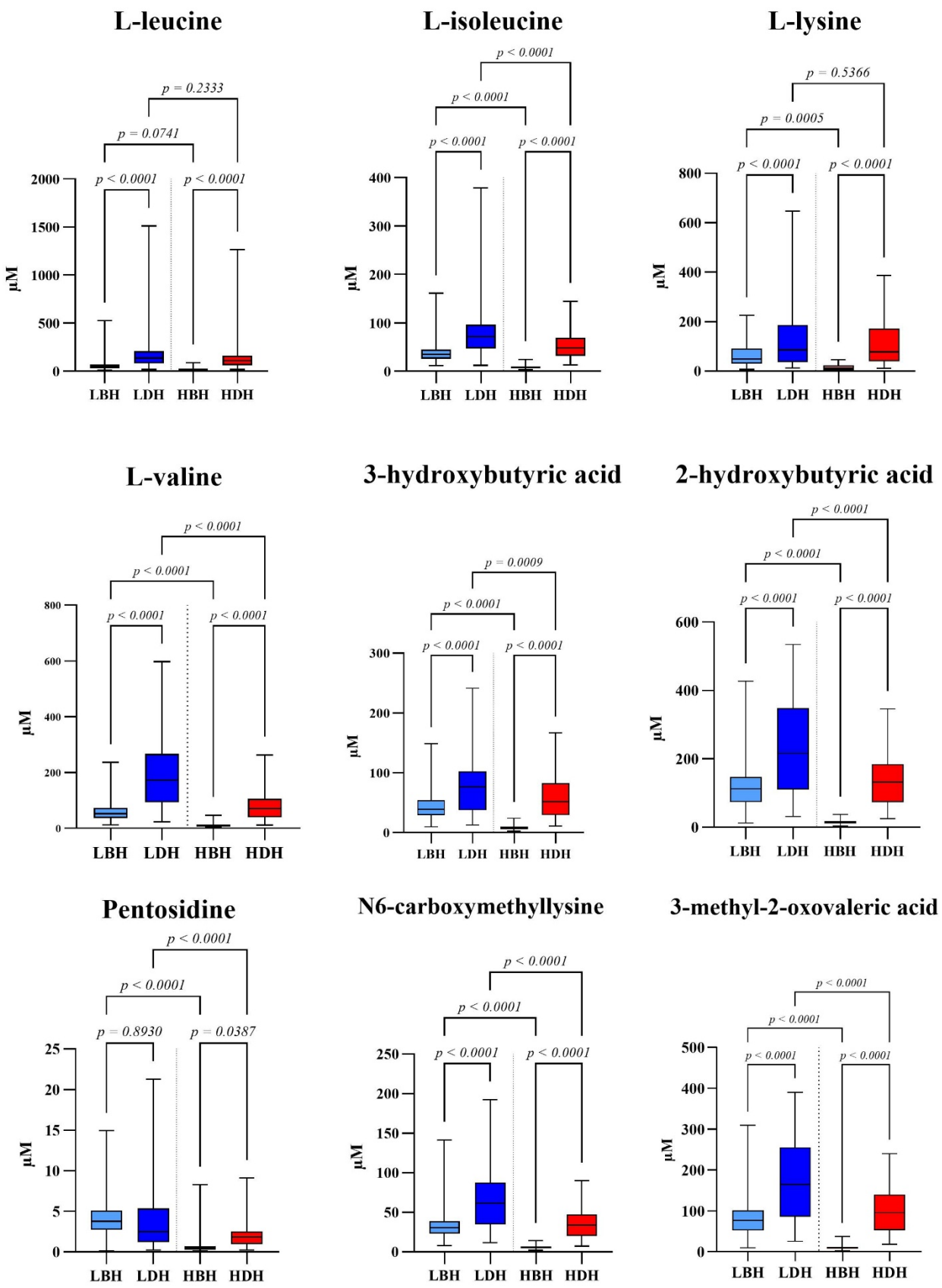

Figure 1. Box plots of compound elevation were associated with Insulin resistance in high and low PM2.5 exposure areas, Significant difference compared between groups using Mann–Witney U test (p <0.0001). The data are expressed as mean ± standard deviation (SD) of concentrations (µM).

The graphs illustrate the impact of PM2.5 on the blood metabolite concentrations across four distinct groups: LBH, LDH, HBH, and HDH. The measured metabolites including BCAAs (L-leucine, L-isoleucine, L-lysine, L-valine), organic acids (3-hydroxybutyric acid, 2-hydroxybutyric acid, 3-methyl-2-oxovaleric acid), and advanced glycation end-products (AGEs) such as pentosidine and N6-carboxymethyllysine were determined. Each box plot represents the distribution of metabolite concentrations. The interquartile range (IQR) representing 50% of the data is shown within the box with the median value indicated by a line inside the box. Whiskers extend to 1.5 times the IQR from the box edges capturing most of the data. The statistical significance of differences between groups is indicated by the *p*-values displayed above each box plot, with a *p*-value less than 0.0001 signifying statistically significant differences.

Branch chain amino acid (BCAA), a mixture of leucine, valine and isoleucine, have important regulatory effects on glucose, lipid, protein metabolism. BCAA can induce IR by promoting fat accumulation. In this study, we determined the precursors for BCAA biosynthesis including L-leucine, L-isoleucine and L-valine. BCAAs are closely related to abnormal glucose and lipid metabolism in animal models and BCAAs are important inducers of insulin resistance (11). The concentrations of BCAAs were significantly higher in the LDH and HDH groups compared to LBH and HBH groups ($p < 0.0001$) suggested a strong link between elevated BCAAs in healthy groups after exposure PM2.5. Among the L-lysine significantly elevated in the LDH compared to the LBH group ($p < 0.0001$). Ketone bodies and AGEs specifically pentosidine and N6-carboxymethyllysine also notably elevated in the LDH and HDH groups ($p < 0.0001$). This indicates increased lipid metabolisms and oxidative stresses, both hallmarks of PM2.5 intoxications. Interestingly, pentosidine and N6-Carboxymethyllysine levels significantly elevated in LDH but not in HDH, and the results are presented in **Figures 1**. Higher precursors might promote the BCAA synthesis and BCAA induce the macromolecule metabolisms. It implied that sub-chronic exposure activates IR and needs to be proved the mechanism further. 3-Methyl-2-oxovaleric acid is an essential intermediate in the catabolism of BCAAs, particularly isoleucine. It is generated through the enzymatic activity of branched-chain aminotransferase and plays a pivotal role in the BCAA degradation pathway. Elevated concentrations of 3-methyl-2-oxovaleric acid have been linked to neurotoxic effects and metabolic imbalances. The level of 3-Methyl-2-oxovaleric acid was higher during PM2.5 exposure indicating that PM2.5 might disrupt isoleucine metabolism. Additionally, impaired function of the branched-chain alpha-keto acid dehydrogenase complex (BCKDC) can result in increased levels of 3-methyl-2-oxovaleric acid. 3-Methyl-2-oxovaleric acid is released by brown and white adipocytes in response to thermogenic stimuli. It has been shown to promote adipose tissue browning and enhance fatty acid β-oxidation in both adipose tissue and skeletal muscle, functioning within an adipose–adipose and adipose–skeletal muscle interorgan signaling network (12).

The organic acid, 3-methyl-2-oxovaleric acid and 2-hydroxybutyric acid were associated with BCAAs metabolism significantly elevated in LDH and HDH group, further supporting the role of altered amino acid metabolism in diabetes (13, 14). Additionally, the BCAA precursor and its metabolites such as L-leucine, L-isoleucine, L-valine, 3-hydroxybutyric acid and 3-methyl-2-oxovaleric acid significant increase in the low- and high-exposure groups suggesting that dietary protein intake substantially might impact these metabolites. However, the L-lysine levels appeared to be similar in the LDH and HDH group. 2-Hydroxybutyric acid, also known as alpha-hydroxybutyric acid, is an organic molecule indicative of metabolic alterations and physiological conditions. It participates in critical metabolic processes, such as energy production and the conversion of cystathione to cysteine in glutathione synthesis. Beyond its role as a metabolic byproduct, 2-hydroxybutyric acid serves as an early biomarker for insulin resistance and oxidative stress-related conditions. Elevated levels of this compound in blood may signal metabolic dysregulation, including lactic acidosis or ketoacidosis, often observed in diabetes. The normal concentration of 2-hydroxybutyric acid in blood typically ranges from 8.00 to 80.0 μM, as reported in previous studies (5). This metabolite has been linked to pancreatic β-cell dysfunction, a critical factor in the development of type 2 diabetes mellitus (T2D). In the current study, among healthy adults, exposure to PM2.5 was positively correlated with elevated levels of 2-hydroxybutyric acid in both high- and

low-exposure areas during the haze period, with recorded concentrations of 138.9 ± 80.2 μM and 232.7 ± 136.6 μM, respectively. Interestingly, participants residing in Mae Jam exhibited lower metabolite concentrations compared to those in Sa Kaew, despite the higher incidence of T2D in Sa Kaew occurring without direct PM2.5 exposure. Following PM2.5 exposure, insulin resistance (IR) biomarkers increased in both regions, with a more pronounced elevation observed in the high-exposure area. These findings highlight the role of PM2.5 in activating IR-related metabolic pathways. Moreover, 3-Hydroxybutyric acid is a small ketone body molecule produced in the liver (13). In mammals, 3-Hydroxybutyric acid is transported to extrahepatic tissues, taken up in peripheral tissues by monocarboxylate transporter (MCT), and oxidized for ATP production. 3-Hydroxybutyric acid becomes an important energy source within extrahepatic tissues. Circulating total ketone body concentrations in healthy adult humans normally exhibit circadian oscillations between approximately 0.1 and 0.25 mM, rise to 1 mM after prolonged exercise or 24 h of fasting, and can accumulate to as high as 20 mM in pathological states such as diabetic ketoacidosis (14). The level of 3-hydroxybutyric acid elevated after sub-chronic exposure to PM2.5 indicating that human body has accumulated from energy production.

Pentosidine and N6-carboxymethyllysine are advanced glycation end products (AGEs) produced during imbalance of oxidative stress and antioxidant. Serum levels of pentosidine and N6-carboxymethyllysine were significantly elevated in individuals with type 2 diabetes compared to non-diabetic controls (15). The levels of pentosidine and N6-carboxymethyllysine significantly enhanced in blood samples after PM2.5 exposure. Increasing of pentosidine and N6-carboxymethyllysine might be from oxidative stress during haze period.

Air pollution in Thailand is linked to fine particulate matter, varying seasonally and by region. Chiang Mai, the largest city in northern Thailand situated on a plain amidst towering mountains, experienced the haze period from January to April. During the haze season, Chiang Mai recorded some of the highest dust levels contributing to global air pollution. Biomass combustion from agricultural practices and wildfires constitutes a significant source of PM2.5 and PM10. Sa Kaew is a city in eastern Thailand situated on the plain adjacent to the sea. Agricultural biomass combustion is a notable contributor to PM2.5, albeit at lower levels than in Chiang Mai. The mean concentration of PM2.5 in high-exposure areas was 31.7 $\mu g/m^3$/day, while in low-exposure areas it was 19.5 $\mu g/m^3$/day. Before haze period, all the IR biomarkers of Sa Kaew, the low-exposure area, differed from Mae Jam. The results indicated that the volunteers who lived in Sa Kaew higher incident of diabetes than Mae Jam. Moreover, the difference of lifestyles, diets and physical activities of the volunteers are the major factors of the differences. After sub-chronic PM2.5 exposure, the levels of IR concentrations in the both areas were greater than the before haze period excepted pentosidine. Additionally, the IR biomarker concentrations were significantly higher (p <0.0001) in the LDH group compared to the HDH group. These results indicate that high exposure to PM2.5 levels exceeding the WHO recommendations increases IR concentrations.

But rather the sort of chemicals that are transmitted from various sources of particulate matter. In spite of this study, a critical need to develop biomarkers and clinical tests or procedures that are not only easily accessible but also cost-effective in order to attenuate and prevent the developing of type 2 diabetes in its early stages. Based on the findings of this study, it is possible that the potential of infrared predictors with additional biomolecules, as well as the existing methods for their detection, will be better understood.

Limitations of this study, Various factors, including the use of personal protective equipment, alcohol consumption, smoking, intake of grilled foods, and genetic variation, may influence oxidative stress and insulin resistance levels.

Conclusion

Sub-chronic exposure to air pollutants, especially particulate matter enhanced the IR biomarkers. Higher levels of BCAA precursors are specific to insulin resistance is so closely related to Type 2 Diabetes Mellitus. The health impact of particulate-matter exposure on humans is ambiguous, further research examining more observation and further exploration are still needed.

Conflict of interest statement: No conflict of interest

References

(1) Jaikang C, Konguthaithip G, Amornlertwatana Y, Autsavapromporn N, Rattanachitthawat S, Monum T. Alterations in the blood kynurenine pathway following Long-Term PM2.5 and PM10 exposure: a Cross-Sectional study. Biomedicines. 2024;12(9):1947.

(2) Ma R, Zhang Y, Sun Z, Xu D, Li T. Effects of ambient particulate matter on fasting blood glucose: a systematic review and meta-analysis. Environmental pollution. 2020; 258:113589.

(3) Gong X, Wang S, Wang X, Zhong S, Yuan J, Zhong Y, et al. Long-term exposure to air pollution and risk of insulin resistance: A systematic review and meta-analysis. Ecotoxicology and Environmental Safety. 2024;271:115909.

(4) Danian, Kahe., Zahra, Sabeti., Parvin, Sarbakhsh., Mohammad, Shakerkhatibi., Akbar, Gholampour., Gholamreza, Goudarzi., Jabraeil, Sharbafi., Saeed, Dastgiri., Ahmad, Separham., Ensiyeh, Seyedrezazadeh. Effect of PM2.5 exposure on adhesion molecules and systemic nitric oxide in healthy adults: The role of metals, PAHs, and oxidative potential. Chemosphere, (2024).

(5) Ryu JY, Hong DH. Association of mixed polycyclic aromatic hydrocarbons exposure with oxidative stress in Korean adults. Scientific Reports [Internet]. 2024 Mar 29;14(1). Available from: https://doi.org/10.1038/s41598-024-58263-9

(6) Sousa AP, Cunha DM, Franco C, Teixeira C, Gojon F, Baylina P, et al. Which role plays 2-Hydroxybutyric acid on insulin resistance? Metabolites. 2021;11(12):835.

(7) Hsu FC, Palmer ND, Chen SH, Ng MCY, Goodarzi MO, Rotter JI, et al. Methods for estimating insulin resistance from untargeted metabolomics data. Metabolomics. 2023;19(8).

(8) Wishart, D. S., Jewison, T., Guo, A. C., Wilson, M., Knox, C., Liu, Y., Scalbert, A. (2013). HMDB 3.0--The Human Metabolome Database in 2013. *Nucleic Acids Res, 41*, D801-807.

(9) Choi, K., Myoung, S., Seo, Y., & Ahn, S. (2021). Quantitative NMR as a Versatile Tool for the Reference Material Preparation. *Magnetochemistry, 7*(1).

(10) de Graaf, R. A., & Behar, K. L. (2003). Quantitative ^{1}H NMR spectroscopy of blood plasma metabolites. *Analytical Chemistry*, *75*(9), 2100-2104.

(11) de Bandt JP, Coumoul X, Barouki R. Branched-Chain Amino Acids and Insulin Resistance, from Protein Supply to Diet-Induced Obesity. Nutrients [Internet]. 2022 Dec 23;15(1):68. Available from: https://doi.org/10.3390/nu15010068.

(12) MacCannell ADv, Roberts LD. Metabokines in the regulation of systemic energy metabolism. Current Opinion in Pharmacology [Internet]. 2022 Sep 19;67:102286. Available from: https://doi.org/10.1016/j.coph.2022.102286.

(13) Zhang Y, Li Z, Liu X, Chen X, Zhang S, Chen Y, et al. 3-Hydroxybutyrate ameliorates insulin resistance by inhibiting PPARγ Ser273 phosphorylation in type 2 diabetic mice. Signal Transduction and Targeted Therapy [Internet]. 2023 May 26;8(1). Available from: https://doi.org/10.1038/s41392-023-01415-6.

(14) Nishitani S, Fukuhara A, Tomita I, Kume S, Shin J, Okuno Y, et al. Ketone body 3-hydroxybutyrate enhances adipocyte function. Scientific Reports [Internet]. 2022 Jun 16;12(1). Available from: https://doi.org/10.1038/s41598-022-14268-w.

(15) Ghanem AA, Elewa A, Arafa LF. Pentosidine and N-Carboxymethyl-Lysine: biomarkers for Type 2 diabetic retinopathy. European Journal of Ophthalmology [Internet]. 2010 May 26;21(1):48–54. Available from: https://doi.org/10.5301/ejo.2010.4447.

Antiproliferative Activity of Alizarin Derivative Al-5 Against Human Cervical Cancer Cell Line

Aye Myat Zon[1], Narissara Namwan[1], Gulsiri Senawong[1], Mongkol Nontakitticharoen[2], and Thanaset Senawong[1,*]

[1] Department of Biochemistry, Faculty of Science, Khon Kaen University, Khon Kaen 40002, Thailand
[2] Department of Chemistry, Faculty of Science, Khon Kaen University, Khon Kaen 40002, Thailand
*Corresponding author's email: sthanaset@kku.ac.th

Abstract:

Cervical cancer is a major public health problem against women. Recent chemotherapy drugs cause side effects and lead to drug resistance. Therefore, searching for new anticancer drugs derived from natural products is urgently needed. This study aimed to investigate the antiproliferative activity of the alizarin derivative AL-5 against human cervical cancer HeLa cells in single and combination drug treatments with the current chemotherapeutic drug carboplatin (CBP). MTT results revealed that alizarin derivative AL-5 inhibited HeLa cells with half-maximal inhibitory concentration (IC_{50}) values of 195.5 ± 0.7, 24.39 ± 0.5, and 18.2 ± 1.1 μM at exposure times of 24, 48, and 72 hours, respectively. In contrast, CBP exhibited IC_{50} values of >400, 226.51 ± 2.84, and 76.06 ± 3.48 μM at exposure times of 24, 48, and 72 hours, respectively. In the non-cancer Vero cells, alizarin derivative AL-5 showed IC_{50} values of >200, 114.49 ± 6.69, and 81.22 ± 17.13 μM, while CBP exhibited 373.67 ± 30.94, 87.14 ± 17.81, and 58.5 ± 12.23 μM at exposure times of 24, 48, and 72 hours, respectively. The combined treatment between CBP (IC_{20} subtoxic dose) and alizarin derivative AL-5 in HeLa cells exhibited the synergistic effect (combination index less than 1) with IC_{50} values of 10.53 ± 0.7 and 10.49 ± 0.5 μM at 48- and 72-hour exposures, respectively. The result showed that the combination of CBP and AL-5 has a synergistic effect on the Hela cell line, enhancing anti-proliferative activity and effectively inhibiting cancer cell growth while minimizing harm to non-cancerous cells. In summary, alizarin derivative AL-5 was more effective than CBP in inhibiting HeLa cell proliferation, with less toxicity to non-cancer Vero cells. Additionally, alizarin derivative AL-5 could enhance the antiproliferative activity of CBP against HeLa cells in combination treatments.

Keywords: Alizarin derivatives; Carboplatin; Drug interaction; MTT assay; HeLa cells

Introduction

Cervical cancer is a significant health issue for women, exhibiting about 6.6% of all cancers diagnosed in females, and accounting for the second most prevalent cancer in Thailand (1, 2). In 2020, approximately 570,000 new cases of cervical cancer were recorded (2). According to the World Health Organization report, approximately 5,100 cervical cancer deaths occur annually in Thailand. Besides, the cumulative risk of developing cervical cancer for individuals aged 0-74 is 1.7% (3). Human papillomavirus (HPV) infection, especially with the high-risk subtypes HPV-16 and HPV-18, is the major cause of cervical cancer (4). Symptoms of cervical cancer patients include bleeding, pelvic pain, and dyspareunia. Treatment of cervical cancer is based on the stage of cervical cancer, however, the common treatments include surgical interventions, hysterectomy, chemotherapy, and radiotherapy that can be either used alone or in combination (5, 6). Although chemotherapy is an efficient treatment to suppress the growth of cervical cancer cells, side effects are a concern such as nausea, neuropathy, immune suppression, and long-term health risks. Surgical interventions could damage nearby organs, infertility, and sexual dysfunction. Moreover, radiotherapy's effect was a concern such as bowel, bladder, and vaginal damage, as well as fatigue (7).

Nowadays, natural products become an intriguing focus on enhancing anticancer activities of current anticancer drugs or lessening problems of side effects and drug resistance from chemotherapy through drug combination treatments (8, 9). Natural products such as alkaloids, flavonoids, and terpenoids have been reported as an alternative due to their strong cytotoxic effects against cervical

cancer cells with low toxicity against noncancer cells. Additionally, natural products can enhance immune responses and help to control HPV (10). Therefore, research and development of new drugs derived from natural compounds and their derivatives are urgently needed. A flowering plant madder (*Rubia tinctorum*) belongs to the Rubiaceae family and is known for its historical use as a natural dye and its application in traditional medicine. Alizarin derived from a root of madder has been reported on the anticancer properties in various types of cancer such as osteosarcoma, pancreatic cancer, breast cancer, cervical cancer, etc. For example, alizarin showed anticancer activity against pancreatic cancer cells with minimal cytotoxicity against the normal cells and showed no side effects in mice (11). Currently, carboplatin (CBP) is a chemotherapy drug for cervical cancer treatment that belongs to platinum-containing compounds. As an alternative to cisplatin, CBP exhibits less nephrotoxic in treating advanced or recurrent cervical cancer (12). In this study, we explored the antiproliferative activity of the alizarin derivative AL-5 against human cervical cancer HeLa cells in alone and combination treatments with the current chemotherapeutic drug CBP.

Materials and Methods

Cell culture

The HeLa and non-cancer Vero cells were maintained in RPMI-1640 medium supplemented with 10% fetal bovine serum, penicillin (100 U/ml), and streptomycin (100 µg/ml) (Gibco-BRL, USA). The cells were incubated at 37 °C in a humidified atmosphere with 5% CO_2. Alizarin derivative AL-5 was obtained from the Department of Chemistry, Faculty of Science, Khon Kaen University, Thailand, while CBP was purchased from Sigma-Aldrich (USA).

Antiproliferation assay

Cell viability was determined by MTT assay. HeLa or Vero cells were seeded into 96-well plates at 8 x 10^3 cells/well for 24 hours. After that, cells were exposed to various concentrations of alizarin derivative AL-5 (6.25, 12.50, 25, 50, 100, and 200 µM) or CBP (12.50, 25, 50, 100, 200, and 400 µM), and 0.5 % DMSO plus 0.5% ethanol and 50 % DMSO plus 50 % DDW at 1:1 ratio were served as solvent controls for alizarin derivative AL-5 and CBP, respectively. Treated cells were incubated at 37 °C for 24, 48, and 72 hours. Half-maximal inhibitory concentration (IC_{50}) values of compounds and a sub-toxic concentration of CBP (IC_{20}) were obtained from their cell viability graphs. In combined treatment experiments, HeLa cells were exposed to a sub-toxic concentration of CBP (IC_{20}) combined with various concentrations of AL-5 (1.56, 3.13, 6.25, and 12.5, 25, 50 µM) at 37 °C for 48 and 72 hours. Then, the old medium was replaced with fresh medium containing 1.2 mM of MTT (100 µl/well) and incubated at 37 °C for 2 hours. After incubation, formazan crystal was dissolved with DMSO and incubated for 15 min. The absorbances were measured at 570 nm and 655 nm (served as reference) wavelengths using the iMark™ Microplate Absorbance Reader. The percentages of cell viability were calculated as follows;

$$\text{Cell viability (\%)} = \frac{\text{A570 treatment - OD655 treatment}}{\text{A570 solvent control - OD655 solvent control}} \times 100$$

Where A represents the absorbance and OD represents the optical density.

Selectivity index (SI)

The degree of selectivity of the compounds was expressed as the selectivity index (SI) value. The SI value > 2 is considered selective toxicity against cancer cells, while the SI value < 2 is considered general toxicity against cancer and normal cells. The SI value was calculated using the following equation;

$$\text{SI} = \frac{IC_{50} \text{ noncancer (Vero) cells}}{IC_{50} \text{ cancer (HeLa) cells}}$$

Determination of drug interaction

The Chou-Talalay method (13) was used to estimate the combination index (CI) and to assess the type of drug interaction between CBP and alizarin derivative AL-5. The following is the equation of CI values for 50% growth inhibition:

$$CI = \frac{D1}{Dx1} + \frac{D2}{Dx2} + \alpha\left[\frac{(D1 \times D2)}{(Dx1Dx2)}\right]$$

Where D1 indicates a dose of drug 1 combined with drug 2 in combination treatment to produce 50 % growth inhibition; Dx1 is a dose of drug 1 single treatment to produce 50 % growth inhibition; D2 represents a dose of drug 2 combined with drug 1 in combination treatment to produce 50 % growth inhibition; Dx2 indicated a dose of drug 2 single treatment to produce 50 % growth inhibition; $\alpha = 1$ for mutually non-exclusive modes of drug action; $CI < 1$ reveals a synergistic effect; $CI = 1$ reveals an additive effect, and $CI > 1$ reveals antagonism.

The dose reduction index (DRI) was calculated as follows;

$$DRI_1 = \frac{Dx1}{D1} \qquad DRI_2 = \frac{Dx2}{D2}$$

Where D is a dose of a drug combined with the other drug to produce 50 % cell viability, while Dx is a dose of a drug alone to produce 50 % cell viability. DRI value more than 1-fold is favored dose reduction whereas the value less than 1-fold is disfavored dose reduction.

Results and Discussion

Antiproliferative activities of Alizarin derivative AL-5 and chemotherapeutic drug carboplatin against human cervical cancer HeLa cells

In order to investigate the antiproliferative effects, all treatments demonstrated in a dose-and time-dependent manner suppress the growth of cervical cancer cells. The effects of alizarin derivative and carboplatin on cell viability in a single drug treatment against human cervical cancer HeLa cells were determined by using MTT assay. The percentages of cell viability and IC_{50} values were displayed in **Figure 1**. Alizarin derivative alone inhibited proliferation of Hela cells with IC_{50} values of 195.5 ± 0.7, 24.39 ± 0.5, and 18.20 ± 1.1 µM at 24-, 48-, and -72 h exposures, respectively (**Figure 1 (a)**). The IC_{50} values of carboplatin against Hela cells were > 400, 226.51± 2.84 and 76.06± 3.48 µM for exposure times of 24, 48, and 72 h, respectively (**Figure 1 (b)**).

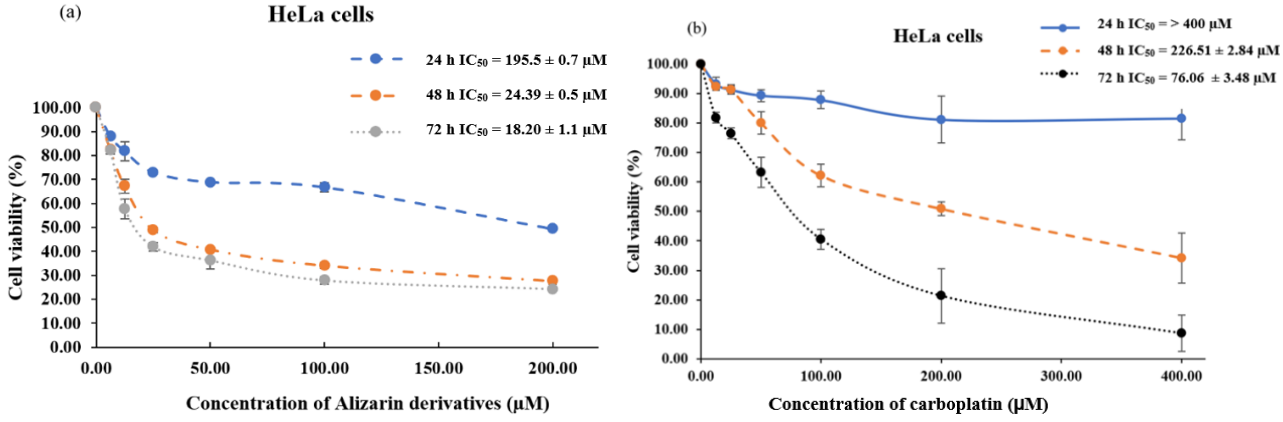

Figure 1 Effects of alizarin derivative AL-5 and carboplatin on the proliferation of HeLa cells. HeLa cells were treated with (a) alizarin derivative AL-5 (6.25-200 µM) and (b) carboplatin (12.5-400 µM). Antiproliferative activity was determined by MTT assay according to the manufacturer protocol. Data

are shown as percentage of cell viability compared with the solvent control treatment. The IC_{50} values are expressed as the mean ± SEM from 3 independent experiments.

Antiproliferative activities of Alizarin derivative AL-5 and chemotherapeutic drug carboplatin against non-cancer Vero cells

The cytotoxic effects of alizarin derivative AL-5 and carboplatin on non-cancer Vero cells were determined by using MTT assay. The alizarin derivative AL-5 significantly reduced the proliferation of Vero cells with IC_{50} values of >200, 114.49 ± 6.69 and 81.22 ± 17.13 µM at exposure times of 24, 48, and 72 h, respectively (**Figure 2 (a)**), whereas carboplatin showed IC_{50} values of 373.67 ± 30.94, 87.14 ± 17.81, and 58.50 ± 12.23 µM at exposure times of 24, 48, and 72 h, respectively (**Figure 2 (b)**). These results indicated that the alizarin derivative AL-5 inhibited the proliferation of HeLa cells more effectively than carboplatin. In addition, the alizarin derivative AL-5 exhibited less cytotoxic effect on non-cancer Vero cells than the current chemotherapeutic drug carboplatin.

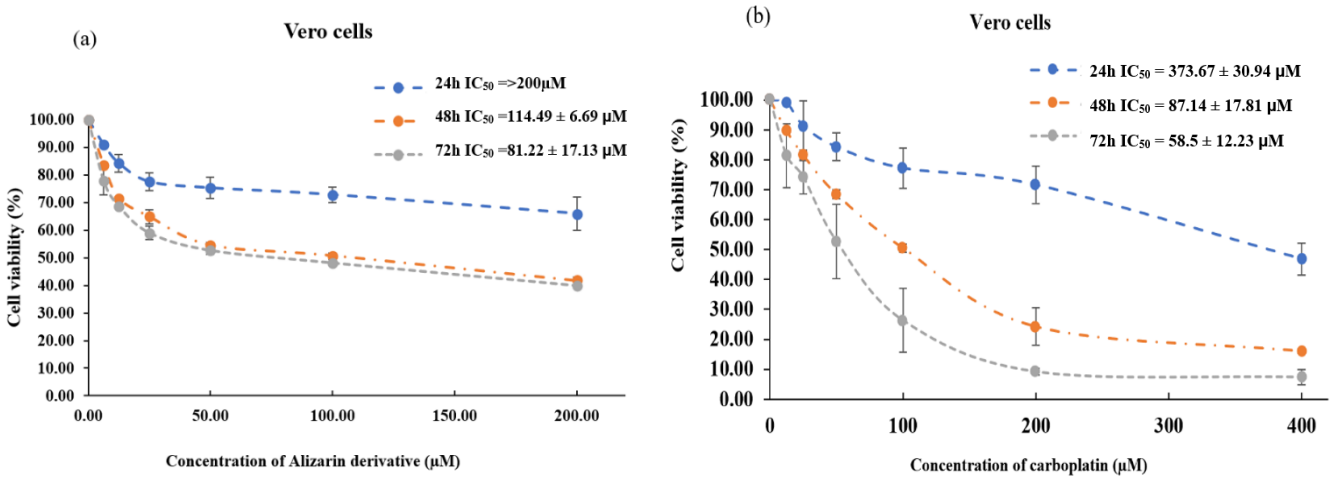

Figure 2 Effect of alizarin derivative AL-5 and carboplatin on the proliferation of Vero cells. Vero cells were treated with (a) alizarin derivative AL-5 (6.25, 12.5, 25, 50, 100, 200 µM) and (b) carboplatin (12.5, 25, 50, 100, 200, 400 µM). Antiproliferative activity was determined by MTT assay according to the manufacturer protocol. Data are shown as the percentage of cell viability compared with the solvent control treatment. The IC_{50} values are expressed as the mean ± SEM from 3 independent experiments.

The IC_{50} values of alizarin derivative AL-5 and carboplatin against human cervical cancer cells (HeLa cells) and non-cancer cells (Vero cells) were summarized in Table 1. For HeLa cells, alizarin derivative inhibited cell proliferation with IC_{50} value of 195.5 ± 0.7 µM while carboplatin inhibited cell proliferation with IC_{50} value of >400 µM at 24 h-exposure. For non-cancer Vero cells, alizarin derivative AL-5 and carboplatin inhibited cell proliferation with IC_{50} values of >200 µM and 373.67 ± 30.94 µM, respectively, at 24 h-exposure. For HeLa cells at 48 h-exposures, alizarin derivative AL-5 and carboplatin showed IC_{50} values of 24.39 ± 0.5 µM and 226.51 ± 2.84 µM, respectively. For Vero cells at 48 h-exposure, alizarin derivative AL-5 and carboplatin inhibited cell proliferation with IC_{50} values of 114.49 ± 6.69 µM and 87.14 ± 17.81 µM, respectively. Accordingly, the SI values of alizarin derivative AL-5 and carboplatin against cervical cancer cells at 48 h exposures were 4.69 and 2.59, respectively. For HeLa cells at 72 h-exposures, alizarin derivative AL-5 and carboplatin showed IC_{50} value of 18.20 ± 1.10 µM and 76.06 ± 3.48 µM, respectively. For Vero cells at 72 h-exposure, alizarin derivative AL-5 and carboplatin inhibited cell proliferation with IC_{50} values of 81.22 ± 17.13 µM and 58.5 ± 12.23 µM, respectively. Therefore, The SI values of

alizarin derivative AL-5 and carboplatin against cervical cancer cells at 72 h exposures were 4.46 and 1.30, respectively.

Tables 1 The IC_{50} and SI values of alizarin derivative and carboplatin against HeLa cells and Vero cells

Anticancer agents	Exposure Time	IC_{50} HeLa cells, µM (mean ± SEM)	IC_{50} Vero cells, µM (mean ± SEM)	SI
Alizarin derivative AL-5	24 h	195.5± 0.70	>200	-
	48 h	24.39± 0.50	114.49± 6.69	4.69
	72 h	18.20± 1.10	81.22± 17.13	4.46
Carboplatin	24 h	> 400	373.67± 30.94	-
	48 h	226.51± 2.84	87.14± 17.81	2.59
	72 h	76.06± 3.48	58.5± 12.23	1.30

SI represents the selectivity index. Data are the means of three independent experiments. Selectivity Index (SI) = IC_{50} Vero cells/ IC_{50} HeLa cells. SI value > 2 indicates selective toxicity against cancer cells (14).

The antiproliferative activities of alizarin derivative AL-5 and chemotherapeutic drug CBP in combination treatments against human cervical cancer HeLa cells

To elucidate the potential of alizarin derivative AL-5 for enhancing the antiproliferative activities of the current chemotherapeutic drug CBP against HeLa cells, we performed combination treatments of alizarin derivative AL-5 with a subtoxic dose (IC_{20} concentration) of CBP. The inhibition rates of fixed dose CBP (IC_{20} = 50.86 and 14.87 µM, at 48 and 72 h, respectively) in combination with various concentrations of alizarin derivative AL-5 (1.56- 50 µM at 48, and 72 h) were determined using MTT assay. The IC_{50} values of combination treatment of CBP (IC_{20}) and AL-5 were 10.53 ± 0.7 and 10.49 ± 0.5 µM at exposure times of 48 and 72 h, respectively, as shown in **Figure 3**.

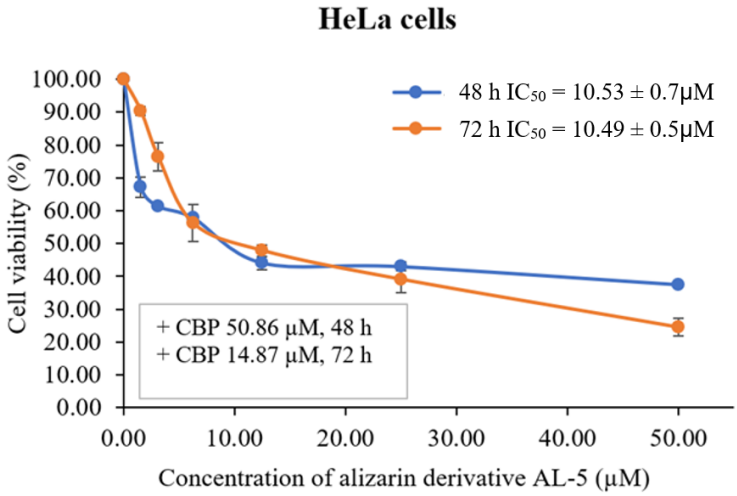

Figure 3 Antiproliferative effects of alizarin derivative AL-5 and CBP on HeLa cells in combination treatments IC_{50} values of alizarin derivative AL-5 against HeLa cells when treated in combination with CBP (sub-toxic dose = IC_{20}).

The combination index (CI) values were calculated using the Chou & Talalay method and the results were shown in Table 2. The CI values for combination treatments of AL-5 and CBP (IC20) against HeLa cells at 48 h and 72 h exposures were 0.75 and 0.88, indicating synergistic effects. In addition, these synergistic effects at 48 and 72 h resulted in a dose reduction of 4.45- and 5.11-fold for CBP and 2.32- and 1.73-fold for AL-5 at 48 h and 72 h exposures, respectively.

Table 2 Combination index (CI) and dose reduction index (DRI) of the combination treatments between CBP and alizarin derivative AL-5 against HeLa cells

Drug combination	Exposure time	CI	DRI	
			CBP	AL-5
CBP 50.86 μM (IC_{20}) + AL-5 (IC_{50})	48 h	0.75 ± 0.03	4.45	2.32
CBP 14.87 μM (IC_{20}) + AL-5 (IC_{50})	72 h	0.88 ± 0.02	5.11	1.73

At the synergistic conditions, the combination treatment of CBP and alizarin derivative AL-5 suppressed HeLa cell viability more effectively than the single drug treatments (**Figure 4 (a)** and **(b)**). However, further studies on mechanisms of drug action in vitro, such as cell cycle arrest induction, apoptosis induction, invasion or metastasis inhibition, are required to reflect anti-cancer hallmarks. Moreover, the study on anticancer activity in animal model is also needed.

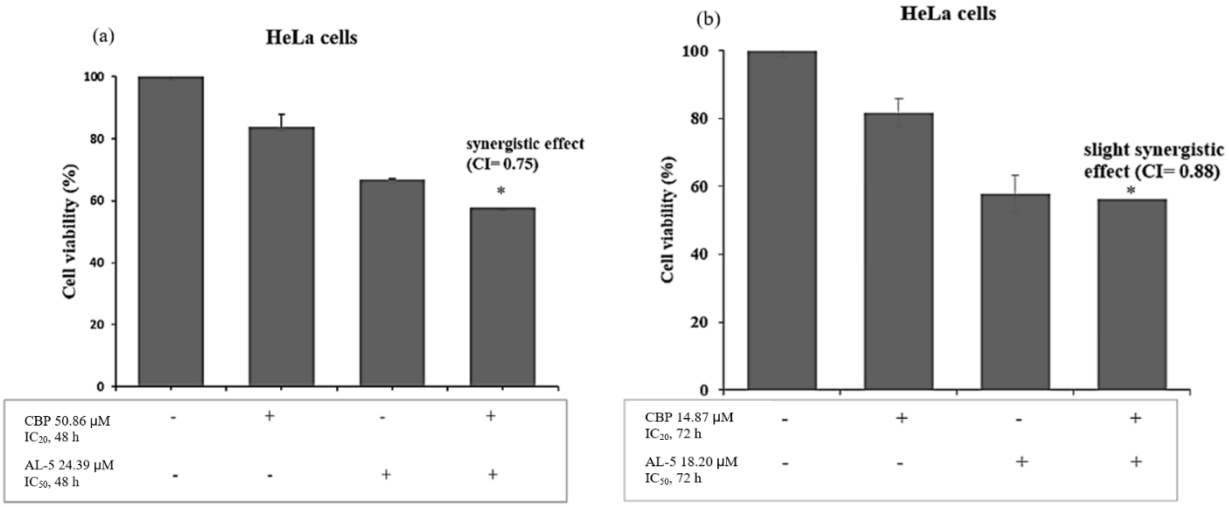

Figure 4 Antiproliferative effects of alizarin derivative AL-5 and CBP on HeLa cells in combination treatments (a) Drug interaction between alizarin derivative AL-5 and CBP against HeLa cells at 48 h exposure. (b) Drug interaction between alizarin derivative AL-5 and CBP against HeLa cells at 72 h exposure. The calculation of cell viability employed the percentage comparison to cells treated with solvent control (0.50% ethanol + 0.50% DMSO). "*" denotes a statistically significant reduction ($p < 0.05$) compared to the single drug treatment of AL-5.

Conclusion

Alizarin derivative AL-5 exhibited antiproliferative activity against cervical cancer HeLa cells in a dose- and time-dependent manner. Alizarin derivative AL-5 exhibited a remarkable cytotoxic effect on HeLa cells at all exposure times compared with carboplatin. The alizarin derivative AL-5 combination treatments showed a synergistic effect with carboplatin (IC_{20}) at both 48 h and 72 h exposures. The findings of this study suggest that alizarin derivative AL-5 enhances the antiproliferative activity of carboplatin against HeLa cells. Alizarin derivative AL-5 could potentially be an alternative therapeutic agent for the treatment of cervical cancer. However, further studies on cell cycle arrest induction, apoptosis induction, invasion or metastasis inhibition, are required.

Conflict of interest statement

The authors declare that there is no conflict of interest in this article.

Acknowledgements

The authors would like thank department of Biochemistry, Faculty of Science, Khon Kaen University for providing a graduate scholarship to Aye Myat Zon. The research on "Development of anti-cancer agents possessing histone deacetylase inhibitory activity from Thai medicinal plants" by Khon Kaen University has received funding support from the National Science Research and Innovation Fund (Fundamental Fund-2567).

References

1. Wongpratate, M., & Bumrungthai, S. Cervical cancer in Thailand: 2023 update. Obstetrics & gynecology science 2024; 67(3): 261–269.
2. Ploysawang, P., Rojanamatin, J., Prapakorn, S., Jamsri, P., Pangmuang, P., Seeda, K., et al. National Cervical Cancer Screening in Thailand. Asian Pacific journal of cancer prevention: APJCP 2021; 22(1): 25–30.
3. World Health Organization. Cervical cancer Thailand 2021 country profile. Available at: URL https://www.who.int/publications/m/item/cervical-cancer-tha-country-profile-2021. Accessed Nov 25, 2024.
4. Sahasrabuddhe V. V. Cervical Cancer: Precursors and Prevention. Hematology/oncology clinics of North America 2024; 38(4): 771–781.
5. Burmeister, C. A., Khan, S. F., Schäfer, G., Mbatani, N., Adams, T., Moodley, J., et al. Cervical cancer therapies: Current challenges and future perspectives. Tumour virus research 2022; 13: 200238.
6. Babakanrad, E., Mohammadian, T., Esmaeili, D., & Payam B. Cervical Cancer: A Review of Epidemiology, Treatments, and Anticancer Drugs. Current Cancer Therapy Reviews 2023; 19(3): 198–212.
7. Marth, C., Landoni, F., Mahner, S., McCormack, M., Gonzalez-Martin, A., Colombo, N., et al. Cervical cancer: ESMO Clinical Practice Guidelines for diagnosis, treatment and follow-up. Annals of oncology : official journal of the European Society for Medical Oncology 2017; 28: iv72–iv83.
8. Chen, P., Ni, W., Xie, T., & Sui, X. Meta-Analysis of 5-Fluorouracil-Based Chemotherapy Combined With Traditional Chinese Medicines for Colorectal Cancer Treatment. Integrative cancer therapies 2019;18: 1534735419828824.
9. Xu, B., Wang, X., Wang, H., Cao, L., Ge, Y., Yuan, B., et al. Efficacy and safety of herbal formulas with the function of gut microbiota regulation for gastric and colorectal cancer: A systematic review and meta-analysis. Frontiers in cellular and infection microbiology 2022; 12: 875225.
10. Park, S. H., Kim, M., Lee, S., Jung, W., & Kim, B. Therapeutic Potential of Natural Products in Treatment of Cervical Cancer: A Review. Nutrients 2021; 13(1): 154.
11. Xu, Z., Hou, Y., Zou, C., Liang, H., Mu, J., Jiao, X., et al. Alizarin, a nature compound, inhibits the growth of pancreatic cancer cells by abrogating NF-κB activation. International journal of biological sciences 2022; 18(7): 2759–2774.
12. Liu, W., Zhang, L., & Yu, M. Potential mechanism of Astragalus polysaccharide increasing chemosensitivity of cervical cancer HeLa cells to carboplatin by modulating the PI3K/Akt signaling pathway. European Journal of Gynaecological Oncology 2023; 44(6): 4-11.
13. Chou, T. C., & Talalay, P. Quantitative analysis of dose-effect relationships: the combined effects of multiple drugs or enzyme inhibitors. Advances in enzyme regulation 1984; 22: 27–55.
14. Tugba Artun, F., Karagoz, A., Ozcan, G., Melikoglu, G., Anil, S., Kultur, S., et al. In vitro anticancer and cytotoxic activities of some plant extracts on HeLa and Vero cell lines. Journal of B.U.ON.: official journal of the Balkan Union of Oncology 2016; 21(3): 720–725.

Investigation of Chondroprotective Effects of Hinokititol on Ages-Induced Chondrocytes

Apichaya Rujiphan, Prachya Kongtawelert, and Peraphan Pothacharoen*
Thailand Excellence Center for Tissue Engineering and Stem Cells,
Department of Biochemistry, Faculty of Medicine, Chiang Mai University, Chiang Mai
*Corresponding author's email: peraphan.pothacharoen@gmail.com

Abstract:

Osteoarthritis (OA) is a debilitating condition characterized by cartilage degradation, inflammation, and pain. Risk factors include joint overuse, obesity, aging, and diabetes. In diabetic patients, hyperglycemia leads to the formation of advanced glycation end products (AGEs), exacerbating inflammation and cartilage destruction. While traditional OA treatments are effective, they often have notable side effects, prompting interest in alternative therapies. *Chamaecyparis obtusa* (hinoki) has anti-inflammatory properties, but its potential chondroprotective effects remain unclear. This study aims to investigate the therapeutic effects of hinoki oil and its active compound, hinokitiol, on AGEs-induced OA using a porcine cartilage explant model. We hypothesize that hinoki oil and hinokitiol may exert chondroprotective effects and slow OA progression. To assess AGEs cytotoxicity in the cartilage explant model using LDH analysis, results showed that AGEs (5–100 μg/ml) exhibited no cytotoxic effects compared to the H_2O_2-treated group. However, when exploring AGE-induced cartilage degradation, HA and s-GAG release significantly increased dose-dependent when cartilage tissues were exposed to AGEs (25–100 μg/ml) for 7 days. Correspondingly, uronic acid content in cartilage tissues decreased significantly by day 7 of AGE treatment compared to the control group. In the long-term cartilage explant model, hinokitiol treatment significantly reduced s-GAG and HA release in a dose-dependent manner compared to the AGEs-only group. For collagen release and retention, hinokitiol significantly decreased collagen release while increasing collagen retention in cartilage tissues. Similarly, hinokitiol treatment significantly increased uronic acid content in cartilage tissues in a dose-dependent manner compared to the AGEs-treated group. These findings suggest that hinokitiol has potential therapeutic effects by protecting cartilage from AGE-induced degradation, making it a promising alternative treatment for OA.

Keywords: Advanced Glycation End products (AGEs); Chondroprotection; Hinokitiol; Inflammation; Osteoarthritis

Introduction

Non-communicable diseases (NCDs), driven by unhealthy lifestyle choices such as poor diet, inadequate rest, and lack of exercise, are a leading cause of global pain and mortality. In 2021, NCDs accounted for 74% of all deaths in Thailand (1). This category includes diabetes, hypertension, cardiovascular diseases, stroke, and other chronic conditions. Diabetes, affecting 537 million globally in 2022 and projected to reach 783 million by 2045 (2), frequently causes complications like diabetic retinopathy, nephropathy, and cardiovascular diseases due to prolonged high blood sugar levels.

Research shows a link between osteoarthritis (OA) and diabetes, with elevated blood sugar promoting the formation of advanced glycation end products (AGEs) through non-enzymatic glycation. AGEs, found in blood and cartilage, disrupt type II collagen turnover, reduce cartilage elasticity, and exacerbate joint degeneration (3). Natural products are increasingly explored for OA treatment due to their anti-inflammatory and cartilage-protective properties. Examples include turmeric (*Curcuma domestica*) for pain relief (4) and mulberry root (*Morus alba L.*) for glycosaminoglycan preservation (5). Hinoki cypress oil, containing *hinokitiol*, has demonstrated anti-inflammatory effects by suppressing MMP expression and promoting type II collagen production in chondrocytes (6).

This study aims to evaluate the chondroprotective and anti-inflammatory effects of Hinoki cypress oil and *hinokitiol* on chondrocytes stimulated with AGEs, proposing their potential use in treating OA associated with hyperglycemia.

Materials and Methods

Porcine cartilage explant preparation

Porcine articular cartilage was harvested from the metacarpophalangeal joints of 6- to 8-month-old pigs and sectioned into discs (~25 cm^3). Samples were incubated in DMEM with 5% penicillin/streptomycin at 37°C, 5% CO_2 for 1 hour, then transferred to fresh medium for 24 hours to ensure sterility. Cartilage pieces (30–35 mg) were placed in 24-well plates and maintained in DMEM at 37°C, 5% CO_2 for experiments.

Cytotoxicity assay in cartilage explant

The cytotoxicity of Hinokitiol and AGEs was evaluated using an LDH colorimetric assay. LDH activity in the culture media was measured by incubating the sample with β-DPNH and pyruvate substrate at 37°C, followed by reactions with 4-dinitrophenylhydrazine and NaOH. A 5% (v/v) H_2O_2 solution served as a positive control. Absorbance at 450 nm was recorded using a microplate reader, and LDH activity (unit/ml) was calculated from a standard curve and expressed as a percentage of LDH release.

Optimization of AGEs concentrations in cartilage explant

Cartilage discs, weighing 30–35 mg, were treated with AGEs (Merck Millipore, Belize, MA, USA) at concentrations between 5 and 100 µg/ml. The culture media were collected on days 0 and 7 to assess the release of sulfated glycosaminoglycans (s-GAG) and hyaluronic acid (HA). On day 7, the cartilage discs were collected for papain digestion.

The effect of Hinokitiol on AGE-induced cartilage degradation.

Cartilage discs were co-treated with 50 µg/ml of AGEs and different concentrations of Hinokitiol (25–100 µM). The culture media were collected and replaced on days 0, 7, 14, 21, 28, and 35 to measure the release of sulfated glycosaminoglycans (s-GAG) and hyaluronic acid (HA). On day 35, the cartilage discs were collected for histological evaluation. The papain-digested cartilage was analyzed for uronic acid, and hydroxyproline content, respectively.

Results and Discussion

The effect of AGEs-induced porcine cartilage degradation

The toxicity of AGEs in cartilage explant model

To evaluate the cytotoxicity of AGEs on cartilage, porcine cartilage samples were exposed to varying concentrations of AGEs (12.5–100 µg/ml) for 7 days. Culture media were collected on days 0 and 7 for lactate dehydrogenase (LDH) analysis. The findings revealed that AGEs at concentrations of 12.5–100 µg/ml did not cause cytotoxic effects on cartilage tissue when compared to the control group (Figure 1A).

Investigation of the Effect of AGEs on Glycosaminoglycan Release from AGEs-Treated Cartilage Tissues

Cartilage tissues were treated with AGEs (5-100 µg/ml) for 7 days to evaluate cartilage degradation. By day 7, s-GAG release into the culture media increased in a dose-dependent manner, peaking at 100 µg/ml, while no significant difference was observed at 5 µg/ml compared to controls, indicating minimal degradation at lower concentrations (Fig. 1B). Similarly, HA release significantly increased at 50 and 100 µg/ml of AGEs, with the highest release at 100 µg/ml. Lower concentrations (5 and 25 µg/ml) showed HA levels comparable to the untreated group (Figure. 1B,1D). These findings demonstrate that AGEs induce cartilage matrix degradation in a dose-dependent manner.

Investigation of the effect of AGEs on uronic acid remaining in porcine cartilage tissues

The uronic acid content in cartilage tissues decreased in a dose-dependent manner (5–100 μg/ml) following AGE treatment compared to the untreated group (Figure 1C). Notably, glycosaminoglycan release showed a significant reduction in uronic acid content in cartilage treated with 5 μg/ml of AGEs when compared to the control group.

The chondroprotective effect of Hinokitiol on AGEs induced porcine cartilage degradation

The toxicity of Hinokitiol with AGEs in cartilage explant model

To evaluate the potential cytotoxicity of Hinokitiol and its combination with AGEs, porcine cartilage tissues were treated with various concentrations of Hinokitiol (12.5–100 μg/ml) or co-treated with 50 μg/ml AGEs for 35 days, with 5% H_2O_2 serving as the positive control (Figure 1.4). Culture media were collected at multiple time points (days 0, 7, 14, 21, 28, and 35) to measure LDH levels. The findings demonstrated that Hinokitiol, at all tested concentrations, did not induce cytotoxic effects on cartilage tissue compared to the untreated control group. (Figure 2A).

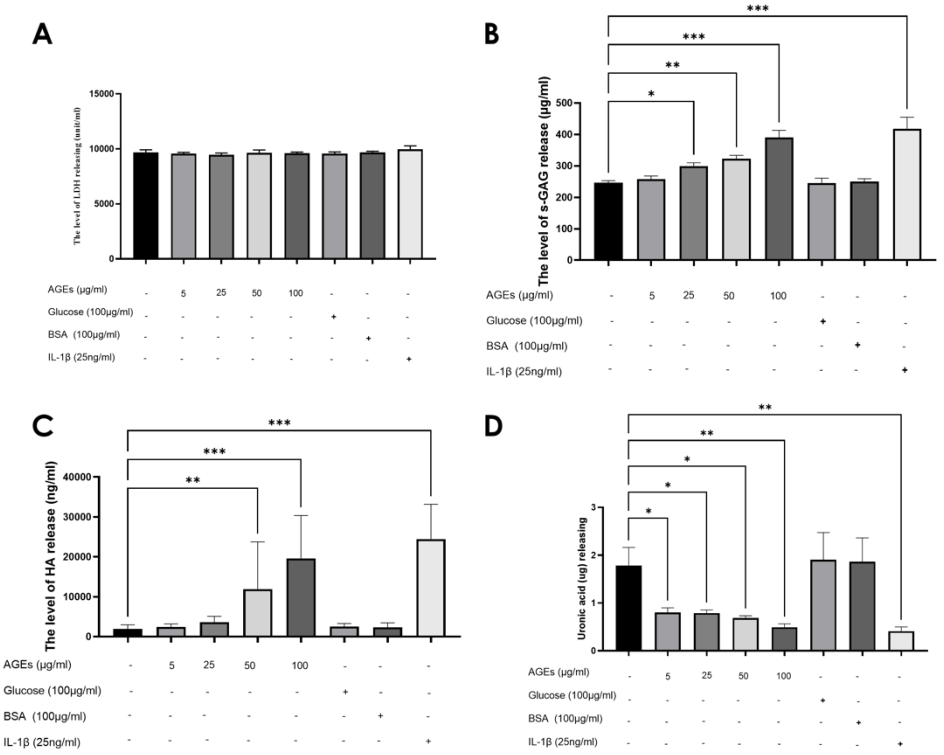

Figure 1 (A) LDH release, (B) s-GAG, (C) HA, and (D) uronic acid levels in cartilage samples treated with AGEs (5–100 μg/ml) for 7 days. Media and tissues were collected for analysis. Data are mean ± SEM from three experiments. *$p < 0.05$ vs. untreated group.

Investigation of the effect of Hinokitiol on glycosaminoglycans releasing from AGEs treated cartilage tissues

To examine the effect of Hinokitiol on AGEs-induced porcine cartilage degradation, cartilage samples were treated with 50 μg/ml AGEs alone or co-treated with Hinokitiol (12.5–100 μg/ml) for 35 days. Culture media were collected on days 0, 7, 14, 21, 28, and 35 to measure s-GAG and HA levels (Figure 2B). The results showed that treatment with 50 μg/ml AGEs. significantly increased the release of s-GAG in the conditioned media compared to the untreated group. In contrast, co-treatment with Hinokitiol (12.5–100 μg/ml) and AGEs significantly reduced s-GAG release in a dose-dependent manner compared to the AGEs-only condition. Similarly, the release of HA in the conditioned media was progressively elevated in the 50 μg/ml AGEs group compared to the untreated

group. However, co-treatment with Hinokitiol (12.5–100 μg/ml) in the presence of AGEs significantly lowered HA levels in a dose-dependent manner compared to the AGEs-alone group. (Figure 2E)

Investigation of the effect of Hinokitiol on Collagen release and remaining in porcine cartilage tissues

Collagen release and retention were assessed in cartilage samples treated with AGEs alone or co-treated with Hinokitiol (12.5–100 μg/ml) over days 0, 7, 14, 21, 28, and 35. The results demonstrated that AGEs treatment alone significantly increased collagen release into the culture media compared to the control group. In contrast, co-treatment with Hinokitiol (12.5–100 μg/ml) markedly reduced collagen release relative to the AGEs-treated group (Figure. 2C). Similarly, the analysis of collagen retention within cartilage revealed that AGEs treatment alone significantly decreased collagen levels in the tissue. However, co-treatment with Hinokitiol (12.5–100 μg/ml) significantly preserved collagen content compared to the AGEs-treated group (Figure. 2F).

Investigation of the effect of Hinokitiol on uronic acid remaining in porcine cartilage tissues

The uronic acid content in cartilage samples treated with AGEs alone or co-treated with Hinokitiol (12.5–100 μg/ml) was assessed on day 35 of the treatment. AGEs treatment alone resulted in a significant reduction in uronic acid content compared to the control group. However, co-treatment with Hinokitiol (12.5–100 μg/ml) significantly increased uronic acid content compared to the AGEs-only treated group. (Figure 2D)

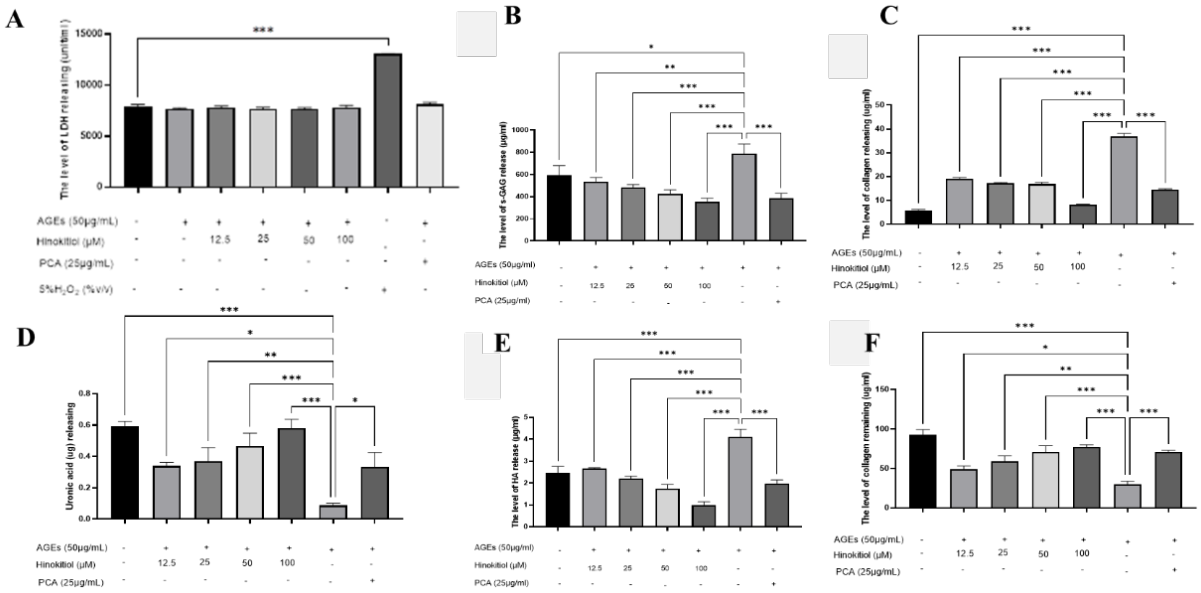

Figure 2 (A) LDH release in the media of cartilage samples treated with AGEs (50 μg/ml) and Hinokitiol (12.5–100 μg/ml) for 35 days. (B) s-GAG and (C) HA release measured in culture media collected on days 0, 7, 14, 21, 28, and 35. (D) Collagen release and (E) retention in cartilage tissues treated with AGEs or co-treated with Hinokitiol. (F) Uronic acid levels in cartilage tissues treated with AGEs or co-treated with Hinokitiol. Data are mean ± SEM from triplicate experiments. *$p < 0.05$ vs. AGEs-treated alone; $p < 0.05$ vs. untreated group.

Conclusion

This study demonstrates that advanced glycation end-products (AGEs) significantly induce porcine cartilage degradation in a dose-dependent manner, as evidenced by increased s-GAG, HA, and collagen release into the culture media and decreased uronic acid and collagen content within cartilage tissues. These findings highlight the detrimental impact of AGEs on cartilage matrix

integrity. Importantly, Hinokitiol exhibited potent chondroprotective effects against AGEs-induced cartilage degradation. Co-treatment with Hinokitiol (12.5–100 μg/ml) significantly reduced the release of s-GAG, HA, and collagen while preserving collagen and uronic acid content within the cartilage tissues. Furthermore, Hinokitiol did not induce cytotoxicity at any tested concentration, as evidenced by unchanged LDH release levels.

Overall, Hinokitiol effectively mitigates AGEs-induced cartilage damage and matrix degradation, suggesting its potential as a therapeutic agent for protecting cartilage integrity in conditions involving AGE accumulation, such as osteoarthritis or diabetes-related joint diseases. However, the study is limited by the use of porcine cartilage as a model, which may not fully replicate the human cartilage environment. Additionally, the in vitro nature of the experiments may not account for complex systemic factors present in vivo. Further investigations, including in vivo studies and clinical trials, are warranted to validate these findings, optimize dosage, and explore the long-term safety and efficacy of Hinokitiol in treating AGEs-related joint diseases.

References

1. Organization WH. Noncommunicable diseases: progress monitor 2022. 2022.
2. International Diabetes Federation. Diabetes around the world in 2021. Available at: https://diabetesatlas.org/. Accessed Dec 11, 2024.
3. Eymard F, Parsons C, Edwards MH, Petit-Dop F, Reginster JY, Bruyere O, et al. Diabetes is a risk factor for knee osteoarthritis progression. Osteoarthritis Cartilage. 2015;23(6):851-9.
4. Kuptniratsaikul V, Thanakhumtorn S, Chinswangwatanakul P, Wattanamongkonsil L, Thamlikitkul V. Efficacy and safety of *Curcuma domestica* extracts in patients with knee osteoarthritis. Journal of alternative and complementary medicine (New York, NY). 2009;15(8):891-7.
5. Yimam M, Lee YC, Wright L, Jiao P, Horm T, Hong M, et al. A Botanical Composition Mitigates Cartilage Degradations and Pain Sensitivity in Osteoarthritis Disease Model. Journal of medicinal food. 2017;20(6):568-76.
6. Li J, Zhou X, Yang K, Chen W, Jiang L, Bao J, et al. Hinokitiol reduces matrix metalloproteinase expression by inhibiting Wnt/β-Catenin signaling in vitro and in vivo. International Immunopharmacology. 2014;23(1):85-91.

Antidiabetic Activity of Partially Purified Polysaccharides from Split Gill Mushrooms (*Schizophyllum commune*)

Nareerat Kumnuanjit[1,2,*] and Decha Sermwittayawong[1,2,*]

[1] Division of Health and Applied Sciences Faculty of Science, Prince of Songkla University, Hatyai, Songkhla, Thailand 90110

[2] Center of Excellence for Biochemistry, Faculty of Science, Prince of Songkla University, Hatyai, Songkhla 90110, Thailand

* Corresponding author's email: nareerat.knj@gmail.com and decha.s@psu.ac.th

Abstract:

Split gill mushrooms (*Schizophyllum commune*) are among the functional mushrooms that have been used as a source for polysaccharide extraction to study the anti-tumor and immunomodulating activities. However, the antidiabetic activity of the polysaccharides has not been well characterized. In this study, we utilized a green procedure involving only ethanol, water, and enzymes to extract and purify polysaccharides from split gill mushrooms. The hot-water extracted polysaccharides were digested with enzymes to eliminate α-glucose and proteins and purified with Diethylethanolamine (DEAE) Sepharose Fast-Flow. The DEAE column chromatography fractionated the sample into three major peaks: Peak 1, Peak 2, and Peak 3, which are eluates from the low, medium, and high salt, respectively. Total protein and carbohydrate analysis showed that the Peak 1 sample contains the highest carbohydrate and the lowest protein contents. Therefore, the Peak 1 sample was selected for further experiments with L6 myotubes. The results showed that the Peak 1 sample dose-dependently stimulated glucose uptake in the cells without affecting the cell viability. These results suggest the antidiabetic activity of the polysaccharides and the potential use of protein-polysaccharides from split gill mushrooms as a functional food for treating diabetes.

Keywords: Split gill mushrooms; Polysaccharides; Glucose uptake; L6 myotubes; Antidiabetic activity

Introduction

Diabetic, a chronic health disease that affects millions of people worldwide, is characterized by the inability of the body to regulate blood glucose. Diabetes mellitus, a group of metabolic disorders associated with elevated blood glucose levels due to the lack of insulin secretion, insulin resistance, or both, has emerged as a major health problem. It is estimated that the number of diabetes patients worldwide will reach 693 million by 2045 (Cho et al., 2018). Thailand is among the countries in Asia with a high prevalence of diabetes. More than 200,000 deaths annually among the Thai population are owing to chronic noncommunicable diseases, and about 30,000 deaths are owing to diabetes, a leading cause of death in Thailand with a prevalence of 9.9% in the adult population (Aekplakorn et al., 2018). Of the more than 200,000 deaths annually due to chronic non-communicable diseases in Thailand, approximately 30,000 (15%) are due to diabetes (Reutrakul & Deerochanawong, 2016). Diabetes mellitus results in severe complications such as neuropathy, nephropathy, retinopathy, and cardiovascular diseases (Clements &Bell, 1985). Postprandial hyperglycemia is mainly responsible for the majority of diabetes-related complications (Ceriello, 2005; Gavin, 2001). Commercially available drugs used for the treatment of diabetes suffer from certain limitations and have side effects (Chaudhury et al., 2017), necessitating the need for novel and more effective antidiabetic agents from natural sources.

Schizophyllum commune is a common and widely distributed edible mushroom naturally growing on decaying woods during the rainy season. It is widely consumed as food and medicine in Thailand (Shweta et al., 2021). *S. commune* has been mostly acknowledged for its medical importance (Han et al., 2005). This mushroom is rich in polysaccharides, namely schizophyllan, a type of β-glucan, which is a polymer of β-(1 → 3) glucose with a single β-(1 → 6) glucose as a side chain at every third glucose residues (Kumari et al., 2008; Rau, 1999; Yanaki et al., 1985).

In general, mushroom polysaccharides are known to possess several biological activitiesare, such as anti-tumor, anti-bacterial, anti-inflammatory, immunomodulatory, and antidiabetic activities. Polysaccharides from split gill mushrooms are well-studied in terms of their anti-tumor and immunomodulating activities (Zhang et al., 2013). However, the antidiabetic activity of polysaccharides from split gill mushrooms has not been well characterized.

In this study, we utilized the hot-water extraction method to extract polysaccharides from the mushrooms, which were subsequently purified with Diethylethanolamine (DEAE) Sepharose Fast-Flow column chromatography. All the purification procedures involve water, ethanol, and enzymes and without using harmful reagents. Polysaccharides eluted from the column were further characterized and the antidiabetic activity is discussed in this report.

Materials and Methods

Preparation of polysaccharides from split gill mushroom

Split gill mushrooms were gifts from Ban hed krang, Hatyai, Songkhla. In brief, 1 kg of fresh mushrooms were washed, air-dried, and diced into small pieces. After drying at 70°C for 2 days, the mushrooms were ground into powder. To perform hot-water extraction, water was added to the mushroom powder in the 1:8 mushroom (g) ratio to water (mL) and boiled at 90-95°C for 4 hours under constant stirring. The sample was allowed to cool down and filtered to separate the supernatant from mushroom residues. Centrifugation was performed to collect the supernatant. The mushroom residues from the extraction were combined and again extracted with hot water. The supernatant from the first and the second extraction was combined. The total protein and total carbohydrates in the sample were analyzed using the protocol described below.

The method for purification of polysaccharides was based on our previous protocol (Sermwittayawong et al., 2018) with some modifications: adding sample evaporation before the precipitation with ethanol and removing the SEVAG extraction step. Briefly, evaporation was performed to reduce the volume of the extract by approximately 50%. Then, absolute ethanol was added to the supernatant at 3:1, ethanol: sample. The mixture was kept for 12-16 hours at 4°C to allow proper polysaccharide precipitation. Precipitated polysaccharides were collected by centrifugation, dissolved with distilled water, dialyzed to remove ethanol, and lyophilized. The crude extract was kept in a desiccator until needed.

The first step after reducing the volume was to eliminate ⟨-glucose using amylase from *Aspergillus oryzae* (Sigma-Aldrich), which was dissolved in P6.7 buffer (50 mM HEPES pH 7.0, 4.5 mM NaCl, and 0.01% sodium azide). Amylase at 0.1 U was mixed with every 1 mg/mL polysaccharide sample. The digestion was performed at 20°C for 24 hours, and the digested product was checked with the 3,5-Dinitrosalicylic acid (DNS) assay. Once the digestion with amylase was satisfied, $CaCl_2$ was added to the sample to a final concentration of 1 mM.

Proteins were eliminated by the digestion with proteinase and proteinase K enzymes. Proteinase at 0.5 U was added to every 1 mL sample, and the digestion was performed at 37°C for 24 hours. Then, 0.04 U proteinase K was added to every 1 mL sample, and the digestion was continued at 55°C for 24 hours. Protein precipitate may appear, and it was removed by centrifugation.

The digested polysaccharides were kept frozen until the next purification step with DEAE ion-exchange column chromatography. The sample was diluted 1:10 with distilled water and passed through a 25-mL DEAE column previously equilibrated with water. Bound polysaccharides were eluted from the column using NaCl at 0.1, 02, 0.4, and 1 M concentrations. Polysaccharides in each fraction were analyzed using the phenol-sulfuric assay (see below), and proteins were estimated by measuring the absorbance at 280 nm. Peak fractions were pooled, dialyzed, and lyophilized. Each peak sample was kept in a desiccator and protected from light until needed.

Total protein determination

Total protein was determined using the Bradford assay. In brief, bovine serum albumin (BSA) was used as a standard protein and was prepared at concentrations 62.5, 125, 250, 500, and 1000

μg/mL. The 5X Bradford solution (0.5 mg/mL Coomassie Brilliant Blue G-250, 23.5% methanol, and 42.5% phosphoric acid) was diluted to 1X solution and was mixed well with each sample (input, fraction 1, fraction 2 and fraction 3) and standard. Each sample was measured the absorbance at 595 nm. The estimation of total protein content was calculated based on the standard curve of BSA.

Total carbohydrate determination

Total carbohydrate was determined using the Phenol-sulfuric assay. In brief, glucose was used as a standard carbohydrate. Two hundred microliters of a 5% phenol solution were added to a 200 μL sample or standard glucose solution in a glass tube. After vortexing, 1 mL of sulfuric acid (H2SO4) was added, and the mixture was incubated at room temperature for 30 minutes. Then, each sample was measured absorbance at 470 nm.

L6 cells maintenance and differentiation

L6 myoblasts (ATCC-CRL-1458) were grown in α-Minimum Essential medium (α-MEM) containing antibiotics and 10% Fetal Bovine Serum (FBS) pH 7.1-7.2. at 37°C in a humidified incubator with 5% CO_2. The cells are maintained in 10-cm dishes and subcultured every 2 days or when the density reaches 60-70%. Cellular differentiation to myotubes were performed as previously described (Mitsumoto et al., 1991). Briefly, myoblasts were seeded in a 48-well plate with the differentiation medium (α-MEM supplemented with antibiotics and 2% FBS). The differentiation medium was replenished every 2 days, and the differentiation was usually completed within 6-8 days or when the formation of myotubes became completed, which could be observed under a light microscope.

The effect of polysaccharides on L6 muscle cells

Differentiated L6 myotubes in a 48-well plate format were treated with various concentrations of polysaccharides for 48 hours. Insulin 500 at nM and Metformin at 2 mM were used as positive controls for stimulating glucose uptake. After 48 hours of incubation, the media were collected for the glucose uptake assay, and cells were treated with MTT solution for the cell viability assay.

Cells viability assay

Cell viability assay was performed as previously described (Sermwittayawong et al., 2018). In brief, cells were treated with media containing 0.5 mg/mL 3-(4,5-dimethylthiazol-2-yl)-2,5-diphenyl tetrazolium bromide (MTT) reagent for 3 hours. Then, the media was removed, and the formazan crystals were dissolved with dimethyl sulfoxide (DMSO). The dissolved formazan in DMSO was used for measuring the absorbance at 570 nm.

Glucose uptake assay

The amount of glucose left in the culturing media could be quantified using a glucose assay kit (GAGO20, Sigma-Aldrich), which was performed according to the instructions provided by the manufacturer. Briefly, media from treated cells were diluted 10-fold with distilled water and transferred 25 μL in 96 well plates. Then, 50 μL of assay reagent was added to each well. Following the incubation at 37°C for 30 minutes, the reaction was stopped by adding 50 μL of 12 N H_2SO_4. The sample was mixed well, and the absorbance at 540 nm was measured. The stimulation of glucose uptake in a treated set is calculated based on this equation:

$$\%\ glucose\ uptake\ stimulation = \frac{([glucose]_{untreated} - [glucose]_{treated})\ x\ 100}{[glucose]_{untreated}}$$

Results and Discussion

Purification of and characterization of polysaccharides from split gill mushrooms

In this study, we extracted polysaccharides using the hot-water extraction technique and purified the samples using only water, ethanol, and enzymes without any harmful reagents, creating a safe and environmentally friendly purification protocol.

The DEAE fractionation yielded 3 major peaks: Peak 1, Peak 2, and Peak 3, which were polysaccharides eluted from 0.1M, 0.2M, and 0.4M NaCl, respectively (Figure 3.1). After pooling the peak fractions separately, the peak samples were dialyzed against water and subsequently lyophilized. We found that from 1 kg of fresh mushroom, we obtained 0.3723 g, 0.0912 g, and 0.115 g for Peak 1, Peak 2, and Peak 3 samples, respectively. These suggest that the yield of the polysaccharide samples per 1 kg fresh weight was relatively low. Additional analysis for the total proteins and total carbohydrates data are shown in Table 1. These data revealed that the Peak 1 sample had the highest carbohydrate content but the lowest protein. Because the goal of the purification was to obtain polysaccharides for experiments, we chose Peak 1 samples, which were protein-polysaccharide complexes, for the subsequent test with the muscle cells.

We have performed a similar protocol for the extraction and purification of polysaccharides from the gray oyster mushrooms [*Pleurotus sajor-caju* (Fr.) Sing.] (Sermwittayawong et al., 2018). The purification involved the use of the SEVAG reagent for the elimination of proteins from the polysaccharides. As a result, the Peak 1 samples was obtained without protein being detected (Sermwittayawong et al., 2018). Unlike our previous report, this study removed the deproteination step using the SEVAG reagent because it requires the use of harmful chemicals. Consequently, we observed a significant amount of protein present in all the peak fractions. However, one major discrepancy between the current and the previous study was the type of mushrooms, which do not share the same level of protein and carbohydrate.

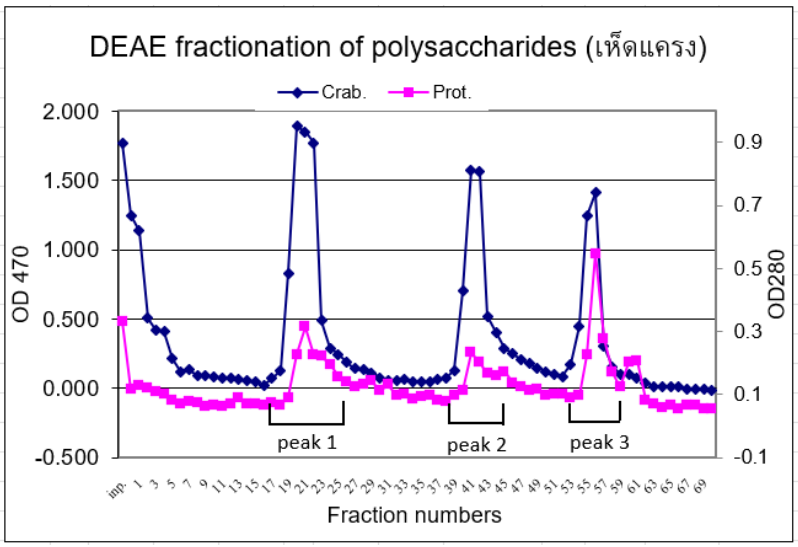

Figure 1: Purification of hot-water extracted polysaccharides from split gill mushroom (*Schizophyllum commune*) with DEAE Sepharose Fast-Flow column.

Table 1: Characterization of the polysaccharide samples purified using the DEAE column chromatography (n=3)

Samples	Total carbohydrate (Ave ± S.D.)	Total protein (Ave ± S.D.)
Input	92.70 ± 6.61	1.63 ± 0.16
Peak 1	103.81 ± 2.39	1.52 ± 0.14
Peak 2	82.06 ± 19.66	2.17 ± 0.10
Peak 3	73.10 ± 18.37	2.20 ± 0.08

The Peak 1 polysaccharide sample stimulate glucose uptake in L6 myotubes

Our previous report showed that polysaccharides from gray oyster mushrooms were able to stimulate glucose uptake in the L6 myotubes in a dose-dependent fashion without reducing cell viability (Sermwittayawong et al., 2018), demonstrating the antidiabetic activity of the mushroom polysaccharides. These findings led us to hypothesized that the polysaccharides from split gill mushrooms could also stimulate glucose uptake in the muscle cells. Thus, we performed the experiment by incubating L6 myotubes with different concentration of Peak 1 sample (62.5, 125, 250 and 500 µg/mL). Five hundred nanomolar insulin and one millimolar metformin were included as a positive controlfor the assay. After treating the cells for 48 hours, the media were collected for a glucose assay, and the cells were used to examine their viability. Results in Figure 2A show that all the treatments confer the cellular viability greater than 80%, suggesting that the polysaccharide samples do not affect to the viability of the muscle cells.

In addition, the glucose assay that analyzed the amount of glucose remains in the media revealed that the increasing concentration of Peak 1 sample results in an increasing percent stimulation of glucose uptake in the L6 myotubes (Figure 2B), while the positive controls (insulin and metformin treatment sets) score a high percent stimulation of glucose uptake. Thus, these results suggest the antidiabetic activity of the Peak 1 sample.

Similar experiments that analyzed the antidiabetic activity of polysaccharide samples with myotubes have been performed. For example, a previous study found that Astragalus polysaccharides (APS) dose-dependently stimulated glucose uptake in L6 myotubes by activating AMP-activated protein kinase (AMPK) complex (Liu et al, 2013). Consistently, our group found that polysaccharides from gray oyster mushrooms also activate the AMPK complex, which promotes glucose to be transported into the cells (Patninan et al., 2023). Therefore, we hypothesize that the Peak 1 sample also promote glucose uptake through AMPK-dependent pathway. This hypothesis remains to be tested in our future experimentation.

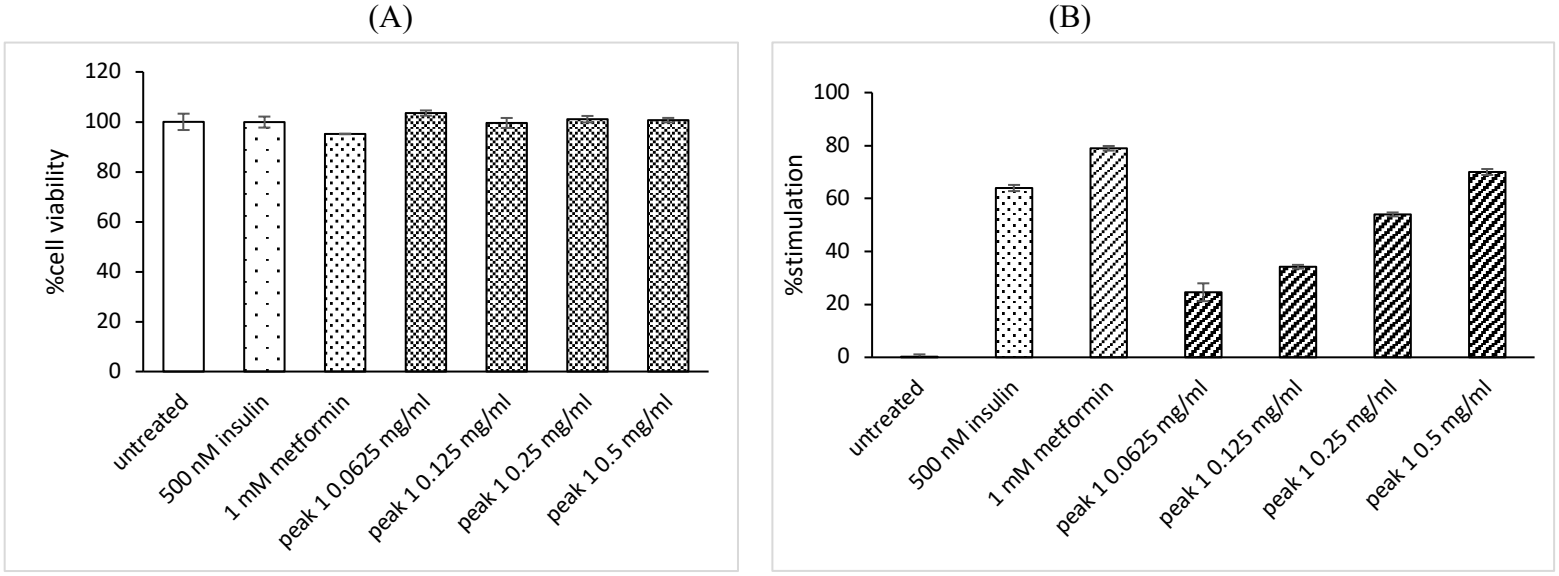

Figure 2: Peak 1 polysaccharide sample dose-dependently stimulates glucose uptake in L6 myotubes without affecting cell viability. (A) shows the effect of Peak 1 sample on cell viability. (B) shows the effect of the sample on the stimulation of glucose uptake in the L6 cells. The experiment was performed at least 3 times. The chart shows the average values with the standard deviation as the error bars (n = 3).

Conclusion

In this study, Polysaccharides have been extracted and isolated from split gill mushroom (*Schizophyllum commune*) through hot-water extraction and purified with DEAE anion-exchanged chromatography, which fractionated the samples into 3 major peaks: Peak 1, Peak 2, and Peak 3 samples. The characterization of the sample revealed that the Peak 1 sample is rich in polysaccharides with the least protein content, and it was chosen for the subsequent antidiabetic analysis. We found that Peak 1 polysaccharide sample is not toxic to L6 myotubes and stimulated glucose uptake in the cells in a dose-dependent manner. Therefore, these results demonstrate the antidiabetic activity of polysaccharide-protein complex from split gill mushrooms, which could potentially be used to treat diabetes mellitus.

Acknowledgements

We would like to thank all the past and present DS lab members for all helps and support. This study was funded by National Science, Research and Innovation Fund (NSRF) and Prince of Songkla University (Grant # SCI6601211S).

References

1. Aekplakorn, W., Chariyalertsak, S., Kessomboon, P., Assanangkornchai, S., Taneepanichskul, S., & Putwatana, P. Prevalence of Diabetes and Relationship with Socioeconomic Status in the Thai Population: National Health Examination Survey, Journal of Diabetes Research, 2018;1–8.
2. Ceriello, A. Postprandial Hyperglycemia and Diabetes Complications. Diabetes, 2005;54(1):1–7.
3. Chaudhury, A., Duvoor, C., Reddy Dendi, V. S., Kraleti, S., Chada, A., Ravilla, R., Marco, A., Shekhawat, N. S., Montales, M. T., Kuriakose, K., Sasapu, A., Beebe, A., Patil, N., Musham, C. K., Lohani, G. P., & Mirza, W. Clinical Review of Antidiabetic Drugs: Implications for Type 2 Diabetes Mellitus Management. Frontiers in Endocrinology, 2017;8.
4. Gavin, J. R. Pathophysiologic mechanisms of postprandial hyperglycemia: The American Journal of Cardiology, 2001;88(6):4–8.
5. Han, C. H., Liu, Q. H., Ng, T. B., & Wang, H. X. A novel homodimeric lactose-binding lectin from the edible split gill medicinal mushroom *Schizophyllum commune*: Biochemical and Biophysical Research Communications, 2005;336(1):252–257.
6. Kumari, M., Survase, S. A., & Singhal, R. S. Production of schizophyllan using Schizophyllum commune NRCM: Bioresource Technology, 2008;99(5):1036–1043. \
7. Mitsumoto, Y., Burdett, E., Grant, A., & Klip, A. Differential expression of the GLUT1 and GLUT4 glucose transporters during differentiation of L6 muscle cells: Biochemical and Biophysical Research Communications, 1991;175(2):652–659.
8. Patninan, K., Sermwittayawong, D., Nuinamwong, S., Khimmaktong, W., Noipha, K., & Nongporn, H.-T. Purified Polysaccharides Extracted from Gray Oyster Mushroom (*Pleurotus sajor-caju* (Fr.) Sing.) Stimulate Glucose Uptake in C2C12 Myotubes through the activation of AMP-Activated Protein Kinase (AMPK) and Glucose Transporter 1 (GLUT1) Proteins: Sains Malaysiana, 2023;52(10):2815–2827.
9. Rau, U. Production of Schizophyllan, 1999; 43–55.
10. Reutrakul, S., & Deerochanawong, C. Diabetes in Thailand: Status and Policy: Current Diabetes Reports, 2016;16(3):28.
11. Sermwittayawong, D., Patninan, K., Phothiphiphit, S., Boonyarattanakalin, S., Sermwittayawong, N., & Hutadilok-Towatana, N. Purification, characterization, and biological activities of purified polysaccharides extracted from the gray oyster mushroom [*Pleurotus sajor-caju* (Fr.) Sing.]: Journal of Food Biochemistry, 2018;42(5):e12606.

12. Yanaki, T., Tabata, K., & Kojima, T. Melting behaviour of a triple helical polysaccharide schizophyllan in aqueous solution: Carbohydrate Polymers, 1985;5(4):275–283.
13. Zhang, Y., Xia, L., Pang, W., Wang, T., Chen, P., Zhu, B., & Zhang, J. A novel soluble β-1,3-D-glucan Salecan reduces adiposity and improves glucose tolerance in high-fat diet-fed mice: British Journal of Nutrition, 2013;109(2):254–262.

NCDs Listener: A Social Listening Tool for Non-communicable Diseases

Ratchanont Thippimanporn, Wuttichai Khamna, Kannika Wiratchawa, and Thanapong Intharah*
Visual Intelligence Laboratory, Department of Statistics, Faculty of Science,
Khon Kaen University, Khon Kaen, 40002, THAILAND
*Corresponding author's email: thanin@kku.ac.th

Abstract:

Over 41 million people worldwide die from NCDs (non-communicable diseases) annually, the majority of which occur in low- and middle-income countries. Social media has become a critical platform for individuals to share experiences and access information about NCDs. Social (media) listening offers valuable insights by analyzing user discussions, but existing tools are closed-source and commercial. This study seeks to simplify the extraction of NCD-related knowledge from social media, making it easier for the public to understand and access information. It also explores how the NCD community shares its lived experiences online. We proposed an open-source social (media) listening tool called NCDs Listener, which is available as an open-source project. The NCDs Listener to collect, analyze, summarize, and visualize data. Comments in Thai or English about NCDs can be collected from public posts. This time, we studied the characteristics of comments from Facebook and Reddit posts that mentioned NCDs to demonstrate the NCDs Listener tool. Use keyword matching and the BERT Model to extract knowledge from comments. The preliminary data was analyzed using descriptive statistics. Additionally, a Generative AI model summarizes the extracted knowledge in human-readable sentences. Our NCDs Listener tool is open-source and can extract knowledge related to NCDs. This knowledge can be used as a guideline for treatment or the development of effective care to meet patients' needs. Our findings demonstrate that aggregated social media data not only provides immediate insights but also serves as a springboard for advanced statistical analyses and cutting-edge data science approaches, opening new avenues for understanding complex social phenomena and predicting emerging trends.

Keywords: Social listening; Non-communicable diseases; Text classification; Data visualization; Generative AI

Introduction

Non-communicable diseases (NCDs) are chronic conditions caused by unhealthy lifestyles, with cardiovascular diseases being the highest, followed by cancers, chronic respiratory diseases, and diabetes (1). Treatment decisions for NCDs often involve a variety of concerns, such as understanding contributing behaviors, recognizing symptoms, and determining effective interventions. While information on NCDs is abundant, accessible and layman-friendly platforms remain limited. Social media has recently played a key role in educating patients, building peer support networks, and sharing experiences (2).

Social (media) listening studies have primarily focused on developing systems that analyze sentiment and track trending topics (3). Plenty of research has been conducted through social listening tools. However, the tools, such as Brand24 and YouScan (4), require expensive monthly subscriptions, which makes them inaccessible to the general public or independent researchers. Furthermore, these tools are often designed to cater to large organizations, limiting their applicability to individuals who wish to analyze social media data on a personal level (4). We developed an open-source tool to analyze public social media posts about NCDs and present the extracted insight as a dashboard. This helps researchers study how the NCD community shares their real-life experiences while reducing the time needed to find relevant information and improving public access to understanding these conditions. The primary distinction between the NCDs Listener and other

existing social media listening tools are as follows; NCDs Listener supports Thai and English languages and is designed especially for extracting knowledge about non-communicable diseases.

This work highlights:

- Developing a Web application, NCDs Listener, a social (media) listening tool, to extract and analyze public sentiment from NCD-related posts, displaying the data in a customizable dashboard.
- Utilizing Natural Language Processing (NLP) techniques and Bidirectional Encoder Representations from Transformers (BERT) to derive meaningful insights from social media data.
- Integrating large language models (LLMs) to enhance the social media listening process

Related Work

Social Listening for Non-Communicable Diseases

Many researchers are working on expanding knowledge on social media listening for non-communicable diseases in literature, and some key contributions are providing support for finding user behaviors and situations in different cases worldwide. Some of the essential papers are included in this section.

For disease-specific social listening studies and various social media listening tools and data collection and analysis techniques, Rodrigues et al. (5) focused on European social media conversations to understand the experiences of lung cancer patients, caregivers, and healthcare professionals. Using Talkwalker and SocialStudio. Chauhan et al. (6) analyzed the experiences of melanoma patients across 14 European countries using SocialStudio and Talkwalker. They identified significant impacts on patients' daily lives and emotions. Manuelita Mazza et al. (7) used social listening on Twitter, patient forums, and blogs to explore metastatic breast cancer patient experiences. Zinaida Perić et al. (8) investigated GVHD patient needs and lifestyles across Europe using Talkwalker to collect data from Twitter, Facebook, Instagram, and YouTube. The research combined quantitative and qualitative methods to analyze quality of life, treatment efficacy, and unmet needs. Our work proposed the utilization of a recent large language model technique to summarize all knowledge in a human-readable paragraph.

Applications of Social Media Listening

Different studies have employed various tools and techniques to analyze social media data, focusing on understanding public sentiment and opinions. For analysis techniques employing NLP, Kamaran H. Manguri et al. (9) analyzed Twitter data from the COVID-19 pandemic using the hashtags #coronavirus and #COVID-19. They applied NLP and Sentiment Analysis. Burzyńska J, Bartosiewicz A, and Rękas M. (10) used the SentiOne tool for NLP to analyze social media data on COVID-19 in Poland. Their analysis revealed increased public discussions and information sharing as the pandemic progressed. For analysis techniques utilizing Latent Dirichlet Allocation (LDA) and Topic Modeling, Shoults CC. et al. (11) employed LDA and t-SNE to analyze social media discussions about telemedicine on Reddit and Twitter, Sanders C. A. et al. (12) conducted sentiment analysis and clustering of Twitter data to study public opinions on face masks during COVID-19. Additionally, quantitative and qualitative analysis, along with bot detection, were employed for social media data analysis; Spitale G., Andorno B. N., and Germani F. (13) analyzed Telegram conversations about the Green Pass in Italy using both quantitative and qualitative methods.

Most research on social media listening relies on platforms like Talkwalker and SocialStudio, with limited use of NLP techniques such as tokenization, stop words removal, sentiment analysis, and topic modeling. In contrast, our open-source NCDs Listener tool uses advanced NLP methods, including tokenization, lemmatization, normalization, and BERT for topic classification. The tool provides insights through descriptive statistics, LLM-based summaries, and dashboard visualizations.

The NCDs Listener Tool

Systems Design

The NCDs Listener system was developed using Python 3.11.9 to collect, analyze, and summarize social media posts related to NCDs. It helps turn these posts into meaningful insights. The system implements a five-step workflow:

1. Data Scraping step: When a user enters a social media post URL into the NCDs Listener tool, the system leverages web scraping tools like Selenium and Beautiful Soup to extract relevant data from the post.

2. Data Preprocessing step: The system cleanses the collected data by removing duplicate comments and filtering out extremely short text entries. Preprocessed data can be exported in CSV format for future analysis.

3. Knowledge Extraction step: The system employs natural language processing (NLP) techniques, including tokenization, stop word removal, normalization, lemmatization, keyword matching, and application of the Bidirectional Encoder Representations from Transformers (BERT) model (14) to identify the type of comments.

4. Data Adjustment step: Users can add diseases and symptoms they wish to include or exclude those they do not want. The system then filters the comments based on the specified diseases and symptoms, tailoring the data to the user's requirements

5. Data Visualization step: The enhanced data is summarized and displayed on an interactive dashboard, featuring a comprehensive summary generated by a Generative AI model. Users can also explore the data from a summary statistics table about the post or export the results to a PDF. The workflow is illustrated in **Figure 1**.

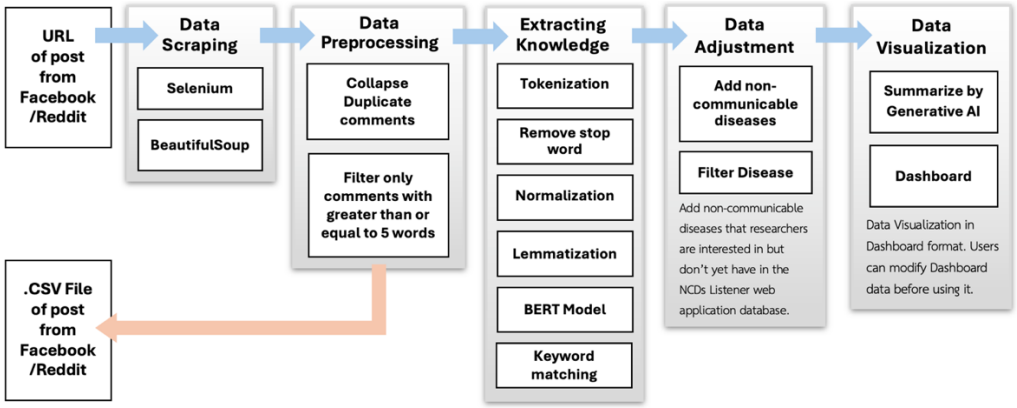

Figure 1. Flow of the NCDs Listener tool.

Artificial Intelligence Models for Insight Extraction

In this work, we employed two AI models in the insight's extraction. First, BERT was used for topic classification. Second, LLMs was used for content summarization

BERT for Topic Classification

The system employs machine learning models to classify the types of comments, enabling users to identify which comments are likely to provide useful information. The BERT model was trained on over 3,000 NCD-related comments in Thai and English. This model can categorize comments into three categories:

1. Experience Stories: Comments that share personal experiences with diseases, including symptoms (before or after diagnosis), treatments, and how the disease has affected quality of life. Such comments often cover all or at least 2 to 3 of these aspects.
2. Questions: Comments that inquire about various aspects of NCDs, such as symptoms, treatments, or disease impacts.

3. Irrelevant or Non-Useful Comments: Comments that are not related to NCDs or lack meaningful information, such as simply stating the name of a disease or unclear descriptions of symptoms.

Large Language Model (LLM) for Summarization

We integrate Generative AI for comment summarization, employing the Google Gemini 1.5 flash model through LangChain (15). This approach applies to a method called Retrieval-Augmented Generation (RAG) to ensure accurate domain-specific and minimize hallucinations in Generative AI. Within the NCDs Listener system, the Generative AI's question-answering capability relies on a predefined set of questions to guide Gemini in generating summaries. Each comment summary reflects the characteristics of the overall community alongside suggestions and noteworthy information related to NCDs.

Prompt template and predefined questions: The prompt template serves as a structured framework to guide the responses of Generative AI. In this context, Generative AI addresses inquiries based on the aggregated comments and responds in English. For predefined questions, the generative AI delivers responses in both Thai and English to meet specific contextual requirements.

A Case Study: Lung Cancer Knowledge from the Crowd

To show the functionalities of the NCDs Listener tool, we focused on lung cancer as a case study. For this analysis, three cancer-related Facebook posts (16-18) were chosen, including a news post discussing cancer mortality rates, a post from a cancer community group, and a personal experience-sharing post. These posts collectively contained 1,797 comments, subsequently filtered to identify 30 comments specifically mentioning lung cancer. The system's data visualization and discovery capabilities were demonstrated through results such as knowledge extraction via keyword matching, classification using the BERT model, and Generative AI-based summarization using Google Gemini.

Results of Knowledge Extraction

From the data analysis and demographic characteristics of the commenters on the three Facebook posts (16,17,18) mentioning lung cancer, **Figure 3A** showed that 21 comments, or 67.74% of all comments (n=31), were classified as real experience sharing. However, a large portion of the comments consisted of name tagging and encouragements, which were classified as not informative. Regarding gender distribution of the patients, as shown in **Figure 3B.** 24 comments, or 77.40% of all comments, included identifiable gender information, with the majority being males (48.40% of comments specific to gender). It is expected that the reason for identifying a large number of male patients may be because the commenters were females who wanted to share their experiences about close individuals such as grandfathers, fathers, husbands, and brothers, who are groups of people with the highest risk behaviors for lung cancer, such as smoking, alcohol consumption, working in close proximity to pollutants such as construction sites. (19, 20)

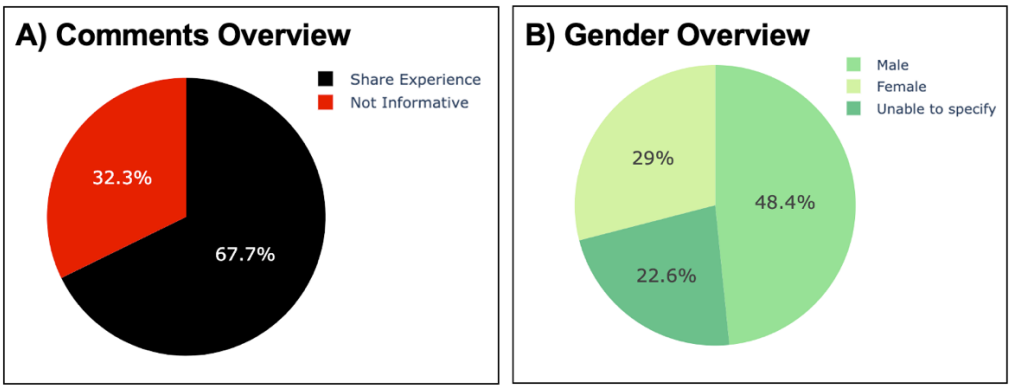

Figure 3. Data visualization shows the demographic characteristics of the commenters; (A) types of comments shared by commenters; (B) gender proportion of commenters.

An in-depth analysis using the NCDs listeners revealed that the most mentioned pre-lung cancer lifestyle behavior was non-smoking (10 comments). However, some comments included other behaviors such as smoking, not drinking, and exercising, as shown in **Figure 4A**. The results reflect that the actual causes of lung cancer may not correspond to the generally accepted risk factors, such as smoking, for lung cancer. (5, 21) Furthermore, **Figure 4B** indicates that three treatment options were mentioned: Chemotherapy (5 comments), Surgery (2 comments), and Radiation Therapy (1 comment). This reflects the perspective that lung cancer is commonly treated with chemotherapy and surgery, aligning with the public perception that these are the primary methods of cancer treatment. (21, 22)

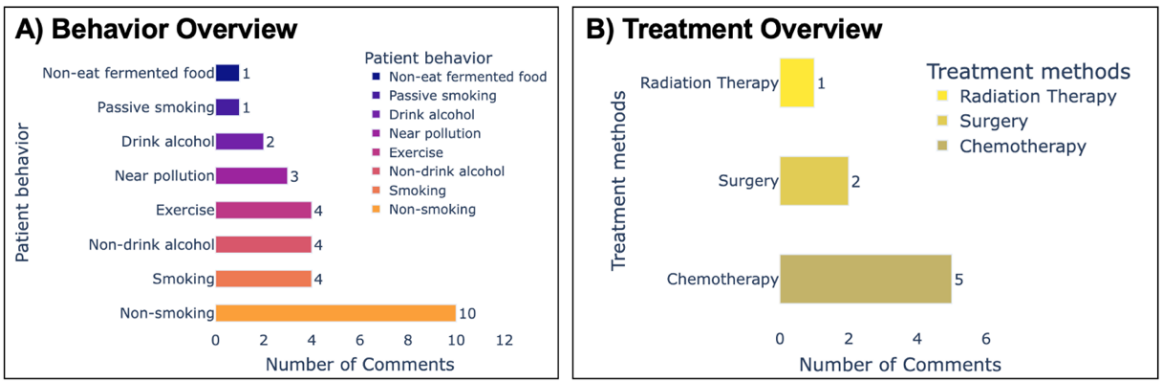

Figure 4. Data visualization shows the relevant cancer chart; (A) patient behavior shared by commenters; (B) treatment mentioned by commenters.

Summarization by the Generative AI Model

While visual data summarization can provide valuable insights, it may not deliver comprehensive conclusions for users. We propose utilizing Generative AI for data summarization based on RAG principles to enhance efficiency. This approach prioritizes accuracy management and minimizes hallucinations by leveraging comments related to lung cancer. The use of comments as meticulously crafted recommendation templates direct data to ensure maximum relevance and precision:

"Answer the question based only on the following context: {context} Question: {question} Respond in the same language."

The result of the comment summary will be generated based on the question as follows:

"Would you summarize the key characteristics of the comments?"

Finally, the results are summarized in a text format that is linked to the user's desired comment (the comment that mentions lung cancer) as follows:

> **"***The comments express a range of opinions and experiences related to lung cancer, predominantly focusing on the seemingly unpredictable nature of the disease. Many commenters express surprise and concern that lung cancer can affect non-smokers, healthy individuals, and even those who exercise regularly. There's a significant amount of shared personal experience, including stories of loved ones battling or succumbing to the disease, and a search for understanding regarding its causes. Genetic predisposition, environmental factors like PM2.5 and asbestos, and even seemingly unrelated factors like diet are discussed as potential contributing elements. Overall, the online conversation reflects a mixture of fear, empathy, and a quest for answers regarding lung cancer's etiology***"**

Based on both the visualization results and the summary of comments generated by Generative AI, most comments predominantly reflected the experiences of others, most commonly men, whose pre-cancer behavior was primarily as non-smokers. Discussions on treatment mainly

focused on chemotherapy. However, the majority of comments expressed concern about the possibility of developing cancer, even among healthy individuals or non-smokers.

Discussion & Conclusion

The NCDs Listener web application is designed to monitor social media data related to NCDs. The results incorporate social data obtained through keyword matching, BERT-based comment extraction, and Generative AI-based comment summarization for comprehensive insights, enabling users to understand societal contexts better. This application is a valuable tool for researchers studying the social characteristics of diseases of interest (5-7). Unlike existing tools primarily focused on marketing (3), this tool adopts a knowledge extraction approach that combines keyword matching with BERT to identify significant data characteristics. It sets it apart from most current research, emphasizing pre-trained models for analyzing emotional responses in comments (5,9,10). Furthermore, the NCDs Listener employs data visualization to present its findings, aligning with methodologies used in comparable studies (5,7,9,10).

Social media serves as a vast and continually evolving source of information, making social media information sources highly significant and valuable in addressing the needs of the masses. The information derived from social media encompasses both primary and in-depth data, which can be utilized to generate knowledge for the public and is crucial for developing effective methods or tools that cater to these needs. However, gathering and analyzing meaningful insights from many individuals is resource-intensive. Consequently, tools have been developed to assist in collecting, analyzing, and summarizing, known as social listening (media) tools.

The NCDs Listener tool was developed to collect and summarize basic and in-depth knowledge about NCDs data from social media. This tool utilizes keyword matching and BERT to classify the characteristics of comments and employs Generative AI to generate knowledge by summarizing comments related to social characteristics. Moreover, the RAG principle enhances accuracy and minimizes hallucination in Generative AI outputs. Additionally, the tool presents insights through data visualization, enabling users to comprehend the social characteristics and insights of NCDs effectively.

This tool is designed to assist doctors, researchers, and the general public address various problems. For instance, it enables doctors to conduct surveys by posing questions to gather public opinions comprehensively. Additionally, it aids doctors and researchers in studies related to treatment by collecting data from social media and filtering opinions relevant to specific diseases of interest. Lastly, the tool facilitates information communication to the general public, enabling them to read, interpret, and summarize with clarity. It can serve as a resource for learning or supporting initial decision-making concerning non-communicable chronic diseases.

References

(1) World Health Organization. Noncommunicable diseases. Available at: URL:https://www.who.int/news-room/fact-sheets/detail/noncommunicable-diseases. Accessed Aug 29, 2024.

(2) Kapoor KK, Tamilmani K, Rana NP, Patil P, Dwivedi YK, Nerur S. Advances in social media research: Past, present and future. Information Systems Frontiers. 2018;20:531-58

(3) Sakamoto D, Matsushita N, Noda M, & Tsuda K. Social listening system using sentiment classification for discovery support of hot topics. Procedia Computer Science. 2018;126:1526-1533.

(4) Geyser W. Top 25 social media listening tools for 2024. Available at: URL :https://influencermarketinghub.com/social-media-listening-tools/. Accessed Sep 3, 2024.

(5) Rodrigues A, Chauhan J, Sagkriotis A, Hughes R, Kenny T. Understanding the lived experience of lung cancer: a European social media listening study. BMC Cancer. 2022;22:(475).

(6) Chauhan J, Aasaithambi S, Márquez-Rodas I, Formisano L, Papa S, Meyer N, Forschner A, Faust G, Lau M, Sagkriotis A. Understanding the lived experiences of patients with melanoma: real-world evidence generated through a European social media listening analysis. JMIR Cancer. 2022;8(2).

(7) Mazza M, Piperis M, Aasaithambi S, Chauhan J, Sagkriotis A, Vieira C. Social media listening to understand the lived experience of individuals in Europe with metastatic breast cancer: a systematic search and content analysis study. Frontiers in Oncology. 2022;12:863641.
(8) Perić Z, Basak G, Koenecke C, Moiseev I, Chauhan J, Asaithambi S, Sagkriotis A, Gunes S, Penack O. Understanding the needs and lived experiences of patients with graft-versus-host disease: real-world European public social media listening study. JMIR Cancer. 2023;9.
(9) Manguri KH, Ramadhan RN, Amin PR. Twitter sentiment analysis on worldwide COVID-19 outbreaks. Kurdistan Journal of Applied Research. 2020;5:54–65.
(10) Burzyńska J, Bartosiewicz A, Ręka s M. The social life of COVID-19: early insights from social media monitoring data collected in Poland. Health Informatics Journal. 2020;26(4):3056-3065.
(11) Shoults CC, Dawson L, Hayes C, Eswaran H. Comparing the discussion of telehealth in two social media platforms: social listening analysis. Telemedicine Reports. 2023;4(1):236–248.
(12) Sanders AC, White RC, Severson LS, Ma R, McQueen R, Alcântara Paulo HC, Zhang Y, Erickson JS, Bennett KP. Unmasking the conversation on masks: natural language processing for topical sentiment analysis of COVID-19 Twitter discourse. AMIA Summits on Translational Science Proceedings. 2021;2021:555-564.
(13) Spitale G, Biller-Andorno N, Germani F. Concerns around opposition to the Green Pass in Italy: social listening analysis by using a mixed methods approach. Journal of Medical Internet Research. 2022;24(2).
(14) Chase H. LangChain: Build context-aware reasoning applications. Available at: URL: https://github.com/langchain-ai/langchain. Accessed Sep 14, 2024.
(15) Devlin J, Chang M, Lee K, Toutanova K. BERT: Pre-training of Deep Bidirectional Transformers for Language Understanding. Proceedings of the 2019 Conference of the North American Chapter of the Association for Computational Linguistics: Human Language Technologies. 2019;4171–86.
(16) Rueng Lao Chao Nee. ตำรวจหนุ่มโพสต์เรื่องราวของตนเอง ผ่านเฟซบุ๊กส่วนตัวเกี่ยวกับโรคมะเร็ง ที่ตนกำลังเผชิญอยู่. Available at: URL: https://www.facebook.com/MorningNewsTV3/posts/pfbid03pjHtzLPnML6x4GU9pvh4Dc8Cmn69Hd3opGcVJ1jKUoaTWs9HoWdys1WuawyWDacl?rdid=1sAmvQWoDYwDJWq4. Accessed Nov 25, 2024
(17) Thyroid Cancer Patient Community of Thailand. แบ่งปันประสบการณ์ได้รับการรักษามะเร็งไทรอยด์ครบสามปี. Available at: URL:https://www.facebook.com/ThaiThyCaCom/posts/pfbid031BwfrFJTy68h3vGpnCpt21Hajv2ZDMpN5cDdaf1nMeHyZ9LKSGoRAbYruVdXeR1Kl?rdid=M5de3aVi1c0y3ckA. Accessed Nov 25, 2024
(18) Pantip. ลูก 8 เดือน จากอาการเหมือนเป็นหวัดสู่โรคทางเดินอาหารสุดท้ายที่มะเร็งสมอง. Available at: URL:https://www.facebook.com/pantipdotcom/posts/pfbid0KAnukjRbzTnNu89338DFSech2H1YLdAoCBT9cQZJd7qtXViPgwZUzGKGj6cXjxcol?rdid=mqnj2q1CrShOz6x7#. Accessed Nov 25, 2024
(19) Social Statistics Division of National Statistical office. The Smoking and Drinking Behaviour Survey 2017. Bangkok: Pimdeekarnpim; 2018.
(20) The Office of Permanent Secretary Ministry of Labour. Labour Statistics Yearbook 2020. Bangkok: Labor Economics Division; 2021
(21) Nattha Phipopchaiyasit. มะเร็งปอด ความเสี่ยงใกล้ตัว. Available at: URL: https://www.nci.go.th/th/New_web2024/service/sv17.html. Accessed Dec 20, 2024
(22) National cancer institute Thailand. การรักษามะเร็งตามหลักสากลที่ปฏิบัติกันอยู่ในประเทศไทย. Available at: URL: https://www.nci.go.th/th/Knowledge/treat.html. Accessed Dec 20, 2024

The Potential Blood Biomarkers for Determining Manner of Death in Suicide Cases

Witchayawat Sunthon[1,2], Giatgong Konguthaithip[1,2], Thitiwat Sopananurakkul[1,2], Yutti Amornlertwatana[1,2], and Churdsak Jaikang[1,2,*]

[1] Department of Forensic Medicine, Faculty of Medicine, Chiang Mai University, Chiang Mai 50200 Thailand

[2] Metabolomics Research Group for Forensic Medicine and Toxicology, Department of Forensic Medicine, Faculty of Medicine, Chiang Mai University, Chiang Mai 50200 Thailand

*Corresponding author's email: churdsak.j@cmu.ac.th

Abstract:

The manner of death (MOD) determination is a crucial step in forensic investigations. The decision of MOD is based on scene investigation, autopsy, histological and toxicological findings. In complicated suicide cases, these evidences may be insufficient to determine the MOD and need potential biomarkers to help judicial determinations. This study aimed to identify potential blood biomarkers for categorizing suicide and non-suicidal death. Heart blood samples were collected from suicide ($n = 45$) and non-suicide cases ($n = 45$) and metabolomic profiles were measured using proton nuclear magnetic resonance spectroscopy. 209 metabolites were investigated in heart blood and 19 metabolites were significantly different between the groups ($p < 0.05$). Particularly, 4-Hydroxyproline and sarcosine significantly decreased in the suicide group, while heparan sulfate significantly increased ($p < 0.01$ and q = 0.04). The Receiver Operating Characteristic (ROC) curve was utilized to evaluate the performance biomarkers. 4-hydroxyproline, sarcosine and heparan sulfate closely related to the suicide with areas under the curve (AUC) values of 0.73 (95% CI: 0.61–0.83),0.72 (95% CI: 0.60–0.81), and 0.71 (95% CI: 0.60–0.82), respectively. These indicate that 4-hydroxyproline, sarcosine and heparan sulfate are potential blood biomarkers for classification suicide and non-suicide cases. This finding highlights the potential of these biomarkers to aid forensic pathologists in determining MOD in suicide cases. Further study on developing predictive models using these metabolites could enhance forensic investigations and contribute to public health and suicide prevention.

Keywords: Suicide; Suicide biomarkers; Forensic metabolome; Manner of death; Metabolomics

Introduction

Suicide is an important global public health issue. It is estimated that approximately 700,000 individuals die by suicide annually(1). Under Thai law, the cause of death and the manner of death (MOD) must be investigated, especially in cases of unnatural death. The manner of death is generally classified into homicide, suicide, accident, natural and undetermined. The correct manner of death is important information for the victim's family, law enforcement, research, public health policy and insurance matters. The scene has been changed by close relatives to disguise the true nature of the event, most often for religious or insurance purposes. Moreover, complicated suicide cases need more information and evidence to conclude the manner of death.

Signs of a struggle, suicide notes, closed-circuit television (CCTV) footage, autopsy findings, and laboratory results serve as circumstantial evidence to assist in determining the manner of death. However, suicide cases occur in obscured locations leading to limited evidence. Suicide notes are seldom found and may not reliably establish intent. Over 90% of suicide cases are associated with psychiatric disorders, substance abuse, anxiety disorders, and schizophrenia(2).

In cases without a history of psychiatric disorder or stress, this situation can raise questions from relatives, law enforcement, and legal professionals. Relatives may reject suicide determination and sometimes allege homicide, often directing suspicion toward the last person who interacted with the deceased. Thus, a precise manner of death determination is crucial for establishing the truth and ensuring justice.

Biomarker discovery has become a crucial area of research and focuses on identifying distinctive features that signify specific diseases or behaviors. Recently advancements in metabolomics, the study of small molecules involved in metabolic processes, enable researchers to investigate biochemical changes linked to various pathological conditions to identify disease biomarkers(3). Prior research has explored metabolomic changes in living individuals with psychiatric disorders, and few studies have focused on post-mortem cases. Using metabolomic profiles from living subjects cannot be applied in forensic cases because of the post-mortem interval (PMI) effect. Therefore, biomarkers related to MOD should be developed to assist forensic pathologists and legal professionals' decisions. This study aims to identify the potential biomarkers to differentiate between suicide and non-suicide cases using blood metabolomics.

Materials and Methods

Chemical and reagents

Acetonitrile, deuterium oxide (D_2O) and 3-(trimethylsilyl)- [2, 2, 3, 3-d4]-1-propionate sodium salt (TSP) were procured from Sigma-Aldrich (St. Louis, MO, USA).

Subjects and study design

This study was approved by the Ethics Committee of the Faculty of Medicine, Chiang Mai University, Thailand (the study code: FOR-2566-0234). Informed consent was received from close relatives before specimen collection. This study included autopsy cases conducted at the Department of Forensic Medicine, Faculty of Medicine, Chiang Mai University, between June 15, 2023, and May 31, 2024. The deceased aged greater than 60 years, inconclusive manner of death, presenting signs of decomposition, and instances where heart blood samples could not be collected were excluded. The study groups comprised suicide (n = 45) and non-suicide groups (n = 45).

Collection and preparation of heart blood specimens

A 3-milliliter heart blood sample was collected in a heparin tube and stored at -80 °C until analysis. The samples were extracted using acetonitrile according to the Somtua method(4). The blood sample was transferred to a plastic tube and extracted with acetonitrile at a 1:3 ratio. The solution was shaken for 10 minutes and subsequently centrifuged at 4000 RPM at 4 °C for 10 minutes. The supernatant was isolated and lyophilized. The 0.6 mL of 0.1 mM TSP prepared in D_2O was used to re-dissolve the dry sample. Metabolite levels were analyzed using a 500 MHz NMR, applying a technique to water suppression.

Acquisition parameters

The proton NMR (^{1}H-NMR) spectrum was acquired on a Bruker AVANCE 500 MHz instrument (Bruker, Bremen, Germany) equipped with a Carr-Purcell-Meiboom-Gill (CPMG, RD-90°, (t-180°), n-acquire) pulse sequence for ^{1}H-NMR analysis. Spectra were collected at 27 °C using water suppression pre-saturation, with the following parameters: 16 scans, a 1-second relaxation delay, a 3.95-second acquisition time, an 8278.146 Hz spectral window, a 0.126 Hz resolution for free induction decay (FID), and a 60.40 microsecond dwell time (DW). A 90° pulse was applied with 16 signal averages (NSAs). Baseline and phase corrections were conducted using TopSpin 4.0.7 software. The spectra ranging from 0.00 to 12.00 ppm were analyzed, with data normalized to the total integrated area. Metabolite resonances were identified using human metabolome databases(5) and TSP was used as an internal standard to quantify 24 energy-related metabolites throughout all samples.

Internal standard and quality control

TSP was designated as the internal standard due to its distinct location at 0.000 ppm and its emergence from a region of higher magnetic field intensity compared to other protons. Quality control (QC) samples were developed by equally mixing portions of each blood sample and ensuring consistent preparation. These specimens were then processed identically into the primary samples

through all previously detailed steps. Non-targeted metabolomic analysis was performed using the specified methods.

Peak assignment and chemical identification

Each chemical compound was identified using the Human Metabolome Database (HMDB), accessed in June 2024. Peak acquisition and J-coupling analysis were performed using Bruker TopSpin software, version 4.0.7. The interpretation of the NMR spectra was based on chemical shift values, spin-spin coupling, signal patterns, and coupling constants. Non-targeted metabolites were matched and the chemical shift of the center peak was less than 0.01 ppm against the HMDB database.

Calculation of non-targeted metabolite concentration by quantitative NMR

The data were imported into MNOVA Software (version 12.0.0, MestreLab Research, Spain) for intensity analysis and identification. The TSP peak was identified and determined at 0.000 ppm. The intensity of the 209 spectra in the chromatogram was identified. Subsequently, the intensity of all metabolite peaks was converted to concentrations using the equation (6) demonstrated below:

$$\frac{I_A}{I_B} = \frac{H_A}{H_B} \times \frac{C_A}{C_B}$$

Where, I = Signal intensity (Integral), H = Number of protons in a functional group, C = Concentration (μM).

Analysis of specific blood metabolomics and biomarkers

The MetaboAnalyst 6.0 free online tool, accessed on September 1, 2024, was used for metabolomics data analysis. Two classes, non-negative numbers for the compound concentrations or peak intensity values, and missing value imputations were checked before data analysis. The data were normalized using quartile, log-transformed (base 10), and auto-scaled for data scaling. The difference in metabolite between suicide and non-suicide groups was analyzed using Partial-least square discriminant analysis (PLS-DA). Variable importance in projection (VIP) was applied for the Importance measure analysis. Wilcoxon rank-sum tests were processed by choosing equal group variance, non-parametric tests, raw, and a p-value threshold of 0.05 to determine significant metabolite differences between suicide and non-suicide groups. The program automatically calculated the p-value and false discovery rate (FDR) in this step. The study applied Receiver Operating Characteristic (ROC) curve analysis to evaluate the specific biomarkers to distinguish between the groups. The ROC curve is widely recognized as an effective evaluation tool, providing a comprehensive, threshold-independent, and visually intuitive method for assessing the discriminative power of biomarkers. The power of the biomarkers is represented by the area under the curve (AUC) as a single, interpretable overall performance metric. The AUC was calculated using classical univariate ROC curve analysis to assess the ability of specific biomarkers to differentiate between the suicide and non-suicide groups. Metabolites with an AUC greater than 0.7 are considered to have acceptable discriminative ability, while those with an AUC less than 0.7 are considered to have fair discriminative ability. Therefore, only metabolites with an AUC greater than 0.7 should be considered as biomarkers.

Statistical analysis

The Kolmogorov-Smirnov test was analyzed to evaluate the normality. The data are presented as quartiles. The differences in central tendency between the two groups were analyzed using Wilcoxon rank-sum tests using MetaboAnalyst 6.0 as aforementioned. Differences in categorical variables, including sex, non-communicable diseases (NCDs), psychiatric disorders, illegal drug use, and alcohol consumption, in the demographic data of subjects between the suicide and non-suicide groups were analyzed using the Chi-square test. An independent samples t-test was applied to evaluate differences in age and BMI between the two groups.

Results and Discussion

Demographic data of participants

Ninety cases were divided into two groups: the suicide group (n = 45) and the non-suicide group (n = 45). The causes of death in the suicide group included hanging (56%), carbon monoxide poisoning (22%), pesticide intoxication (11%), gunshot injury (4%), falls from height (4%), and exsanguination (3%). The non-suicide group included cases of homicide, natural death, and accidents. Psychiatric disorders were determined based on medical history, information provided by the deceased's relatives, or the presence of psychiatric drugs in the blood samples. The number of males, age, body mass index (BMI), non-communicable diseases (such as diabetes mellitus, hypertension, and dyslipidemia), exposure to illegal drugs (particularly methamphetamine and THC), and alcohol drinkers between the groups did not significantly differ. For the number of psychiatric disorders between the two groups, the suicide group included 17 cases compared to 7 cases in the non-suicide group. The number of psychiatric disorders was significantly greater in the suicide group than in the non-suicide group. The data are presented in Table 1.

Table 1. Demographic data of suicide and non-suicide group.

Factors	Suicide (n=45)	Non-suicide (n=45)	p-value
Sex: Male (%)	32 (71%)	36 (80%)	0.33
Age (year-old)	41±9.9	40.2±12.4	0.49
Body mass index (kg/m^2)	23.08±4.39	24.37±4.86	0.19
Noncommunicable diseases	12 (26.7%)	7 (15.6%)	0.20
Psychiatric disorder	17 (37.8%)	7 (15.6%)	0.02*
Illegal drugs users	3 (6.7%)	8 (17%)	0.11
Alcohol drinkers	20 (44.4%)	16 (35.6%)	0.40

Continuous variables are presented as mean ± SD, and p-values were calculated using the independent samples t-test. Categorical variables are presented as numbers in each group, and p-values were calculated using the chi-square test.
* Significant difference between the groups.

Several factors including time since death, sex, age, chronic diseases, and drug use impact on forensic metabolomic analysis(4, 7). In this study, sex, age, body mass index (BMI), non-communicable diseases (NCDs), illegal drug use and alcohol consumption did not differ between the suicide and non-suicide groups. However, the number of psychiatric disorders was significantly higher in the suicide group compared to the non-suicide group. Psychiatric disorders, particularly mood disorders, are major risk factors for suicide(2).

Identification of specific blood biomarkers associated with suicide cases

This is the first study to investigate the complete suicide metabolomic profiles to identify potential biomarkers for differentiating suicides from non-suicides in forensic cases. In post-mortem cases, the metabolomic profile may be influenced by the PMI. However, there is limited data on post-mortem metabolomics, especially 4-hydroxyproline, sarcosine, and heparan sulfate.

All 209 metabolites were analyzed using partial least squares discriminant analysis (PLS-DA) to assess the metabolomic profile for each group, with the results shown in Figure 1. (A). PLS-DA component 1 (8%) is represented on the X-axis, and component 2 (11.2%) on the Y-axis. There are some separate areas of metabolic profiles between the suicide and non-suicide groups. It revealed specific metabolomic profiles that can differentiate suicide cases from non-suicide cases. Therefore, variable importance in projection (VIP) scores were used to evaluate the specific metabolites between the groups. The metabolites which had VIP scores more than 1.0 were considered potential biomarkers. The top 15 VIP score values of metabolite including 4-hydroxyproline, sarcosine, heparan sulfate, pyridoxamine, biopterin, citrulline, 5-carboxycytosine, triglycerides, malic acid, cytidine, thymine, N-acetyl-D-glucosamine, epinephrine, and L-histidine are shown in Figure 1. (B).

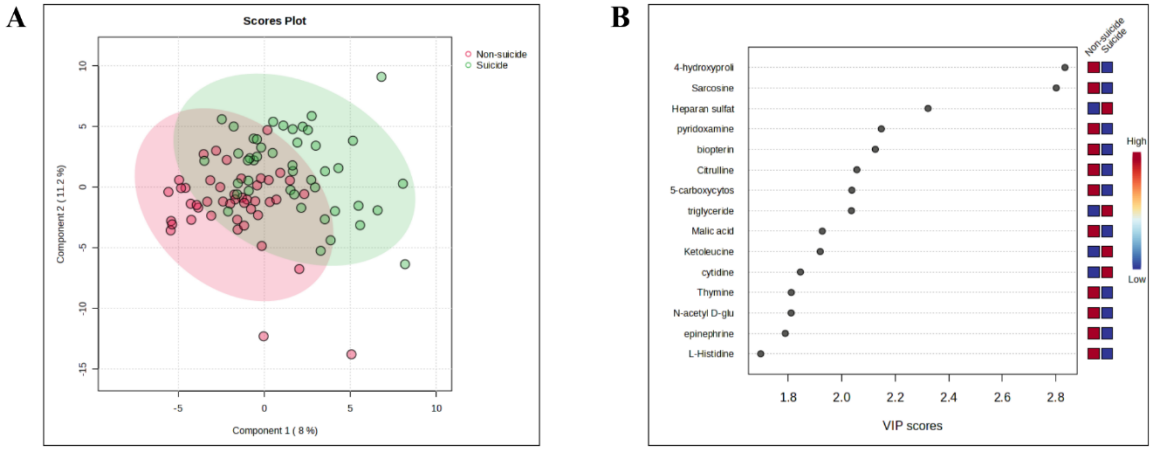

Figure 1. Metabolomic profile of suicide and non-suicide cases. **(A)** PLS-DA analysis of suicide and non-suicide cases. **(B)** The top 15 metabolites with the highest VIP scores. The data were analyzed using the MetaboAnalyst 6.0 online tool.

The t-test identified significant differences in metabolite levels between the two groups, with 19 metabolites showing $p < 0.05$ (details in Table 2). After FDR correction, 4-hydroxyproline and sarcosine were significantly lower in suicide cases, while heparan sulfate was higher ($p < 0.01$, $q = 0.04$). ROC analysis confirmed biomarker performance: AUC 0.73 (95% CI: 0.61–0.83) for 4-hydroxyproline, 0.72 (95% CI: 0.60–0.81) for sarcosine, and 0.71 (95% CI: 0.60–0.82) for heparan sulfate (Figure 2). These metabolites, with AUCs exceeding 0.7, demonstrated potential for differentiating suicide from non-suicide. Lower AUCs for other metabolites may reflect variations in ancestry, diet, living conditions, or post-mortem intervals.

Table 2. Nineteen significantly different metabolites between the suicide and non-suicide groups

Metabolites	Suicide			Non-suicide			p-value	q-value
	Q1	Q2	Q3	Q1	Q2	Q3		
4-Hydroxyproline	30.29	64.42	273.83	43.24	145.66	325.43	<0.001	0.04*
Sarcosine	14.15	26.99	103.30	19.02	38.46	162.44	<0.001	0.04*
Heparan sulfate	6.18	16.23	61.47	6.28	16.50	59.03	<0.001	0.04*
Triglyceride	9.32	19.46	57.61	8.37	22.00	48.72	<0.001	0.19
N-acetyl glycine	31.37	82.17	331.90	41.51	104.72	395.80	0.01	0.39
Acetoacetic acid	23.24	58.11	198.12	32.74	64.66	302.48	0.01	0.39
GAL[a]	13.18	24.83	113.24	17.62	39.83	170.55	0.01	0.44
Cholesterol	11.78	31.45	89.03	13.02	28.46	85.27	0.02	0.44
Ornithine	256.35	470.58	1103.87	244.09	589.04	1590.79	0.02	0.44
Thymine	15.16	33.45	218.52	19.98	54.05	263.57	0.03	0.44
Malic acid	70.13	152.07	522.16	54.67	170.75	497.58	0.03	0.44
Pyridoxamine	25.71	80.37	186.78	31.77	83.48	236.95	0.03	0.44
SnG[b]	6.63	21.44	77.22	8.14	18.39	69.69	0.03	0.44
Hypotaurine	27.48	57.29	227.59	30.47	63.73	173.25	0.03	0.44
Biopterin	15.80	24.78	121.33	21.05	44.12	162.01	0.03	0.44
Acetyl-CoA	3.87	24.23	62.95	4.84	12.13	57.58	0.03	0.44
L-Histidine	2.99	5.20	28.39	4.36	10.05	45.03	0.04	0.48
L-Cystathionine	24.65	68.50	177.43	26.51	66.06	191.00	0.05	0.48
5-Carboxycytosine	3.15	5.94	34.23	4.44	9.19	51.28	0.05	0.48

[a]GAL is Gamma-aminobutyryl-lysine
[b]SnG is Sn-glycerophosphocholine
*Significant differences between the groups after FDR (q-value) were evaluated using MetaboAnalyst 6.0.
The data is presented as quartiles. The difference in central tendency between the two groups (p-value) was assessed using Wilcoxon rank-sum tests.

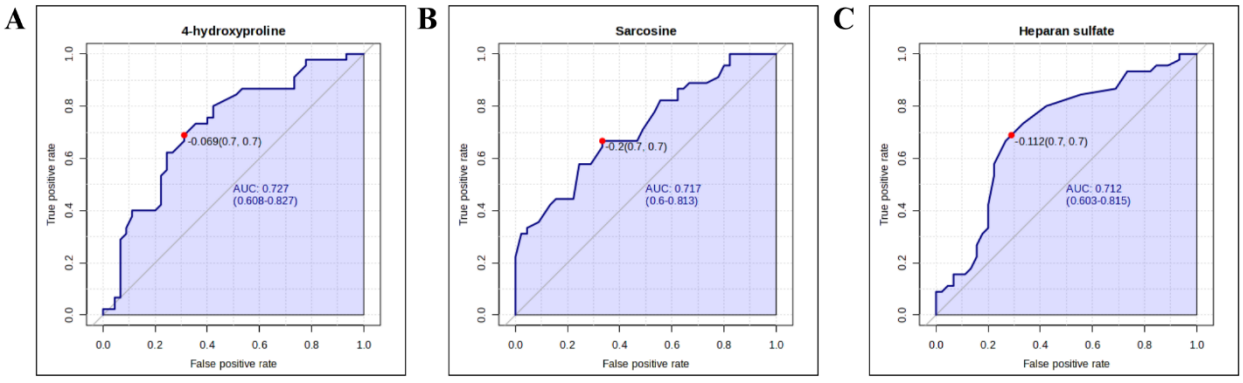

Figure 2. ROC curves for 3 metabolites with AUC values more than 0.7 and p-values less than 0.01. **(A)** 4-Hydroxyproline: AUC = 0.73, 95% CI = 0.61–0.83., **(B)** Sarcosine: AUC = 0.72, 95% CI = 0.60–0.81., **(C)** Heparan sulfate: AUC = 0.71, 95% CI = 0.60–0.82. The data were analyzed using classical univariate ROC curve analysis through MetaboAnalyst 6.0 online.

4-Hydroxyproline, a proline derivative, is produced by hydroxylation in collagen and serves as an important precursor for glycine, which is necessary for glutathione synthesis, DNA, heme, and proteins and scavenges reactive oxygen species. Previous studies in living subjects have shown a correlation between hydroxyproline and proline levels in urine with mental health issues, including stress and anxiety, suggesting a relationship between chronic stress and mental health(8, 9). This study found lower 4-hydroxyproline levels in suicide cases compared to non-suicides, with no existing evidence linking decreased 4-hydroxyproline specifically to suicide or postmortem conditions. However, research in rat models shows a significant drop in hydroxyproline levels in skeletal muscles as the postmortem interval (PMI) increases, reflecting collagen breakdown after death(10).

Our results revealed decreased sarcosine levels in suicide cases compared to non-suicide cases. In living subjects, sarcosine (N-methyl glycine) is a type 1 glycine transporter inhibitor that enhances glutamatergic neurotransmission(11). The glutamatergic system dysfunction has been observed in cases of major depressive disorder(12). The decreased levels of sarcosine found in our study are linked to the psychological and physiological stressors that may lead to suicide. These findings are consistent with previous studies in living subjects(11-13), which report decreased sarcosine levels in suicide cases, suggesting that PMI does not influence these levels.

Our study observed elevated heparan sulfate levels in complete suicide cases. Heparan sulfate, a sulfated polysaccharide, is present on cell surfaces and within the extracellular matrix in various proteoglycan forms. It plays an important role in both neuroinflammation and systemic inflammatory responses(14). Inflammation is associated with the pathophysiology of suicide through various mechanisms(15). The increased heparan sulfate levels in our study may reflect neuroinflammatory or systemic inflammatory processes associated with suicide.

Sarcosine and heparan sulfate levels are consistent in both living and postmortem subjects, while 4-hydroxyproline shows a different pattern, possibly influenced by PMI. This may result from postmortem metabolic changes in 4-hydroxyproline, though human data is lacking. Sarcosine and heparan sulfate not only aid in suicide classification but also provide insight into biochemical pathways linked to suicidal behavior.

This study identified potential biomarkers to differentiate between suicide and non-suicide, showing promise in forensic applications. The research was conducted on subjects with a PMI of less than 24 hours in Thailand. Future studies should examine suicide cases with a PMI greater than 24 hours, different populations, or under varying environmental conditions. Additionally, research on predictive models for distinguishing suicide from non-suicide is needed to further develop a tool to assist forensic pathologists and legal professionals in determining MOD.

Conclusion

4-hydroxyproline, sarcosine and heparan sulfate are key blood metabolites that significantly differ between suicide and non-suicide cases, presenting a novel approach to forensic investigation. This finding underscores the potential of these biomarkers to help forensic pathologists determine MOD in cases of suicide. Further study to develop model prediction as the tool for MOD determination in suicide cases using these metabolites is valuable for forensic applications. This approach not only enhances forensic investigations but could also inform public health and suicide prevention strategies by identifying biomarkers associated with suicide risk.

Conflict of interest statement

The researchers declare that they have no known financial conflicts of interest or personal relationships that could have affected the work presented in this paper

Acknowledgments

This work was supported by the Faculty of Medicine, Chiang Mai University, grant no 42-67. The researchers would like to sincerely thank the deceased donors and their families for their support and permission to collect research samples.

References

1. Pallocci M, Passalacqua P, Zanovello C, Coppeta L, Ferrari C, Milano F, et al. Forensic Characterisation of Complex Suicides: A Literature Review. Forensic Sciences. 2024;4(3):277-88.
2. Sher L, Oquendo MA. Suicide: An Overview for Clinicians. Med Clin North Am. 2023;107(1):119-30.
3. Rinschen MM, Ivanisevic J, Giera M, Siuzdak G. Identification of bioactive metabolites using activity metabolomics. Nat Rev Mol Cell Biol. 2019;20(6):353-67.
4. Somtua P, Jaikang C, Konguthaithip G, Intui K, Watcharakhom S, O'Brien TE, et al. Postmortem Alteration of Purine Metabolism in Coronary Artery Disease. Metabolites. 2023;13(11).
5. Dona AC, Kyriakides M, Scott F, Shephard EA, Varshavi D, Veselkov K, et al. A guide to the identification of metabolites in NMR-based metabonomics/metabolomics experiments. Comput Struct Biotechnol J. 2016;14:135-53.
6. de Graaf RA, Behar KL. Quantitative ^{1}H NMR spectroscopy of blood plasma metabolites. Anal Chem. 2003;75(9):2100-4.
7. Dawidowska J, Krzyżanowska M, Markuszewski MJ, Kaliszan M. The Application of Metabolomics in Forensic Science with Focus on Forensic Toxicology and Time-of-Death Estimation. Metabolites. 2021;11(12).
8. Lee KW, Kim SJ, Park JB, Lee KJ. Relationship between depression anxiety stress scale (DASS) and urinary hydroxyproline and proline concentrations in hospital workers. J Prev Med Public Health. 2011;44(1):9-13.
9. Chen H, Wang J, Chen S, Chen X, Liu J, Tang H, et al. Abnormal energy metabolism, oxidative stress, and polyunsaturated fatty acid metabolism in depressed adolescents associated with childhood maltreatment: A targeted metabolite analysis. Psychiatry Res. 2024;335:115795.
10. Saber TM, Omran BHF, El Deib MM, El-Sharkawy NI, Metwally MMM, Abd-Elhakim YM. Early postmortem biochemical, histological, and immunohistochemical alterations in skeletal muscles of rats exposed to boldenone undecylenate: Forensic implication. J Forensic Leg Med. 2021;83:102248.
11. Curtis D. A possible role for sarcosine in the management of schizophrenia. Br J Psychiatry. 2019;215(6):697-8.
12. Henter ID, de Sousa RT, Zarate CA, Jr. Glutamatergic Modulators in Depression. Harv Rev Psychiatry. 2018;26(6):307-19.
13. Huang CC, Wei IH, Huang CL, Chen KT, Tsai MH, Tsai P, et al. Inhibition of glycine transporter-I as a novel mechanism for the treatment of depression. Biol Psychiatry. 2013;74(10):734-41.
14. Zhang X, Wang B, Li JP. Implications of heparan sulfate and heparanase in neuroinflammation. Matrix Biol. 2014;35:174-81.
15. Brundin L, Bryleva EY, Thirtamara Rajamani K. Role of Inflammation in Suicide: From Mechanisms to Treatment. Neuropsychopharmacology. 2017;42(1):271-83.

^{1}H-NMR-Based Bone Metabolomics Signature for Sex Identification

Thitiwat Sopananurakkul, Witchayawat Sunthon, Yutti Amornlertwatana, and Churdsak Jaikang*
Department of Forensic Medicine, Faculty of Medicine, Chiang Mai University, Chiang Mai 50200 Thailand
Corresponding author's email: churdsak.j@cmu.ac.th

Abstract:

Sex is an important factor for person identification in forensic science. Bone is a static tissue and the most likely to remain intact through decomposition processes. Debris bone samples have limited utility for sex identification and need effective methods for investigation. Proton- nuclear magnetic resonance spectroscopy (^{1}H-NMR) uses a small sample and does not destroy the samples. The aim of this study was to identify potential biomarker in bone for sex identification by using ^{1}H-NMR metabolomic technique. Bone samples were collected from male (n = 62) and female (n = 60). The sponge rib bone was digested and lyophilized before analysis with ^{1}H-NMR. The sponge rib bone contained 197 Chemical compounds. L-glyceric acid and 2-Aminoadipic acid was higher in males (p<0.01; q =0.01). Conversely, L-aspartic acid was higher in females (p=0.04). L-glyceric acid, 2-Aminoadipic acid, and L-aspartic are specific and can apply for sex determination. ROC curve analysis was revealed that L-aspartic acid is the best compound for sex differentiation (AUC=0.76). These findings may result from different metabolomic pathways in both sexes, such as LDH activities, the production of pituitary hormones, and mitochondrial functions. In conclusion, the ^{1}H-NMR-based bone metabolomics signature has potential for sex determination. Further large-scale studies are needed to validate the specificity and sensitivity of these biomarkers for distinguishing between male and female.

Keywords: Sex; Metabolomics; Rib; NMR; Forensic metabolomics

Introduction

Bone is an important component of the musculoskeletal system(1) and the strongest tissue in the human body. The bone has an active metabolism within bone tissue, especially the living cells in the bone marrow. Bone consists of two main components: cortical bone and cancellous bone. The bone marrow, located in the cancellous bone, contains cells vital for bone homeostasis, such as osteoblasts, involved in bone formation; osteoclasts, which facilitate bone resorption; and hematopoietic cells, which produce blood cells(2).

The skeletal remains of an unknown individual can be challenging to identify using conventional methods, such as DNA analysis and anthropological studies, especially when the bone is fragmented(3). In these circumstances, body identification is of utmost importance. Therefore, new reliable techniques must be developed to solve this problem and identify the deceased individual. Rib bones are easily accessible during a forensic autopsy because the routine process involves the opening of the thoracic cavity. Consequently, the collection of the rib bones can be integrated into the standard procedures of forensic autopsies.

In some circumstances, especially explosions, mass disaster, and the dismemberment of bodies conventional methods for sex identification cannot easily to identify the unknown deceased. New method or specific biomarker to sex need to be developed to assist sex estimation. Sex-specific metabolomics in bone tissue is a modern technique and related to forensic metabolomics. NMR technique is a technique requires only a small samples, thus eliminating the difficulties associated with using fragmented skeletal remains. Therefore, sex-specific biomarkers in human rib bones have the potential to be an alternative method for sex differentiation.

Metabolomics is an -omics science that emphasizes the study of metabolites and the products of cellular metabolism. This field offers both qualitative and quantitative insights into metabolites

and explores metabolomic pathways. By analyzing metabolic profiles, metabolomics can identify biomarkers for various diseases, specific metabolomic pathways, and metabolic disorders(4, 5).

Nuclear magnetic resonance (NMR) is a method that uses the magnetic properties of the metabolites of living cells. The method can provide information of molecules, molecular structures, and metabolic pathways. Proton-magnetic resonance (^{1}H-NMR) utilizes the properties of hydrogen atoms in a cell to identify the compounds without destroying the samples.

Nowadays, in the field of forensic science, metabolomics studies are increasingly utilized to explore postmortem intervals, estimate age, determine causes of death, and conduct toxicological analyses(6). These studies provide the identification of potential biomarkers that can be used in forensic practices. However, these studies are not fully explored and are still in the research phase. Ongoing research is focused on developing sensitivity and accuracy for practical use(7).

The objective of this study is to investigate potential biomarkers that can differentiate between male and female rib bones in the Thai population. This research will focus on the unique characteristics present in rib bones, utilizing ^{1}H-NMR techniques to explore any significant differences that can indicate the biological sex of the individuals.

Materials and Methods

Chemical reagents

Acetonitrile was purchased from Supelco, Merck (Darmstadt, Germany). 3-(trimethylsilyl)-[2,2,3,3-d4]-1-propionate sodium salt (TSP) and deuteri-um oxide (D_2O) were purchased from Sigma-Aldrich (St.Louis,MA,USA)

Bone sample collection

In this study, rib bone samples were obtained from the deceased who were autopsied at the Department of Medicine at the Faculty of Medicine, Chiang Mai University. This study was approved from the Ethic Committee of the Faculty of Medicine, Chiang Mai University, Thailand (Study code: HOS-2566-0322, Research ID: 0322) Rib bone samples from the 4th and 5th ribs were excised to approximately 1x2x0.5 cm in size. Following collection, these samples were stored at -80°C to preserve their integrity until further processing. Samples with no medical record or history of systemic illness or chronic drug use were excluded.

Bone samples preparation

The cancellous bone samples were manually extracted using a curette instrument. The extracted samples were then treated with 6M hydrochloric acid (HCl) at 100°C for 24 hours. Following this treatment, the samples were evaporated to remove water. Sub-sequently, TSP which dissolved in D_2O was added to the dried samples to prepare them for analysis using ^{1}H-NMR.

^{1}H-NMR analysis

The analysis was conducted using ^{1}H-NMR at 500 MHz with a water suppression technique. The parameters were set as follows: pulse sequence = 16 scans, relaxation decay = 1 second, acquisition time = 3.95 seconds, spectral window = 8,278.146 Hz, free induction decay (FID) resolution = 0.126 Hz, and dwell time (DW) = 60.40 microsec-onds. The results were the chemical shifts, which were selected for each individual sample. TSP was used as the internal standard for the analysis due to its chemical shift appearing at 0 ppm in 500 MHz ^{1}H-NMR. The chemical shifts were identified using the Human Metabolome Database (HMDB)(8), retrieved in June 2024.

Data analysis

Descriptive data analysis for age, BMI, weight, and height was analyzed using IBM SPSS Statistics version 27. The normality of the data was assessed with the Kolmogorov-Smirnov test. After the normality testing, comparisons were made using an independent t-test.

The data retrieved from the chemical shifts were analyzed, and peaks were identified using MNOVA software. The baseline of the spectra was adjusted to 0, and the internal standard peak (TSP)

was calibrated to 0.00 ppm. Consequently, all identified chemical shifts were used to calculate concentrations, using the formula shown below(9).

$$\frac{I_A}{I_B} = \frac{H_A}{H_B} \times \frac{C_A}{C_B}$$

I = Signal intensity (Integral), H = Number of protons in a functional group, C = Concentration.

Metabolomics measurements

The concentration of each sample was analyzed using the online software MetaboAnalyst (version 6.0, http://www.metaboanalyst.ca/MetaboAnalyst). The data were classified into two groups (male and female). Subsequently, the data were normalized by median, log-transformed (base 10), and auto-scaled for data scaling. The normalized data were then analyzed using partial least squares discriminant analysis (PLS-DA)(7), an independent t-test, a volcano plot, and enrichment analysis. Enrichment analysis was conducted using KEGG human metabolic pathways (December 2023).

Results and Discussion

Descriptive analysis

A total of 122 rib bones were collected from female (60 samples) and male (62 samples). The mean age at death of female group and male group are 53.1 and 49.2 years respectively with no statistically significant differences. The results are shown in Table 1. Both groups also show no significant differences in height, weight and body mass index. Therefore, these results indicate that both groups have similar characteristics.

Table 1. Demographic data of the rib bone samples.

Parameters	Female (N=60)	Male (N=62)	*p*-value
Age (years)	53.1±16.0	49.2±17.7	0.40
Height (cm)	155.8±6.7	167.2±7.3	0.36
Weight (kg)	63.1±15.2	63.7±17.9	0.29
Body mass index (kg/ m^2)	26.1± 6.2	22.5± 5.0	0.21

Identification chemical compounds contained in rib bone

197 chemical compounds were identified in cancellous bone of human rib bone by ^{1}H-NMR technique. The group of chemical compounds that were identified are organic acid derivatives, organic oxygen compounds and organicheterocyclic compounds were the most abundant chemical compounds and presented in Figure 1.

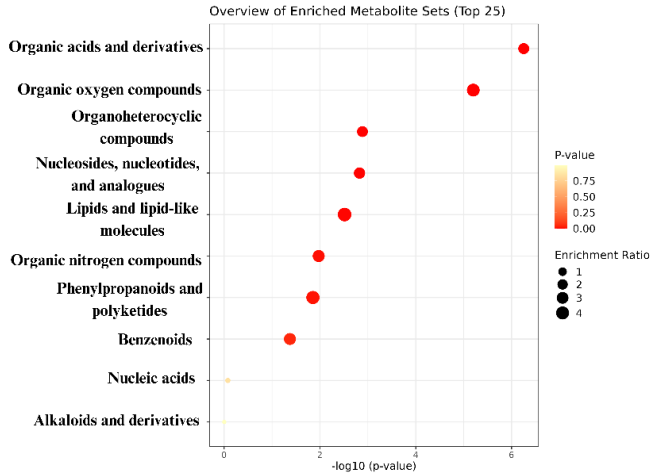

Figure 1. The enrichment analysis shows the different chemical groups between male and female using super-class chemical structures for metabolite set library.

Metabolomics study

The multivariate partial least squares-discriminant analysis (PLS-DA) was implemented(10) and showed two defined cluster for male and female groups (accuracy = 0.88, R2 = 0.86, Q2 = 0.5, permutation test: $p < 0.0001$). The results, as shown in Figure 2, indicate a clear separation between female and male samples, signifying distinct metabolic profiles. The Variable Importance in Projection (VIP) scores plot reveals that L-glyceric acid has the highest VIP score. Independent t-test analysis of the identified metabolites shows 47 compounds with statistically significant differences (p-Value < 0.05) between male and female samples. Of these, 13 compounds remained significant after applying the False Discovery Rate (FDR) correction (FDR q-Value < 0.05)(11), shown in table 2. As a result, L-glyceric acid was the most significant compound with p-value and q-value less than 0.01. This finding suggests that L-glyceric acid has the potential to be a biomarker for differentiating between males and females.

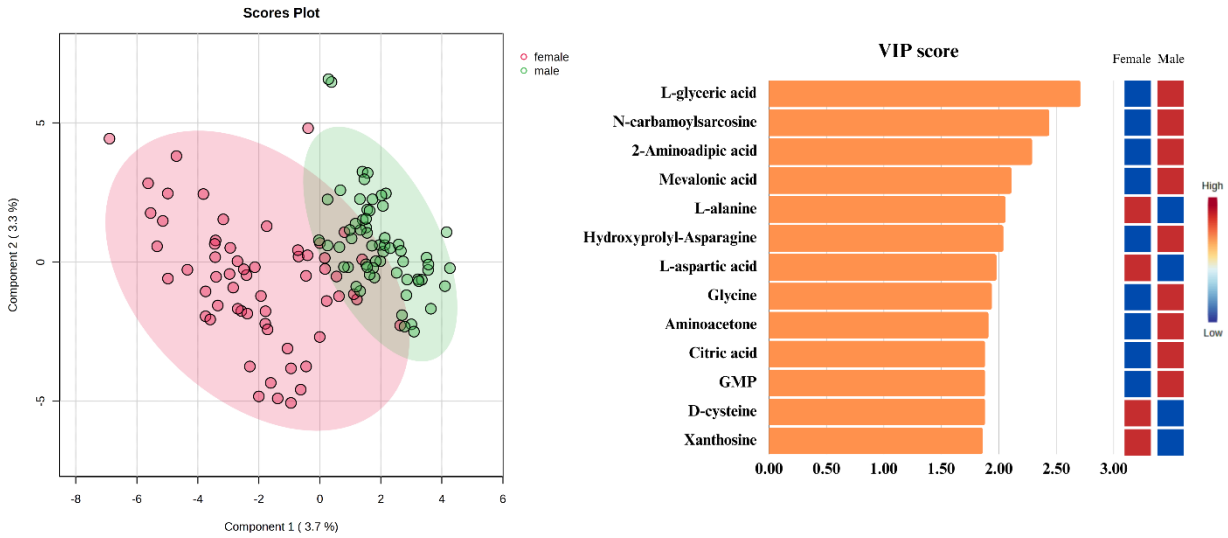

Figure 2. The PLS-DA score plot shows a distinct difference between the male (green) and female (pink) groups, with the female group displaying greater dispersion compared to the male group. The VIP score plot shows several key compounds that differentiate between the male and female groups.

Table 2. The independent T-test of normalized data with fold change and log_2(FC) of associated compounds.

Compounds	Fold change	Log_2(FC)	p-Value	FDR
L-glyceric acid	0.66	-0.61	< 0.01	< 0.01
N-carbamoylsarcosine	0.78	-0.36	< 0.01	0.01
2-Aminoadipic acid	0.09	-3.47	< 0.01	0.01
Mevalonic acid	0.77	-0.38	< 0.01	0.03
L-alanine	1.38	0.47	< 0.01	0.03
Hydroxyprolyl-Asparagine	0.75	-0.41	< 0.01	0.03
L-aspartic acid	2.89	1.53	< 0.01	0.04
Glycine	0.89	-0.17	< 0.01	0.04
Aminoacetone	0.80	-0.32	< 0.01	0.04
Citric acid	0.82	-0.29	< 0.01	0.04
GMP	1.01	0.01	< 0.01	0.04
D-cysteine	1.57	0.65	< 0.01	0.04
Xanthosine	1.93	0.95	< 0.01	0.04

The volcano plot shows that 10 compounds were upregulated in female, while 4 compounds were upregulated in males. 2-aminoadipic acid has an FC of 0.09 with a log_2(FC) of -3.47, indicating a significantly higher concentration in males. In contrast, L-aspartic acid has higher concentration in females with, has an FC of 2.89 with a log_2(FC) of 1.53, shown in Fig 3 and Table 3. As a result, these findings highlight that 2-aminoadipic acid and L-aspartic acid are potential biomarkers for sex differentiation.

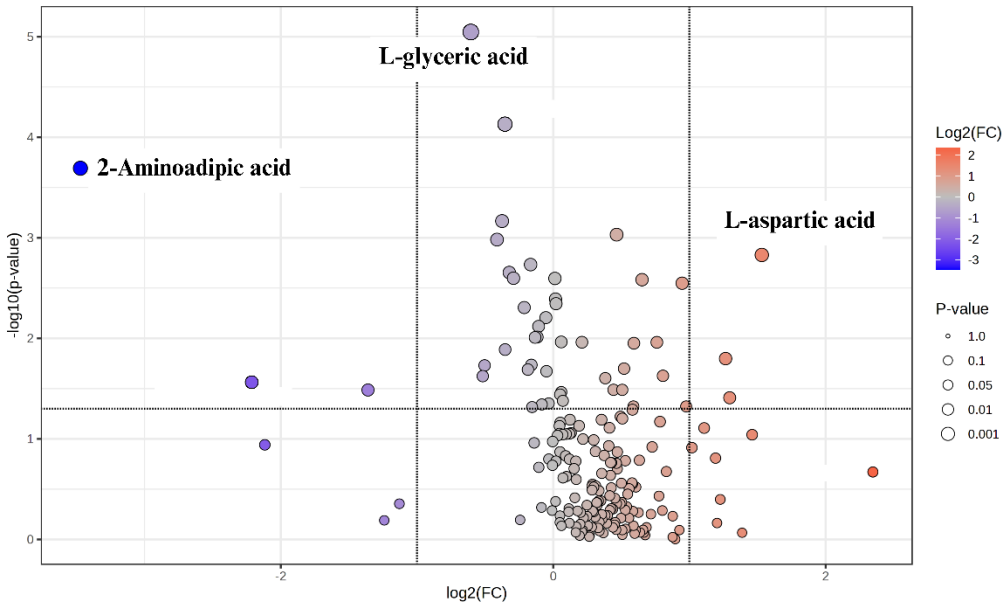

Figure 3 The volcano plot shows the fold change (FC) of statistically significant compounds. Circles on the left (blue) show the compounds that upregulate in male group. Circles on the right (red) show the compounds that upregulate in female group.

The receiver operating characteristic (ROC) curve analysis was done to analyze individual biomarkers. The result reveals that L-aspartic acid has the highest value of area under the curve (AUC) at 0.76, indicating the best potential biomarker for sex differentiation. The biomarkers with AUC more than 0.6 were also considered to be other potential biomarkers for sex differentiation, shown in Table 4. The result shows that 2-Aminoadipic acid has the lowest Log_2(FC) value at -4.04, while L-aspartic acid has the highest value with Log_2(FC) of 0.95.

Table 3. A list of compounds with mean±SD of unnormalized data of both groups and Fold change (FC) with p-value and FDR of normalized data.

Compounds	Male	Female	Fold change (FC)	Log_2(FC)	*p*-value	FDR
L-glyceric acid**	971.24±1168.85	409.33±382.99	0.66	-0.61	<0.01	<0.01
N-carbamoylsarcosine	313.20±202.69	164.40±155.43	0.78	-0.36	<0.01	0.01
2-Aminoadipic acid*	756.82±1583.00	46.12±40.74	0.09	-3.47	<0.01	0.01
Mevalonic acid	440.90±267.45	253.53±249.57	0.77	-0.38	<0.01	0.03
L-alanine	85.73±48.15	78.07±41.30	1.38	0.47	<0.01	0.03
Hydroxyprolyl-Asparagine	120.24±109.76	60.30±52.58	0.75	-0.41	<0.01	0.03
L-aspartic acid*	24.07±20.36	46.50±34.46	2.89	1.53	<0.01	0.04
Glycine	931.44±935.15	553.69±496.84	0.89	-0.17	<0.01	0.04
Aminoacetone	253.33±124.56	149.55±105.32	0.80	-0.32	<0.01	0.04
Citric acid	147.03±131.60	86.60±104.56	0.82	-0.29	<0.01	0.04
GMP	6.07±4.35	4.02±3.60	1.01	0.01	<0.01	0.04
D-cysteine	498.40±425.10	539.82±311.74	1.57	0.65	<0.01	0.04
Xanthosine	9.95±9.03	12.46±8.53	1.93	0.95	<0.01	0.04
Cysteic acid	220.09±239.39	242.80±134.35	1.69	0.76	0.01	0.09
N2-gamma-glutamylglutamine	23.67±26.61	22.58±12.49	1.51	0.59	0.01	0.09
Lanthionine*	143.16±497.23	158.37±261.13	2.40	1.27	0.02	0.12
5-methylcytosine	47.84±41.09	65.49±46.60	1.75	0.81	0.02	0.14
L-Altruronic acid*	480.10±1392.90	77.21±90.36	0.22	-2.21	0.03	0.15
L-lysine*	72.97±117.51	19.77±10.84	0.39	-1.36	0.03	0.17
L-tryptophan*	4.44±5.15	6.61±5.77	2.45	1.30	0.04	0.19
Thioguanine	7.99±7.71	7.35±4.95	1.50	0.59	<0.05	0.20
L-2,4-diaminobutyric acid	427.23±374.49	577.03±583.46	1.97	0.98	<0.05	0.20

* Indicate the compounds with Log_2(FC) < -1 or > 1

** Indicate the compound that has the highest statistically significant difference

This study, the potential biomarkers for sex differentiation are L-glyceric acid, 2-aminoadipic acid, and L-aspartic acid. L-glyceric acid and 2-aminoadipic acid are higher level in the male population, while L-aspartic acid is higher concentration in the female population. These indicate that males might have higher LDH activity than female leading to increase L-glyceric acid levels(12). There are limit data to describe the roles of 2-aminoadipic acid and L-aspartic acid on sex separation(13, 14). The authors suggested that higher levels of L-aspartic acid in females might be resulted from sex-specific mitochondrial function and production of pituitary hormones(14). In contrast, the higher levels of 2-aminoadipic acid in males might result from sex-specific lysine degradation(13).

Table 4. A list of compounds using ROC curve analysis for individual biomarkers with AUC (area under the curve) > 0.6.

Compounds	AUC	*p*-value	$Log_2(FC)$
L-aspartic acid	0.76	<0.01	0.95
Cysteic acid	0.74	0.01	0.14
5-methylcytosine	0.72	0.02	0.45
Xanthosine	0.72	<0.01	0.32
L-tryptophan	0.70	0.04	0.57
N2-gamma-glutamylglutamine	0.69	0.01	-0.07
L-alanine	0.68	<0.01	-0.14
L-glyceric acid	0.68	<0.01	-1.25
D-cysteine	0.67	<0.01	0.12
Glycylsarcosine	0.67	0.03	0.08
N-carbamoylsarcosine	0.67	<0.01	-0.93
Hydroxyprolyl-Asparagine	0.64	<0.01	-0.99
Thioguanine	0.63	<0.05	-0.12
2-Aminoadipic acid	0.63	<0.01	-4.04
Mevalonic acid	0.63	<0.01	-0.80
L-2,4-diaminobutyric acid	0.61	<0.05	0.43

Conclusion

This study discovered sex-specific compounds in human rib bone tissue. Utilizing ^{1}H-NMR spectroscopy, it has the potential to differentiate between male and female samples and solve sex identification problem from fragmented skeletal remains. L-glyceric acid, 2-aminoadipic acid, and L-aspartic acid as potential biomarkers for sex determination. However, these results need to apply in a large sample sizes and a more diverse population, including individuals with metabolic disorders and bone diseases, for better representation of the general population. Future studies should also investigate potential metabolites in practical scenarios, such as cases involving fragmented bone tissue, to optimize the forensic application of metabolomics for reliable sex determination.

Conflict of interest statement

The authors declare no conflict of interest.

Acknowledgements:

This work was supported by the Faculty of Medicine, Chiang Mai University, grant no 42-67. The researchers would like to sincerely thank the deceased donors and their families for their support and permission to collect research samples.

References

1. Fan J, Jahed V, Klavins K. Metabolomics in Bone Research. Metabolites. 2021;11(7).
2. Welhaven HD, Vahidi G, Walk ST, Bothner B, Martin SA, Heveran CM, et al. The Cortical Bone Metabolome of C57BL/6J Mice Is Sexually Dimorphic. JBMR Plus. 2022;6(7):e10654.
3. Inkret J, Podovsovnik E, Zupanc T, Haring G, Pajnic IZ. Intra-bone nuclear DNA variability in Second World War metatarsal and metacarpal bones. Int J Legal Med. 2021;135(4):1245-56.
4. Zhao H, Li X, Zhang D, Chen H, Chao Y, Wu K, et al. Integrative Bone Metabolomics-Lipidomics Strategy for Pathological Mechanism of Postmenopausal Osteoporosis Mouse Model. Sci Rep. 2018;8(1):16456.

5. Costanzo M, Caterino M, Sotgiu G, Ruoppolo M, Franconi F, Campesi I. Sex differences in the human metabolome. Biol Sex Differ. 2022;13(1):30.
6. Bonicelli A, Mickleburgh HL, Chighine A, Locci E, Wescott DJ, Procopio N. The 'ForensOMICS' approach for postmortem interval estimation from human bone by integrating metabolomics, lipidomics, and proteomics. Elife. 2022;11.
7. Mittelstrass K, Ried JS, Yu Z, Krumsiek J, Gieger C, Prehn C, et al. Discovery of sexual dimorphisms in metabolic and genetic biomarkers. PLoS Genet. 2011;7(8):e1002215.
8. Dona AC, Kyriakides M, Scott F, Shephard EA, Varshavi D, Veselkov K, et al. A guide to the identification of metabolites in NMR-based metabonomics/metabolomics experiments. Comput Struct Biotechnol J. 2016;14:135-53.
9. de Graaf RA, Behar KL. Quantitative ^{1}H NMR spectroscopy of blood plasma metabolites. Anal Chem. 2003;75(9):2100-4.
10. Gromski PS, Muhamadali H, Ellis DI, Xu Y, Correa E, Turner ML, et al. A tutorial review: Metabolomics and partial least squares-discriminant analysis--a marriage of convenience or a shotgun wedding. Anal Chim Acta. 2015;879:10-23.
11. Scheubert K, Hufsky F, Petras D, Wang M, Nothias LF, Duhrkop K, et al. Significance estimation for large scale metabolomics annotations by spectral matching. Nat Commun. 2017;8(1):1494.
12. Cohen L, Block J, Djordjevich J. Sex related differences in isozymes of serum lactic dehydrogenase (LDH). Rev Tuberc Pneumol (Paris). 1966;30(12):55-60.
13. Leandro J, Houten SM. The lysine degradation pathway: Subcellular compartmentalization and enzyme deficiencies. Mol Genet Metab. 2020;131(1-2):14-22.
14. Holeček M. Aspartic Acid in Health and Disease. Nutrients. 2023;15(18):4023.

Metabolomics Profile in Dentine Involved in Cancer: Implications for Personal Identification

Chaniswara Hengcharoen[1], Tawachai Monum[1], Karune Verochana[2], Giatgong Konguthaithip[1], Paknaphat Watwaraphat[1], and Churdsak Jaikang[1,*]

[1] Chiang Mai University, Faculty of Medicine, Department of Forensic Medicine, Chiang Mai, 50200 Thailand.

[2] Chiang Mai University, Faculty of Dentistry, Department of Dentistry, Chiang Mai, 50200 Thailand

*Corresponding author's e-mail: churdsak.j@cmu.ac.th

Abstract:

Personal identification is a crucial step in forensic science. In decomposed and skeletal remains cases are limited evidences for identification. Underlying diseases is one factor that can use for personal identification**.** Now a day, cancer is a major cause of death then, identification of cancer biomarkers in remained tissue might be help in forensic identification. The aim of this study was to investigate the potential cancer biomarker contained in dentine using nuclear magnetic resonance (NMR) spectroscopy- based metabolomics. A total of 44 second molars (22 from healthy volunteers and 22 from cancer patients) were included. Dentine powder was prepared by removing enamel, pulverizing the tissue, and conducting ^{1}H-NMR spectroscopy. Metabolites were identified using the Human Metabolome Database (HMDB), and statistical methods, including Partial Least Squares Discriminant Analysis (PLS-DA), volcano plots, and Receiver Operating Characteristic (ROC) analysis, were employed to identify significant biomarkers. Thirty-six metabolites were significantly associated with cancer and eleven metabolites presented high potential cancer diagnostic. O-phosphotyrosine, L-kynurenine, N-acetyl-L-phenylalanine, and 9-methyladenine, were linked to immune modulation pathway, nucleotide metabolism, and amino acid dysregulation. Elevated L-kynurenine associated immune suppression and cancer activation. While 9-methyladenine and 7-methylguanine reflected cancer-associated epigenetic changes. Integrating dentine metabolomics could refine cancer biomarkers for personal identification. However, a small sample size and cancer type heterogeneity are limitation.

Keywords: Cancer biomarkers; Dentine metabolomics; NMR spectroscopy; Forensic metabolomics; Metabolomic profiling.

Introduction

Sex, age, ethnicity, and height are key factors for the personal identification in legal and forensic medicine. In some cases, especially in advanced decomposition or trauma presents challenges, the personal identification is limited. Disease plays a pivotal role in personal identification and as it can leave distinct biochemical and metabolic signatures in biological tissues. These disease-specific markers, often detectable through advanced techniques like metabolomic profiling, provide valuable insights into an individual's health status. By leveraging such unique metabolic alterations, forensic and diagnostic applications can more accurately identify individuals and associate them with specific health conditions or disease histories. Cancer, a major cause of death in Thailand, is present 140,000 new cases and 84,000 cancer-related deaths annually. Common cancers such as liver, lung, breast, cervical cancers and leukemia (1) represent significant health burdens.

Metabolomics, the study of small biomolecules, can identify biomarkers reflecting pathological conditions, exposure to toxins, or organ-specific diseases. Metabolomics is often studied in blood, urine, and other fluids, but research on bones and teeth is limited. Teeth, especially second molars, are ideal for metabolomic studies because dentine is strong and preserves long-term metabolic changes, including cancer markers. Dentinal tubules connect the pulp to the dentine matrix, allowing systemic changes to be detected. Odontoblasts enhance this process by responding to stress or disease.

Dentine's stability makes it valuable for studying systemic metabolic changes, offering insights into cancer and applications in forensics and medicine. Advanced techniques like nuclear

magnetic resonance (NMR) spectroscopy help identify biochemical markers with minimal sample damage (2, 3). Studies have found many compounds in dental tissues, such as amino acids, organic acids, sugars, and fatty acids, with reports identifying 25 to 63 chemical components (4, 5). Biomolecular markers in teeth have been used to estimate age, sex(6), and causes of death (7), as well as to detect toxins and drugs. This study uses metabolomics and NMR spectroscopy to analyze dental tissues from cancer patients, aiming to improve personal identification accuracy. By combining these methods with traditional forensic techniques, this research advances forensic science, especially in cases with damaged or limited samples.

Materials and Methods

Chemicals

Hydrochloric acid (HCl) was obtained from Merck (Darmstadt, Germany). Deuterium oxide (D_2O) and 3-(trimethylsilyl) propanoic acid sodium salt (TSP) were purchased from Sigma-Aldrich (St. Louis, MA, USA).

Teeth sample collection

A total of 44 non-carious permanent second molars were collected, with 22 samples from healthy individuals and 22 from cancer patients, all aged 20 or older. The teeth were provided by the Department of Forensic Medicine, Faculty of Medicine, Chiang Mai University, Thailand, under ethical approval (FOR-2566-0323). The samples were cleaned with saline and distilled water, dried, and stored at -20°C.

Dentine preparation

Samples were cleaned following Pellegrini et al., sliced into 1 mm sections using a precision saw, and the enamel was removed using a high-speed diamond drill. All preparation steps were performed under coolant conditions to prevent heat damage.

^{1}H-NMR spectroscopy

Dentine samples were pulverized using a freezing mill and digested with 0.6 M HCl at 100°C for 24 hours. The lyophilized solution was mixed with 0.1 M TSP in D_2O and analyzed with a Bruker AVANCE 500 MHz NMR spectrometer at 27°C. Peak assignments were determined using Bruker TopSpin software and the Human Metabolome Database (HMDB).

Chemical Identification and Quantification

Metabolites were identified using HMDB based on chemical shifts, coupling types, and other molecular properties, with a tolerance of ±0.02 for chemical shifts. Concentrations were calculated using a formula incorporating substance and TSP intensities, hydrogen counts, and TSP concentration (8, 9).

Statistical analysis for metabolomic data

Data normalization and statistical analysis were conducted using MetaboAnalyst 6.0 with median normalization, log transformation, and auto-scaling to manage variability and skewness, ensuring comparability across samples. Median normalization minimizes outlier effects, log transformation compresses data range for better handling of non-normal distributions, and auto-scaling standardizes variables for equal contribution. Partial Least-Squares Discriminant Analysis (PLS-DA) identified significant metabolic differences, with model reliability evaluated by R^2 and Q^2. R^2 is value to measure of model fit to the original data, and Q^2 provides an internal measure of consistency between the original and cross-validation predicted data.

This method, ideal for high-dimensional data, simplifies complexity while enhancing group separation. Volcano plots (fold change > 2, $p < 0.05$) highlighted key metabolites, and Receiver operating characteristic (ROC) analysis (area under the curve (AUC) > 0.8)(10) assessed diagnostic

accuracy, with AUC values near 1 indicating high discriminatory power. Venn diagrams integrated multiple analyses to identify overlapping cancer-specific metabolites.

Results and Discussion

Demographic data of participants

Forty-four cases were divided equally into a healthy control group (n=22) and a cancer group (n=22), with cancer types detailed in Table 1. Diagnoses were confirmed using medical records and family information. Both groups had the same gender distribution (12 females and 10 males each) and similar mean ages: 54.6 ± 15.0 years for the healthy group and 55.7 ± 15.7 years for the cancer group. The results are presented in Table 2.

Table 1. Type of cancer in cancer group

Cancer Type	Number of Cases	Percentage (%)
Hypopharyngeal Cancer	1	5
Lymph Node Cancer	2	10
Prostate Cancer	2	10
Intestinal Cancer	2	10
Ampulla of Vater Cancer	1	5
Pancreatic Cancer	1	5
Buccal Cancer	1	5
Lung Cancer	2	10
Salivary Gland Cancer	1	5
Liver Cancer	2	10
Adrenal Gland Cancer	1	5
Unspecified Cancer	4	20

Table 2. Characteristics of healthy and cancer groups.

Variables	Healthy (n=22)	Cancer (n=22)	p-value
Sex:			1.000
Male (%)	12 (54.54%)	12 (54.54%)	
Female (%)	10 (45.45%)	10 (45.45%)	
Age (year-old)	54.6 ± 15.0	55.7 ± 15.7	0.807

Continuous variables are presented as mean ± SD, and p-values were calculated using the independent samples t-test. Categorical variables are presented as numbers in each group, and p-values were calculated using the chi-square test.

Identification of specific cancer biomarkers contained in dentine samples

Partial Least Squares Discriminant Analysis (PLS-DA) showed differences in metabolic profiles between the healthy and cancer groups. Component 1 (36.7% variance) and Component 2 (8.9% variance) revealed partial separation in the cancer profiles (Figure 2a). Out of 209 analyzed metabolites, 91 had VIP scores above 1, with the top 15 highlighted as key biomarkers (Figure 2b). Fold-change analysis identified 22 metabolites with levels more than twice as high in the cancer group (red spots) and 41 metabolites with levels twice as high in the healthy group (blue spots), shown in the volcano plot (Figure 2c). Additionally, univariate ROC analysis identified 56 potential biomarkers, with the top 15 showing AUC values ranging from 0.8905 to 0.94215, demonstrating strong diagnostic potential (Figure 3).

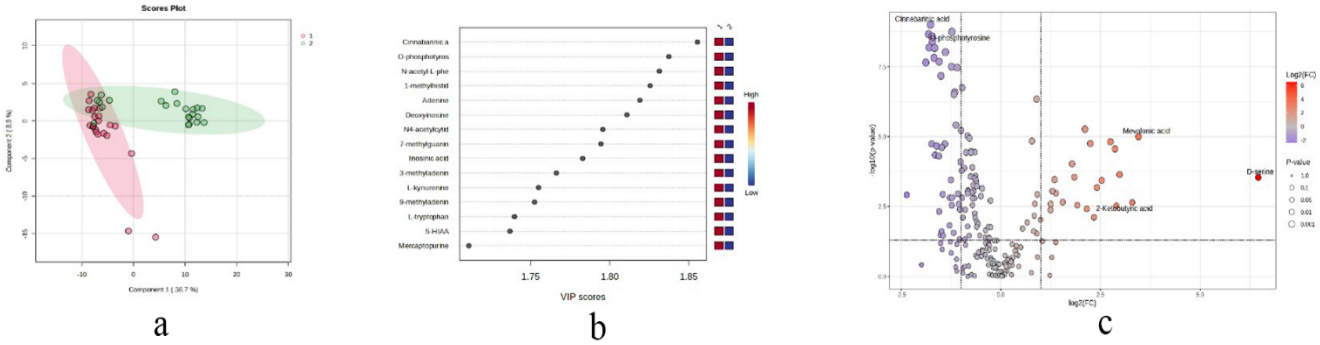

Figure 2. Metabolomic Profiles of Healthy and Cancer cases. **(a.)** PLS-DA analysis of healthy and cancer cases. **(b.)** The top 15 metabolites with the hightest VIP scores. The data were analyzed using the MetaboAnalyst 6.0 online tool. (**c.**) Volcano plot shows 56 metabolites with FC > 2 or < 0.5 and $p < 0.05$.

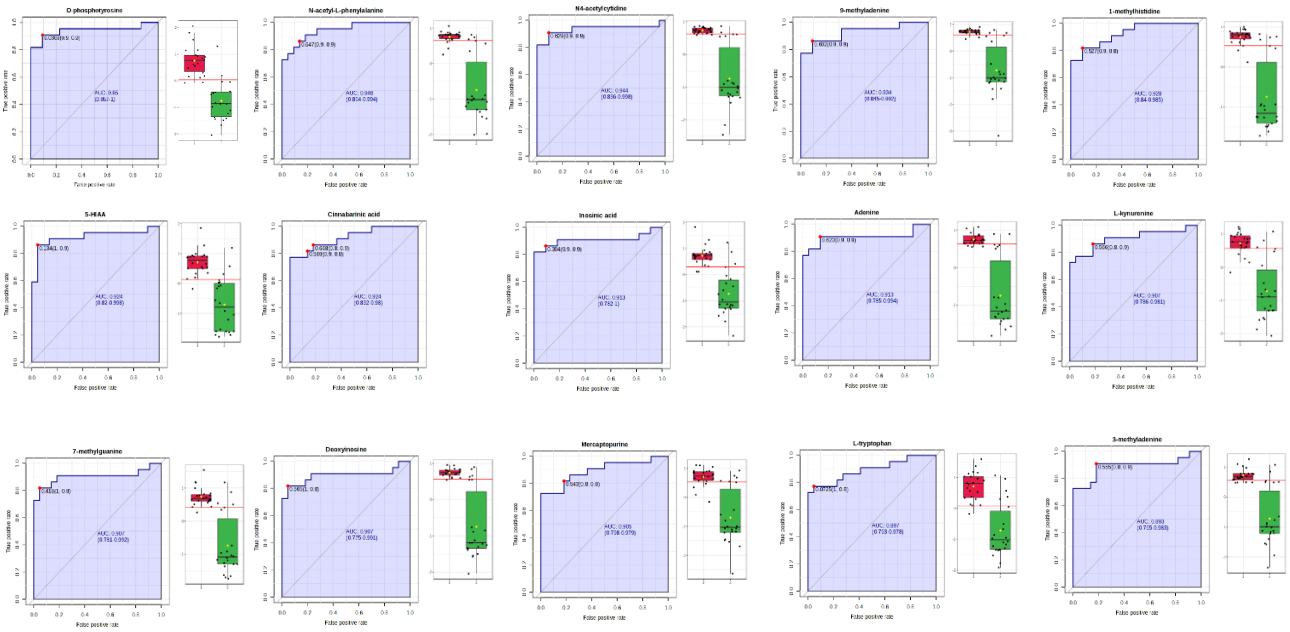

Figure 3. The univariate receiver operating characteristic (ROC) analysis highlights the top 15 metabolites associated with cancer. The accompanying box-and-whisker plots illustrate the relative concentrations of these metabolites, with red indicating cancer samples and blue representing healthy samples. These visualizations emphasize the significant differences in metabolite levels between the two groups.

Identification of potential biomarkers related to Cancer

A Venn diagram was used to identify potential cancer biomarkers based on three criteria: a VIP score >1 in the PLS-DA model, a mean metabolite concentration difference ($FC > 2$; $p < 0.05$) in the volcano plot, and an AUC > 0.8 in univariate ROC analysis. Out of 91, 63, and 56 metabolites meeting these criteria, the Venn diagram showed 36 overlapping metabolites (Figure 4). Details of the overlapping metabolites with an ROC > 0.9 are presented in Table 3.

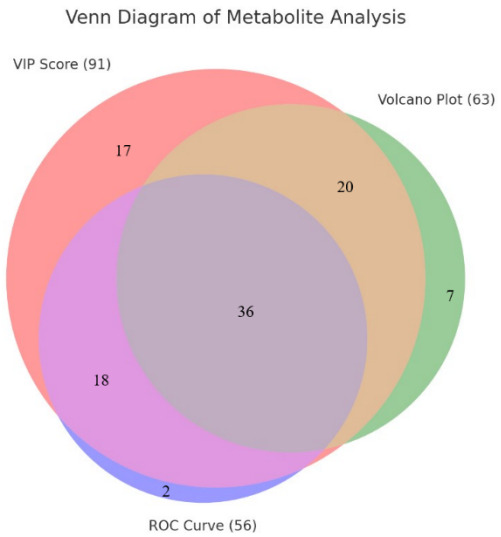

Figure 4. Venn diagram shows data set of VIP score, volcano plot and univariate ROC analysis. The diagram presents 36 potential biomarkers for Cancer.

Table 3 Overlapping Metabolites with ROC > 0.9

Metabolites	HMDB ID	VIP	FC	p-value	ROC
O-phosphotyrosine	HMDB0011185	1.8373	0.42678	1.81E-09	0.94215
N-acetyl-L-phenylalanine	HMDB0000512	1.8314	0.28458	2.19E-09	0.94215
N4-acetylcytidine	HMDB0005923	1.7956	0.28796	6.60E-09	0.93595
9-methyladenine	HMDB0140713	1.7525	0.27112	2.26E-08	0.92769
1-methylhistidine	HMDB0000001	1.8255	0.3029	2.65E-09	0.92562
5-HIAA	HMDB0000763	1.737	0.46864	3.43E-08	0.92149
Cinnabarinic acid	HMDB0004078	1.8554	0.29414	1.00E-09	0.91942
Inosinic acid	HMDB0000175	1.7829	0.38157	9.57E-09	0.90909
Adenine	HMDB0000034	1.8191	0.30491	3.23E-09	0.90702
L-kynurenine	HMDB0000684	1.755	0.34158	2.11E-08	0.90289
7-methylguanine	HMDB0000897	1.6561	0.31652	6.83E-09	0.90289

Metabolites with ROC > 0.9, showing their names, HMDB IDs, VIP scores, fold changes, p-values, and ROC values, highlight their potential as significant biomarkers.

This study identified 36 metabolites significantly associated with cancer, with 11 showing high diagnostic potential (AUC > 0.9). Key metabolites like O-phosphotyrosine, L-kynurenine, N-acetyl-L-phenylalanine, and 9-methyladenine are linked to critical pathways(11), such as immune modulation, nucleotide metabolism, and amino acid dysregulation. These findings indicate that cancer cells undergo metabolic changes in several ways. Elevated L-kynurenine levels suggest immune evasion mechanisms(12). while 9-methyladenine(13) and 7-methylguanine(14) highlight epigenetic changes, including DNA methylation, that contribute to tumor progression by silencing tumor suppressor genes and activating oncogenes.

This research extends beyond traditional biomarker studies in biological fluids by exploring dental tissues, specifically dentine, as a stable and resilient substrate for metabolomic profiling. Dentine's chemical stability provides a promising alternative for diagnostic and forensic applications, particularly when soft tissues are unavailable or degraded.

However, limitations exist. The study focuses on metabolic pathways like tryptophan-kynurenine and nucleotide metabolism, which may not be as significant in all cancer types(15). For example, while melanoma and lung cancer may heavily depend on these pathways, other cancers, such as breast cancer or certain leukemias, may rely more on lipid metabolism or glycolysis. This variability presents challenges for universal applicability across different cancer types. Additionally, the inclusion of multiple cancer types in the cohort may reduce biomarker specificity, and the small sample size (n=44) limits the generalizability of the findings. These challenges emphasize the need for larger, stratified cohorts to validate results and improve biomarker accuracy.

To increase the study's impact, we recommend integrating these findings into a broader systems biology framework. Mapping the identified metabolites onto cancer-specific metabolic networks could provide insights into pathway interactions, such as how immune modulation and epigenetic changes contribute to metabolic reprogramming. Combining metabolomics with other omics approaches, like genomics and proteomics, could offer a more comprehensive understanding of cancer biology and enhance biomarker specificity for individual cancer types. Future research should address these limitations by expanding the cohort size, stratifying samples by cancer type and stage, and utilizing advanced computational tools, such as machine learning, to integrate multi-omics data. These strategies could uncover predictive biomarkers, refine therapeutic targets, and enable personalized diagnostics.

By establishing dentine metabolomics as a viable approach for cancer biomarker discovery, this study broadens the scope of metabolomics and offers new opportunities for non-invasive diagnostics and forensic applications. A systems biology perspective could further enhance our understanding of cancer biology, advancing precision medicine and clinical diagnostics.

Conclusion

This study demonstrates the potential of dentine metabolomics for identifying cancer biomarkers, emphasizing its stability and accessibility as a substrate for profiling key cancer-related pathways, such as immune modulation and nucleotide metabolism. By positioning dentine as a viable alternative to traditional soft tissues, the research expands the scope of metabolomics, contributing to advancements in non-invasive cancer diagnostics and forensic science. Integrating dentine metabolomics into multi-omics approaches could enhance biomarker specificity, uncover pathway interactions, and reveal novel therapeutic targets. Future research should address limitations, including small sample size and cancer heterogeneity, to fully unlock its potential in personalized medicine and forensic applications.

Conflict of Interest Statement

The authors declare no conflicts of interest related to this research.

References

1. กรมการแพทย์เผยคนไทยป่วยมะเร็งรายใหม่ปีละ 1.4แสนคน เสียชีวิต 8.3หมื่นคน [Internet]. Hfocus เจาะลึกระบบสุขภาพ; 2024 [updated 2 Febuary 2024. Available from: https://www.hfocus.org/content/2024/02/29679.
2. Ni Q, Chen S. Assessment of structural changes of human teeth by low-field nuclear magnetic resonance (NMR). Meas Sci Technol. 2010;21(1):15803.
3. Zia K, Siddiqui T, Ali S, Farooq I, Zafar MS, Khurshid Z. Nuclear Magnetic Resonance Spectroscopy for Medical and Dental Applications: A Comprehensive Review. Eur J Dent. 2019;13(1):124-8.
4. Zhou J, Ning K, Yang Y, Zou L, Xue J, Kong X, et al. 1H-NMR -based metabolic analysis on biocompatibility of dental biomaterials. Process Biochemistry. 2022;114:163-73.

5. G K, T M, C J. C. Determination of Biomolecules Contained in Human Dentine Samples by Proton Nuclear Magnetic Resonance Spectroscopy (1H-NMR). 2022;8(1).
6. Ankur Shah MFaSC. Reasons for extractions of permanent teeth in western India: A prospective study. International Journal of Applied Dental Sciences. 2019;5(1):180-4.
7. Maciejczyk M, Nesterowicz M, Zalewska A, Biedrzycki G, Gerreth P, Hojan K, et al. Salivary Xanthine Oxidase as a Potential Biomarker in Stroke Diagnostics. Front Immunol. 2022;13:897413.
8. Choi K MS, Seo Y, Ahn S. Quantitative NMR as a Versatile Tool for the Reference Material Preparation. Magnetochemistry. 2021;7(1).
9. DFC G, MD. PDF hosted at the Radboud Repository of the Radboud University Nijmegen. Radboud Repository. 2023;213(1):71.
10. Şeref Kerem Çorbacıoğlu GA. Receiver operating characteristic curve analysis in diagnostic accuracy studies: A guide to interpreting the area under the curve value. TURKISH JOURNAL OF EMERGENCY MEDICINE. 2023;23(4):195-8.
11. Seo S-K, Kwon B. Immune regulation through tryptophan metabolism. Experimental & Molecular Medicine. 2023;55(7):1371-9.
12. Schlichtner S, Yasinska IM, Klenova E, Abooali M, Lall GS, Berger SM, et al. L-Kynurenine participates in cancer immune evasion by downregulating hypoxic signaling in T lymphocytes. Oncoimmunology. 2023;12(1):2244330.
13. Du D, He J, Ju C, Wang C, Li H, He F, et al. When N7-methyladenosine modification meets cancer: Emerging frontiers and promising therapeutic opportunities. Cancer Letters. 2023;562:216165.
14. D'Ambrosi S, García-Vílchez R, Kedra D, Vitali P, Macias-Cámara N, Bárcena L, et al. Global and single-nucleotide resolution detection of 7-methylguanosine in RNA. RNA Biology. 2024;21(1):476-93.
15. Yan J, Chen D, Ye Z, Zhu X, Li X, Jiao H, et al. Molecular mechanisms and therapeutic significance of Tryptophan Metabolism and signaling in cancer. Molecular Cancer. 2024;23(1):241.

Keyword Index

Supported by

S.M. CHEMICAL

everlife
RI Technologies

P.Intertrade Equipment Co., Ltd.

LIFE SCIENCE AP

BD

Applied Chemical & Instrument Co.,Ltd.

AMS
บริษัท แอดวานซ์
เมดิคอล
ซายน์ จำกัด

BANG TRADING 1992 CO., LTD.

BIOSCIENCE

UNION SCIENCE

MERCK

ESCO
LIFESCIENCES GROUP

BARA SCIENTIFIC
Solution of Success

For more information

Tel: 053-935322 or 053-935325

https://www.agribiomed2025.org

https://w1.med.cmu.ac.th/biochem/